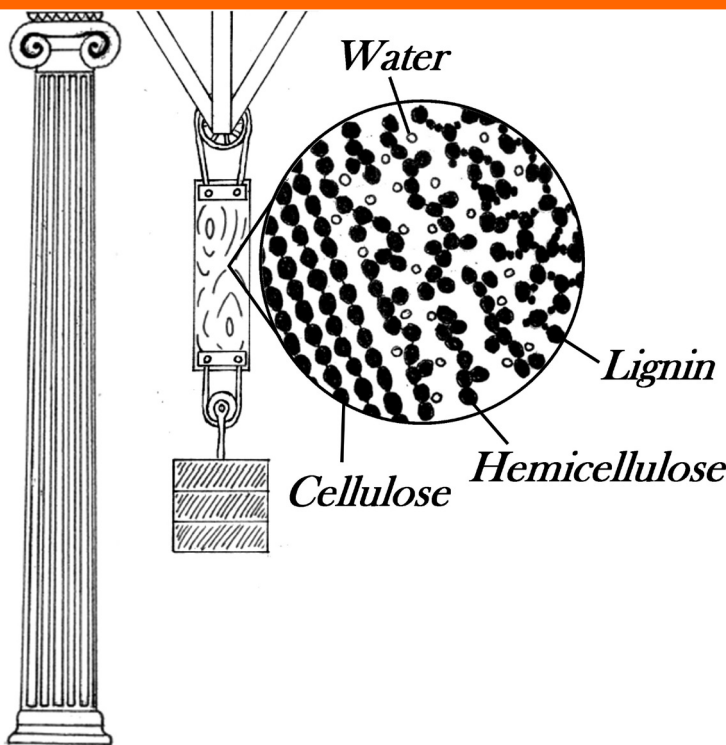


Wood – water interactions

Linking molecular level mechanisms
with macroscopic performance



Emil Tang Engelund

PhD Thesis

**Department of Civil Engineering
2011**

DTU Civil Engineering Report R-258 (UK)
November 2011

Wood-water interactions

Linking molecular level mechanisms with macroscopic performance

Copyright ©, Emil Tang Engelund, 2011

Printed by Rosendahls-Schultz Grafisk

Department of Civil Engineering

Technical University of Denmark

ISBN number: 9788778773401

ISSN number: 1601-2917

Report number: R-258

WOOD – WATER INTERACTIONS

**Linking molecular level mechanisms
with macroscopic performance**

Emil Tang Engelund

Industrial PhD-thesis

Sponsored by the Ministry of Science, Technology and Innovation

Department of Civil Engineering

Technical University of Denmark

2011

ABSTRACT

Predicting the performance of wood for decades ahead is important when using the material for structural purposes. The performance is closely related to the hierarchical material structure of wood and the dependent interaction with water in the structure. Accurately predicting wood performance therefore requires an understanding of material structure from molecular to macroscopic level as well as of the impact of water molecules.

The objective of this work is to investigate the performance of wood in terms of mechanical response of the material and effect of water. To understand the latter, one must first know in which parts of the wood structure, water is located. If parts of the water in wood are held in capillaries in the wood structure, these water molecules interact with the material differently than those held within wood cell walls. In this study, the occurrence of capillary water in wood is investigated at high levels of relative humidity (RH), where capillary water might be present. Three different techniques are employed in overlapping RH regimes. The three techniques give similar results and show that the amount of capillary water is insignificant up to at least 99.5 % RH. Thus, for wood in equilibrium with surrounding climate in the RH range 0-99.5 %, water is only significantly present within cell walls.

A structural model of a wood cell is developed in this study using Finite Element Method for predicting the mechanical performance of wood. The starting point for the model is the physical behaviour on the molecular level since water interferes with wood at this level. The elastic material properties of the wood cell wall are explained by the organisation of wood constituents and their properties. The effect of water as well as temperature is incorporated by considering the amount of hydrogen bonds between wood constituents and the stiffness of these bonds. The mechanical response of wood includes a substantial time-dependent response, which previously has been explained by sliding between wood constituents on the molecular level. In this study, this is incorporated in the model as time-dependent shearing of the material planes of the cell wall. The calculated results of the model is verified against various experimental results from literature as well as from measurements presented in this work. It is shown that the structural model is able to describe a diverse range of mechanical responses of wood cells in both elastic and time-dependent domains. Furthermore, comparison of results from experiments and model suggests that the mechanical response of wood tissue, i.e. the hierarchical level above single wood cells, is a sum of responses from both wood cells and intercellular layer, i.e. the middle lamella.

SAMMENFATNING

Når træ anvendes til konstruktioner, er det yderst vigtigt at dets mekaniske opførsel kan forudsiges langt ud i fremtiden. Træs opførsel hænger nøje sammen med både den hierarkiske opbygning af materialet og interaktionen med fugt i materialet. At kunne forudsige træs opførsel kræver derfor en dybere forståelse af materialets struktur fra molekylært til makroskopisk niveau samt mekanismen hvormed fugten påvirker materialet.

Formålet med denne afhandling er at afdække træs mekaniske opførsel og fugtens effekt herpå. For at kunne forstå sidstnævnte, er det nødvendigt først at undersøge hvor fugten er til stede i træets struktur. Hvis en del af fugten findes i kapillarer i træet, påvirker den materialet på en anden måde end vandmolekyler bundet i træets cellevægge. I dette projekt er tilstedeværelsen af kapillarbundet fugt i træ undersøgt under høje relative luftfugtigheder (RF), hvor sandsynligheden for at finde kapillarbundet fugt er størst. Tre forskellige måleteknikker er anvendt med overlap i intervallet i RF for hver teknik. Alle tre teknikker gav ensartede resultater, og det vist at mængden af kapillarbundet fugt er forsvindende lille for luftfugtigheder under 99,5 % RF. Det konkluderes derfor at træ i ligevægt med luftfugtigheder mellem 0-99,5 % RF i langt overvejende grad har fugten bundet i cellevæggene.

I denne afhandling udvikles endvidere en strukturel model af en træcelle ved brug af Finite Element-metoden. Formålet er at forudsige træs mekaniske opførsel ud fra denne model. Udgangspunktet for modellen er den fysiske opførsel på molekylært niveau, eftersom det er på dette niveau fugten interagerer med træet. Cellevæggenes elastiske materialeegenskaber forklares ud fra deres kemiske opbygning. Effekten af både fugt og temperatur forudsiges ud fra antallet af hydrogenbindinger mellem træets bestanddele og stivheden af disse. Træs mekaniske opførsel er i betydelig grad tidsafhængig. Baggrunden for den tidsafhængige opførsel er tidligere blevet forklaret ved glidninger på molekylært niveau mellem træets bestanddele. Dette medtages i denne afhandling gennem tidsafhængige forskydningsdeformationer i cellevæggens materialeplaner. Resultaterne fra den strukturelle model verificeres mod forsøgsresultater fra litteraturen såvel som fra forsøg beskrevet i denne afhandling. Det vises at modellen er i stand til at beskrive en bred vifte af træs forskelligartede elastiske og tidsafhængige fænomener. Endvidere vises det at træs mekaniske opførsel er en sum af bidrag fra træets celler og materialet mellem cellerne, kaldet midtlamellen.

ACKNOWLEDGEMENTS

Even though only my name is on the front cover, this thesis would not have materialised were it not for the contributions of a whole range of people. Firstly, I would like to thank my supervisors Staffan Svensson, Lisbeth G. Thygesen, and Niels Morsing for their guidance and patience when nearly all my initial experiments went wrong, our numerous discussions, and most of all for letting me find my own way through the PhD project. Secondly, for technical support in acquiring most of the experimental results of this thesis I am greatly indebted to Ulla Gjøøl Jacobsen and Anne-Mari Olsson. Thirdly, I would like to give thanks to Preben Hoffmeyer; not only for our fruitful collaboration during my PhD project but also for the many years of inspired discussions and supervision during my time at university.

This thesis is the product of my Industrial PhD project which incorporated the Department of Civil Engineering at Technical University of Denmark, Forest and Landscape at University of Copenhagen, and Centre for Wood Technology at Danish Technological Institute. Having three offices scattered around the Greater Copenhagen area has provided me the opportunity to socialise with amazing colleagues at all three institutions, which I am grateful for. Furthermore, through financial support from the Ministry of Science, Technology and Innovation and COST Action FP0802 I have been able to travel to conferences, courses and a scientific visit. Hereby, I have met colleagues and friends within the scientific community who have enriched me both professionally and personally. In that connection I am grateful for the welcome I received at Innventia, Stockholm; in particular by Anne-Mari, Elina, Jasna, Lennart, Silvia, and Tommy. I would also like to express my appreciation to the organizers of COST Action FP0802, especially Karin Hofstetter, for arranging the course “Wood at the microscale” which was a turning point in the project. Last but not least, I would to thank some of those people that made the last couple of years a fun and enjoyable time. These include my friends from the Industrial PhD program: Jörg, Sverrir and Ali with whom I have spent many great occasions with all-you-can-eat stegt flæsk, beer, fun, and kebab. Also included are all the wonderful, crazy, funny, and charming people I have met via boxing and dancing. They have reminded me that there is more to life than work (and wood science). Most important of all, however, is Dorte whose love I cherish every day.

Amager, Copenhagen, August 2011

Emil Tang Engelund

LIST OF PAPERS

This thesis is based on the following six papers:

- Paper I** Water sorption in wood and modified wood at high values of relative humidity. Part I: Results for untreated, acetylated and furfurylated Norway spruce
Thygesen L. G., Engelund E. T. and Hoffmeyer P.
Holzforschung (2010) 64:315-323
- Paper II** Water sorption in wood and modified wood at high values of relative humidity. Part II: Appendix. Theoretical assessment of the amount of capillary water in wood microvoids
Engelund E. T., Thygesen L. G. and Hoffmeyer P.
Holzforschung (2010) 64:325-330
- Paper III** Equilibrium moisture content in Norway spruce during the first and second desorptions
Hoffmeyer P., Thygesen L. G. and Engelund E. T.
Holzforschung (2011) 65:875-882
- Paper IV** Modelling time-dependant behaviour of softwood using deformation kinetics
Engelund E. T. and Svensson S.
Holzforschung (2011) 65:231-237
- Paper V** Tensile creep and recovery of Norway spruce influenced by temperature and moisture
Engelund E. T. and Salmén L.
Submitted to Holzforschung
- Paper VI** Predicting the reorientation of microfibrils in plant fibres under tensile strain
Engelund E. T. and Svensson S.
Unsubmitted manuscript

In addition, the work has resulted in the following publications

Service life prediction of wood claddings by in-situ measurement of wood moisture content: status after 5 years of outdoor exposure

Engelund E. T., Lindegaard B. and Morsing N.

Proceedings of the 40th annual meeting of the International Research Group on Wood Protection (2009), Beijing

Optimising hydrogen bonding in solid wood

Engelund E. T.

Proceedings of the 5th meeting of the Nordic-Baltic Network in Wood Material Science and Engineering (2009), Copenhagen

Acquisition of sorption isotherms for modified woods by the use of dynamic vapour sorption instrumentation. Principles and practice

Engelund E. T., Klamer M. and Venås T. M.

Proceedings of the 41st annual meeting of the International Research Group on Wood Protection (2010), Biarritz

Numerical modelling of softwood time-dependent behaviour based on microstructure

Engelund E.T.

Book of abstracts of the COST Action FP0802 workshop "Wood structure/function-relationships" (2010), Hamburg

Numerical modelling of the time-dependent mechanical behaviour of softwood

Engelund E. T.

Proceedings of the 6th meeting of the Nordic-Baltic Network in Wood Material Science and Engineering (2010), Tallinn

Glæden ved det enkle (in Danish)

Engelund E. T.

Dissemination Award for Industrial PhD students (2010), second prize contribution

Adsorption boundary curve influenced by step interval of relative humidity investigated by Dynamic Vapour Sorption equipment

Engelund E. T., Klamer M. and Venås T. M.

Proceedings of the 42nd annual meeting of the International Research Group on Wood Protection (2011), Queenstown

LIST OF SYMBOLS

Symbol	Unit	Description
A	s ⁻¹	Parameter related to the rate of deformation
A ₀	s ⁻¹	Reference value of parameter A
A _{HC}	s ⁻¹	Parameter related to the rate of deformation of hemicellulose
A _{LG}	s ⁻¹	Parameter related to the rate of deformation of lignin
B	-	Parameter related to the rate of deformation
B _{HC}	-	Parameter related to the rate of deformation of hemicellulose
B _{LG}	-	Parameter related to the rate of deformation of lignin
c _{HG}	-	Volume concentration of hemicellulose
c _{LG}	-	Volume concentration of lignin
E	Pa	Modulus of elasticity
E _{ref}	Pa	Reference modulus of elasticity related to the Nissan theory
EMC	%	Equilibrium moisture content described as mass fraction
G	Pa	Shear modulus (elastic)
ΔG [‡]	J/mol	Activation free energy
h	J s	Planck's constant
k	J/K	Boltzmann's constant
k _{HB}	N/m	Average force constant of hydrogen bonds
K _{MC}	/%	Coefficient of change in modulus of elasticity with moisture content
K _T	K ⁻¹	Coefficient of change in modulus of elasticity with temperature
M _{polymer unit}	g/mol	Molar mass of a polymer unit
M _{water}	g/mol	Molar mass of water
MC	%	Moisture content described as mass fraction
MC _c	%	Critical moisture content related to the Nissan theory
MC _{ref}	%	Reference moisture content related to the Nissan theory
MFA	°	Microfibril angle
N	m ⁻³	Number of effective hydrogen bonds per unit volume
N ₀	m ⁻³	Number of effective hydrogen bonds at zero moisture content per unit volume
n _{sorption site}	-	Number of sorption sites on a polymer unit

t	s	Time
T	K	Absolute temperature
T _{ref}	K	Reference temperature related to the Nissan theory
V _h	m ³	Volume swept by the motion of a moving segment
V _m	m ³	Volume of a moving segment
W	J	Mechanical work
β _{sw}	-	Swelling coefficient
β _{sw,cell}	-	Swelling coefficient of wood cell wall
β _{sw,polymer}	-	Swelling coefficient of wood polymers
ε	-	Strain
ε _v	-	Viscous strain
v	s ⁻¹	Specific rate of reactions, often described by the symbol k' in the literature
θ	-	Transmission coefficient, often described by the symbol κ in the literature
σ	Pa	Stress
Φ	%	Hypothetical saturation moisture content of a polymer unit, often described by the symbol W in the literature

CONTENT

MOTIVATION.....	1
STRUCTURE OF THE THESIS.....	4
SOFTWOOD STRUCTURE	7
• THE CELLULOSE MICROFIBRIL.....	7
• THE TRACHEID CELL	9
• SOFTWOOD TISSUE	13
WATER IN WOOD.....	15
• WOOD CELL AFFINITY TO WATER	15
• SORPTION ISOTHERM.....	16
• SORPTION HYSTERESIS	22
• FIRST DESORPTION AND EFFECT OF DRYING PROCEDURE.....	25
MECHANICAL BEHAVIOUR.....	29
• EFFECTS OF WATER ON THE ELASTIC PROPERTIES OF THE CELL WALL	30
• EFFECTS OF WATER ON THE TIME-DEPENDENT PROPERTIES OF THE CELL WALL	36
• MODELLING THE ELASTIC AND TIME-DEPENDENT BEHAVIOUR OF THE CELL WALL	40
• NUMERICAL MODELLING OF THE ELASTIC BEHAVIOUR OF TRACHEIDS	47
• NUMERICAL MODELLING OF THE TIME-DEPENDENT BEHAVIOUR OF TRACHEIDS	52
• THE MECHANICAL BEHAVIOUR OF SOFTWOOD	59
SUGGESTED FUTURE RESEARCH.....	61
• WATER SORPTION AND DIFFUSION	61
• MECHANOSORPTION	63
REFERENCES.....	65
APPENDED PAPERS	79

INTRODUCTION

Motivation

Modern society is filled with products made of or derived from wood, e.g. paper and packaging materials, furniture, tools, and structural components in buildings. The last decades have seen a growing European consumption of wood (Kangas and Baudin 2003) of which about half is used for construction purposes (CEI Bois 2008). There is good reason to believe that wood will remain an important building material for future generations. For instance, growing concerns over environmental issues and global warming have led to new sustainable building practices (Rocco et al. 2010). These encourage the use of materials with small or moderate environmental footprint, which favours renewable resources such as wood (Rocco et al. 2010). The choice of wood is, however, also favoured by a natural human affinity for wood; we have an innate fondness of the visual and tactile characteristics of wood (Nyruud and Bringslimark 2010).

In order to build safe and durable structures, a proper understanding of physical characteristics of the building materials is required. The serviceability of a structure is not only a question of the strength of components, i.e. whether the building will stand for a required service life. The serviceability also incorporates lasting functionality of the structure. Thus, structures are designed to avoid function interfering deformations, e.g. the sagging of a beam should not exceed the serviceability limit criteria. When building with wood, this latter requirement is many times the designing factor. This is because of the significant time-dependent mechanical response of the material. For instance, after one year of service the deflection of a wooden joist has typically increased 50 % compared to the immediate deflection. The time-dependent response, however, is variable and heavily influenced by both moisture and temperature. One of the primary goals of wood science for many decades has therefore been to predict the time-dependent mechanical behaviour as function of moisture and temperature.

The first attempts at predicting the time-dependent mechanical behaviour of wood were purely empirical. Thus, correlations in experimental results led to mathematical models. The empirical approach is illustrated in figure I.1, where measured parameters by extrapolation directly lead to the predicted parameters. One example is the work of Clouser (1959) based on experiments with small wood beams in bending. In this work, a power law function was fitted to the deflection over time. The parameters determined in this way are, however, not linked to any physical reality (Hunt 1997). They can thus not provide a deeper scientific understanding of the behaviour of wood.

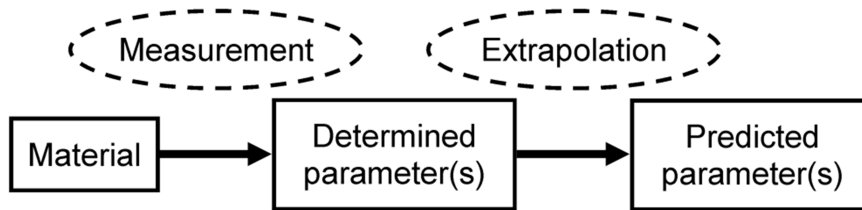


Figure I.1: Empirical approach for predicting wood properties.

Another approach is the introduction into wood science of various theoretical mathematical models from other scientific fields where they have been successfully applied. These models are based on assumptions regarding the physical reality, and therefore their parameters may or may not have physical meaning when used for wood. Often, the models fail to describe experimental results. This is possibly because of deviations between the physical reality in which the models have been established and that in which they are set to operate. The approach is illustrated in figure I.2 where measured parameters serve as input data in a theoretical model from which predicted parameters are drawn.

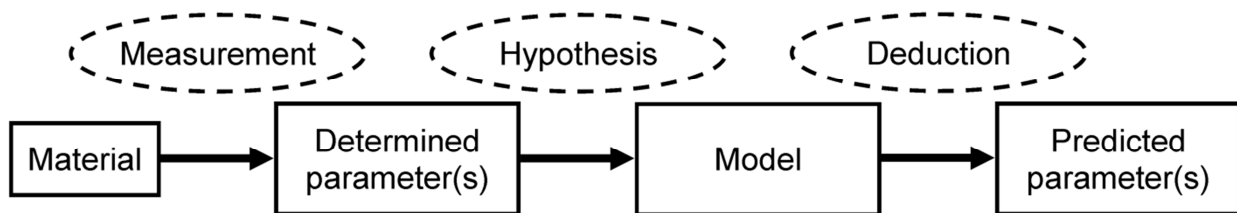


Figure I.2: Theoretical approach for predicting wood properties.

One example of this is the work of Hanhijärvi (1995) which describes a simple mathematical model for predicting the time-dependent mechanical behaviour of solid materials. In fact, the model is similar to the one used in this work. It is a statistical mechanical description of how fast time-dependent processes occur. However, the model as it is does not consider the microstructure of the material concerned, and it fails to describe experimental data. Therefore, Hanhijärvi (1995) expands the model by introducing the sum of terms of similar form but with different parameter values. Hereby, predictions of the model are improved by incorporating several (physical unjustified) parameters as are many other mathematical models. Consequently, the physical interpretation of parameters is difficult (Hunt 1997; Gril et al. 2004), and models start resembling empirical fitting models, rather than physical realistic models. A deeper scientific insight into the physics behind wood behaviour is therefore lost. A further review of both empirical and theoretical mathematical models is given by Morlier and Palka (1994). None of these models are able to describe the time-

dependent mechanical behaviour of wood from coherent physical theory. It must here be stated that the works of Hanhijärvi (1995) and Clouser (1959) are not brought forward as examples of useless research efforts. On the contrary, it shows the progression of wood science from basic experiments and simple mathematical models towards more complex experiments and elaborate models. It is thus natural that successors of these scientists stand on their shoulders and try to renew and rethink the theories in order to further advance our knowledge on wood behaviour.

This work attempts a mathematical description of the mechanical behaviour of wood based on established theories from other scientific fields, while considering the physical reality the mathematical model is operating in, i.e. wood. Thus, the model must not violate physics, e.g. degenerate established physical theories, nor make violations to the structural constraints. This kind of approach is illustrated in figure I.3 where a structural analysis of the material in question is the basis for constructing the theoretical model. The measured parameters are used for verifying the model from which predicted parameters are drawn.

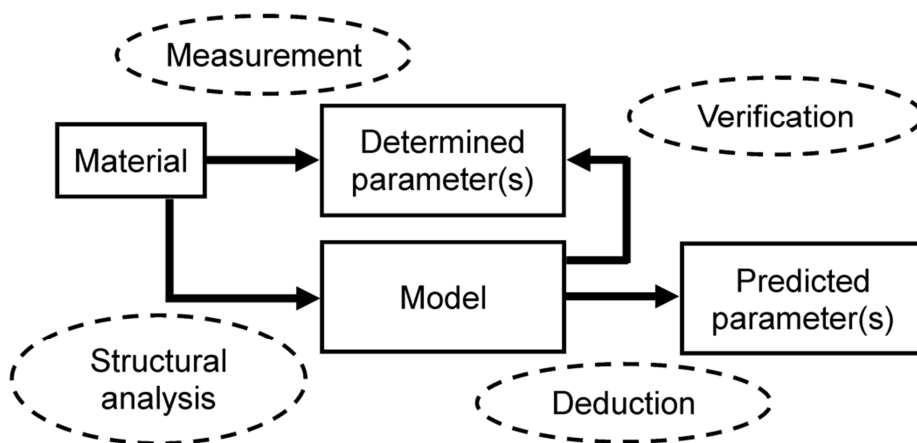


Figure I.3: Theoretical approach for predicting wood properties incorporating the structure of the material.

Such approach has previously been used to describe the elastic mechanical behaviour of wood. For instance, both Mark (1967) and Salmén (1982) described the elastic mechanical behaviour of wood based on present knowledge about wood microstructure. More recently, Persson (2000) used numerical modelling to describe the elastic mechanical behaviour. Similarly, several micromechanical modelling studies have been performed on wood recently and are reviewed by Hofstetter and Gamstedt (2009). However, so far no study has successfully described the time-dependent mechanical behaviour of wood.

Structure of the thesis

This thesis rests on both experimental and theoretical work done by the author and co-workers as well as scientific investigations reported in the literature. To clarify which parts of the thesis are contributions of the author and co-workers, a brief review of the structure of the thesis is here stated.

- Chapter 1, “Softwood structure”, is a state-of-the-art on structure and composition of softwood. The chapter is entirely based on relevant literature, and no contributions of the author are added. The chapter serves as an introduction to the hierarchical structure of wood which is important for the mathematical modelling performed in Chapter 3.
- Chapter 2, “Water in wood”, deals with the interaction of softwood with water. The contribution of the author and co-workers is mixed with contributions during the last 100 years from scientific investigation on the subject. First half of subchapter “Sorption isotherm” and entire subchapter “First desorption and effect of drying procedure” are based on work done by the author. The rest of the chapter relies on data and observations from the literature with some new interpretations by the author. The work of the author and co-workers related to this chapter is also described in Paper I, II, and III. The chapter describes where in the wood structure water is present and how water interacts with wood. This information is crucial for the mathematical description of effects of water on mechanical behaviour in Chapter 3.
- Chapter 3, “Mechanical behaviour”, focuses on our current understanding of the mechanical behaviour of softwood cells, and on basis of this shows how the behaviour can be mathematically described. The first two subchapters “Effects of water on the elastic properties of the cell wall” and “Effects of water on the time-dependent properties of the cell wall” are reviews of the literature relevant for establishing the modelling presented in the rest of the chapter. The subsequent four subchapters “Modelling the elastic and time-dependent behaviour of the cell wall”, “Numerical modelling of the elastic behaviour of tracheids”, “Numerical modelling of the time-dependent behaviour of tracheids”, and “Effect of water on the mechanical behaviour of softwood” are all based on work done by

the author and co-workers. The work related to this chapter is also described in Paper IV, V, and VI. The chapter explains elastic behaviour from theories describing the amount of hydrogen bonds between wood polymers, whereas the time-dependent response is described by shearing processes at the molecular level where wood polymers are displaced relative to each other. Many of the assumptions of this chapter are directly based on wood microstructure and effects of water described in Chapter 1 and 2.

- Chapter 4, “Suggested future research”, attempts to briefly introduce two related wood phenomena which are relevant for the numerical modelling presented in Chapter 3.

CHAPTER 1

Softwood structure

Wood is a hierarchical material with several levels of organisation. Predicting the behaviour of wood therefore requires substantial knowledge of composition and structural organisation from molecular level to macroscopic structure. The governing components at the molecular level are the biopolymers cellulose, hemicelluloses, and lignin. These are organised into a composite and form the cell walls of the tracheid cells, which in turn are arranged into wood tissue. The structure and variation at these different levels have a potential influence on macroscopic wood performance. The following gives a brief review of current knowledge about the organisation of softwood at the molecular, the cell wall, and tissue levels.

The cellulose microfibril

Cellulose is the most highly ordered and stable wood polymer. The repeating unit of cellulose is cellobiose shown in figure 1.1, consisting of two glucose monomers. These monomers are polymerized to a degree of polymerisation of about 10,000 in wood (Goring and Timell 1962).

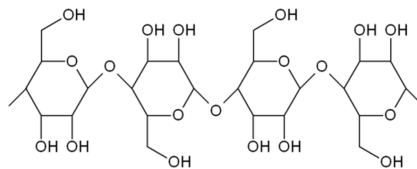


Figure 1.1: Two cellobiose units connected to form a small part of a cellulose chain.

The cellulose chains are aligned and arranged into microfibrils which are long aggregates (Atalla et al. 2008) that for softwood consists of 36 chains each (Ding and Himmel 2006; Li and Renneckar 2011). The cross-section of a softwood microfibril is hexagonal as illustrated in figure 1.2 and has a thickness of about 3.1 nm and a width of about 5.3 nm (Li and Renneckar 2011). Various other values have been reported for the microfibrillar dimensions (Andersson et al. 2003; Emons 1988; Ha et al. 1998; Hult et al. 2001; Hult et al. 2003; Ohad and Danon 1964). The variation between studies result from limitations of the measurement techniques and sample preparation procedures employed (Ding and Himmel 2006). Microfibrils from other natural sources may, however, have different dimensions, e.g. algae microfibrils are typically quite large (Sugiyama et al. 1985). The length of a microfibril is less certain than the cross-sectional dimensions (Hanley et al. 1997;

Somerville et al. 2004). The length can, however, be estimated based on the degree of polymerisation of glucose monomers and their length. Detailed experimental studies have revealed that the length of a cellobiose unit, i.e. two glucose monomers, is close to 1.04 nm (Nishiyama et al. 2002; Nishiyama et al. 2003). With a degree of polymerization of glucose of 10,000, this yields an expected length of microfibrils around 5 μm , i.e. about 1,000 times the width of the microfibrils.

In the softwood microfibril, the cellulose chains are ordered in eight sheets (Li and Renneckar 2011), see figure 1.2. Every sheet is held together by strong hydrogen bonds between hydroxyl groups, whereas the interaction between sheets are governed by weaker hydrogen bonds and van der Waals interactions (Li and Renneckar 2011; Qian et al. 2005; Qian 2008). It has been proposed (Atalla and Vanderhart 1984) that two different stable conformations of native cellulose microfibrils exist; cellulose I α and cellulose I β . The proportions of I α and I β depends on the plant species studied (Vanderhart and Atalla 1984). Traditionally, cellulose in the microfibril is called “crystalline” and the forms I α and I β are characterized by differences in the crystalline unit cell and hydrogen bonding pattern. The two forms are, however, very much alike and can be found in the same microfibril (Imai and Sugiyama 1998; Sugiyama et al. 1991; Wada and Okano 2001). It has been suggested that the core of microfibrils was composed of I β surrounded by I α (Yamamoto et al. 1996), but recent studies have shown that the two forms are mixed in the microfibrils (Horikawa and Sugiyama 2009). The exact distribution, however, remains unclear.

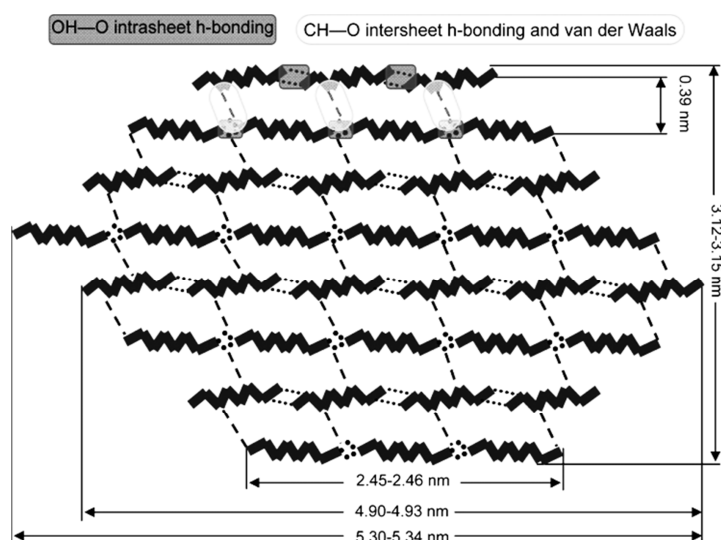


Figure 1.2: Cross-section of a microfibril with 36 cellulose chains arranged in a hexagonal pattern. Reprinted with permission from (Li and Renneckar 2011). Copyright (2011) American Chemical Society.

Previously, microfibrils were thought to be made up of portions of crystalline cellulose interrupted by regions of less ordered cellulose (Mark 1928; Mark 1940; Mukherjee et al. 1951); see (Hon 1994) for a historical account of models for the arrangement of cellulose in microfibrils. Recent experimental findings show, however, that the microfibrils are continuous ordered aggregates (Ding and Himmel 2006) twisted along the length (Hanley et al. 1997). This is confirmed by molecular dynamics studies (Matthews et al. 2006; Yui et al. 2006), and it thus seems that the aggregated cellulose has an inherited tendency for twisting along the length. The twisting of microfibrils probably depends on the dimensions of the cross section (Atalla et al. 2008).

Experimental studies have revealed that part of the cellulose in microfibrils is less-ordered, and this part has been termed “amorphous”. Unlike previous models of microfibrils, the amorphous cellulose is not interrupting ordered portions of crystalline cellulose. Instead, it is now clear that the so-called amorphous cellulose in fact is cellulose chains found at the surfaces of microfibrils (Larsson et al. 1999; Newman and Hemmingson 1995). This is confirmed by evaluating the crystallinity, i.e. percentage of “crystalline” cellulose, of different sized microfibrils from various natural sources. The variation in size gives a variation of surface-to-volume ratio, and this ratio is directly correlated with the measured crystallinity of the various microfibrils (O’Sullivan 1997). For wood, about 33 % of the hydroxyl groups of cellulose are located on the surfaces of microfibrils (O’Sullivan 1997). Although surface cellulose is not amorphous in the strict sense of the word, the bonding pattern for these chains might be less ordered than for core cellulose chains (O’Sullivan 1997; Xu et al. 2007).

The tracheid cell

The cellulose microfibril is the most significant structural unit of plant cells. Several different types of plant cells exist but the most abundant cell in softwood is the tracheid. It constitutes about 95 % of the softwood volume (Higuchi 1997). Tracheids are about 2-4 mm long and 0.02-0.04 mm wide hollow tubes (Brändström 2001). The inner void volume of the cell is called cell lumen and the material surrounding the lumen is termed cell wall. In tracheids, the latter has thickness of 0.002-0.008 mm (Brändström 2001). The cell wall of tracheids can be divided into the primary (P) and secondary wall of which the latter typically consists of three distinct layers: S1, S2 and S3, see figure 1.3. The dominant wall layer is the S2 layer which constitutes around 80 % of the cell wall (Fengel and Stoll 1973).

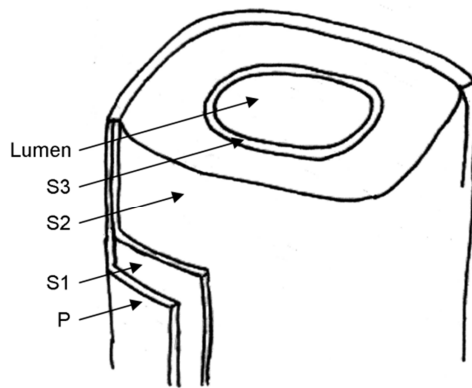


Figure 1.3: Cell wall layers of a softwood tracheid cut open. *P* = primary wall, *S1-S3* = secondary wall.

In all of the wall layers, the microfibrils have a helical structure as seen in figure 1.4; however, the inclination of the helix varies between wall layers. In the S1 and S3 layers, the helix has a very low inclination (Brändström et al. 2003), whereas microfibril inclination in the S2 layer typically is quite large (Barnett and Bonham 2004). The microfibrils in the primary wall are not as aligned and arranged as those in the secondary wall (Stevanic 2008). The inclination of microfibrils in each layer is often described by the microfibril angle (MFA). This is defined as the angle between the microfibrils and the longitudinal direction of the tracheid as seen in figure 1.4. Since the S2 layer is the dominant layer, it is common that the MFA of the S2 layer is denoted the MFA of the tracheid.

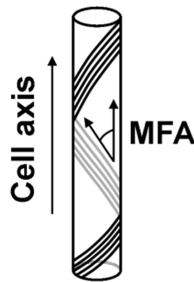


Figure 1.4: Schematic illustration of a wood cell showing the helical structure of microfibrils.

Besides cellulose microfibrils, the most important constituents of the cell wall are hemicelluloses and lignin. The former is a family of several wood polymers with the arabinoglucuronoxylan and galactoglucomannans being the most abundant hemicelluloses in softwood (Sjöström 1993). They are branched polymers with a lower degree of polymerization than cellulose and consist of various different saccharides, see figure 1.5.

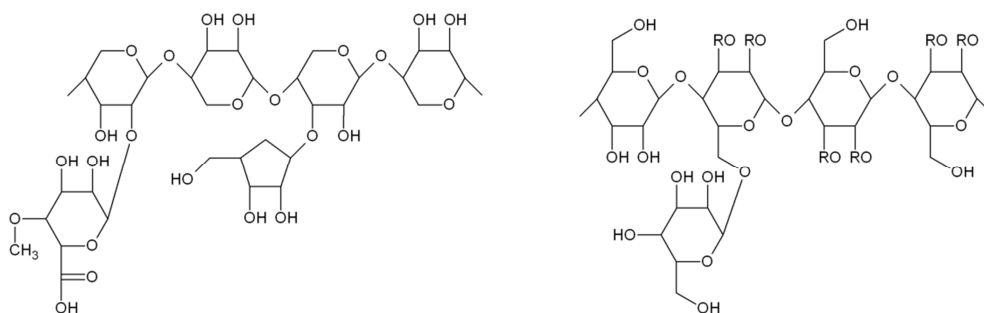


Figure 1.5: Chemical structures of the two most common softwood hemicelluloses: arabinoglucuronoxylan (left) and galactoglucomannan (right). $R = \text{CH}_3\text{CO}$ or H . Based on (Sjöström 1993).

Lignin is an aromatic branched polymer. Three types of building blocks, called mono-lignols, exist of which softwood is mainly made up by the mono-lignol coniferyl alcohol (Sjöström 1993), see figure 1.6. Due to differences in the mode of lignin polymerization, two different types of lignin are found in softwood; condensed and non-condensed (Joseleau and Ruel 2007; Ruel et al. 2006).

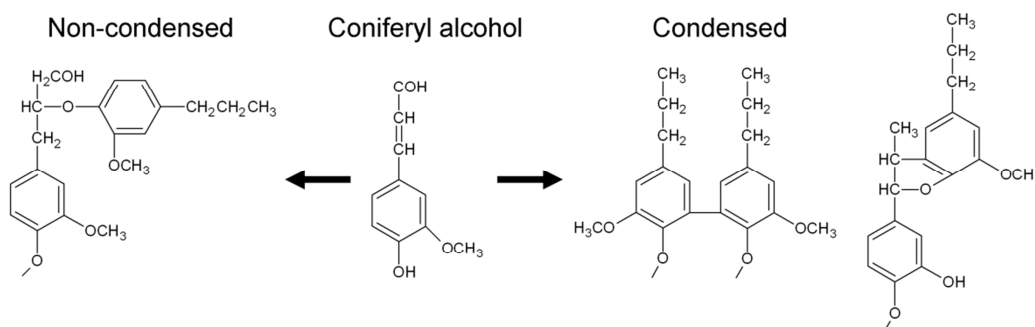


Figure 1.6: Typical covalent bonding in lignin. Based on (Christiernin 2006; Terashima and Seguchi 1988).

The arrangement of the different polymers is illustrated schematically in figure 1.7. Experimental studies using both electron microscopy and atomic force microscopy have revealed aggregations of microfibrils termed macrofibrils (Donaldson 2007; Fahlén and Salmén 2003; Fahlén and Salmén 2005). These have varying sizes dependent on the number of microfibrils present in a given macrofibril. Another study shows that the microfibrils follow a wavy pattern along their length (Bardage et al. 2004; Ding and Himmel 2006; Fahlén 2005). Salmén and Burgert (2009) therefore suggest that the microfibrils have various contact points with other microfibrils along their length. In a given cross-sectional plane of the cell wall, microfibrils in contact with each other in that particular plane give the impression of macrofibrils (Xu et al. 2007). In a neighbouring cross-section, however, the observed macrofibrils may consist of microfibrils that were found in different macrofibrils in the first cross-section.

Between microfibrils, the hemicelluloses and lignin are found. Glucomannan hemicellulose is the component closest to the cellulose microfibrils (Åkerholm and Salmén 2001; Åkerholm and Salmén 2004), whereas non-condensed lignin is farthest from the microfibrils. In between these two, the xylan and condensed lignin are found (Ruel et al. 2006) which are covalently bonded to each other (Salmén and Olsson 1998). Experimental studies indicate that glucomannan (Liang et al. 1960; Stevanic and Salmén 2009; Åkerholm 2003), xylan (Liang et al. 1960; Marchessault and Liang 1962; Stevanic and Salmén 2009), and lignins (Fromm et al. 2003; Åkerholm and Salmén 2003) are all oriented parallel to the microfibrils.

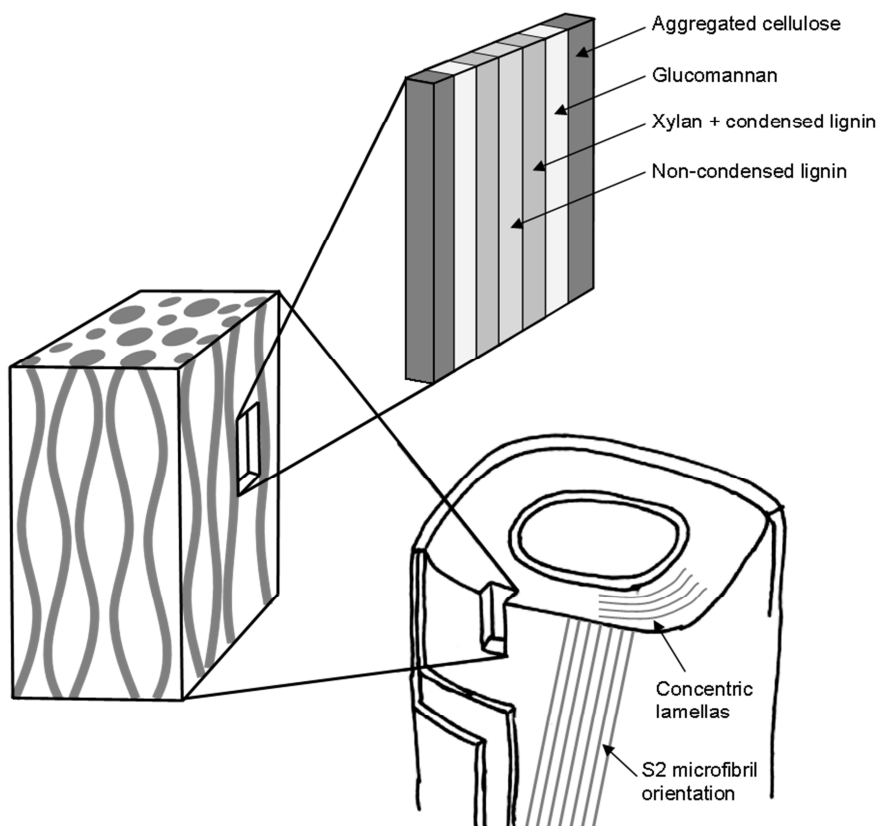


Figure 1.7: Structural arrangement of chemical constituents (upper right), wavy pattern along the microfibrils in the S2 layer (left), and concentric arrangement of lamellas in the cell wall (lower right). Based on (Salmén and Burgert 2009).

The cell wall appears to have a lamellar structure (De Micco et al. 2010; Fahlén and Salmén 2002; Fromm et al. 2003; Ruel et al. 1978) with concentric lamellar orientation as shown in figure 1.7. This is possibly a result of the deposition of the different layers during cell growth. The last component to be deposited in the cell wall is non-condensed lignin which is mostly found between

the lamellae (Ruel et al. 2006). The less cross-linked mode of polymerization of this lignin compared with condensed lignin is a result of spatial constraint from the already deposited structure (Jurasek 1995; Roussel and Lim 1995).

Softwood tissue

The softwood tracheids are held together in tissues by the middle lamella, see figure 1.8. This layer is almost entirely composed of condensed lignin (Christiernin 2006; Meshitsuka and Nakano 1985; Terashima and Fukushima 1988).

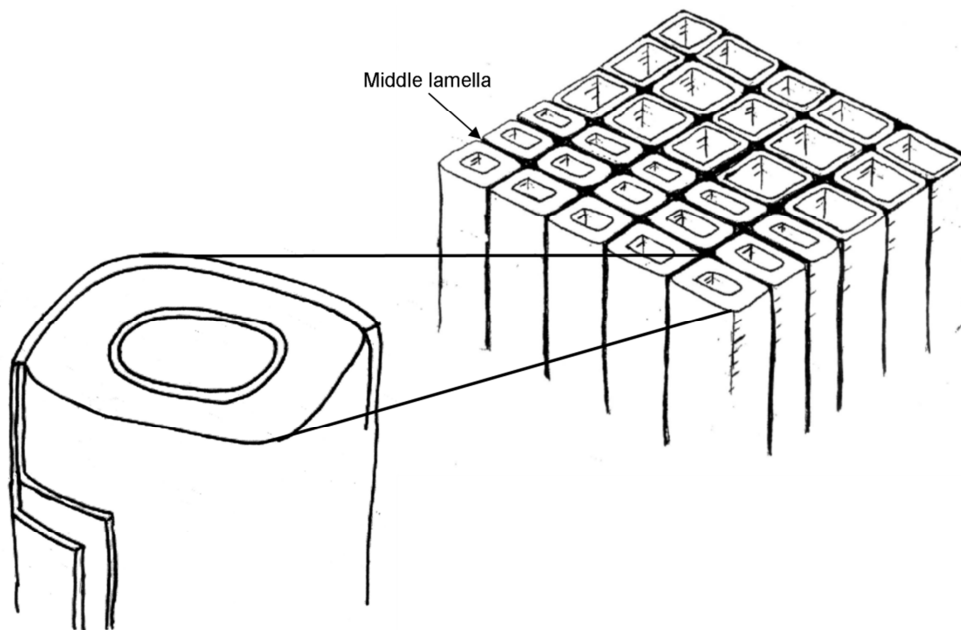


Figure 1.8: Tracheids in a softwood tissue held together by the middle lamella.

In geographical regions with seasonal changing climate, e.g. temperate regions, softwood tissue formed varies over the season. In spring when trees reassume growth after being dormant during winter, the tissue formed consists of tracheids with thin cell walls and wide lumens. This tissue is known as earlywood. As growth progresses the cells formed start having smaller and smaller lumens and thicker cell walls until the end of the growing season. The tissue formed in this part of the season is called latewood. For some wood species, the intermediate tissue between earlywood and latewood is referred to as transition wood. The change might, however, also occur abruptly rather than gradually. The difference in cell geometry between earlywood and latewood results in a higher density of the latter (Vintila 1939).

CHAPTER 2

Water in wood

Water has an undisputable effect on the properties of wood. The wood cells are formed in an aqueous environment inside the tree, and have a natural affinity for water. For wood engineering purposes, water is of great importance since it alters the mechanical behaviour of wood dramatically. Understanding sorption of water in the cells is therefore important in terms of predicting macroscopic wood performance. The general concept of water in wood used in the following is largely based on the work of Salmén and co-workers (Berthold et al. 1994; Berthold et al. 1996; Berthold et al. 1998; Olsson and Salmén 2004a).

Wood cell affinity to water

The wood cell wall is made from polymers which are all more or less hydrophilic. Therefore, wood can accommodate a substantial amount of water inside its cell walls. The most important chemical component in terms of attracting water molecules are hydroxyl groups found in all wood polymers. Other chemical groups such as carboxyl groups may also attract water (Berthold et al. 1994) but their amount in the cell wall is negligible. All chemical groups capable of attracting water molecules are termed sorption sites. Their affinity to water derives from their ability to form hydrogen bonds with water molecules (Jeffrey and Saenger 1991). The most sorption sites are found in hemicelluloses followed by cellulose and lignin (Christensen and Kelsey 1959). Since condensed lignin has fewer hydroxyl groups than non-condensed lignin, there should be more sorption sites available in the latter. There exists, however, no experimental proof of this. Conformational analysis indicates that the amorphous nature of hemicelluloses and lignin makes all their sorption sites more or less equally energetically favourable for water molecules (Pizzi et al. 1987a). For cellulose only the surfaces of microfibrils are accessible for water (Hofstetter et al. 2006; Matthews et al. 2006; Wickholm et al. 1998). Due to the rigid structure of cellulose microfibrils, the calculated sorption energy of their sorption sites shows greater variation than for the amorphous wood polymers (Pizzi et al. 1987b).

Traditionally, water in wood has been divided into several classifications. As Stamm (1950) shows the different classifications do not always agree. Following the classifications held by Salmén and co-workers, water in wood cells can be held as non-freezing bound water, freezing bound water, and free water. Non-freezing bound water is water specifically bound to sorption sites.

For hydroxyl groups, the amount of water molecules they can bind is one in average but no more than two per sorption site (Berthold et al. 1994; Pizzi et al. 1987b). Freezing bound water is more loosely bound than non-freezing bound water. It appears as clusters of water around strongly polar sorption sites such as carboxylic acid groups (Berthold et al. 1996). Thus, freezing bound water is only indirectly bound to the hydrophilic sites of wood polymers and it is only found when air humidity is high (Berthold et al. 1994). The negligible amount of strong polar groups in untreated wood means that no freezing bound water is found in untreated wood (Paper I). Another study suggests, however, that freezing bound water can be found at moisture content (MC), i.e. mass ratio of moisture to wood, down to at least 8 % MC (Handa et al. 1982) which roughly corresponds to an air humidity of 40 % at room temperature (Forest Products Laboratory 2010). Free water in wood is held in voids in the cell structure by capillary forces. Thus, the term free only signifies that water molecules are not bound to specific sorption sites. Stamm (1950) refers to this type of water in wood as capillary water.

Sorption isotherm

The amount of moisture in wood depends on the surrounding climate. The maximum amount of water which can be accommodated within wood cell walls is termed the fibre saturation point (FSP), although the exact definition varies among researchers (Paper III). For softwood the FSP is in the range of 40 % MC (Griffin 1977; Hernández and Bizoñ 1994; Hill et al. 2005; Stone and Scallan 1967). After harvesting and in the absence of direct contact with liquid water, the moisture content of wood is controlled by temperature and relative humidity (RH). This dependence can be described by sorption isotherms for given constant temperatures as seen in figure 2.1. Besides RH and temperature, the equilibrium moisture content (EMC) of wood depends on its moisture history. For instance, drying (desorption) from a saturated state in certain climatic conditions yields a higher EMC than moistening (adsorption) from a dry state to the same conditions. This will be described in the next subchapter.

The sorption isotherm of wood has a sigmoid shape. The physical background for this shape has over the decades been attributed to various phenomena and attempted predicted by different mathematical models. Sorption behaviour at low to intermediate relative humidity has been explained by water molecules gradually covering internal surfaces of the wood (Stamm and Hansen 1938). At high RH, the upward bend of the sorption isotherm has been attributed to capillary condensation (Babbitt 1942; Barkas 1937; Kollmann 1962; Sheppard 1933; Spalt 1958;

Stamm 1950), i.e. sorption of free water. However, capillary condensation has been speculated only to be possible above 90 % RH, whereas the upward bend occurs around 60-70 % RH (Stamm 1964). It appears now that capillary condensation does not play any significant role in the water vapour sorption of wood (Paper I, II).

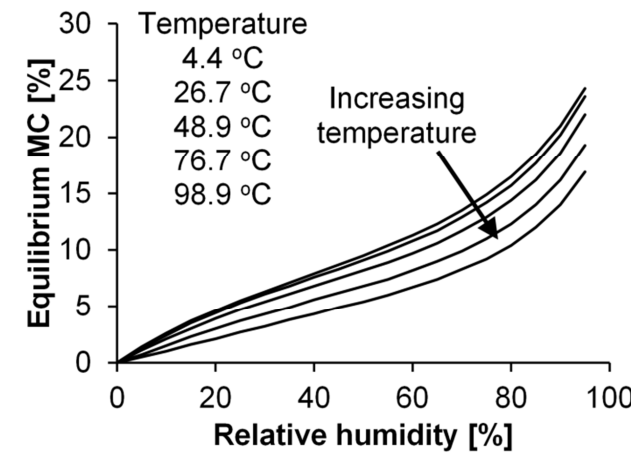


Figure 2.1: Softwood sorption isotherms in the range 0-95 % RH (Forest Products Laboratory 2010).

Assuming an idealized tracheid geometry, it is possible to calculate the amount of water held as free water in pits and lumens of softwood by the Kelvin equation (Paper II). This is illustrated in figure 2.2 from which it is seen that the theoretical calculations dismiss capillary condensation as being significant in sorption of water vapour by wood. Even at RH as high as 99.9 % the contribution of free water to the EMC is still below 0.5 %.

The role of capillary condensation has also been investigated experimentally (Paper I). Comparison of desorption isotherms at high RH for untreated and acetylated softwood are in agreement with conclusions found from theoretical calculations. The acetylation process replaces a certain amount of sorption sites with other functional groups which do not bind water. Thus, the EMC of acetylated wood is reduced by the fraction of sorption sites replaced. Due to the small size of the replacing functional groups, capillary condensation remains unaffected by the procedure (Paper I). Thus, if capillary condensation plays a significant role in sorption behaviour at high RH, the upward bend of the sorption isotherm would be similar for both untreated and acetylated samples. However, if the amount of water held in the wood at high RH is directly related to the amount of available sorption sites, the EMC of acetylated wood should be reduced by a constant fraction.

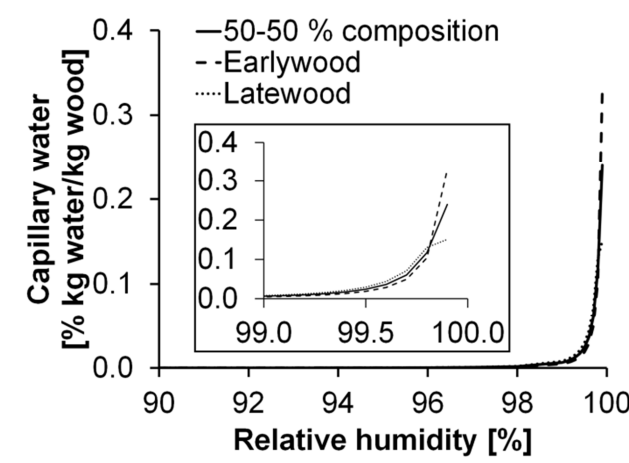


Figure 2.2: Calculated amount of capillary water in an idealized softwood structure. Data from (Paper II).

The desorption data in figure 2.3 clearly shows that the EMC of acetylated wood is reduced by a constant fraction. Therefore, since capillary condensation plays an insignificant role in sorption behaviour at high RH, sorption behaviour must be governed by mechanisms related to the binding of water to sorption sites in the cell wall.

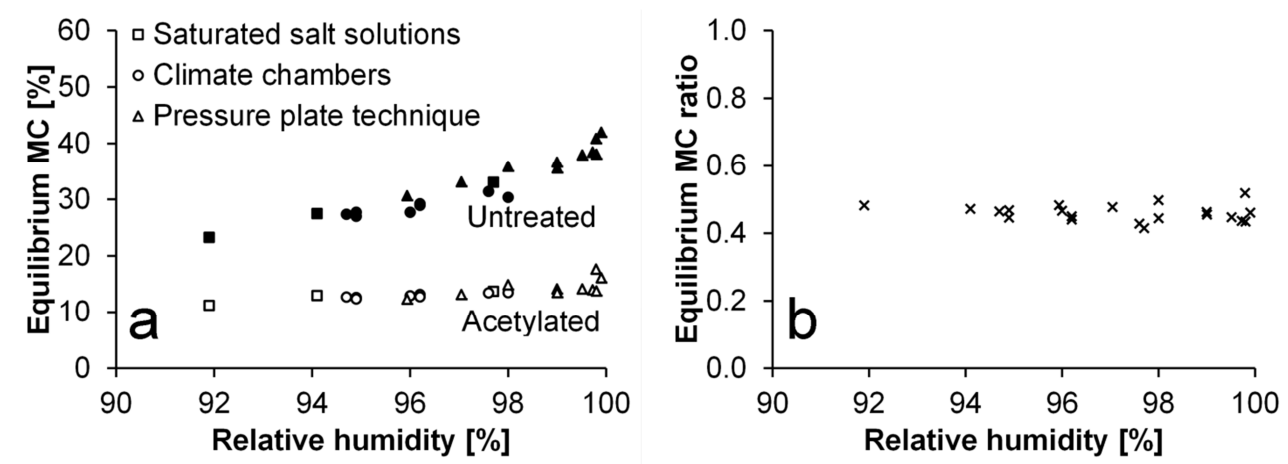


Figure 2.3: a) Desorption data for untreated and acetylated spruce samples. For each data point the method for establishing constant relative humidity is indicated. b) Ratio of moisture content of acetylated samples to that of untreated ones as function of relative humidity. Data from (Paper I).

The sorption isotherm of wood reflects to a large extent that of its constituents. Thus, the amount of water bound to either of the wood polymers is in a constant relation with the wood EMC as illustrated in figure 2.4. It is clear that hemicelluloses dominate the sorption behaviour due to their large amount of sorption sites. Lignins have the lowest sorptive capacity, whereas cellulose is intermediate between these two. The latter is not shown in figure 2.4 due to problems with isolating

cellulose without changing the degree of crystallinity, i.e. percentage of accessible sorption sites. However, transforming the sorption data to number of water molecules per accessible sorption site in cellulose reveals a sorption isotherm of similar shape as that for wood (Berthold et al. 1994).

The sorption isotherms of many polymeric materials have a sigmoid shape. For amorphous polymers it has been suggested that the upward bend is related to softening of polymers (Mauze and Stern 1984; Pierlot 1999; Vrentas and Vrentas 1991). Softening is the transition from a glassy to rubbery state of amorphous polymers. The glassy state is characterized by high viscosity and rigidity of the polymers, whereas polymers in rubbery state have a much lower viscosity and rigidity. When a hydrophilic polymeric material experiences a change in moisture content it is accompanied by shrinkage/swelling, i.e. a change in volume. The capacity to accommodate water molecules must therefore be related to the rigidity of the polymers.

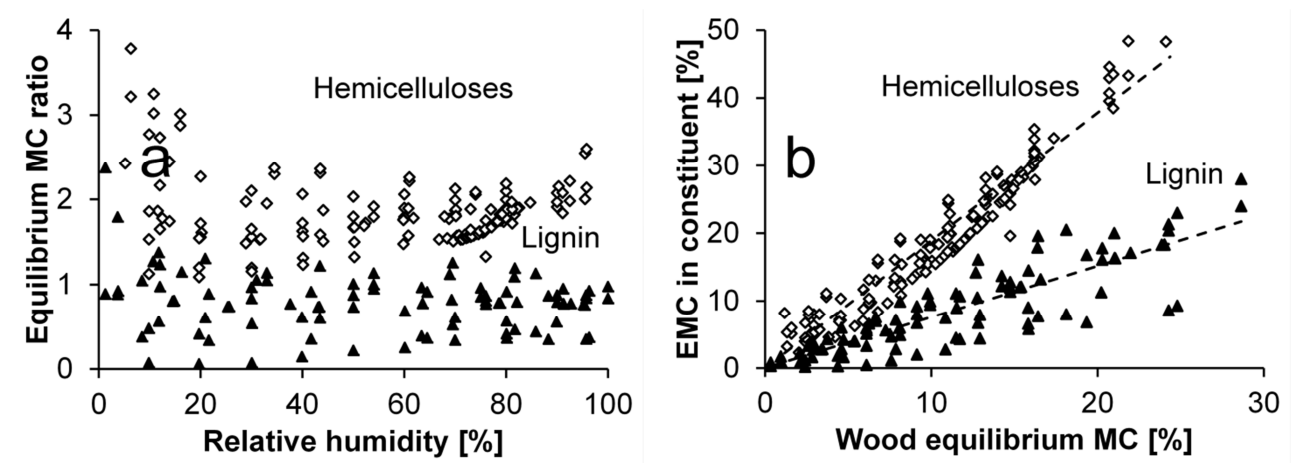


Figure 2.4: a) EMC ratio between hemicellulose (diamonds) or lignin (triangles) and wood as function of RH, and b) EMC of hemicellulose (diamonds) and lignin (triangles) as function of wood EMC. Experimental data for hemicelluloses (temperatures 16-80 °C) and lignin (20-25 °C) (Christensen and Kelsey 1958; Christensen and Kelsey 1959; Cousins 1976; Cousins 1978; Goring 1963; Olsson and Salmén 2004b; Reina et al. 2001; Sadoh 1960; Sadoh and Christensen 1964; Seborg et al. 1938). The wood EMC is calculated from the standard softwood isotherm at the different experimental temperatures (Forest Products Laboratory 2010).

Softening is accompanied by a marked decrease in rigidity of the polymers which also reflected is in an increasing diffusivity (Meares 1954), i.e. the ability of adsorbed molecules to move inside the polymers. At room temperature, softening of hemicelluloses occur around 75 % RH (Olsson and Salmén 2004b). It depends, however, on both temperature and EMC of the wood as illustrated in

figure 2.5. The figure clearly shows that the softening curve for hemicellulose crosses the isohumes, i.e. lines of constant RH, in the region 70-90 % RH at room temperature.

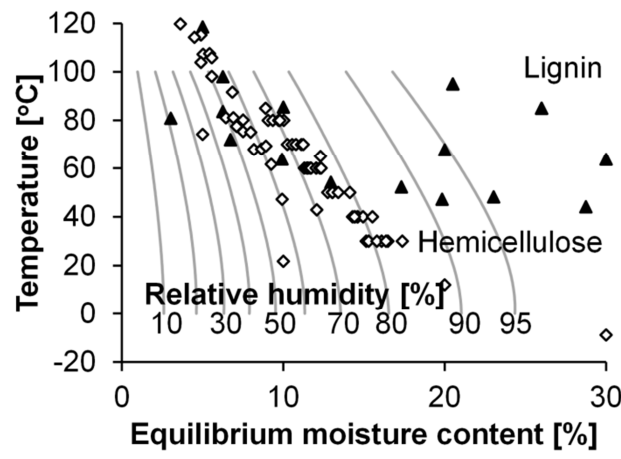


Figure 2.5: Softening of hemicelluloses (diamonds) and lignin (triangles) as function of wood EMC. Experimental data from (Becker and Noack 1968; Irvine 1984; Kelley et al. 1987; Olsson and Salmén 2004b; Stevens et al. 1983). Grey lines marks isohumes, i.e. lines of constant RH, derived from the standard softwood sorption isotherm (Forest Products Laboratory 2010).

That softening of amorphous polymers can have such an effect on the sorption isotherm is illustrated by several experimental investigations on various polymers (Berens 1975; Chiou et al. 1985; Kamiya et al. 1986; Wissinger and Paulaitis 1987). The results indicate that when polymers are in the glassy state, the inclination of the vapour sorption isotherm, i.e. the derivative $dEMC/dRH$, decreases with increasing RH. When polymers are in the rubbery state for all vapour pressures, the sorption isotherm is either linear or has an upward bend at high vapour pressures (Berens 1975), i.e. increasing inclination with increasing RH. However, when the sorption isotherm covers conditions both above and below the softening point, a sigmoid shaped isotherm appears (Chiou et al. 1985; Wissinger and Paulaitis 1987). In figure 2.6, sorption isotherms for hemicelluloses and lignin are shown. The hemicellulose isotherm is below the softening point at low RH and above at high RH, see figure 2.5, whereas the lignin isotherm is below the softening point for all RH. Whereas the hemicellulose sorption isotherm has a sigmoid shape, the lignin isotherm shows decreasing inclination with increasing RH. Furthermore, it seems that the onset of the upward bend of the hemicellulose isotherm is slightly lowered with increasing temperature. This could be related to the influence of moisture on softening as illustrated in figure 2.5 or to differences in chemical composition of the extracted hemicelluloses. Nonetheless, the curves

indicate that the upward bend of the wood sorption isotherm at room temperature are due to softening of hemicelluloses.

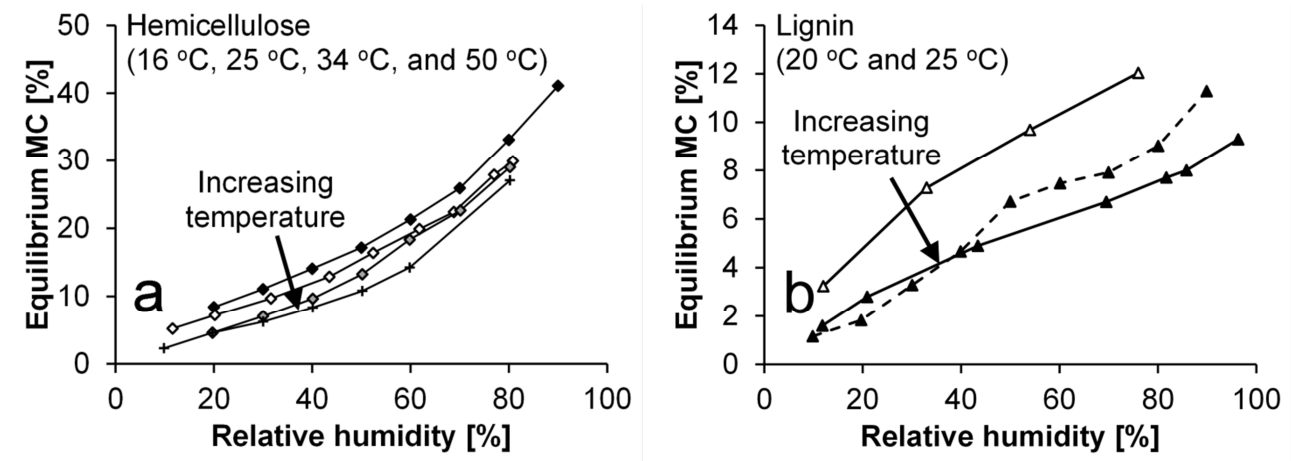


Figure 2.6: a) Sorption isotherms for hemicelluloses at 16 °C (Sadoh 1960), 25 °C (Sadoh and Christensen 1964), 34 °C (Olsson and Salmén 2004b), and 50 °C (Olsson and Salmén 2004b), and b) sorption isotherms for lignin at 20 °C (Cousins 1976) and at 25 °C (Christensen and Kelsey 1958; Reina et al. 2001).

The sorption isotherm of wood at low RH levels resembles that of glassy polymers below their softening point (Vrentas and Vrentas 1991). Water molecules entering the wood cell wall in a completely dry state will be adsorbed to the most favourable sorption sites. These are presumably the weakest intramolecular hydrogen bonds (Cocinero et al. 2009) or tiny voids on the molecular scale, i.e. free volume (Vrentas and Vrentas 1996) where water molecules do not have to create space for them to be accommodated. This could also explain the slightly lower degree of dimensional change for moisture changes in the low end of the sorption isotherm, i.e. up to about 5 % MC (Hartley and Avramidis 1996; Weichert 1963). The first water molecules entering the cell wall might even increase the structural order of the hydrogen bonding pattern. Such behaviour has been experimentally observed in monosaccharides and confirmed by molecular modelling of one water molecule interacting per sugar unit (Çarçabal et al. 2005). Since there are about three sorption sites per sugar unit in wood polymers, one water molecule per sugar unit corresponds to around 0.33 H₂O per sorption site. Figure 2.7 shows the average number of water molecules per accessible sorption site, i.e. not counting the unavailable hydroxyl group within microfibrils. It appears that 0.33 H₂O per sorption site corresponds roughly to 5-6 % MC.

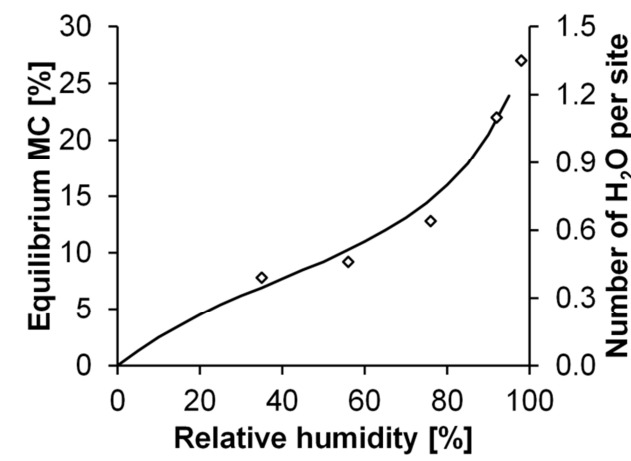


Figure 2.7: Sorption isotherm for wood at room temperature (Forest Products Laboratory 2010) and average number of water molecules per sorption site (Berthold et al. 1996).

Sorption hysteresis

As mentioned previously, the EMC of wood depends on the moisture history. This is typical for amorphous polymers in the glassy state (Fleming and Koros 1986) and is called sorption hysteresis. Sorption hysteresis can be illustrated by the isotherms for moisture uptake (adsorption) from dry condition and moisture release (desorption) from saturation condition. Of these isotherms, the desorption isotherm lies above the adsorption isotherm. Thus, a lower vapour pressure is needed to maintain a given moisture content during desorption than during adsorption (Vrentas and Vrentas 1996). Any other isotherm generated from a different moisture history than desorption from saturated condition or adsorption from dry condition, will either coincide or lie between these two isotherms.

For polymeric materials like wood, sorption is accompanied by shrinkage/swelling. The structure of amorphous polymers is collapsing during desorption, whereas adsorption will re-open and swell the structure. Above their softening point, amorphous polymers can freely adjust to accommodate the volume change produced by adsorption or desorption (Meares 1954) as illustrated in figure 2.8. In the glassy state, however, movement of polymers is restricted. Therefore, an amount of free volume is “frozen” as polymers enter the glassy state (Vrentas and Vrentas 1991). Thus, it is more or less locked in a local thermodynamic equilibrium state which not necessarily equals the global thermodynamic equilibrium state. The occurrence of free volume can be seen from the total volume of swollen glassy polymers, which is greater than the sum of volumes of glassy polymers and swelling agent (Fleming and Koros 1986). Furthermore, examination of the

experimental results by Fleming and Koros (1986) shows that the swelled volume for similar amounts of swelling agent is larger during desorption than adsorption (Vrentas and Vrentas 1996).

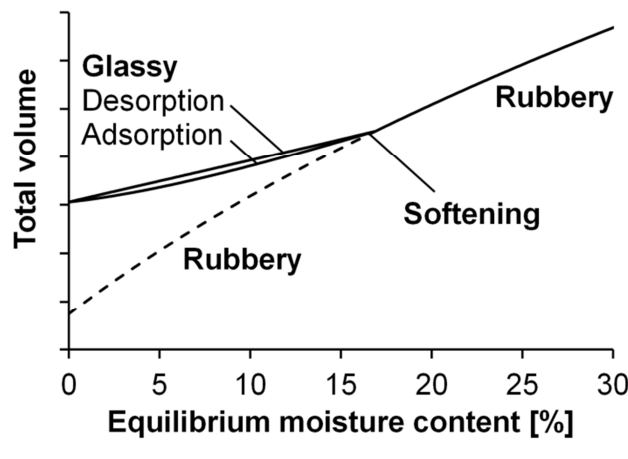


Figure 2.8: Schematic illustration of total volume as function of EMC for amorphous polymers below and above the softening point. Curves generated based on theoretic model by Vrentas and co-workers (Vrentas et al. 1988; Vrentas and Vrentas 1991; Vrentas and Vrentas 1996).

This is similar to findings for wood, where the volume for a given EMC is greatest during desorption. The difference in swollen volume is, however, small (Arevalo and Hernández 2001; Chauhan and Aggarwal 2004; Djolani 1972; Hartley and Avramidis 1996; Hernández 1993; Seifert 1972). As the structure collapses during desorption, the polymer structure cannot fully adjust, whereas during adsorption, a greater external pressure is required to re-open the structure. Therefore, at a given RH the EMC is greater during desorption than adsorption as illustrated in figure 2.9. If the polymers were in the rubbery state, however, equilibrium between RH and EMC would yield an even lower EMC than for equilibrium after adsorption in the glassy state (Vrentas and Vrentas 1991). Sorption hysteresis disappears for amorphous polymers when entering the rubbery state (Kamiya et al. 1986; Kamiya et al. 1992; Vrentas and Vrentas 1991), where the polymer chains once again are free to adjust to changes in external or internal condition. Hereby, thermodynamic equilibrium within the polymer is re-established.

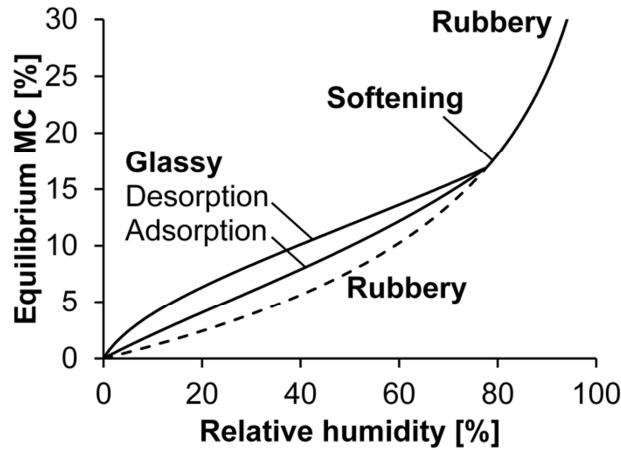


Figure 2.9: Schematic sorption isotherms for amorphous polymers above and below their softening point. Curves generated based on theoretical model by Vrentas and co-workers (Vrentas et al. 1988; Vrentas and Vrentas 1991; Vrentas and Vrentas 1996).

Extracted hemicelluloses and lignin from wood exhibit sorption hysteresis at room temperature as illustrated in figure 2.10. For hemicellulose, however, the hysteresis is diminished at high EMC when the polymer is in the rubbery state. The sorption hysteresis of lignin, on the other hand, is present from dry to saturated conditions. It therefore appears that differences in free volume in the glassy state of the wood polymers can explain sorption hysteresis of wood.

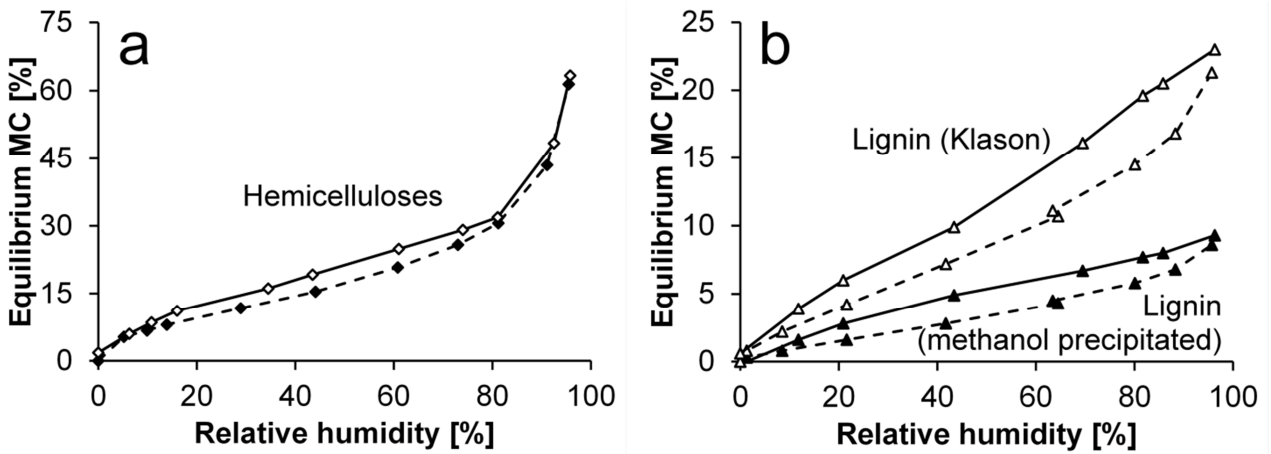


Figure 2.10: Adsorption and desorption isotherms at 25 °C for a) hemicellulose and b) lignin extracted by two different methods. Experimental data from (Christensen and Kelsey 1958).

For wood, however, sorption hysteresis remains even above the softening points of both hemicelluloses and lignin. This could be explained by the constraints from the rigid microfibrils on nearby amorphous wood polymers that raise their softening point as described by Struik (1987a;

1987b). A proportion of amorphous wood polymers might therefore never find their optimal configuration at any climate condition due to these constraints. In theory, this could imply that upon the first change in climatic conditions after felling a tree, the wood will never again be in the same thermodynamic state. The sorption and swelling behaviour of wood would therefore not be reversible. This supports the commonly accepted notion, but challenged in this thesis, that the first desorption after felling deviates from any subsequent desorption, no matter how much water is added to the cell wall before desorption commences.

First desorption and effect of drying procedure

For many decades it has been a commonly accepted notion that the first desorption after harvesting, i.e. from the green condition of wood, yields the highest EMC at a given RH. More specifically, it is commonly accepted that after drying, any subsequent desorption from saturated condition produces lower values of EMC above 60-70 % RH ‘indicating that there is an initial irreversible loss in hygroscopicity’ (quote by Skaar 1988), i.e. the ability to accommodate water within the cell wall. The scientific basis for the notion that the second desorption universally gives lower EMCs than the first is often ascribed to Spalt (1958), though similar observations had earlier been reported for cotton (Urquhart 1929; Urquhart and Eckersall 1930), beech wood (Barkas 1936), wood pulp (Seborg et al. 1938) and cellulose objects (Hermans 1949). Recent investigations (Paper III) show that the lower EMCs produced during the second desorption was due to incomplete saturation of the cell wall, i.e. the FSP was not reached before desorption commenced. This is clear from figure 2.11 where desorption from green condition, i.e. the first desorption, is compared with second desorptions. In figure 2.11a, the comparison is made with samples saturated over saturated water vapour; a method equivalent to that employed by Spalt (1958). This method yields lower EMCs, however, if the sample is water saturated by vacuum saturation in liquid water, the curves for first and second desorptions are much more similar as seen in figure 2.11b.

There are, however, deviations between first and subsequent desorptions although of smaller magnitude than previously reported. This is illustrated in figure 2.12 which depicts the ratio of EMC of green samples, i.e. for the first desorption, and EMC of dried and re-saturated samples, i.e. second desorptions. First of all, it seems that vacuum water saturation is able to press slightly more water into the cell wall than what appears naturally in green condition. Secondly, the drying method employed influences the magnitude of deviations between first and second desorptions.

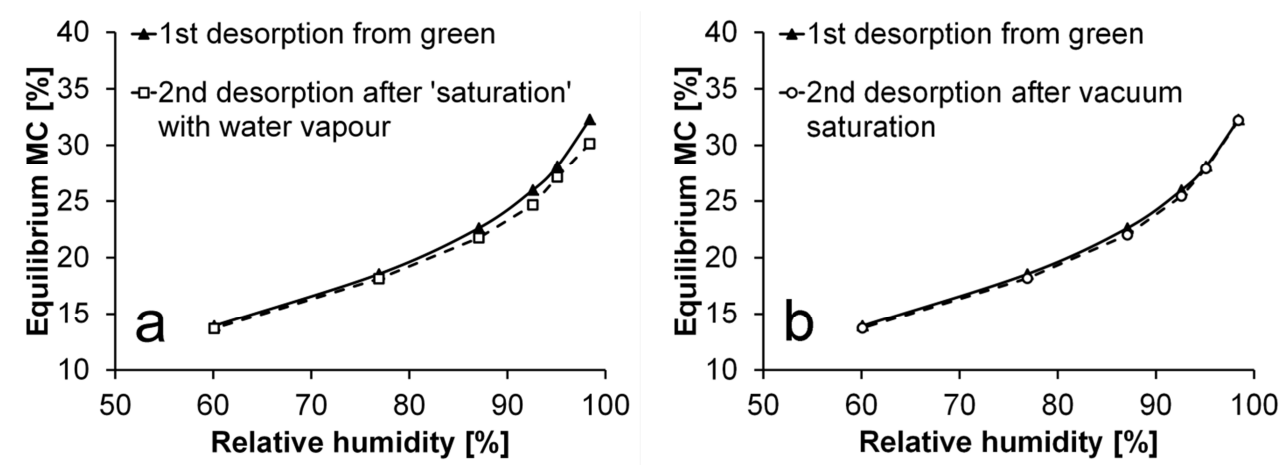


Figure 2.11: Desorption isotherm from green condition, i.e. initial desorption, compared with second desorptions from two different conditions: a) 'saturation' by prolonged exposure to saturated water vapour and b) vacuum saturation in liquid water. Data from (Paper III).

The most gentle of the investigated drying methods is vacuum drying over a desiccant. This method generally produces lower EMCs but the deviations disappear at full saturation. A greater deviation between first and second desorptions is seen for oven-dried samples. However, at very high RH the oven-dried wood is suddenly capable of accommodating more water in the cell wall than both the green and the green, vacuum saturated wood.

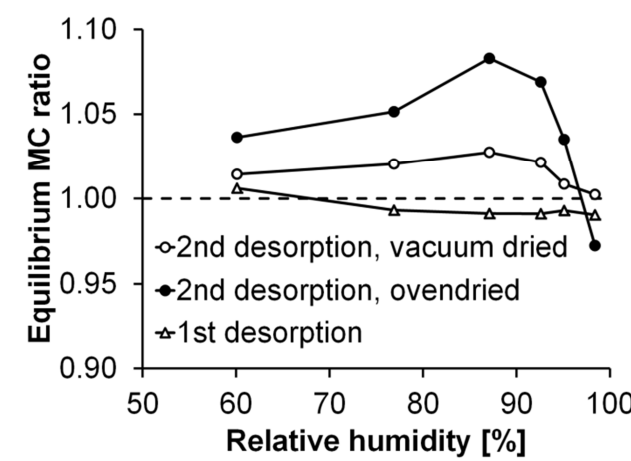


Figure 2.12: Ratios of EMC of green samples to that of differently dried and saturated samples as function of RH. All samples have been vacuum saturated before desorption. Data from (Paper III).

As described previously, the structure is gradually collapsing during desorption and hydrogen bonds between wood polymers are established during this process. It has been suggested that some of these might be energetically very favourable and therefore hard to break again (Urquhart 1929).

Thus, some fraction of the sorption sites accessible in green condition should become permanently inaccessible after the first desorption. This could explain why dried wood holds less moisture for a given RH below 95 % than during first desorption. The argument is, however, contradicted by the results at very high RH in figure 2.12 where dried wood is seen to hold as much, if not more, moisture at saturation than before the first desorption. This could be explained by capillary condensation in microvoids or microcracks caused by the drying procedure (Paper III). These might develop as a result of chemical degradation and removal of cell wall material (Stamm 1956) or because of drying stresses. The microvoids or microcracks would cause an increased hygroscopicity at high RH due to capillary condensation, but a decreased hygroscopicity at lower RH due to loss of sorption sites in the cell wall (Hoffmeyer et al. 2003). Nevertheless, experimental investigations of neverdried and overdried wood show no capillary water present in either type of wood (Paper III). The higher EMC of overdried wood at very high RH must therefore constitute a greater amount of bound water in the cell wall. The conclusion is that the mechanism causing such behaviour of overdried wood remains unexplained.

CHAPTER 3

Mechanical behaviour

In order to understand and describe the mechanical behaviour of wood, interactions at several different levels need to be considered. For instance, the organisation of polymers at the molecular level and amount of moisture adsorbed affects the stiffness of microfibrils and surrounding matrix material. On a higher level, however, the behaviour is also affected by the orientation of microfibrils in the cell wall. Furthermore, on an even higher level the organisation of cells in the wood tissue will also impact mechanical behaviour. A mathematical description has to incorporate effects on all these levels. Figure 3.1 illustrates the direction followed in this chapter, starting with effects on the molecular level and ending at the description of softwood tissue.

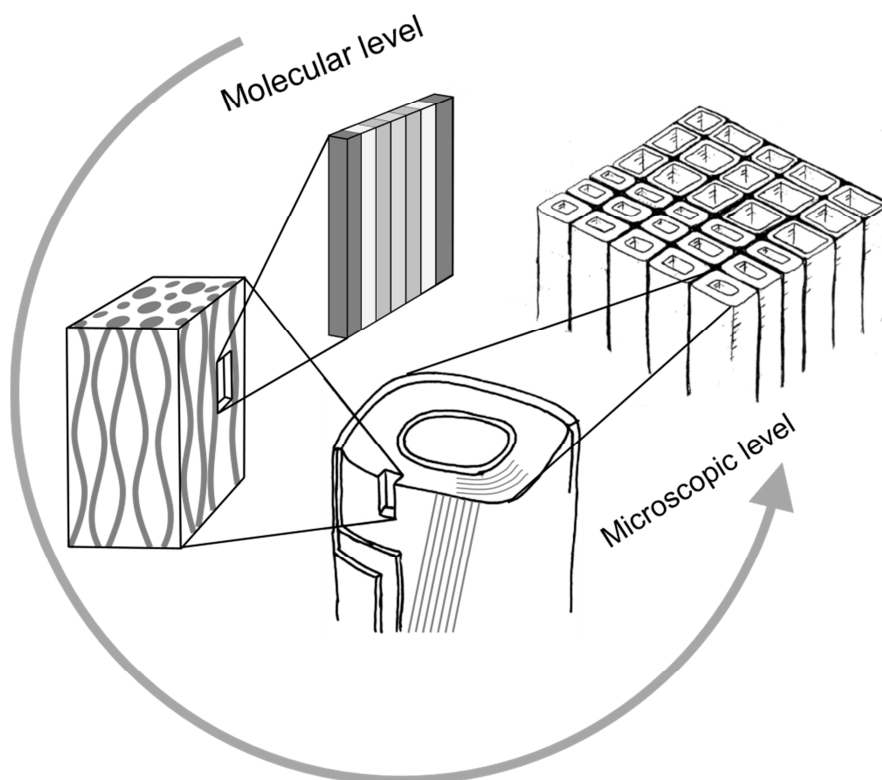


Figure 3.1: Organization of softwood from molecular level to microscopic level and direction of this chapter.

The first two subchapters briefly review current knowledge on mechanical behaviour of wood polymers and the effects of moisture. The third subchapter incorporates this knowledge into a mathematical description of the behaviour of the composite cell wall material. The following fourth and fifth subchapters show how the orientation of composite material affects the mechanical

behaviour of modelled softwood tracheids. This is done by using numerical modelling to describe and predict the mechanical behaviour. Finally, the sixth subchapter focuses on the mechanical behaviour of softwood.

Effects of water on the elastic properties of the cell wall

The response of wood polymers to a mechanical excitation depends on the chemical bonds within and between them. The response differs, however, between the cellulose microfibrils and the amorphous wood polymers surrounding these. In the direction of the microfibrils, applied loads are carried both by covalent and hydrogen bonds of the aggregated cellulose. This is evident from infrared and Raman spectroscopic investigations which show elongation of both covalent and hydrogen bonds upon stretching (Eichhorn et al. 2001; Hinterstoisser et al. 2003). On the other hand, the covalent bonds of lignin do not seem to respond (Eichhorn et al. 2001; Gierlinger et al. 2006) or only vaguely respond to extension of the wood cell (Åkerholm and Salmén 2003). This is confirmed by molecular modelling showing that loading “amorphous cellulose” in tension does not affect covalent bonds at low extensions, but only lengthens hydrogen bonds (Chen et al. 2004b). Other modelling studies show that it is the secondary chemical bonds such as hydrogen bonds and van der Waals interactions that dominates the strain energy, i.e. are responsible for most of the deformation, upon loading amorphous polymers (Fan 1995; Hossain et al. 2010; Jang and Jo 1999a; Jang and Jo 1999b). Deformation in terms of stretching and bending of hydrogen bonds as a response to mechanical excitation of the cell wall has been extensively documented by spectroscopic techniques (Gierlinger et al. 2006; Hinterstoisser et al. 2003; Stevanic and Salmén 2006). It is therefore expected that the only chemical bonds affected by mechanical excitation of hemicelluloses and lignin are hydrogen bonds. Thus, the mechanical properties of hemicelluloses and lignin are assumed entirely dominated by hydrogen bonding, whereas those for cellulose also are heavily influenced by its covalent bonds.

The substantial influence of moisture on the mechanical performance of the wood cell wall is derived from the significant role of hydrogen bonding. The predominant sorption site is the hydroxyl group and this is also the one responsible for hydrogen bonding between wood polymers in the absence of an attached water molecule. When water molecules enter the cell wall, hydrogen bonds between wood polymers are broken and replaced by bonds to water molecules. Furthermore, the spacing between wood polymers is increased to accommodate moisture. Both of these effects are depicted in figure 3.2.

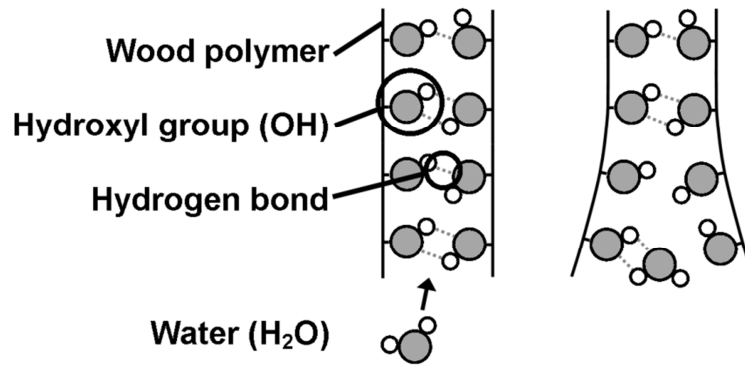


Figure 3.2: Schematic illustration of the effect of a water molecule on amount of hydrogen bonds between wood polymers and their spacing.

Since water molecules cannot enter the aggregated cellulose, swelling occurs only in the hemicellulose and lignin fractions, hereby causing an increased spacing between microfibrils (Donaldson 2008). The swelling will also result in increased cell wall dimensions. As the dimensions of cell lumens are more or less constant, macroscopic swelling of wood is directly proportional to that of its cell walls (Murata and Masuda 2006). On the macroscopic scale, however, swelling in the tangential direction is greater than in the radial direction. This is presumably due to an interaction effect between earlywood and latewood, since on the cell wall level swelling in both directions is similar (Murata and Masuda 2006).

The swelling of wood is linear with equilibrium moisture content (EMC) in the range 5-20 % moisture content (MC) (Hartley and Avramidis 1996; Stamm 1959), and the inclination of this linearity is termed the swelling coefficient, β_{sw} . For softwood, β_{sw} has typically a value of 0.36-0.45 and 0.17-0.23 for the tangential and radial directions, respectively (Hartley and Avramidis 1996; Murata and Masuda 2006; Seifert 1972). The coefficient for swelling of the cell wall is similar to that for macroscopic tangential swelling (Murata and Masuda 2006). In the longitudinal direction of wood, β_{sw} is small for normal mature wood since water molecules only increase the distance between wood polymers, and a majority of these are aligned more or less in the longitudinal direction of wood. Thus, Hunt and Shelton (1988) found longitudinal β_{sw} in the range 0.004-0.011 for Scots pine.

The breaking of hydrogen bonds by water molecules has a marked influence on the elastic properties of wood polymers. This effect can be explained by the theory of hydrogen bond dominated solid materials (Caulfield 1990; Nissan 1957a; Nissan 1957b; Nissan 1976a; Nissan 1976b; Nissan and Batten 1990).

Nissan (1957b) found that for solid materials dominated by hydrogen bonds, the effective number of hydrogen bonds is related to the modulus of elasticity by

$$E = k_{\text{HB}}N^{1/3} \quad (1)$$

where E is modulus of elasticity [Pa], k_{HB} is the average force constant of hydrogen bonds [N/m] and N is the number of effective hydrogen bonds per unit volume [m^{-3}]. When the amount of moisture increases, the number of effective hydrogen bonds is reduced resulting in a decreasing modulus. A lengthening of the intact hydrogen bonds, i.e. unbroken by water molecules, might also be expected due to swelling. Nonetheless, the average force constant of the intact hydrogen bonds is assumed to be constant with respect to moisture (Nissan 1977a; Nissan et al. 1985). Even though this assumption may be questioned, the variation in force constant with distance is small for hydrogen bonds of distances typical for wood (Novak 1974). It is therefore assumed that the force constant is only a function of temperature, whereas the number of hydrogen bonds is only a function of moisture. The term “number of effective hydrogen bonds” relates to the distribution in orientation of hydrogen bonds in the solid material. Typically, this number equals one third of the total amount of hydrogen bonds in the solid (Nissan 1976b). Mechanical excitation of a solid with a random distribution of hydrogen bond orientations is mathematically equivalent to distributing one third of the bonds parallel to each main direction (Nissan and Batten 1990). The amount of intact hydrogen bonds relative to the amount in dry condition, N/N_0 , can be related to the relative amount of moisture. This quantity is described by the relative moisture coverage, MC/Φ . In this subchapter, amount of moisture is described by moisture content (MC) rather than EMC, since global moisture equilibrium is not required for the validity of the relations (Berger 1988; Berger and Habeger 1989). The relative moisture coverage is the ratio of moisture content in a wood polymer to the hypothetical moisture content required to attach one water molecule to each polymer sorption site, Φ [%]. It is found from

$$\Phi = \frac{n_{\text{sorption site}}M_{\text{water}}}{M_{\text{polymer unit}}} \quad (2)$$

where $n_{\text{sorption site}}$ is the number of sorption sites available at each polymer unit [-], M_{water} is the molar mass of water [g/mol], and $M_{\text{polymer unit}}$ is the molar mass of the given polymer unit [g/mol]. For hemicelluloses, no theoretical value of Φ has been derived. In terms of basic chemical structure and number of sorption sites, however, hemicelluloses are roughly similar to cellulose. Batten and

Nissan (1987) have calculated Φ for cellulose based on a molar mass of 324 g/mol for a cellobiose unit which contain six hydroxyl groups. With a molar mass of water of 18 g/mol this yields a value for Φ of 33.3 %. For lignin, the value of Φ of 12.3 % has been derived by Nissan (1977b).

When a hydrogen bonded solid material in dry condition absorbs moisture, water molecules are assumed to interact with one hydrogen bond each (Nissan 1976b). If the total number of effective hydrogen bonds in dry condition is N_0 and the number of bonds between wood polymers is N , the number of bonds broken by water molecules is $N_0 - N$. Nissan (1976b) assumes that the free energy of interaction of a water molecule is similar both for interacting with bonds between wood polymers and with bonds between wood polymers and bound water. All vacant sorption sites are hereby viewed as equally energetically favourable to an entering water molecule which agrees well with the theory described in Chapter 2. Whether a sorption site with one water molecule attached is as energetically favourable as a vacant sorption site may be questioned. However, sorption sites, which predominantly are hydroxyl groups, and water molecules are quite similar chemically. Therefore, the energy difference between vacant sites and those with one water molecule is presumably not large enough to invalidate the assumption of equal attractiveness stated in the Nissan theory. Because of the equal attractiveness of all N_0 effective bonds in the material, an entering water molecule may interact with all of these bonds, whether broken by another water molecule or not. Hereby, an increase in amount of water molecules does not equal a similar decrease in amount of wood polymer bonds. The relation between relative amount of hydrogen bonds between wood polymers and relative moisture coverage can instead be described by

$$\frac{d\left(\frac{N}{N_0}\right)}{d\left(\frac{MC}{\Phi}\right)} = -\frac{N}{N_0} \quad (3)$$

which is a linear first order differential equation with the following solution

$$\ln\left(\frac{N}{N_0}\right) = -\frac{MC}{\Phi} \quad (4)$$

for MC [%] between zero and a critical moisture content, MC_c [%]. The boundary condition is that the ratio N/N_0 is unity at zero relative moisture coverage. Above MC_c the water molecules tend to break more than one bond between wood polymers each (Nissan 1976b). For wood polymers, this transition from the low moisture regime to the high moisture regime occurs at a wood moisture

content of about 5 % (Nissan 1957b). This amount of moisture corresponds with approximately one water molecule per sugar unit as illustrated in figure 2.7 in Chapter 2. Below 5 % MC, entering water molecules result in less swelling and perhaps even an ordering of the hydrogen bonding pattern as discussed in Chapter 2. Above 5 % MC a larger degree of swelling is observed, which indicate that a greater number of hydrogen bonds are broken per entering water molecule, C. This is accounted for as

$$\frac{d\left(\frac{N}{N_0}\right)}{d\left(\frac{MC}{\Phi}\right)} = -C \frac{N}{N_0} \quad (5)$$

which results in the following relation

$$\ln\left(\frac{N}{N_0}\right) = -\frac{MC_c}{\Phi} - C\left(\frac{MC - MC_c}{\Phi}\right) \quad (6)$$

for MC greater than MC_c . The boundary condition is N/N_0 being equal at MC_c for both (3) and (5). The number of bonds broken per water molecule in the high moisture regime, i.e. parameter C, is independent of amount of water already present in the cell wall (Nissan 1977a). This is in line with experimental investigations of the sorption of plasticizing gases in polymers (Kamiya et al. 1992). The effect of moisture on modulus of elasticity can be expressed by the ratio E/E_0 where E_0 is modulus of elasticity at zero moisture content. The ratio is related to N/N_0 by the simple relation

$$\frac{E}{E_0} = \frac{k_{HB}}{k_{HB}} \left(\frac{N}{N_0}\right)^{1/3} = \left(\frac{N}{N_0}\right)^{1/3} \quad (7)$$

The relation is based on the general assumption that moisture only affects the number of hydrogen bonds and not their average force constant. The number of bonds between wood polymers as function of relative moisture coverage is illustrated in figure 3.3 along with E/E_0 . The dependence of modulus of elasticity on moisture content can be conveniently expressed as

$$\frac{d\ln\left(\frac{E}{E_0}\right)}{dMC} = -K_{MC} \quad (8)$$

Where

$$K_{MC} = \frac{1}{3\Phi} \text{ [%]} \text{ for } MC \leq MC_c$$

$$K_{MC} = \frac{c}{3\Phi} \text{ [%]} \text{ for } MC > MC_c$$

Based on literature values of Φ , the value of K_{MC} for hemicellulose and lignin in the low moisture regime is $1.0 \cdot 10^{-2} \text{ \%}$ and $2.7 \cdot 10^{-2} \text{ \%}$, respectively. In the high moisture regime, the values are $6.7 \cdot 10^{-2} \text{ \%}$ and $7.2 \cdot 10^{-2} \text{ \%}$, respectively (Caulfield 1990; Nissan 1977b). The value of K_{MC} for cellulose is zero since water does not affect the mechanical properties of cellulose. It is worth noting that the modulus of elasticity has been found to be directly correlated with moisture content independently of moisture history (Berger et al. 1989; Higgins 1958; Ishimaru et al. 2001). This indicates that although sorption hysteresis may lead to various equilibria between moisture content and ambient climate, as described in Chapter 2, the number of effective hydrogen bonds within the material is always directly correlated with amount of water molecules present.

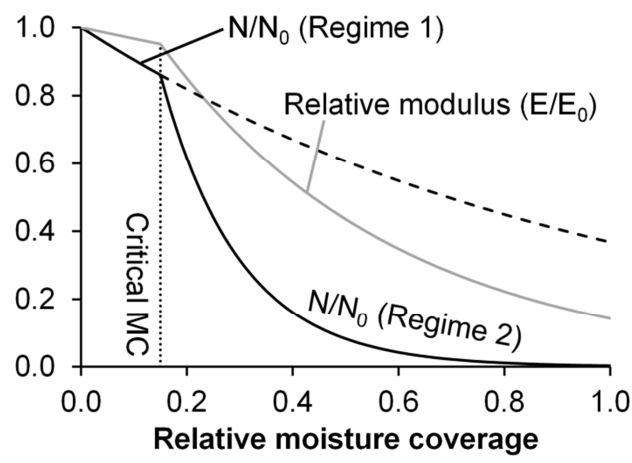


Figure 3.3: Schematic illustration of the relative number of effective hydrogen bonds and relative modulus as function of relative moisture coverage.

Another climatic factor influencing the modulus of elasticity is temperature. Increasing the temperature will extend and hereby weaken hydrogen bonds (Imamura et al. 2006; Lutz and van der Maas 1994). The number of hydrogen bonds will, however, remain constant. This can be described by a decreasing force constant of hydrogen bonds in (1).

Batten and Nissan (1987) derived the following relation from the Lippincott-Schroeder potential function for hydrogen bonds (Lippincott and Schroeder 1955).

$$\frac{d \ln E}{dT} = -K_T \quad (9)$$

The value of K_T [K^{-1}] for solids dominated by hydrogen bonding varies between literature sources but is reportedly within the range $1.8\text{--}6.3 \cdot 10^{-3} K^{-1}$ (Caulfield 1990). Based on theoretical considerations, Nissan and co-workers suggest a value of K_T of $2.4 \cdot 10^{-3} K^{-1}$ (Batten and Nissan 1987; Caulfield 1990; Nissan and Batten 1990; Nissan and Batten 1997). The influence of moisture and temperature on modulus of elasticity given by (8) and (9) can be assembled to yield the following relation for the combined effect of both climatic factors

$$E(MC, T) = E_{ref} \cdot \exp[-K_{MC}(MC - MC_{ref}) - K_T(T - T_{ref})] \quad (10)$$

where E is elastic modulus [GPa], MC is moisture content in the constituent [%], T is temperature [K], and the index refers to the reference condition. The assumption behind (10) is still that moisture only affects the number of hydrogen bonds, whereas temperature only affects the average force constant of the bond, i.e. no interaction effect is included. The shear modulus of a hydrogen bonded solid material depends on the number of unbroken hydrogen bonds in the same way as the elastic modulus. Therefore, the shear modulus can be described by (10) with the elastic modulus, E replaced by the shear modulus, G , but with similar parameter values, K_{MC} and K_T (Nissan 1977b). The Poisson's ratios remain unaffected by moisture (Baum et al. 1981) and is assumed to be unaffected by temperature as well.

Effects of water on the time-dependent properties of the cell wall

The wood cell wall does not only respond elastically to a mechanical excitation. Often, there is a significant non-elastic response dependent on the duration of the mechanical excitation. The mechanism behind this time-dependent mechanical behaviour has been ascribed to sliding between microfibrils (Balashov et al. 1957; Lotfy et al. 1972; Olsson and Salmén 2001). Hereby, hydrogen bonds between adjacent wood polymers are broken and re-formed in new configurations (Bonfield et al. 1996; van der Put 1989) as the polymers gradually slide past each other. If water molecules interfere with the hydrogen bonding between polymers, the sliding is further facilitated. This is documented by molecular modelling (Chen et al. 2004a). The result is greater rate of time-

dependent mechanical processes seen in experimental studies on various polymeric fibres (Holland et al. 1946; Steinberger 1936).

The process of sliding of polymers can be described by deformation kinetics (Eyring et al. 1958; Tobolsky and Eyring 1943) which is derived from the theory of absolute reaction rates developed by Eyring and co-workers (Eyring 1935; Eyring 1938; Kauzmann and Eyring 1940; Wynne-Jones and Eyring 1935) and extended to the deformation of solid materials (Krausz and Eyring 1971; Krausz and Eyring 1975). In deformation kinetic theory, the sliding of polymers is viewed as an activated process where a length section of a polymer has to attain a certain energy level in order to move across an energy barrier and form a new configuration of hydrogen bonds, see figure 3.4. The energy state related to the top of the barrier is termed the activated state (Eyring 1936). In a state of stress free rest, the potential energy of each mobile unit oscillates due to thermally induced molecular motions (Kauzmann and Eyring 1940). A certain percentage of mobile units will hereby have a potential energy equal to the activation energy, i.e. be in the activated state and free to move.

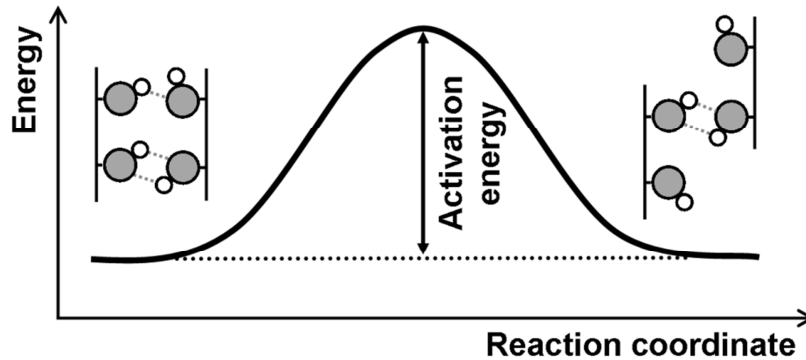


Figure 3.4: Energy barrier for shearing of polymers with hydrogen bonds between hydroxyl groups.

The specific rate of reaction, i.e. number of jumps per second, is described by

$$v = \theta \frac{kT}{h} \exp\left(\frac{-\Delta G^\ddagger}{kT}\right) \quad (11)$$

where v is the specific rate [s^{-1}], θ is the transmission coefficient [-], k is Boltzmann's constant [J/K], h is Planck's constant [J s], T is absolute temperature [K], and ΔG^\ddagger is termed the activation free energy. The transmission coefficient represents the probability that upon mounting the energy barrier, the activated segment moves across the barrier, i.e. do not return to the original state (Wynne-Jones and Eyring 1935). Typically, this coefficient is unity or close to unity (Eyring 1962;

Krausz and Eyring 1975). The ratio kT/h is the rate of decomposition, i.e. from falling from the activated state into the lower energy state on the other side of the barrier. It is a universal frequency which is derived from statistical mechanics. The exponential term is related to the fractional amount of activated segments at a given temperature and is derived from thermodynamics.

For chemical and physical reactions in general, the lowest energy barriers of a given reaction are favoured. Thus, movement of an activated segment in a given direction will occur via the intermediate state with lowest free energy. Although the process is described as breaking and reforming of hydrogen bonds, a more continuous process is likely. For instance, Jeffrey and Saenger (1991) believe that three-centre bonds play an important role in the shifting of hydrogen bonds during water movement. The same is possibly true for the shearing of wood polymers past each other. This is illustrated in figure 3.5 where the energy barrier depends on whether the intermediate state is a “no bond” state or a “three-centre bond” state.

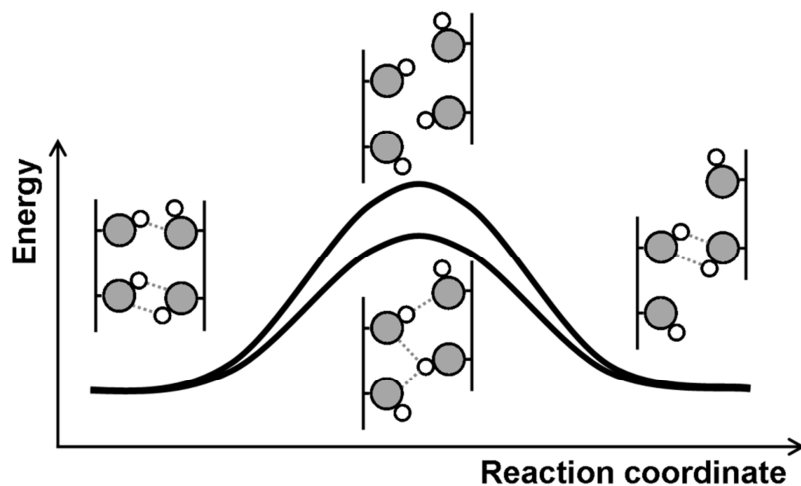


Figure 3.5: Energy barrier for two intermediate states in breaking and forming of a hydrogen bond: a no-bond intermediate (upper) and a three-centre hydrogen bond intermediate (lower).

Since the energy barrier for sliding of wood polymers is symmetric the probability of mobile units moving both forwards and backwards is equal. Therefore, the overall movement is zero if no force is applied. If a force is applied, however, the energy needed to cross the energy barrier is shifted as seen in figure 3.6.

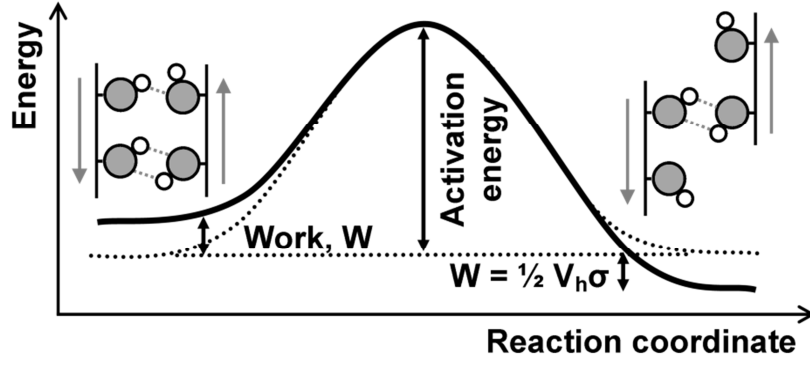


Figure 3.6: Energy barrier shifted due to shearing forces.

Hereby, movement along the direction of force is favoured over that in the opposite direction. The rate of resulting deformation can be found by incorporating the mechanical work and contribution of each movement of a segment to the deformation. The mechanical work raises the ground state energy level on one side of the barrier and lowers the level on the opposite side as seen in figure 3.6. The total mechanical work done on the system is therefore the sum of work done on each side of the barrier. The resulting rate of deformation is (Halsey et al. 1945; Tobolsky and Eyring 1943)

$$\frac{d\varepsilon_v}{dt} = \frac{V_h}{V_m} \frac{kT}{h} \exp\left(-\frac{\Delta G^\ddagger}{kT}\right) \left[\exp\left(\frac{W}{kT}\right) - \exp\left(-\frac{W}{kT}\right)\right] = \frac{V_h}{V_m} \frac{kT}{h} \exp\left(-\frac{\Delta G^\ddagger}{kT}\right) 2\sinh\left(\frac{V_h\sigma}{2kT}\right) \quad (12)$$

where ε_v is shear strain [-], t is time [s], W is half the total mechanical work [J], and σ is shear stress [Pa]. The parameters V_h and V_m [m^3] are volume swept by the motion and volume of the moving segment itself, respectively. The V_h/V_m ratio is a measure of the relative length of each movement. (12) can also be written

$$\frac{d\varepsilon_v}{dt} = A(MC, T) \cdot 2\sinh[B(T) \cdot \sigma] \quad (13)$$

where

$$A(MC, T) = \frac{V_h}{V_m} \frac{kT}{h} \exp\left(-\frac{\Delta G^\ddagger}{kT}\right) \quad \text{and} \quad B = \frac{V_h}{2kT}$$

The volume of the moving segment in cellulosic materials can be estimated to be 0.68 nm^3 based on the molecular dimensions of a cellulose residue (Halsey et al. 1945; Kingston and Clarke 1961). This is close to the volume of the cellulose unit cell experimentally determined to around 0.65 nm^3 at room temperature (Hidaka et al. 2010; Hori and Wada 2005). The volume is, however, often found by fitting the model to experimental data yielding values between 0.27 nm^3 and 0.94 nm^3 for

cellulose acetate (Reichardt et al. 1946; Reichardt and Eyring 1946), cotton (Holland et al. 1946), and viscose rayon (Eyring and Halsey 1946; Holland et al. 1946). For lignin, the value of V_m is more uncertain since the theory of deformation kinetics has not been applied to this compound before.

The volume swept by the motion of the moving segment, V_h is often found from the ratio V_h/V_m . For cellulosic material this ratio has been calculated to 0.47 (Halsey et al. 1945), but a value of 0.5 is often assumed (Reichardt et al. 1946). A ratio of 0.5 for hemicelluloses corresponds to moving a hydroxyl group from one bonding site to the neighbouring site as depicted in figure 3.5. The ratio for lignin is, as with the volume V_m , uncertain due to the complex structure and bonding pattern of the lignin molecule and lack of data. For many polymeric materials, however, a ratio between 0.5-1.0 is typical (Krausz and Eyring 1975; Ree et al. 1951).

Modelling the elastic and time-dependent behaviour of the cell wall

The elastic moduli and Poisson's ratio of the composite cell wall in the material directions can be calculated by assuming a layered composite of the three main wood polymers, see figure 3.7. This is in good agreement with the actual distribution and structure of the cell wall illustrated in figure 1.7 in Chapter 1. The properties in the longitudinal direction, i.e. along the microfibrils, and the transverse direction is found from Voigt (1889) and Reuss (1929) bounds (Böhm 2004; Paper IV). The shear modulus of the composite cell wall is in (Paper V) found from a mathematical model given by Kerner (1956).

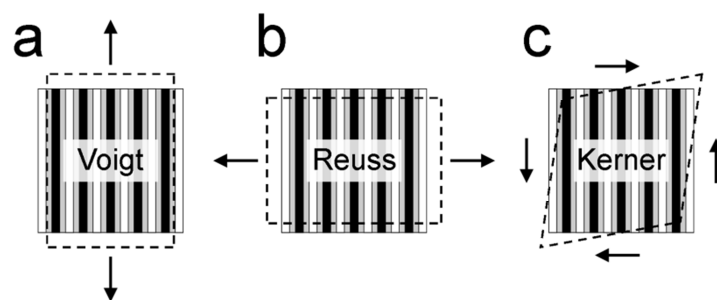


Figure 3.7: Schematic illustration of a three-phase layered composite material. Three modes of deformation are shown: a) tension along layers, b) tension perpendicular to layers, and c) shearing. The moduli for the three modes of deformation are calculated using Voigt, Reuss and Kerner models, respectively.

In order to use this model, one of the three phases must be defined as matrix material which embeds the other two phases. Lignin is selected as matrix material which embeds both cellulose microfibrils

and hemicelluloses. The Poisson's ratio in the LT plane can be found from Voigt bounds, whereas in the TT plane it is assumed equal to that of the matrix material, i.e. lignin (Paper IV). The calculation of elastic properties presented here and in (Paper V) is an improvement of the model presented in (Paper IV). In the latter a simpler model is used for calculating moduli of the composite cell wall in which cellulose microfibrils are embedded in a hemicellulose/lignin matrix.

Calculating composite elastic and shear moduli of the cell wall requires knowledge of volume concentrations of the three constituent phases. This concentration depends on amount of moisture in the cell wall since only hemicelluloses and lignin swell upon a moisture increase. These two polymers comprise about 56 % of the entire wood volume (Berg and Gradin 1999). The swelling of hemicelluloses and lignin can be estimated by assuming a swelling coefficient of the cell wall, $\beta_{sw,cell}$ of 0.40 which is similar to the macroscopic tangential β_{sw} . Since a majority of wood polymers are oriented in the longitudinal direction of wood, it is reasonable to directly relate the transverse swelling of wood cell walls with the swelling of hemicelluloses and lignin. The increase in volume by water entering these two polymer phases are assumed to be equal, i.e. the swelling coefficient $\beta_{sw,polymer}$ is similar for both polymers. From these considerations, the $\beta_{sw,polymer}$ can be estimated from (14).

$$\beta_{sw,cell} = (c_{HC} + c_{LG})\beta_{sw,polymer} \quad (14)$$

where c denotes the volume concentration and the indices "HC" and "LG" refer to hemicelluloses and lignin, respectively. The result is a $\beta_{sw,polymer}$ of 0.71 for hemicelluloses and lignin. Based on this parameter, the change in volume concentration of the three main wood polymers with moisture can be found. Table 3.1 shows the volume concentration for the S2 layer. The volume concentrations in dry condition are according to Berg and Gradin (1999).

Table 3.1: Volume concentrations of wood polymers in the S2 layer at different levels of EMC.

Moisture	0 % MC	5 % MC	10 % MC	15 % MC	20 % MC
Cellulose	45.0 %	44.1 %	43.3 %	42.5 %	41.7 %
Hemicelluloses	35.0 %	35.5 %	36.1 %	36.6 %	37.1 %
Lignin	20.0 %	20.3 %	20.6 %	20.9 %	21.2 %

Based on these volume concentrations, the composite elastic properties can be found if the properties of the constituents are known. These are described by the theory of hydrogen bonded dominated solid materials. However, three of the parameter values are different than those

previously described. For hemicelluloses, the hypothetical moisture content at full coverage, Φ differs between the units of xylan and glucomannan shown in figure 1.5 in Chapter 1. The molar mass of a xylan unit is 835 g/mol, whereas that for glucomannan has a range of 796-1049 g/mol depending on the chemical nature of the six RO-sites. The number of sorption sites differs between xylan and glucomannan in that the previous has 12 sorption sites, whereas the latter has between 9 and 15. Furthermore, the amount of glucomannan in the cell wall is about twice the amount of xylan (Sjöström 1993). This yields a value of Φ in the range 18.4-31.1 %, which is lower than that calculated for cellulose of 33.3 %. A value of Φ of 24.2 % is selected for hemicelluloses.

For lignin, it seems obvious that Φ differs between non-condensed and condensed lignins due to their difference in amount of sorption sites. In figure 1.6 in Chapter 1, the methoxy groups of the three types of lignin are most capable of acting as sorption sites. Whereas non-condensed lignin subunits have four of these groups, condensed types have two or three groups. On the basis of the molar mass of each of the types of lignin subunits, the value of Φ is in the range 11.2-20.9 %. By taking into account the uneven distribution of these subunits of lignin (Christiernin 2006), an average value of 18.6 % for Φ is found. These different values of Φ for hemicellulose and lignin than previously reported in this chapter, have implications for the value of K_{MC} in the low moisture regime. Based on the newly derived Φ , the values of K_{MC} become $1.38 \cdot 10^{-2} /%$ and $1.80 \cdot 10^{-2} /%$ for hemicellulose and lignin, respectively. In the high moisture regime, K_{MC} remains similar to the previously reported values.

For cellulose, the parameter K_T must differ along the microfibrils from that derived from the Lippincott-Schroeder potential for hydrogen bonds. The reason for this is the significant impact of covalent bonds on the elastic modulus in this direction. The covalent bonds are less affected by temperature than hydrogen bonds, which is why the thermal expansion along microfibrils is very small compared to their transverse thermal expansion (Hori and Wada 2005). Figure 3.8 shows the longitudinal modulus of elasticity (E_L) for cellulose as function of temperature. A value for K_T of $0.75 \cdot 10^{-3} \text{ K}^{-1}$ seems more appropriate for cellulose in this direction. If only the computational simulations by Bergenstråhle et al. (2007) were considered the value of K_T would be $1.4 \cdot 10^{-3} \text{ K}^{-1}$. In the transverse directions, the value of K_T of $2.4 \cdot 10^{-3} \text{ K}^{-1}$ is used since in these directions the elastic response is governed by hydrogen bonds.

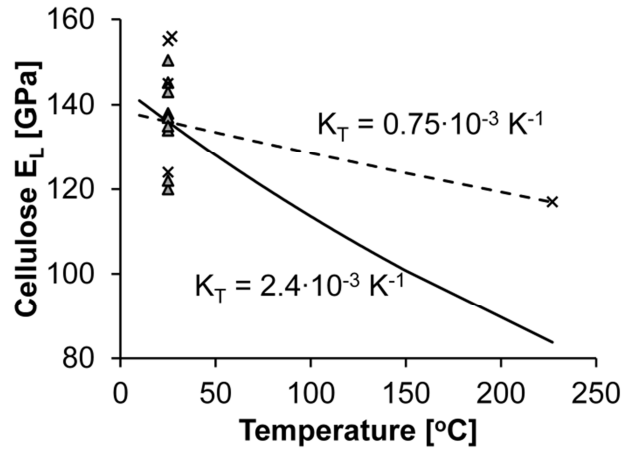


Figure 3.8: Moduli of elasticity along cellulose microfibrils as function of temperature. Data from experimental studies (triangles) (Iwamoto et al. 2009; Matsuo et al. 1990; Nishino et al. 1995; Sakurada et al. 1962; Šturcová et al. 2005) and computer simulations (crosses) (Bergensträhle et al. 2007; Šturcová et al. 2005; Tanaka and Iwata 2006) are included.

It could be argued that an interaction effect between moisture and temperature should be incorporated in the calculation of the modulus of elasticity (10). However, according to Kamiya et al. (1992), the number of hydrogen bonds broken per water molecule is proportional to the partial molar volume of adsorbed water. If there is a difference in thermal expansion between wood polymers and adsorbed water, the number of bonds broken per water molecule will also change. The thermal expansion of both wood polymers and adsorbed water is dominated by the expansion of similar hydrogen bonds, i.e. between hydrogen and oxygen. Therefore, the change in partial molar volume with temperature should be approximately similar. The volumetric thermal expansion coefficient of cellulose has been measured to $1.11 \cdot 10^{-4} \text{ K}^{-1}$ (Hori and Wada 2005), whereas the coefficient for bound water in wood has not been determined experimentally. However, ice, which is a solid material dominated by hydrogen bonding between water molecules, has a volumetric thermal expansion coefficient of $1.5 \cdot 10^{-4} \text{ K}^{-1}$ (Butkovich 1959; La Place and Post 1960). Furthermore, water molecules bound to proteins have been found to have a volumetric thermal expansion coefficient of $0.8 \cdot 10^{-4} \text{ K}^{-1}$ (Hiebl and Maksymiwi 1991). Thus, the thermal expansion of both wood polymers and water is expected to be reasonably similar. This supports the exclusion of an interaction effect between moisture and temperature in (10). Furthermore, analysis of dynamic mechanical data for wood (Gao 1994) shows an insignificant interaction effect between moisture and temperature in predicting the dynamic modulus of elasticity.

Calculated elastic and shear moduli of the three constituents are illustrated in figure 3.9, along with experimental data for some of the moduli of hemicelluloses and lignin. The mathematical description of elastic and shear moduli of each constituent is based on the mass of water molecules relative to that of the constituent, i.e. constituent EMC. In order to describe the elastic properties of the composite cell wall, the constituent EMC must be converted to wood EMC. Because the sorption sites in all three major constituents are more or less equally energetically favoured as discussed in Chapter 2, moisture is distributed between constituents in proportion to their volume concentration and number of sorption sites. This causes the linear relations between constituent EMC and wood EMC illustrated in figure 2.4b in Chapter 2. The linear correlations for hemicelluloses and lignin are 1.80 and 0.72, respectively. Furthermore, as described in Chapter 2 capillary condensation plays an insignificant role in the binding of moisture in wood. It is therefore safe to assume that all water molecules at a given wood EMC is found within the cell wall interacting with hydrogen bonds of the material. Based on the linear correlations for converting constituent EMC into wood EMC, the elastic and shear moduli of the three constituents is illustrated in figure 3.9 as function of moisture in the wood.

The Poisson's ratios in the LT-plane used for the three constituents are 0.2 for cellulose and hemicelluloses (Chen et al. 2004a; Peura et al. 2007) and 0.33 for lignin (Cousins 1976). These are assumed to be unaffected by both moisture and temperature. The resultant elastic properties of the cell wall calculated by Voigt, Reuss, and Kerner models are shown in figure 3.10. It is clear that the stiffening effect of cellulose microfibrils is predominant in the longitudinal direction. In the other directions, the influence of decreasing moduli of the amorphous wood polymers with increasing EMC is more pronounced. The Poisson's ratios in the LT and TT-planes for the composite cell wall are 0.23 and 0.33, respectively.

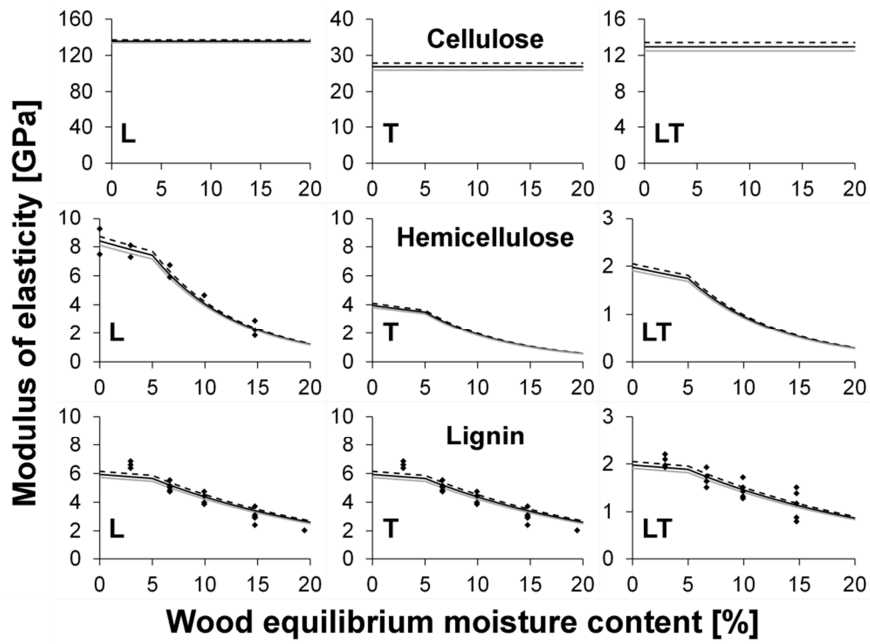


Figure 3.9: Calculated moduli of elasticity along and normal to (L, T) and in the shear plane (LT) of the material directions for cellulose, hemicellulose, and lignin. Moduli are given as function of moisture for three temperatures: 10 °C (dotted), 25 °C (black), and 40 °C (grey). Experimental data from (Cousins et al. 1975; Cousins 1976; Cousins 1978; Srinivasan 1941) is included for hemicellulose and lignin.

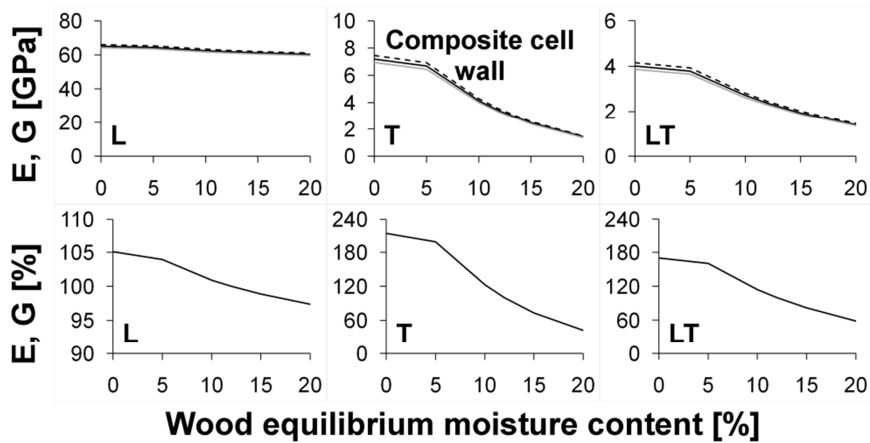


Figure 3.10: Calculated moduli of elasticity in GPa (upper) and normalized with the value at 12 %MC (lower) along and normal to (L, T) and in the shear plane (LT) of the material directions for the composite cell wall. Moduli are given as function of moisture for three temperatures: 10 °C (dotted), 25 °C (black), and 40 °C (grey).

The sliding of wood polymers on the molecular scale is equivalent to shearing deformations on the scale of the composite cell wall, i.e. microscopic scale. These time-dependent deformations are therefore introduced by adding them to the elastic shearing deformations. However, the shearing depends on movement of more than one type of molecular unit since both hemicelluloses and lignin are involved (Paper V). The time-dependent shearing of hemicelluloses and lignin has different V_h , V_m , and activation free energy, and is described by two deformation processes. Due to the layered structure of the cell wall shown in figure 3.7, these two processes act in series and their weighted contribution is added to the overall shearing of the composite cell wall. The stable molecular configuration and bonding of cellulose microfibrils (Bergenstr hle et al. 2007) prevents time-dependent shearing in this constituent, except in the boundary layer with the hemicelluloses. The time-dependent part of the cell wall shearing can be described by

$$\frac{d\varepsilon_v}{dt} = c_{HC}A_{HC} \cdot 2\sinh(B_{HC} \cdot \sigma) + c_{LG}A_{LG} \cdot 2\sinh(B_{LG} \cdot \sigma) \quad (15)$$

Where c is volume concentration and the indices ‘‘HC’’ and ‘‘LG’’ denotes hemicelluloses and lignin, respectively. The parameters A and B depend on the volumes V_h and V_m , the activation free energy and absolute temperature. Of these, the first three may differ between hemicelluloses and lignin. It seems reasonable to describe the time-dependent shearing in hemicelluloses by a V_m of 0.65 nm^3 due to the similarity in molecular structure between cellulose and hemicellulose. As noted previously, the value of V_m for lignin is more uncertain. Crystallographic investigations and molecular dynamics simulations indicate a unit cell volume of a lignin dimer of $0.966\text{-}1.020 \text{ nm}^3$ (Langer et al. 2005; Petridis and Smith 2009). Half of this volume could be appropriate for describing the movement of a single non-condensed lignin molecular segment. For the condensed type of lignin, it is possible that the volume is larger. This is because the condensed lignin does not have any rotational freedom between two cross-linked coniferyl alcohol groups, and the moving volume would comprise two coniferyl groups and probably be closer to 1 nm^3 . No matter the type of lignin, the volumes described here are considerably larger than what has been assumed for a single coniferyl alcohol (Jurasek 1995) with a length of 0.86 nm and a diameter of 0.42 nm at the widest place. These dimensions yield a volume of only 0.152 nm^3 .

It is assumed that the ratio V_h/V_m is independent of temperature, since it describes the relative length of a molecular jump. The volumes are, however, not independent of temperature due to thermal expansion. Nonetheless, Ree and Eyring (1955) suggest that the kinetic parameter B of (13) is independent of temperature since the flow volume changes linearly with temperature. The validity of this assumption may be questioned, since the volume of the moving molecular segment

does not vanish at zero absolute temperature. The effect of temperature on the parameter B is, nevertheless, smaller if thermal expansion is considered than if the volume V_h is held constant. For cellulose the volume of the unit cell changes linearly with temperature with linear thermal expansion coefficients around $1 \cdot 10^{-4} \text{ K}^{-1}$ (Hidaka et al. 2010; Hori and Wada 2005). This is of the same order as the coefficient for softwood in transverse directions which is $0.3\text{-}0.8 \cdot 10^{-4} \text{ K}^{-1}$ (Hendershot 1924; Kubler et al. 1973; Weatherwax and Stamm 1956), as well as the coefficient for other wood polymers of about $0.5\text{-}1.1 \cdot 10^{-4} \text{ K}^{-1}$ (Ramiah and Goring 1965). A thermal expansion coefficient of V_m of $1 \cdot 10^{-4} \text{ K}^{-1}$ is selected.

Numerical modelling of the elastic behaviour of tracheids

The mechanical behaviour of tracheids does not only depend on amount and layered arrangement of wood polymers in the cell wall. Also the orientation of main directions of the cell wall in the tracheid is of importance, i.e. the orientation of microfibrils. In this study, the mechanical behaviour of tracheids is assumed to be controlled by the behaviour of its dominant S2 layer. Even though the orientation of wood polymers varies between the different layers of the cell wall, only the S2 layer is considered when constructing a numerical model of a softwood tracheid. Using such an approach, the elastic behaviour of single wood cells has previously been modelled with required accuracy and precision (Berg and Gradin 1999). To mathematically describe the mechanical behaviour of a tracheid it is convenient to define two coordinate systems as illustrated in figure 3.11.

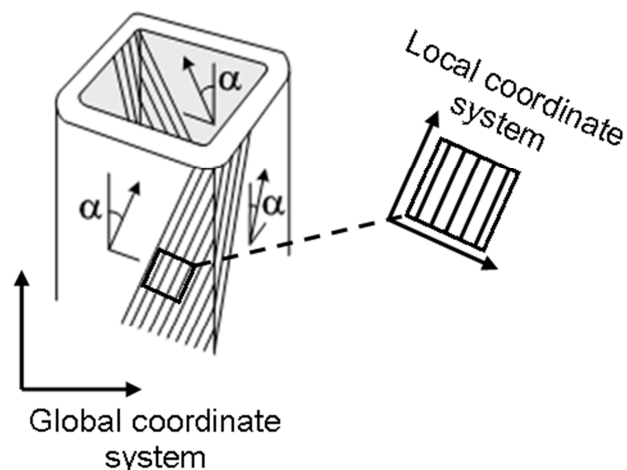


Figure 3.11: Global and local coordinate systems for tracheid model.

The global coordinate system is oriented along the longitudinal direction of the tracheid. In this coordinate system, macroscopic mechanical excitation of the tracheid such as applied force or deformation is described along with observed macroscopic response. The macroscopic response of the tracheid originates from the mechanical response of wood polymers on the molecular level. The response on this level is mathematically described by the elastic and shear moduli of the cell wall. These are most easily described in the local coordinate system which follows the orientation of the cellulose microfibrils, i.e. the longitudinal direction of the cell wall. The local coordinate system is thus rotated in relation to the global coordinate system with an inclination corresponding to the microfibril angle (MFA) of the tracheid. The geometry of a tracheid can be modelled as a hollow rectangular tube with rounded corners (Paper V), see figure 3.11. By defining composite cell wall properties as described previously, the mechanical behaviour of a tracheid can be investigated by numerical modelling.

The change in dimensions which accompany a change in EMC can be incorporated in the numerical model by applying a β_{sw} in the transverse directions of 0.40 similar to the macroscopic tangential β_{sw} . The unequal swelling of the cell wall in the main directions results presumably in a change in MFA for tracheids with low MFA. This can be seen from figure 3.12 illustrating results from the numerical model. It can be seen that at low initial MFA, the MFA might change up to 3-4° for a 15 % change in EMC. At high MFA, the effect is reversed, although the change in MFA with EMC is very small.

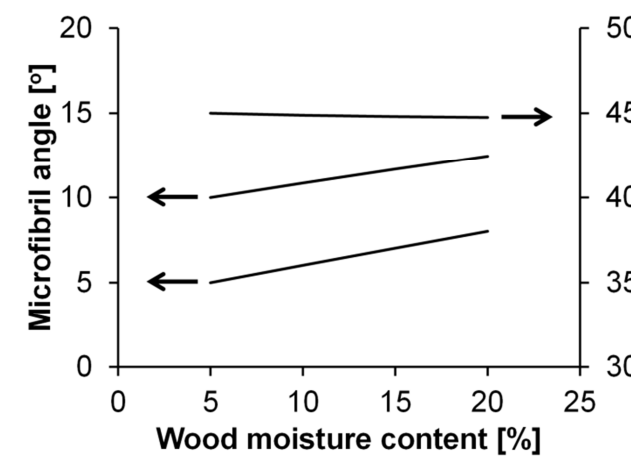


Figure 3.12: Predicted MFA as function of EMC for both high and low initial MFA.

Little experimental evidence has been produced (Jentzen 1964) to support the changing MFA with moisture. However, it may be important when describing the mechanical behaviour of wood with

low MFA, since the behaviour of tracheids is closely connected to MFA. This is illustrated in figure 3.13 which depicts the cell wall modulus of elasticity in the longitudinal direction of the cell as function of MFA. Clearly, the numerical model is able to describe the decrease in stiffness of the composite cell wall with increasing MFA and moisture content. The effect of the latter is also evident when comparing the relative modulus of elasticity of softwood in figure 3.14 with predictions of the numerical model.

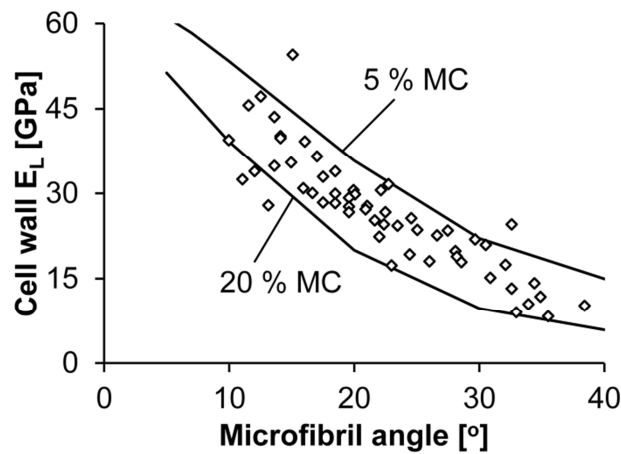


Figure 3.13: Cell wall longitudinal modulus of elasticity as function of MFA predicted by the numerical model at two levels of EMC. Included are experimental results by Cave (1968).

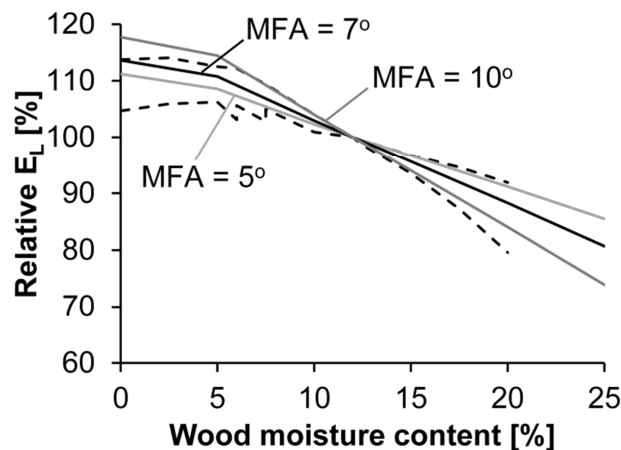


Figure 3.14: Predictions by the numerical model of the relative longitudinal modulus of elasticity of softwood as function of EMC. The modulus is relative to the value at 12 % MC. Dashed boundary curves from compiled experimental results (Gerhards 1982).

The experimental results reviewed by Gerhards (1982) and shown in figure 3.14 indicate, however, a slightly increasing modulus of elasticity with increasing EMC in the range 0-5 % MC. This effect has also been observed in more recent studies (Green and Kretschmann 1994; Kretschmann and Green 1996; Takahashi et al. 2006). Such increase is not reflected in the elastic behaviour of the numerical model. One explanation for this behaviour is the previously noted ordering of the hydrogen bonding pattern by small amounts of water.

The relation between the mechanical behaviour in the longitudinal direction, MFA and EMC is illustrated by figures 3.12, 3.13, and 3.14: at low initial MFA, a change in EMC may cause a significant change in MFA which would lead to a significant change in modulus of elasticity. Reorientation of microfibrils is not only affected by a change in EMC. A mechanical excitation of a tracheid in its longitudinal direction will also cause the MFA to change (Paper VI). Figure 3.15 illustrates change in MFA for different woody fibres under tensile strain predicted by a simple mechanical model described in (Paper VI). Good agreement between predicted and observed behaviour is seen independently of the value of MFA at zero strain.

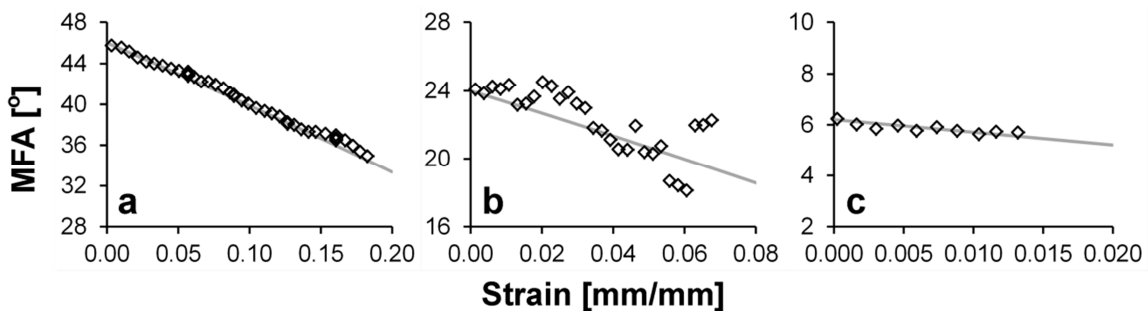


Figure 3.15: MFA in woody fibres under tensile strain. Grey lines mark predictions of a continuum mechanical model (Paper VI). Included are experimental data for a) and b) Norway spruce with initial MFA of 46° (Keckes et al. 2003) and 24° (Kölln 2004), respectively, and c) flax with initial MFA of 6° (Kölln 2004). Data from (Paper VI).

The effect of temperature on the longitudinal modulus of elasticity of softwood is depicted in figure 3.16. An interaction effect of temperature and moisture is seen in the experimental data when moisture content is changed from zero to 12 %. This change is likely accompanied by a change in MFA as illustrated in figure 3.12. Therefore, to evaluate the effect of temperature at different moisture contents, different levels of MFA must be considered. In figure 3.16 the predicted modulus of elasticity is included as function of temperature for two different cases: 8 % MC and MFA of 5°, and 20 % MC and MFA of 10°. A slight change in the temperature sensitivity is seen

between the two cases, i.e. the numerical model predicts an interaction effect between temperature and moisture. It should be noted that this effect arises despite the fact that no interaction effect is incorporated at the molecular level. The reason for this effect is the difference in temperature sensitivity between the covalent and hydrogen bonds. Along the microfibrils, the less temperature sensitive covalent bonds reduce the effect of temperature in this direction. Thus, the modulus of elasticity of tracheids with higher MFA, e.g. due to a greater MC, will be more sensitive to temperature. However, the magnitude of this sensitivity of modulus of elasticity to temperature varies significantly between different studies as illustrated in figure 3.16. The validity of the small temperature sensitivity of the numerical model may be questioned. It seems clear, nonetheless, that the interaction effect of temperature and moisture can at least partly be explained by the difference in temperature sensitivity of the dominating molecular bonds in the directions along and perpendicular to the microfibrils.

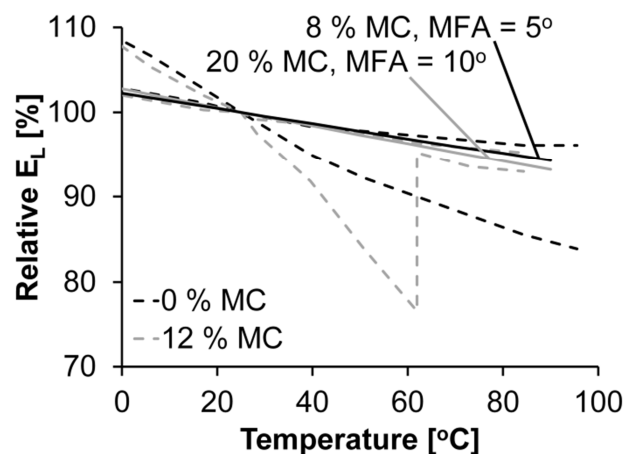


Figure 3.16: Predictions by the numerical model of the relative longitudinal modulus of elasticity of softwood as function of temperature. The modulus is relative to the value at 25 °C. Dashed boundary curves from compiled experimental results (Gerhards 1982).

In the transverse directions, the numerical model is unable to produce reasonable values for the modulus of elasticity. For loading of wood in the transverse directions, the stiffening effect of the microfibrils in the S1 and S3 layers therefore needs to be incorporated as suggested by other authors (Bergander and Salmén 2000). This is reasonable since the weighted modulus of the S2 layer in the transverse direction is of similar magnitude as that of the S1 and S3 layers in the same direction. The contribution of each of these, however thinner cell wall layers, can therefore not be disregarded as done in the present numerical model.

Numerical modelling of the time-dependent behaviour of tracheids

When a constant load is applied to wood specimens or single tracheids, the deformation will increase over time, whereas if a constant deformation is applied the load necessary to sustain the deformation will decrease over time. These two processes are termed creep and relaxation, respectively, and are due to time-dependent shearing within the cell wall (Paper IV; Paper V). Experimental investigations of the influence of temperature and moisture on the time-dependent response of softwood tissue illustrate how these two parameters affect the tracheids differently (Paper V). Figure 3.17 shows the time-dependent response during creep under 10 MPa tensile load and creep recovery after tensile loading at three temperature levels and two levels of EMC.

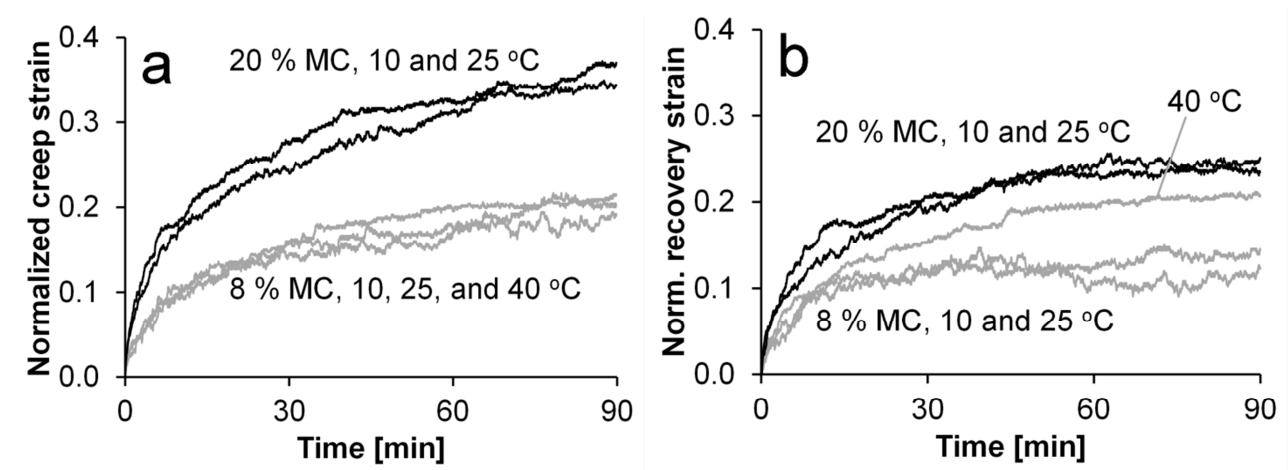


Figure 3.17: a) creep strain of Norway spruce tissue under 10 MPa tensile loading, b) creep recovery strain after tensile loading. Two levels of EMC and three temperatures are employed. Only the time-dependent strain is shown and this is normalized by the elastic strain. Data from (Paper V).

Only time-dependent strains are shown which have been normalized with the elastic strain. It appears from figure 3.17a that temperature affects the elastic and creep response equally since the normalized curves coincide. The same phenomenon is seen for creep recovery in figure 3.17b except for the sample at 40 °C and 8 % MC. These findings contradict, however, experimental results for bending tests which show that creep recovery (Davidson 1962) is in fact affected by temperature in the range 20-60 °C. Although a different mode of loading is employed in the quoted study, further tensile experiments on softwood tissue are needed to draw final conclusions.

The effect of moisture on creep and recovery behaviour is not similar for elastic and time-dependent responses; the relative response is greater at higher EMC. The different impact of temperature and moisture can be linked to their effect on the chemical bonds on the molecular level.

Increasing the temperature will affect all chemical bonds, whether covalent or secondary like hydrogen bonds, hereby increasing bond lengths and weakening bonds. Moisture, on the other hand, predominantly interferes with hydrogen bonds. Even though hydrogen bonds dominate the elastic behaviour of the amorphous wood polymers, covalent bonds in the cellulose microfibrils greatly influence the elastic behaviour of the composite cell wall. The time-dependent response of wood tissue during creep as depicted in figure 3.17a is a result of the combined responses of tracheids and middle lamella gluing these together (Paper IV; Paper V). During creep recovery, the elastic energy stored in microfibrils will cause a full or almost full reversal of the response of the tracheids. This is also predicted by the numerical model as illustrated in figure 3.18.

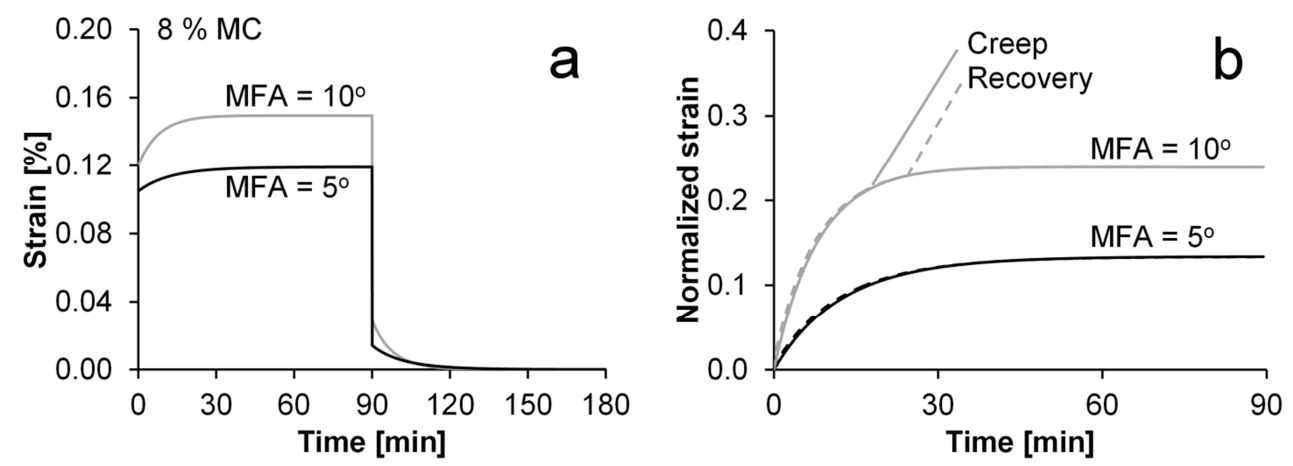


Figure 3.18: a) numerical model predicted creep at 10 MPa and recovery after load duration of 90 minutes for two levels of initial MFA, b) creep (solid) and recovery (dashed) strain normalized with the elastic strain.

The developed strains in the middle lamella are, however, not reversed. By isolating the tracheid response during creep, similar curves for creep and creep recovery of the tracheids are obtained indicating full or almost full strain reversal, see figure 3.19a. The mechanical response of a tracheid can therefore be characterized by a decreasing rate of the time-dependent processes which eventually more or less levels off for both creep and relaxation as illustrated in figure 3.19.

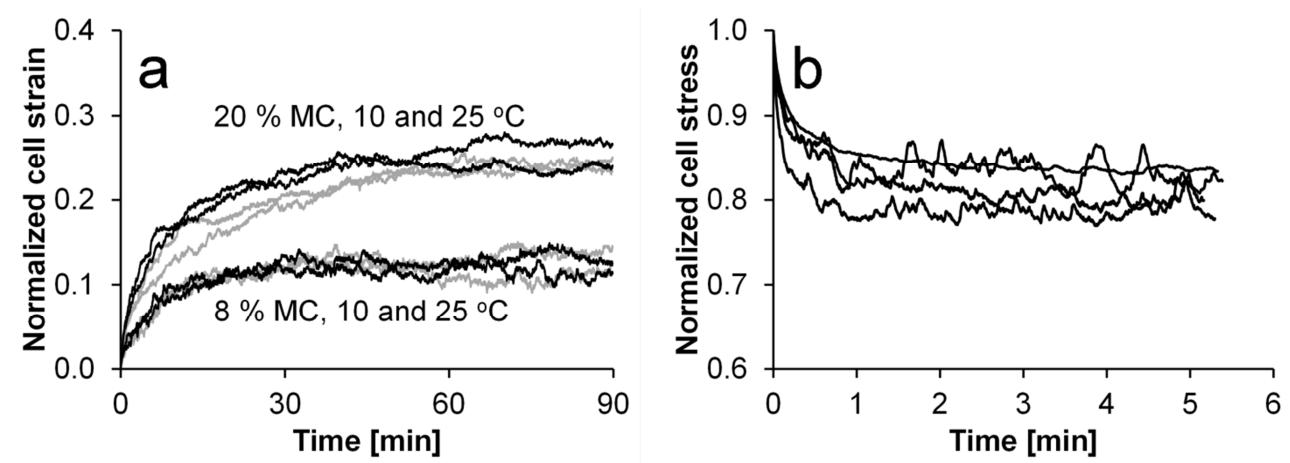


Figure 3.19: a) normalized creep strain (black) and creep recovery strain (grey) response of only the tracheids. Experimental data from (Paper V), b) normalized cell stress under relaxation of single tracheids. Experimental data from (Eder et al. 2006).

For tracheids bundled in a tissue, the time-dependent response of the middle lamella will continue as seen in experiments on softwood tissues (Paper IV; Paper V). For a constant load, the response of the middle lamella is apparently linear with time. This is supported by creep experiments in bending for temperatures of 40 °C and below (Davidson 1962).

In the following, due to a scarcity of experimental data to fully evaluate (15), the simpler model of (13) describing a single energy barrier is used as done in (Paper IV). In order to illustrate the performance of the numerical model, the kinetic parameter A is varied to generate differences in shearing rates. Furthermore, the elastic properties as function of moisture and temperature are varied in accordance with previously described theory. In the following, the reference value A_0 of parameter A in (13) corresponds to a activation free energy of about 100 kJ/mol at room temperature, which is within the range of 85-140 kJ/mol reported for time-dependent deformation of viscose rayon (Eyring and Halsey 1946; Halsey et al. 1945; Holland et al. 1946), cotton (Holland et al. 1946; Lasater et al. 1953), cellulose acetate (Halsey et al. 1945; Reichardt et al. 1946; Reichardt and Eyring 1946), and wood (Bonfield et al. 1996; Kingston and Clarke 1961). The value of B used in the following is based on the volume of a hemicellulose unit. The tracheid model is fully capable of describing the behaviour observed in figure 3.19. As illustrated by the results from a simulated creep test in figure 3.20 and a simulated relaxation test in figure 3.21, the numerical model predicts levelling off of strain and stress in the respective types of experiment. It is clear that the magnitude of the final level of strain or stress is determined by MFA

and elastic properties, but not the rate of time-dependent processes. Whether the time-dependent process is fast, i.e. high value of A or slow, the final level of stress or strain is the same.

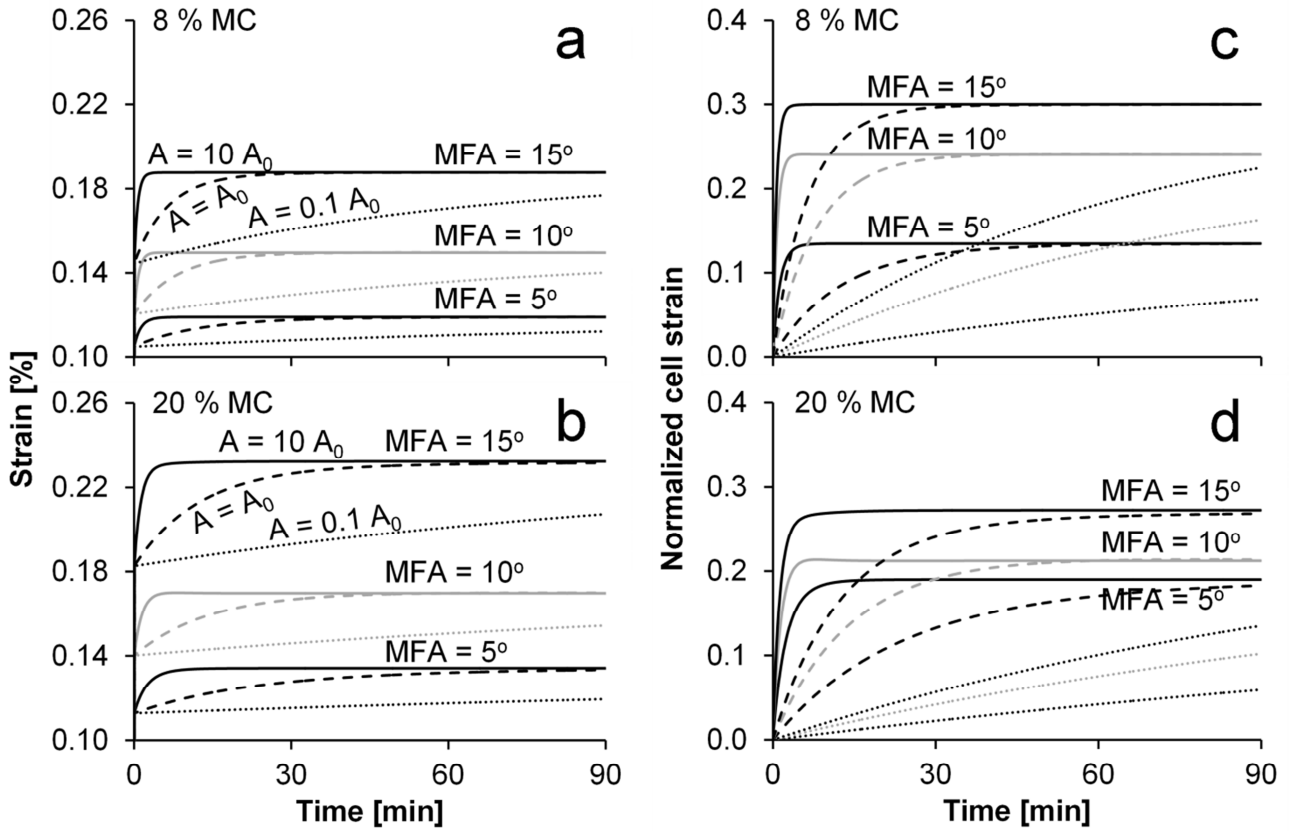


Figure 3.20: Predicted strain response at 10 MPa for three levels of initial MFA at a) 8 % MC and b) 20 % MC, and time-dependent strain normalized with elastic strain for c) 8 % MC and d) 20 % MC. The kinetic parameter A is varied by two orders of magnitude. Based on the kinetic model of (Paper IV).

These observations imply that time-dependent mechanical behaviour of tracheids is controlled by moisture and MFA. Part of the observed difference between creep at 8 % MC and 20 % MC in figure 3.17 must therefore be explained by a difference in MFA in these two moisture states. This is supported by the predicted change in MFA with EMC as shown in figure 3.12. If an initial MFA of about 5° in the tracheids at 8 % MC is assumed, figure 3.12 predicts the MFA of tracheids at 20 % MC to be about 3° higher. The low initial MFA at 8 % MC is in accordance with measured MFA of latewood fibres by Bergander and Salmén (2000). In figure 3.22, the experimental results are fitted with good agreement by the numerical model with such two levels of MFA. The kinetic parameter A is doubled for the 20 % MC model in order to achieve a better fit to data. This corresponds with an expected decreased activation free energy with increased EMC.

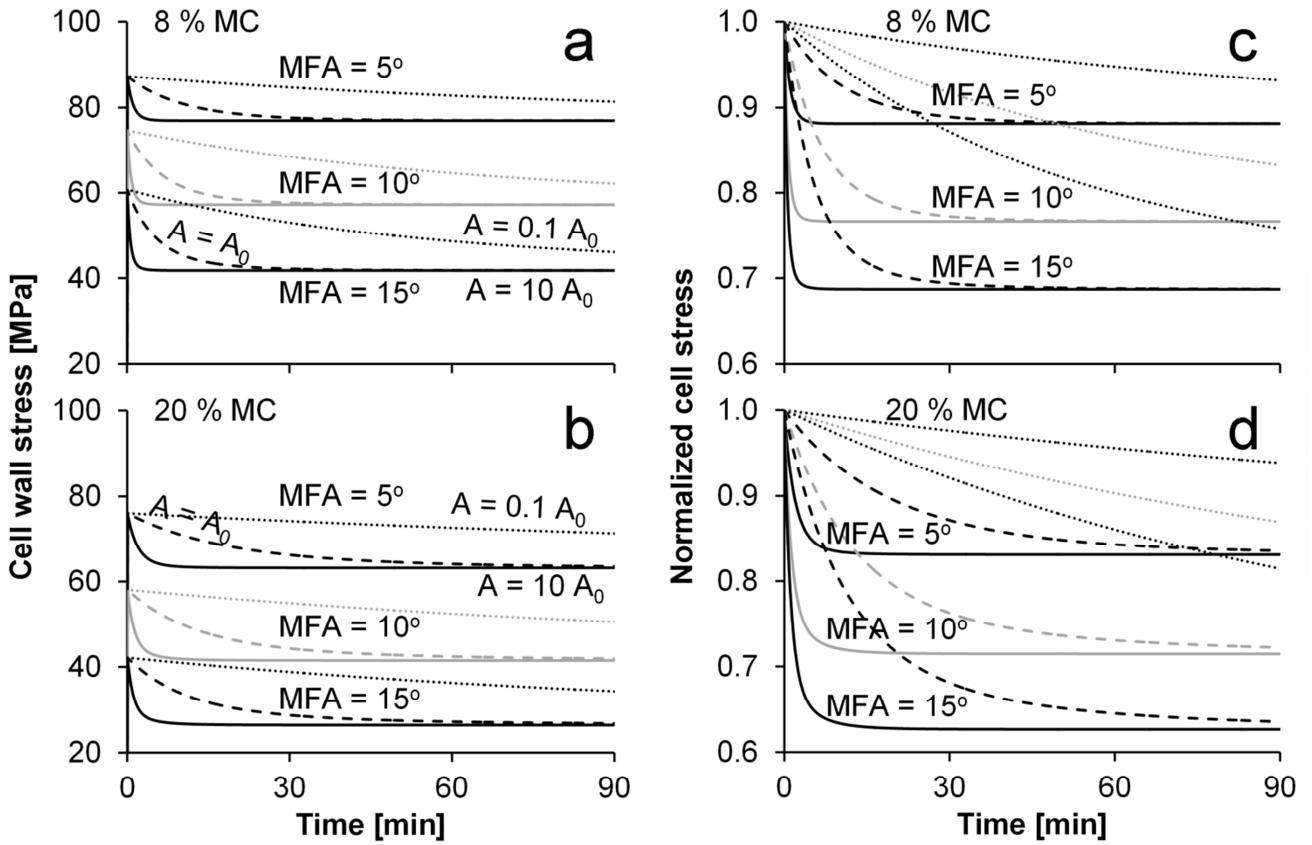


Figure 3.21: Predicted stress response at 0.15 % strain for three levels of initial MFA at a) 8 % MC and b) 20 % MC. Time-dependent stress normalized with stress immediately after constant deformation is applied at c) 8 % MC and d) 20 % MC. The kinetic parameter A is varied by two orders of magnitude. Based on the kinetic model of (Paper IV).

The effect of temperature found in the present study is, as described previously, not in accordance with results from literature. The predictions of the numerical model are, however, in agreement with experimental results achieved in the present study. In figure 3.23 strain development over time and normalized cell strain are shown for the temperature levels employed in the experiments. It is clear that when strains are normalized with elastic response, the curves coincide for all temperature levels. This obvious conflict between the experimental and numerical results of the present study and the experimental results of Davidson (1962) cannot be resolved until further experimental results are obtained. One possibility is that the contradiction is due to the difference in mode of loading employed.

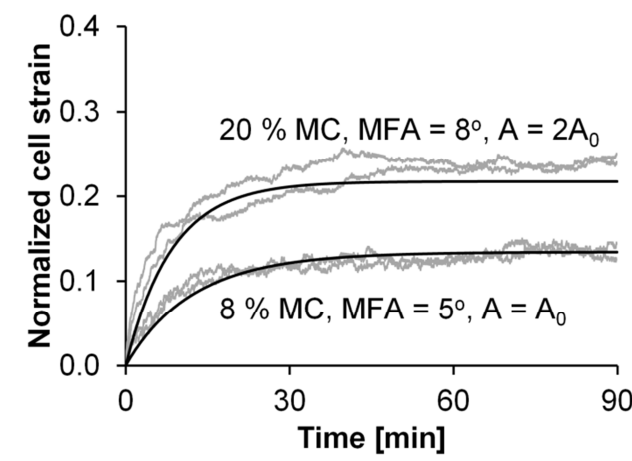


Figure 3.22: Experimental creep curves fitted with predicted curves of the numerical model.

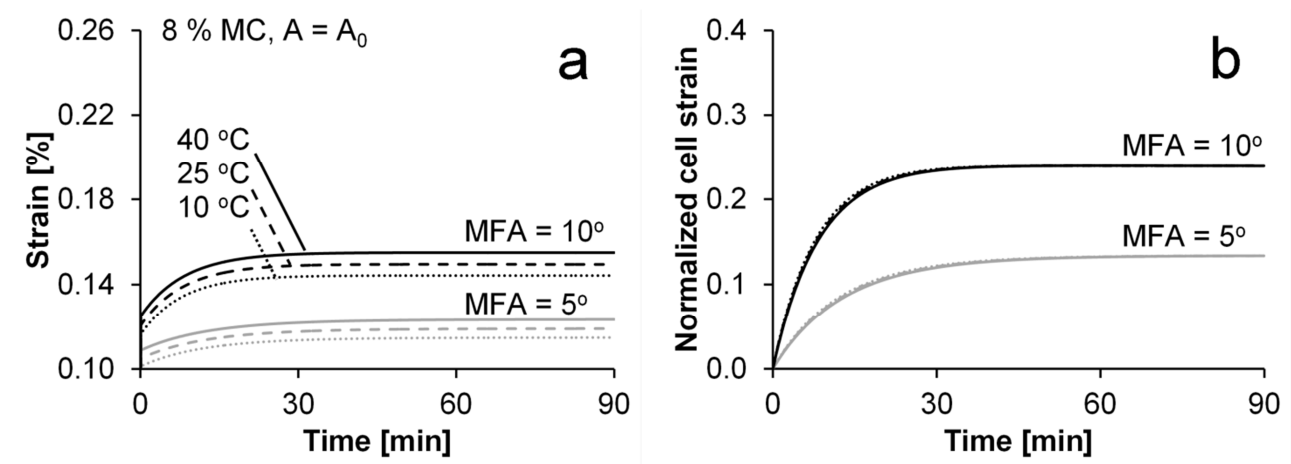


Figure 3.23: a) Predicted strain response at 10 MPa for two levels of initial MFA at three temperatures, and b) predicted time-dependent strain normalized with elastic strain. Based on the kinetic model of (Paper IV).

The reorientation of the microfibrils, i.e. changes in MFA, illustrated in figure 3.15 is not limited to the elastic domain. As observed in tensile experiments (Hill 1967), the numerical model predicts a reorientation, although only less than 0.1° occurring during both creep and relaxation for initial MFA levels of $5\text{-}10^\circ$ for 10 MPa tensile stress.

In general, the numerical model is able describe several different phenomena concerning the mechanical behaviour in the longitudinal direction of softwood tracheids. This fact, plus the simple hypotheses about structure and physical mechanisms causing this lends the numerical model credibility. It also allows a study of the nature of the mechanical response of tracheids. Figure 3.24 illustrates the strain energy distribution between the directions along the

microfibrils, perpendicular to these and in shearing for both creep and stress relaxation to similar strain after 90 minutes. A decrease over time in strain energy due to shear forces is seen. This reflects the redistribution over time due to viscous sliding of microfibrils past each other causing a relatively higher proportion of strain energy along the microfibrils; even though the total strain energy for relaxation is decreasing. Thus, with time the tracheid redistributes stress from hydrogen bonded segments in shear to covalent and hydrogen bonds in tension.

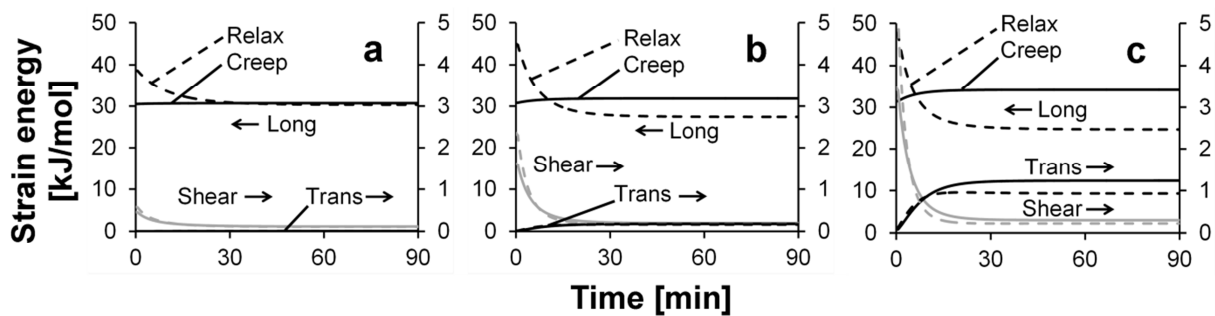


Figure 3.24: Predicted distribution of elastic energy along the microfibrils (long), perpendicular to these (trans) and in shearing (shear) for similar strain after 90 min. obtained by either creep or stress relaxation with an initial MFA of a) 5°, b) 10°, and c) 15°.

The direct effect of water molecules entering the cell wall is breaking of hydrogen bonds between wood polymers and swelling to accommodate the water. On the scale of the tracheid the effect is a marked weakening of transverse elastic and shear moduli and a reorientation of microfibrils, i.e. a change in MFA. The uneven decrease of the different elastic moduli can for instance be seen between 8 % MC and 20 % MC. In this moisture range, the longitudinal and transverse elastic modulus and shear modulus of the cell wall are reduced by 7 %, 72 % and 57 %, respectively. This results in a change in mechanical behaviour of the tracheid. Figure 3.25 illustrates this change in creep response when the elastic moduli are reduced by the before mentioned percentages for three levels of MFA. It is clear that the reduction in transverse elastic and shear moduli has a greater effect on the response than the reduction in longitudinal modulus.

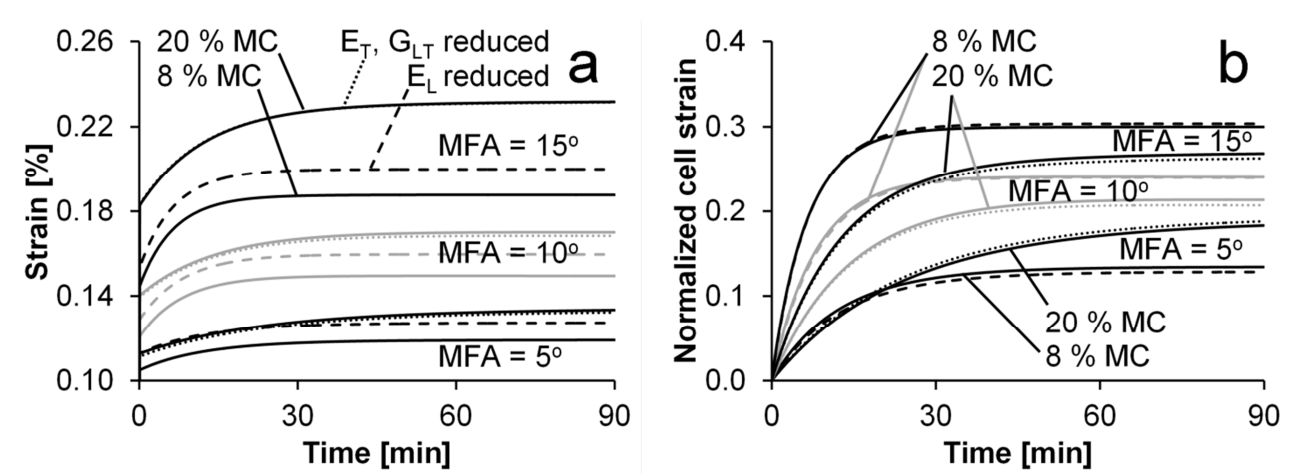


Figure 3.25: a) Predicted creep strain for three levels of initial MFA at 8 % MC (upper solid line) and 20 % MC (lower solid line). Also included are creep curves for tracheids with reduced transverse and shear moduli (dotted line) and reduced longitudinal modulus (dashed line) of the cell wall compared with the moduli at 8 % MC. The previous almost coincide with the curves for 20 % MC for all levels of initial MFA. b) Normalized predicted creep strain. The dotted lines almost coincide with the curves for 20 % MC, whereas the dashed lines almost coincide with the curves for 8 % MC.

The mechanical behaviour of softwood

On the macroscopic scale, the mechanical response of tracheids is supplemented by the response of the middle lamella. Thus, whereas tracheids of softwood tissue under constant load approach a final level of strain, which marks the equilibrium between applied mechanical excitation and internal stress distribution, the middle lamella will continue to develop strain over time. Upon unloading, only the strain developed in tracheids will be reversed due to the elastic energy stored in microfibrils, causing an increase in MFA (Hill 1967). The time-dependent strain developed in the middle lamella, however, is not recoverable. When water molecules enter the softwood structure, it will also affect the response of the middle lamella, however, at present more data is needed to evaluate this effect. Furthermore, it should be noted that the present model needs incorporation of the mechanical response of the S1 and S3 layers for it to be able to predict and describe the transverse mechanical response of a tracheid.

CHAPTER 4

Suggested future research

The results of the preceding three chapters point toward several interesting new foci of future research. In the following, several topics which could elucidate the relation between molecular level mechanisms and macroscopic wood performance are briefly reviewed.

Water sorption and diffusion

The effect of water on mechanical behaviour of tracheids is in the preceding chapters described for constant moisture conditions. When using wood for engineering purposes, however, the ambient climate typically varies over time. This results in variations in moisture conditions of the wood as it strives toward equilibrium with the current ambient climate. Upon a change in ambient conditions, two phenomena occur concurrently: sorption and diffusion. The first involves a change in phase of water molecules between gaseous phase and bound phase adsorbed to sorption sites within the cell wall. The latter describes the transport of water molecules from regions of high water activity to those with lower and is typically described by Fick's law. The diffusion occurs, however, in both phases of water present below the fibre saturation point, i.e. the gaseous phase in lumens and the bound water phase in cell walls. Therefore, a model based on two Fickian differential equations is needed for describing diffusion of water in wood. Such a model has been established (Frandsen et al. 2007; Krabbenhøft and Damkilde 2004) and further developed by Eitelberger et al. (2011). The two Fickian differential equations are coupled by an equation describing sorption. Eitelberger et al. (2011) convincingly describe sorption as a diffusion process: adsorption by diffusion from the interface between the tracheid wall and the lumen air and into the cell wall, and desorption by the opposite process.

The mechanical response of the cell wall to a change in amount of moisture, i.e. swelling induced stresses, is not incorporated in the sorption model by Eitelberger et al. (2011). It is likely that these stresses influence sorption of moisture. Experimental studies (Christensen 1959; Downes and Mackay 1958) show that swelling stresses influence sorption kinetics. Furthermore, Christensen and Hergt (1969) experimented with conditioning thinly cut wood samples to the same climate after they had reached "equilibrium" at various length of time. Hereafter, the samples were subjected to a higher vapour pressure which resulted in adsorption and swelling. The longer the time of conditioning at "equilibrium", the slower was the approach to the new equilibrium state.

Furthermore, the time to reach half of the moisture change was faster the higher the change in ambient vapour pressure. This is a sign that stresses in samples with long conditioning time had decreased the most, whereas samples kept shortest at the first climate still had significant swelling stresses. Therefore, upon changing the climate, the resulting swelling stresses were higher and sorption commenced faster (Christensen 1967). However, the first part of the sorption histories were almost similar indicating a first sorption controlled mainly by elastic swelling stresses, whereas subsequent uptake of moisture depends on stress relaxation. This is in line with experimental results by Newns (1956; 1959). In a related study, Newns (1975b) found that the rate during the second stage of sorption could be related to the hyperbolic sine of the induced swelling pressure. This indicates that sorption is controlled by deformation kinetics similar to those controlling shearing of the cell wall. Similar conclusions are drawn by Christensen and Hergt (1969) and Berens (1977). If the sorption isotherm is split into contributions of the moisture adsorbed in first and second stages, the previous is seen as a Langmuir-shaped isotherm, whereas the latter is shaped as an exponentially increasing curve (Newns 1975a). This could perhaps be seen as the initial stage sorption isotherm depicts the true relation between air humidity and swelling pressure. The second stage curve would therefore come automatically when relaxation of the adsorbent is inserted in the numerical model, since stress relaxation results in an increased moisture content in order to uphold equilibrium with the given constant external air humidity (Newns 1975a).

In order to describe and predict the magnitude of swelling stresses and rate of shearing, the mechanical properties must be accurately described. The elastic properties change upon a change in moisture content as described by Nissan's model (10), but the parameters controlling the rate of shearing also changes as seen in figure 3.22 in Chapter 3. Furthermore, adsorption and desorption is accompanied by a change in temperature which affects the mechanical properties of the wood cell wall (Berger and Habeger 1989; Coffin and Habeger 2001). The magnitude of change in temperature depends on the heat of sorption, also termed sorption enthalpy, at given moisture content. The sorption enthalpy decreases as the moisture content is increased (Skaar 1988), but the physical background for this decrease is not well understood. Many authors have suggested that the binding energy of water in the cell wall decreased with increasing moisture content. This explanation does not, however, fit experimental results from spectroscopy nor the theory for hydrogen bonding described in this work. The binding energy of water in wood is directly coupled to the attractive force between polymer and water. If the attractive force of the wood-water bonds did change with moisture content, experimental results from spectroscopy would

show a change in the natural vibration frequency of the bonds. This is analogous to the classical mechanical description of vibrations where an increased stiffness of a vibrating structure leads to a higher natural frequency. No such change can be seen in the results of Hofstetter et al. (2006) who investigated the binding of water in wood. It therefore seems that the variation of sorption enthalpy with moisture content is not related to variations in bonding force. Another explanation for the variation in sorption enthalpy is related to the diffusion process from cell wall surface to the interior of the cell wall as equilibrium is approached. At low moisture content, the energy required to swell the cell wall is greater due to a higher material stiffness than at higher moisture content. Thus, more energy is related to attain equilibrium at low than at high moisture content. No matter the cause, a more detailed study of sorption and diffusion processes of water in the wood cell wall will need to address the changes in mechanical properties occurring during these processes.

Mechanosorption

When wood under load exhibits varying moisture content, the strain over time will fluctuate but have a greater magnitude than if the wood exhibited constant high moisture content (Armstrong and Christensen 1961; Armstrong and Kingston 1960; Armstrong and Kingston 1962; Gibson 1965; Hearmon and Paton 1964; Kingston and Armstrong 1951). The behaviour is thus a combined effect of moisture sorption and mechanical excitation and is termed “mechanosorption” or “accelerated creep”. The latter term implies that the physical mechanism behind the phenomenon is related to that causing creep (Hanhijärvi and Hunt 1998). Despite significant research effort no generally accepted theory for mechanosorption exists.

Experimental investigations indicate that tensile creep curves of single tracheids under moisture cycling do not exceed the creep curves of single tracheids at constant high moisture content (Coffin and Boese 1997; Sedlachek 1995). The mechanosorptive effect in single tracheids seems therefore to be a result of the added responses of creep and anisotropic swelling of the tracheids (Haslach 1994). The reason for this contradictory behaviour between wood tissue and tracheids is explained by Habeger et al. (2001) by a difference in moisture generated stresses due to moisture gradients. For small specimens such as single tracheids, moisture gradients are thought not to have a sufficient magnitude to result in significant mechanosorption. Results from other investigations reject, however, that mechanosorption in single tracheids does not exceed creep strain at high moisture content (Dong et al. 2010; Olsson et al. 2007). Nonetheless, mechanosorption in

larger wood specimens is presumably significantly affected by the response of the middle lamella in terms of swelling and mechanical behaviour.

An initial attempt to predict the mechanical response of a tracheid in tension during moisture cycling was made by varying the moisture content in the range 8-20 % MC. This was done by assuming a uniform distribution of moisture, i.e. no moisture gradients were incorporated. The change in moisture was very rapid in accordance with observations by Sedlachek (1995) that moisture equilibrium was achieved within 15 seconds. Following each change in moisture, the conditions were held constant for about 10 minutes prior to the next change. Figure 4.1 illustrates the predictions of the numerical model. Apparently, the numerical model is able to qualitatively predict the behaviour observed by Sedlachek (1995).

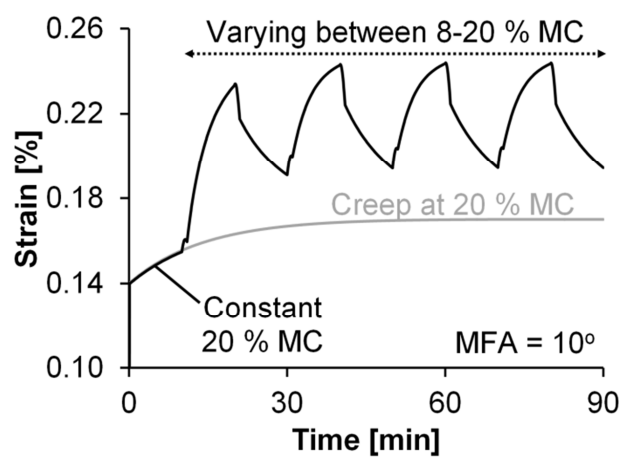


Figure 4.1: Predicted strain response at 10 MPa constant stress for constant MC at 20 % followed by desorption-adsorption cycles. The creep response at constant 20 % MC is included for comparison.

A significant amount of work is, however, needed to fully implement mechanosorption in the numerical model and verify the results. For instance, temperature changes and subsequent changes in mechanical properties discussed in the previous subchapter need to be incorporated. However, experimental results indicate that a change in moisture content does not affect the modulus of elasticity beyond what can be expected from the local moisture constant or local temperature in the cell wall (Berger and Habeger 1989). Prediction of the mechanosorptive phenomenon therefore seems possible with the current numerical model under condition that sorption and diffusion processes are incorporated into the model.

References

- Andersson, S., Serimaa, R., Paakkari, T., Saranpää, P., Pesonen, E. (2003) Crystallinity of wood and the size of cellulose crystallites in Norway spruce (*Picea abies*). *Journal of Wood Science*. 49:531-537
- Arevalo, R., Hernández, R. E. (2001) Influence of moisture sorption on swelling of mahogany (*Swietenia macrophylla* King) wood. *Holzforschung*. 55:590-594
- Armstrong, L., Christensen, G. N. (1961) Influence of moisture changes on deformation of wood under stress. *Nature*. 191:869-870
- Armstrong, L. D., Kingston, R. S. T. (1960) Effect of moisture changes on creep in wood. *Nature*. 185:862-863
- Armstrong, L. D., Kingston, R. S. T. (1962) The effect of moisture content changes on the deformation of wood under stress. *Australian Journal of Applied Science*. 13:257-276
- Atalla, R. H., Brady, J. W., Matthews, J. F., Ding, S.-Y., Himmel, M. E. (2008) Structures of plant cell wall celluloses. *In Biomass Recalcitrance - Deconstructing the Plant Cell Wall for Bioenergy* (Himmel, M. E., ed.), Blackwell Publishing Ltd., Oxford, UK, 188-212
- Atalla, R. H., Vanderhart, D. L. (1984) Native cellulose - a composite of two distinct crystalline forms. *Science*. 223:283-285
- Babbitt, J. D. (1942) On the adsorption of water vapour by cellulose. *Canadian Journal of Research Section A-Physical Sciences*. 20:143-172
- Balashov, V., Preston, R. D., Ripley, G. W., Spark, L. C. (1957) Structure and mechanical properties of vegetable fibres, 1: The influence of strain on the orientation of cellulose microfibrils in sisal leaf fibre. *Proceedings of the Royal Society of London Series B-Biological Sciences*. 146:460-468
- Bardage, S., Donaldson, L., Tokoh, C., Daniel, G. (2004) Ultrastructure of the cell wall of unbeaten Norway spruce pulp fibre surfaces. *Nordic Pulp & Paper Research Journal*. 19:448-452
- Barkas, W. W. (1936) Wood-water relationships, 2: The fibre saturation point of beech wood. *Proceedings of the Physical Society*. 48:576-588
- Barkas, W. W. (1937) Wood-water relationships, Part III: Molecular sorption of water by Sitka spruce wood. *Proceedings of the Physical Society*. 49:237-242
- Barnett, J. R., Bonham, V. A. (2004) Cellulose microfibril angle in the cell wall of wood fibres. *Biological Reviews*. 79:461-472
- Batten, G. L., Nissan, A. H. (1987) Unified theory of the mechanical properties of paper and other H-bond-dominated solids, Part I. *Tappi Journal*. 70:119-123
- Baum, G. A., Brennan, D. C., Habeger, C. C. (1981) Orthotropic elastic constants of paper. *Tappi Journal*. 64:97-101
- Becker, H., Noack, D. (1968) Studies on dynamic torsional viscoelasticity of wood. *Wood Science and Technology*. 2:213-230
- Berens, A. R. (1975) Solubility of vinyl chloride in poly(vinyl chloride). *Angewandte Makromolekulare Chemie*. 47:97-110
- Berens, A. R. (1977) Diffusion and relaxation in glassy polymer powders, 1: Fickian diffusion of vinyl-chloride in poly(vinyl chloride). *Polymer*. 18:697-704

- Berg, J. E., Gradin, P. A. (1999) A micromechanical model of the deterioration of a wood fibre. *Journal of Pulp and Paper Science*. 25:66-71
- Bergander, A., Salmén, L. (2000) Variations in transverse fibre wall properties: Relations between elastic properties and structure. *Holzforschung*. 54:654-660
- Bergensträhle, M., Berglund, L. A., Mazeau, K. (2007) Thermal response in crystalline I beta cellulose: A molecular dynamics study. *Journal of Physical Chemistry B*. 111:9138-9145
- Berger, B. J. (1988) The influence of temperature test frequency and moisture sorption on the viscoelastic moduli of cellulose. PhD thesis. Lawrence University, Appleton, WI, USA.
- Berger, B. J., Habeger, C. C. (1989) Influences of non-equilibrium moisture conditions on the in-plane, ultrasonic stiffnesses of cellulose. *Journal of Pulp and Paper Science*. 15:J160-JJ165
- Berthold, J., Desbrières, J., Rinaudo, M., Salmén, L. (1994) Types of adsorbed water in relation to the ionic groups and their counterions for some cellulose derivatives. *Polymer*. 35:5729-5736
- Berthold, J., Olsson, R. J. O., Salmén, L. (1998) Water sorption to hydroxyl and carboxylic acid groups in carboxymethylcellulose (CMC) studied with NIR-spectroscopy. *Cellulose*. 5:281-298
- Berthold, J., Rinaudo, M., Salmén, L. (1996) Association of water to polar groups: Estimations by an adsorption model for ligno-cellulosic materials. *Colloids and Surfaces A-Physicochemical and Engineering Aspects*. 112:117-129
- Böhm, H. J. (2004) A short introduction to continuum micromechanics. *In Mechanics of microstructured materials* (Böhm, H. J., ed.), Springer-Verlag, Vienna, Austria, pp 1-40
- Bonfield, P. W., Mundy, J., Robson, D. J., Dinwoodie, J. M. (1996) The modelling of time-dependant deformation in wood using chemical kinetics. *Wood Science and Technology*. 30:105-115
- Brändström, J. (2001) Micro- and ultrastructural aspects of Norway spruce tracheids: A review. *IAWA Journal*. 22:333-353
- Brändström, J., Bardage, S. L., Daniel, G., Nilsson, T. (2003) The structural organisation of the S-1 cell wall layer of Norway spruce tracheids. *IAWA Journal*. 24:27-40
- Butkovich, T. R. (1959) The thermal expansion of ice. *Journal of Applied Physics*. 30:350-353
- Çarçabal, P., Jockusch, R. A., Hünig, I., Snoek, L. C., Kroemer, R. T., Davis, B. G., Gambin, D. P., Compagnon, I., Oomens, J., Simons, J. P. (2005) Hydrogen bonding and cooperativity in isolated and hydrated sugars: mannose, galactose, glucose, and lactose. *Journal of the American Chemical Society*. 127:11414-11425
- Caulfield, D. F. (1990) Effect of moisture and temperature on the mechanical properties of paper. *Solid mechanics advances in paper related industries: Proceedings of National Science Foundation workshop*, Syracuse, NY, USA. 50-62
- Cave, I. D. (1968) Anisotropic elasticity of plant cell wall. *Wood Science and Technology*. 2:268-278
- CEI Bois (2008) Tackle climate change – use wood. CEI Bois, Brussels, Belgium
- Chauhan, S. S., Aggarwal, P. (2004) Effect of moisture sorption state on transverse dimensional changes in wood. *Holz Als Roh- und Werkstoff*. 62:50-55
- Chen, W., Lickfield, G. C., Yang, C. Q. (2004a) Molecular modeling of cellulose in amorphous state, Part II: Effects of rigid and flexible crosslinks on cellulose. *Polymer*. 45:7357-7365
- Chen, W., Lickfield, G. C., Yang, C. Q. (2004b) Molecular modeling of cellulose in amorphous state, Part I: Model building and plastic deformation study. *Polymer*. 45:1063-1071

- Chiou, J. S., Maeda, Y., Paul, D. R. (1985) Gas and vapor sorption in polymers just below T_g. *Journal of Applied Polymer Science*. 30:4019-4029
- Christensen, G. N. (1959) The rate of sorption of water vapour by wood and pulp. *Appita Journal*. 13:112-123
- Christensen, G. N. (1967) Sorption and swelling within wood cell walls. *Nature*. 213:782-784
- Christensen, G. N., Hergt, H. F. A. (1969) Effect of previous history on kinetics of sorption by wood cell walls. *Journal of Polymer Science Part A-1-Polymer Chemistry*. 7:2427-2430
- Christensen, G. N., Kelsey, K. E. (1958) The sorption of water vapour by the constituents of wood: determination of sorption isotherms. *Australian Journal of Applied Science*. 9(3):265-282
- Christensen, G. N., Kelsey, K. E. (1959) The sorption of water vapor by the constituents of wood. *Holz als Roh- und Werkstoff*. 17:189-203
- Christiernin, M. (2006) Composition of lignin in outer cell-wall layers. PhD thesis. Royal Institute of Technology, KTH, Stockholm, Sweden
- Clouser, W. S. (1959) Creep of small wood beams under constant bending load. Tech. Rep. 2150. US Department of Agriculture, Forest Service, Forest Products Laboratory, Madison, WI, USA
- Cocinero, E. J., Gamblin, D. P., Davis, B. G., Simons, J. P. (2009) The building blocks of cellulose: The intrinsic conformational structures of cellobiose, its epimer, lactose, and their singly hydrated complexes. *Journal of the American Chemical Society*. 131:11117-11123
- Coffin, D. W., Boese, S. B. (1997) Tensile creep behavior of single fibers and paper in a cyclic humidity environment. *Proceedings of the 3rd International Symposium on Moisture and Creep Effects on Paper and Containers*, Rotorua, New Zealand. 39-52
- Coffin, D. W., Habeger, C. C. (2001) The mechanics of sorption-induced transients in the loss tangent. *Journal of Pulp and Paper Science*. 27:385-390
- Cousins, W. J. (1976) Elastic-modulus of lignin as related to moisture-content. *Wood Science and Technology*. 10:9-17
- Cousins, W. J. (1978) Youngs modulus of hemicellulose as related to moisture-content. *Wood Science and Technology*. 12:161-167
- Cousins, W. J., Armstrong, R. W., Robinson, W. H. (1975) Youngs modulus of lignin from a continuous indentation test. *Journal of Materials Science*. 10:1655-1658
- Davidson, R. W. (1962) The influence of temperature on creep in wood. *Forest Products Journal*. 12:377-381
- De Micco, V., Ruel, K., Joseleau, J. P., Aronne, G. (2010) Building and degradation of secondary cell walls: are there common patterns of lamellar assembly of cellulose microfibrils and cell wall delamination? *Planta*. 232:621-627
- Ding, S. Y., Himmel, M. E. (2006) The maize primary cell wall microfibril: A new model derived from direct visualization. *Journal of Agricultural and Food Chemistry*. 54:597-606
- Djolani, B. (1972) Hysteresis and second order effects of the moisture sorption in the wood at temperatures of 5, 21, 35 and 50 Celsius. *Annales des Sciences Forestieres (Paris)*. 29:465-474
- Donaldson, L. (2007) Cellulose microfibril aggregates and their size variation with cell wall type. *Wood Science and Technology*. 41:443-460
- Donaldson, L. (2008) Microfibril angle: Measurement, variation and relationships - A review. *IAWA Journal*. 29:345-386

- Dong, F., Olsson, A. M., Salmén, L. (2010) Fibre morphological effects on mechano-sorptive creep. *Wood Science and Technology*. 44:475-483
- Downes, J. G., Mackay, B. H. (1958) Sorption kinetics of water vapor in wool fibers. *Journal of Polymer Science*. 28:45-67
- Eder, M., Burgert, I., Stanzl-Tschegg, S. (2006) Relaxation experiments on wood fibres and tissues. *Proceedings of the Third International Conference of the European Society of Wood Mechanics*, Vila Real, Portugal. 141-147
- Eichhorn, S. J., Sirichaisit, J., Young, R. J. (2001) Deformation mechanisms in cellulose fibres, paper and wood. *Journal of Materials Science*. 36:3129-3135
- Eitelberger, J., Svensson, S., Hofstetter, K. (2011) Theory of transport processes in wood below the fiber saturation point: Physical background on the microscale and its macroscopic description. *Holzforschung*. 65:337-342
- Emons, A. M. C. (1988) Methods for visualizing cell-wall texture. *Acta Botanica Neerlandica*. 37:31-38
- Eyring, H. (1935) The activated complex and the absolute rate of chemical reactions. *Chemical Reviews*. 17:65-77
- Eyring, H. (1936) Viscosity, plasticity, and diffusion as examples of absolute reaction rates. *Journal of Chemical Physics*. 4:283-291
- Eyring, H. (1938) The theory of absolute reaction rates. *Transactions of the Faraday Society*. 34:0041-0048
- Eyring, H. (1962) Transmission coefficient in reaction rate. *Reviews of Modern Physics*. 34:616-619
- Eyring, H., Halsey, G. (1946) The mechanical properties of textiles, 3. *Textile Research Journal*. 16:13-25
- Eyring, H., Ree, T., Hirai, N. (1958) The viscosity of high polymers - the random walk of a group of connected segments. *Proceedings of the National Academy of Sciences of the United States of America*. 44:1213-1217
- Fahlén, J. (2005) The cell wall ultrastructure of wood fibres - effects of the chemical pulp fibre line. PhD thesis. Royal Institute of Technology, KTH, Stockholm, Sweden
- Fahlén, J., Salmén, L. (2002) On the lamellar structure of the tracheid cell wall. *Plant Biology*. 4:339-345
- Fahlén, J., Salmén, L. (2003) Cross-sectional structure of the secondary wall of wood fibers as affected by processing. *Journal of Materials Science*. 38:119-126
- Fahlén, J., Salmén, L. (2005) Pore and matrix distribution in the fiber wall revealed by atomic force microscopy and image analysis. *Biomacromolecules*. 6:433-438
- Fan, C. F. (1995) Yielding of a model glassy polycarbonate under tension - a molecular mechanics simulation. *Macromolecules*. 28:5215-5224
- Fengel, D., Stoll, M. (1973) Variation of cell cross area, thickness of cell-wall and of wall layers of sprucewood tracheids within an annual ring. *Holzforschung*. 27:1-7
- Fleming, G. K., Koros, W. J. (1986) Dilation of polymers by sorption of carbon-dioxide at elevated pressures, 1: Silicone-rubber and unconditioned polycarbonate. *Macromolecules*. 19:2285-2291
- Forest Products Laboratory (2010) Wood handbook - wood as an engineering material, Centennial edition. Tech. Rep. FPL-GTR-190, US Department of Agriculture, Forest Service, Forest Products Laboratory, Madison, WI, USA
- Frandsen, H. L., Damkilde, L., Svensson, S. (2007) A revised multi-Fickian moisture transport model to describe non-Fickian effects in wood. *Holzforschung*. 61:563-572
- Fromm, J., Rockel, B., Lautner, S., Windeisen, E., Wanner, G. (2003) Lignin distribution in wood cell walls determined by TEM and backscattered SEM techniques. *Journal of Structural Biology*. 143:77-84

- Gao, H. (1994) Dynamic mechanical analysis of wood and wood-based composites. PhD thesis. Oregon State University, Corvallis, OR, USA
- Gerhards, C. C. (1982) Effect of moisture-content and temperature on the mechanical properties of wood - an analysis of immediate effects. *Wood and Fiber*. 14:4-36
- Gibson, E. J. (1965) Creep of wood - role of water and effect of a changing moisture content. *Nature*. 206:213-215
- Gierlinger, N., Schwanninger, M., Reinecke, A., Burgert, I. (2006) Molecular changes during tensile deformation of single wood fibers followed by Raman microscopy. *Biomacromolecules*. 7:2077-2081
- Goring, D. A. I., Timell, T. E. (1962) Molecular weight of native celluloses. *Tappi*. 45:454-460
- Goring, D. A. I. (1963) Thermal softening of lignin, hemicellulose and cellulose. *Pulp and Paper Magazine of Canada*. T517-T527
- Green, D. W., Kretschmann, D. E. (1994) Moisture content and the properties of clear southern pine. Res. Pap. FPL-RP-531, US Department of Agriculture, Forest Service, Forest Products Laboratory, Madison, WI, USA
- Griffin, D. M. (1977) Water potential and wood-decay fungi. *Annual Review of Phytopathology*. 15:319-329
- Gril, J., Hunt, D., Thibaut, B. (2004) Using wood creep data to discuss the contribution of cell-wall reinforcing material. *Comptes Rendus Biologies*. 327:881-888
- Ha, M. A., Apperley, D. C., Evans, B. W., Huxham, M., Jardine, W. G., Viëtor, R. J., Reis, D., Vian, B., Jarvis, M. C. (1998) Fine structure in cellulose microfibrils: NMR evidence from onion and quince. *Plant Journal*. 16:183-190
- Habeger, C. C., Coffin, D. W., Hojjatie, B. (2001) Influence of humidity cycling parameters on the moisture-accelerated creep of polymeric fibers. *Journal of Polymer Science Part B-Polymer Physics*. 39:2048-2062
- Halsey, G., White, H. J., Eyring, H. (1945) Mechanical properties of textiles, 1. *Textile Research Journal*. 15:295-311
- Handa, T., Fukuoka, M., Yoshizawa, S., Kanamoto, T. (1982) The effect of moisture on the dielectric relaxations in wood. *Journal of Applied Polymer Science*. 27:439-453
- Hanhijärvi, A. (1995) Deformation kinetics based rheological model for the time-dependent and moisture induced deformation of wood. *Wood Science and Technology*. 29:191-199
- Hanhijärvi, A., Hunt, D. (1998) Experimental indication of interaction between viscoelastic and mechano-sorptive creep. *Wood Science and Technology*. 32:57-70
- Hanley, S. J., Revol, J. F., Godbout, L., Gray, D. G. (1997) Atomic force microscopy and transmission electron microscopy of cellulose from *Micrasterias denticulata*; evidence for a chiral helical microfibril twist. *Cellulose*. 4:209-220
- Hartley, I. D., Avramidis, S. (1996) Static dimensional changes of Sitka spruce and Western hemlock influenced by sorption conditions. *Journal of the Institute of Wood Science*. 14:83-88
- Haslach, H. W. (1994) The mechanics of moisture accelerated tensile creep in paper. *Tappi Journal*. 77:179-186
- Hearmon, R. F. S., Paton, J. M. (1964) Moisture content changes and creep of wood. *Forest Products Journal*. 14:357-359
- Hendershot, O. P. (1924) Thermal expansion of wood. *Science*. 60:456-457
- Hermans, P.H. (1949) *Physics and chemistry of cellulose fibers*. New York-Amsterdam-London-Brussels Elsevier Publishing Co. Inc., pp 180-196
- Hernández, R. E. (1993) Influence of moisture sorption history on the swelling of Sugar maple wood and some tropical hardwoods. *Wood Science and Technology*. 27:337-345

- Hernández, R. E., Bizoň, M. (1994) Changes in shrinkage and tangential compression strength of Sugar maple below and above the fiber saturation point. *Wood and Fiber Science*. 26:360-369
- Hidaka, H., Kim, U. J., Wada, M. (2010) Synchrotron X-ray fiber diffraction study on the thermal expansion behavior of cellulose crystals in tension wood of Japanese poplar in the low-temperature region. *Holzforschung*. 64:167-171
- Hiebl, M., Maksymiw, R. (1991) Anomalous temperature-dependence of the thermal expansion of proteins. *Biopolymers*. 31:161-167
- Higgins, H. G. (1958) Structure and properties of paper, 9: Some critical problems. *APPITA*. 12:1-17
- Higuchi, T. (1997) *Biochemistry and molecular biology of wood*. Springer-Verlag, Berlin
- Hill, C. A. S., Forster, S. C., Farahani, M. R. M., Hale, M. D. C., Ormondroyd, G. A., Williams, G. R. (2005) An investigation of cell wall micropore blocking as a possible mechanism for the decay resistance of anhydride modified wood. *International Biodeterioration & Biodegradation*. 55:69-76
- Hill, R. L. (1967) Creep behavior of individual pulp fibers under tensile stress. *Tappi*. 50:432-440
- Hinterstoisser, B., Åkerholm, M., Salmén, L. (2003) Load distribution in native cellulose. *Biomacromolecules*. 4:1232-1237
- Hoffmeyer, P., Jensen, S.K., Jones, D., Klinke, H.B., Felby, C. (2003) Sorption properties of steam treated wood and plant fibres. *Proceedings of the First European Conference on Wood Modification, Ghent, Belgium*. 177-189
- Hofstetter, K., Hinterstoisser, B., Salmén, L. (2006) Moisture uptake in native cellulose - the roles of different hydrogen bonds: a dynamic FT-IR study using Deuterium exchange. *Cellulose*. 13:131-145
- Hofstetter, K., Gamstedt, K. (2009) Hierarchical modelling of microstructural effects on mechanical properties of wood – a review. *Holzforschung*. 63:130-138
- Holland, H. D., Halsey, G., Eyring, H. (1946) Mechanical properties of textiles, 6: A study of creep of fibers. *Textile Research Journal*. 16:201-210
- Hon, D. N. S. (1994) Cellulose - a random-walk along its historical path. *Cellulose*. 1:1-25
- Hori, R., Wada, M. (2005) The thermal expansion of wood cellulose crystals. *Cellulose*. 12:479-484
- Horikawa, Y., Sugiyama, J. (2009) Localization of crystalline allomorphs in cellulose microfibril. *Biomacromolecules*. 10:2235-2239
- Hossain, D., Tschopp, M. A., Ward, D. K., Bouvard, J. L., Wang, P., Horstemeyer, M. F. (2010) Molecular dynamics simulations of deformation mechanisms of amorphous polyethylene. *Polymer*. 51:6071-6083
- Hult, E. L., Iversen, T., Sugiyama, J. (2003) Characterization of the supermolecular structure of cellulose in wood pulp fibres. *Cellulose*. 10:103-110
- Hult, E. L., Larsson, P. T., Iversen, T. (2001) Cellulose fibril aggregation - an inherent property of kraft pulps. *Polymer*. 42:3309-3314
- Hunt, D. G., Shelton, C. F. (1988) Longitudinal moisture-shrinkage coefficients of softwood at the mechano-sorptive creep limit. *Wood Science and Technology*. 22:199-210
- Hunt, D. G. (1997) Dimensional changes and creep of spruce, and consequent model requirements. *Wood Science and Technology*. 31:3-16
- Imai, T., Sugiyama, J. (1998) Nanodomains of I-alpha and I-beta cellulose in algal microfibrils. *Macromolecules*. 31:6275-6279

- Imamura, K., Sakaura, K., Ohyama, K., Fukushima, A., Imanaka, H., Sakiyama, T., Nakanishi, K. (2006) Temperature scanning FTIR analysis of hydrogen bonding states of various saccharides in amorphous matrixes below and above their glass transition temperatures. *Journal of Physical Chemistry B*. 110:15094-15099
- Irvine, G. M. (1984) The glass transitions of lignin and hemicellulose and their measurement by differential thermal-analysis. *Tappi Journal*. 67:118-121
- Ishimaru, Y., Arai, K., Mizutani, M., Oshima, K., Iida, I. (2001) Physical and mechanical properties of wood after moisture conditioning. *Journal of Wood Science*. 47:185-191
- Iwamoto, S., Kai, W. H., Isogai, A., Iwata, T. (2009) Elastic modulus of single cellulose microfibrils from tunicate measured by atomic force microscopy. *Biomacromolecules*. 10:2571-2576
- Jang, S. S., Jo, W. H. (1999a) Analysis of the mechanical behavior of amorphous atactic poly(oxypropylene) by atomistic modeling. *Macromolecular Theory and Simulations*. 8:1-9
- Jang, S. S., Jo, W. H. (1999b) Yielding and plastic behaviour of amorphous atactic poly(oxypropylene) under uniaxial compression: an atomistic modeling approach. *Polymer*. 40:919-925
- Jeffrey, G. A., Saenger, W. (1991) *Hydrogen bonding in biological structures*. Springer-Verlag, New York
- Jentzen, C. A. (1964) The effect of stress applied during drying on some of the properties of individual pulp fibers. The Institute of Paper Chemistry, Lawrence College, Appleton, WI, USA
- Joseleau, J. P., Ruel, K. (2007) Condensed and non-condensed lignins are differentially and specifically distributed in the cell walls of softwoods, hardwoods and grasses. *Cellulose Chemistry and Technology*. 41:487-494
- Jurasek, L. (1995) Toward a three-dimensional model of lignin structure. *Journal of Pulp and Paper Science*. 21:J274-J279
- Kamiya, Y., Bourbon, D., Mizoguchi, K., Naito, Y. (1992) Sorption, dilation, and isothermal glass-transition of poly(ethyl methacrylate)-organic gas systems. *Polymer Journal*. 24:443-449
- Kamiya, Y., Mizoguchi, K., Naito, Y., Hirose, T. (1986) Gas sorption in poly(vinyl benzoate). *Journal of Polymer Science Part B-Polymer Physics*. 24:535-547
- Kangas, K., Baudin, A. (2003) Modelling and projections of forest products demand, supply and trade in Europe. Geneva Timber and Forest Discussion Papers, ECE/TIM/DP/30, United Nations, Geneva, Switzerland
- Kauzmann, W., Eyring, H. (1940) The viscous flow of large molecules. *Journal of the American Chemical Society*. 62:3113-3125
- Keckes, J., Burgert, I., Frühmann, K., Müller, M., Kölln, K., Hamilton, M., Burghammer, M., Roth, S. V., Stanzl-Tschegg, S., Fratzl, P. (2003) Cell-wall recovery after irreversible deformation of wood. *Nature Materials*. 2:810-814
- Kelley, S. S., Rials, T. G., Glasser, W. G. (1987) Relaxation behavior of the amorphous components of wood. *Journal of Materials Science Letters*. 22:617-624
- Kerner, E. H. (1956) The elastic and thermo-elastic properties of composite media. *Proceedings of the Physical Society of London Section B*. 69:808-813
- Kingston, R. S. T., Armstrong, L. D. (1951) Creep in initially green wooden beams. *Australian Journal of Applied Science*. 2:306-325
- Kingston, R. S. T., Clarke, L. N. (1961) Some aspects of the rheological behavior of wood, II: Analysis of creep data by reaction-rate. *Australian Journal of Applied Science*. 12:227-240
- Kollmann, F. (1962) Eine Gleichung der Sorptionsisotherme. *Naturwissenschaften*. 49:206-207

- Kölln, K. (2004) Morphology and mechanical characteristics of cellulose fibres – investigations with X-ray and neutron scattering. PhD thesis. Christian-Albrechts-Universität, Kiel, Germany
- Krabbenhøft, K., Damkilde, L. (2004) A model for non-Fickian moisture transfer in wood. *Materials and Structures*. 37:615-622
- Krausz, A. S., Eyring, H. (1971) Chemical kinetics of plastic deformation. *Journal of Applied Physics*. 42:2382-2385
- Kretschmann, D. E., Green, D. W. (1996) Modeling moisture content-mechanical property relationships for clear southern pine. *Wood and Fiber Science*. 28:320-337
- Kubler, H., Liang, L., Chang, S. (1973) Thermal expansion of moist wood. *Wood and Fiber Science*. 5:257-267
- Langer, V., Lundquist, K., Miksche, G. E. (2005) erythro-2-(2,6-dimethoxy-4-methylphenoxy)-1-(4-hydroxy-3,5-dimethoxyphenyl)propane-1,3-diol. *Acta Crystallographica Section E-Structure Reports Online*. 61:O1001-O1003
- La Placa, S. J., Post, B. (1960) Thermal expansion of ice. *Acta Crystallographica*. 13:503-505
- Larsson, P. T., Hult, E. L., Wickholm, K., Pettersson, E., Iversen, T. (1999) CP/MAS C-13-NMR spectroscopy applied to structure and interaction studies on cellulose I. *Solid State Nuclear Magnetic Resonance*. 15:31-40
- Lasater, J. A., Nimer, E. L., Eyring, H. (1953) Mechanical properties of cotton fibers, 1: Relaxation in air and water. *Textile Research Journal*. 23:237-242
- Li, Q., Renneckar, S. (2011) Supramolecular structure characterization of molecularly thin cellulose I nanoparticles. *Biomacromolecules*. 12:650-659
- Liang, C. Y., Bassett, K. H., McGinnes, E. A., Marchessault, R. H. (1960) Infrared spectra of crystalline polysaccharides VII – thin wood sections. *Tappi*. 43:1017-1024
- Lippincott, E. R., Schroeder, R. (1955) One-dimensional model of the hydrogen bond. *Journal of Chemical Physics*. 23:1099-1106
- Lotfy, M., El-osta, M., Wellwood, R. W. (1972) Short-term creep as related to microfibril angle. *Wood and Fiber Science*. 4:26-32
- Lutz, E. T. G., van der Maas, J. H. (1994) Hydrogen-bonds in crystalline carbohydrates - a variable-temperature FT-IR study. *Journal of Molecular Structure*. 324:123-132
- Marchessault, R. H., Liang, C. Y. (1962) Infrared spectra of crystalline polysaccharides, 8: Xylans. *Journal of Polymer Science*. 59:357-378
- Mark, H. (1928) The physical ground base of micellar theory. *Naturwissenschaften*. 16:892-900
- Mark, H. (1940) Intermicellar hole and tube system in fiber structure. *Journal of Physical Chemistry*. 44:764-788
- Mark, R. E. (1967) Cell wall mechanics of tracheids. Yale University Press, New Haven
- Matsuo, M., Sawatari, C., Iwai, Y., Ozaki, F. (1990) Effect of orientation distribution and crystallinity on the measurement by X-Ray-diffraction of the crystal-lattice moduli of cellulose-I and cellulose-II. *Macromolecules*. 23:3266-3275
- Matthews, J. F., Skopec, C. E., Mason, P. E., Zuccato, P., Torget, R. W., Sugiyama, J., Himmel, M. E., Brady, J. W. (2006) Computer simulation studies of microcrystalline cellulose I beta. *Carbohydrate Research*. 341:138-152
- Mauze, G. R., Stern, S. A. (1984) The dual-mode solution of vinyl chloride monomer in poly(vinyl chloride). *Journal of Membrane Science*. 18:99-109
- Meares, P. (1954) The diffusion of gases through polyvinyl acetate. *Journal of the American Chemical Society*. 76:3415-3422

- Meshitsuka, G., Nakano, J. (1985) Structural characteristics of compound middle lamella lignin. *Journal of Wood Chemistry and Technology*. 5:391-404
- Morlier, P., Palka, L. C. (1994) Basic knowledge. *In: Creep in timber structures* (Morlier, P., ed.), Rilem Report 8, E & FN Spon, New York, 9-42
- Mukherjee, S. M., Sikorski, J., Woods, H. J. (1951) Micellar structure of native cellulose. *Nature*. 167:821-822
- Murata, K., Masuda, M. (2006) Microscopic observation of transverse swelling of latewood tracheid: effect of macroscopic/mesoscopic structure. *Journal of Wood Science*. 52:283-289
- Newman, R. H., Hemmingson, J. A. (1995) C-13 NMR distinction between categories of molecular order and disorder in cellulose. *Cellulose*. 2:95-110
- Newns, A. C. (1956) The sorption and desorption kinetics of water in a regenerated cellulose. *Transactions of the Faraday Society*. 52:1533-1545
- Newns, A. C. (1959) The sorption and desorption kinetics of water in a regenerated cellulose. *Journal of Polymer Science*. 41:425-434
- Newns, A. C. (1975a) Some effects of formaldehyde crosslinking on kinetics of water-vapor sorption in cellulose. *Polymer*. 16:2-4
- Newns, A. C. (1975b) Sorption and desorption-kinetics of cellulose and water system, 3: Rates of sorption on lowest sorption limb of a hysteresis loop. *Journal of the Chemical Society-Faraday Transactions I*. 71:278-284
- Nishino, T., Takano, K., Nakamae, K. (1995) Elastic-modulus of the crystalline regions of cellulose polymorphs. *Journal of Polymer Science Part B-Polymer Physics*. 33:1647-1651
- Nishiyama, Y., Langan, P., Chanzy, H. (2002) Crystal structure and hydrogen-bonding system in cellulose I-beta from synchrotron x-ray and neutron fiber diffraction. *Journal of the American Chemical Society*. 124:9074-9082
- Nishiyama, Y., Sugiyama, J., Chanzy, H., Langan, P. (2003) Crystal structure and hydrogen bonding system in cellulose I-alpha from synchrotron x-ray and neutron fiber diffraction. *Journal of the American Chemical Society*. 125:14300-14306
- Nissan, A. H. (1957a) The rheological behaviour of hydrogen-bonded solids, 1: Primary considerations. *Transactions of the Faraday Society*. 53:700-709
- Nissan, A. H. (1957b) The rheological behaviour of hydrogen-bonded solids, 2: Derivative phenomena. *Transactions of the Faraday Society*. 53:710-721
- Nissan, A. H. (1976a) Three modes of dissociation of H-bonds in hydrogen-bond dominated solids. *Nature*. 263:759
- Nissan, A. H. (1976b) H-bond dissociation in hydrogen-bond dominated solids. *Macromolecules*. 9:840-850
- Nissan, A. H. (1977a) Effects of water on Young's modulus of paper. *Tappi*. 60:98-101
- Nissan, A. H. (1977b) Elastic-modulus of lignin as related to moisture-content. *Wood Science and Technology*. 11:147-151
- Nissan, A. H., Batten, G. L. (1990) On the primacy of the hydrogen-bond in paper mechanics. *Tappi Journal*. 73:159-164
- Nissan, A. H., Batten, G. L. (1997) The link between the molecular and structural theories of paper elasticity. *Tappi Journal*. 80:153-158
- Novak, A. (1974) Hydrogen bonding in solids: correlation of spectroscopic and crystallographic data. *Structure and Bonding*. 18:177-216

- Nyrud, A. Q., Bringslimark, T. (2010) Is interior wood use psychologically beneficial? A review of psychological responses toward wood. *Wood and Fiber Science*. 42:202-218
- Ohad, I., Danon, D. (1964) On dimensions of cellulose microfibrils. *Journal of Cell Biology*. 22:302-305
- Olsson, A. M., Salmén, L. (2001) Molecular mechanisms involved in creep phenomena of paper. *Journal of Applied Polymer Science*. 79:1590-1595
- Olsson, A. M., Salmén, L. (2004a) The association of water to cellulose and hemicellulose in paper examined by FTIR spectroscopy. *Carbohydrate Research*. 339:813-818
- Olsson, A. M., Salmén, L. (2004b) The softening behavior of hemicelluloses related to moisture. *Hemicelluloses: Science and Technology*. 864:184-197
- Olsson, A. M., Salmén, L., Eder, M., Burgert, I. (2007) Mechano-sorptive creep in wood fibres. *Wood Science and Technology*. 41:59-67
- O'Sullivan, A. C. (1997) Cellulose: the structure slowly unravels. *Cellulose*. 4:173-207
- Persson, K. (2000) Micromechanical modelling of wood and fibre properties. PhD thesis. Lund University, Lund, Sweden
- Petridis, L., Smith, J. C. (2009) A molecular mechanics force field for lignin. *Journal of Computational Chemistry*. 30:457-467
- Peura, M., Kölln, K., Grotkopp, I., Saranpää, P., Müller, M., Serimaa, R. (2007) The effect of axial strain on crystalline cellulose in Norway spruce. *Wood Science and Technology*. 41:565-583
- Pierlot, A. P. (1999) Water in wool. *Textile Research Journal*. 69:97-103
- Pizzi, A., Bariska, M., Eaton, N. J. (1987a) Theoretical water sorption energies by conformational-analysis, 2: Amorphous cellulose and the sorption isotherm. *Wood Science and Technology*. 21:317-327
- Pizzi, A., Eaton, N. J., Bariska, M. (1987b) Theoretical water sorption energies by conformational-analysis, 1: Crystalline cellulose-I. *Wood Science and Technology*. 21:235-248
- Qian, X. H. (2008) The effect of cooperativity on hydrogen bonding interactions in native cellulose I beta from ab initio molecular dynamics simulations. *Molecular Simulation*. 34:183-191
- Qian, X. H., Ding, S. Y., Nimlos, M. R., Johnson, D. K., Himmel, M. E. (2005) Atomic and electronic structures of molecular crystalline cellulose I beta: A first-principles investigation. *Macromolecules*. 38:10580-10589
- Ramiah, M. V., Goring, D. A. I. (1965) Thermal expansion of cellulose, hemicellulose and lignin. *Journal of Polymer Science Part C-Polymer Symposium*. 27-48
- Ree, T., Chen, M. C., Eyring, H. (1951) Molecular theory of damping in fibers. *Textile Research Journal*. 21:789-804
- Ree, T., Eyring, H. (1955) Theory of non-Newtonian flow, 1: Solid plastic system. *Journal of Applied Physics*. 26:793-800
- Reichardt, C. H., Eyring, H. (1946) Mechanical properties of textiles, 11: Application of the theory of the 3-element model to stress-strain experiments on cellulose acetate filaments. *Textile Research Journal*. 16:635-642
- Reichardt, C. H., Halsey, G., Eyring, H. (1946) Mechanical properties of textiles, 10: Analysis of Steinberger data on creep of cellulose acetate filaments. *Textile Research Journal*. 16:382-389
- Reina, J. J., Domínguez, E., Heredia, A. (2001) Water sorption-desorption in conifer cuticles: The role of lignin. *Physiologia Plantarum*. 112:372-378

- Reuss, A. (1929) Berechnung der Fließgrenze von Mischkristallen auf Grund der Plastizitätsbedingung für Einkristalle. *Zeitschrift für Angewandte Mathematik und Mechanik*. 9:49-58
- Rocco, V. M., Pochettino, T., Moro, A. (2010) The renewable sources materials incidence of on building performance – the wood case study. *Proceedings of the World Conference on Timber Engineering*, Trentino, Italy
- Roussel, M. R., Lim, C. (1995) Dynamic-model of lignin growing in restricted spaces. *Macromolecules*. 28:370-376
- Ruel, K., Barnoud, F., Goring, D. A. I. (1978) Lamellation in S2 layer of softwood tracheids as demonstrated by scanning-transmission electron-microscopy. *Wood Science and Technology*. 12:287-291
- Ruel, K., Chevallier-Billosta, V., Guillemin, F., Sierra, J. B., Joseleau, J. P. (2006) The wood cell wall at the ultrastructural scale - formation and topochemical organization. *Maderas. Ciencia y tecnologia*. 8:107-116
- Sadoh, T. (1960) Studies on the sorption of water vapour by wood hemicellulose, 2: Amount of vapour adsorbed. *The scientific reports of Kyoto Prefectural University, Agriculture*. 12:113-118
- Sadoh, T., Christensen, G. N. (1964) Rate of sorption of water vapour by hemicellulose. *Australian Journal of Applied Science*. 15:297-308
- Sakurada, I., Nukushina, Y., Ito, T. (1962) Experimental determination of elastic modulus of crystalline regions in oriented polymers. *Journal of Polymer Science*. 57:651-660
- Salmén, L. (1982) Temperature and water induced softening behaviour of wood fiber based materials. PhD thesis. Royal Institute of Technology, KTH, Stockholm, Sweden
- Salmén, L., Burgert, I. (2009) Cell wall features with regard to mechanical performance. A review COST Action E35 2004-2008: Wood machining - micromechanics and fracture. *Holzforschung*. 63:121-129
- Salmén, L., Olsson, A. M. (1998) Interaction between hemicelluloses, lignin and cellulose: Structure-property relationships. *Journal of Pulp and Paper Science*. 24:99-103
- Seborg, C. O., Simmonds, F. A., Baird, P. K. (1938) Sorption of water vapor by papermaking materials: Irreversible loss of hygroscopicity due to drying. *Paper Trade Journal*. 107:223-228
- Sedlachek, K. M. (1995) The effect of hemicelluloses and cyclic humidity on the creep of single fibers. PhD thesis. Institute of Paper Science and Research, Atlanta, GA, USA
- Seifert, J. (1972) Sorption and swelling of wood and wood base materials, 2: Swelling behavior of wood and wood base materials. *Holz Als Roh- und Werkstoff*. 30:294-303
- Sheppard, S. E. (1933) The structure of xerogels of cellulose and derivatives. *Transactions of the Faraday Society*. 29:0077-0085
- Sjöström, E. (1993) Wood chemistry – fundamentals and applications. Academic Press, San Diego
- Skaar, C. (1988) Wood-water relations. Springer-Verlag, Berlin Heidelberg
- Somerville, C., Bauer, S., Brininstool, G., Facette, M., Hamann, T., Milne, J., Osborne, E., Paredes, A., Persson, S., Raab, T., Vorwerk, S., Youngs, H. (2004) Toward a systems approach to understanding plant-cell walls. *Science*. 306:2206-2211
- Spalt, H. A. (1958) The fundamentals of water sorption by wood. *Forest Products Journal*. 8:288-295
- Srinivasan, P. S. (1941) The elastic and thermal properties of timber. *Quarterly Journal of the Indian Institute of Science*. 4:222-314, quoted from (Cousins et al. 1975)
- Stamm, A. J. (1950) Bound water and hydration. *Tappi*. 33:435-439
- Stamm, A. J. (1959) Bound water diffusion into wood in the fiber direction. *Forest Products Journal*. 9:27-32

- Stamm, A. J., Hansen, L. A. (1938) Surface-bound versus capillary-condensed water in wood. *Journal of Physical Chemistry*. 42:209-214
- Steinberger, R. L. (1936) Creep in cellulose acetate filaments. *Textile Research Journal*. 6:191-206
- Stamm, A. J. (1956) Thermal degradation of wood and cellulose. *Industrial and Engineering Chemistry*. 48:413-417
- Stamm, A. J. (1964) *Wood and cellulose science*. The Ronald Press Company, New York
- Stevanic, J. S. (2008) Ultrastructure of the primary cell wall of softwood fibres studied using dynamic FT-IR spectroscopy. lic.tech. thesis. Royal Institute of Technology, KTH, Stockholm, Sweden
- Stevanic, J. S., Salmén, L. (2006) The primary cell wall studied by dynamic 2D FT-IR: Interaction among components in Norway spruce (*Picea abies*). *Cellulose Chemistry and Technology*. 40:761-767
- Stevanic, J. S., Salmén, L. (2009) Orientation of the wood polymers in the cell wall of spruce wood fibres. *Holzforschung*. 63:497-503
- Stevens, V., Kühne, G., Wienhaus, O. (1983) Untersuchungen zum thermoplastischen Verhalten von Ligninen. *Wissenschaftliche Zeitschrift der Technischen Universität Dresden*. 32:149-154
- Stone, J. E., Scallan, A. M. (1967) Effect of component removal upon porous structure of cell wall of wood, 2: Swelling in water and fiber saturation point. *Tappi*. 50:496-501
- Struik, L. C. E. (1987a) The mechanical and physical aging of semicrystalline polymers, 1. *Polymer*. 28:1521-1533
- Struik, L. C. E. (1987b) The mechanical behavior and physical aging of semicrystalline polymers, 2. *Polymer*. 28:1534-1542
- Šturcová, A., Davies, G. R., Eichhorn, S. J. (2005) Elastic modulus and stress-transfer properties of tunicate cellulose whiskers. *Biomacromolecules*. 6:1055-1061
- Sugiyama, J., Harada, H., Fujiyoshi, Y., Uyeda, N. (1985) Lattice images from ultrathin sections of cellulose microfibrils in the cell-wall of *Valonia macrophysa* Kutz. *Planta*. 166:161-168
- Sugiyama, J., Vuong, R., Chanzy, H. (1991) Electron diffraction study on the two crystalline phases occurring in native cellulose from an algal cell wall. *Macromolecules*. 24:4168-4175
- Takahashi, C., Nakazawa, N., Ishibashi, K., Iida, I., Furuta, Y., Ishimaru, Y. (2006) Influence of variation in modulus of elasticity on creep of wood during changing process of moisture. *Holzforschung*. 60:445-449
- Tanaka, F., Iwata, T. (2006) Estimation of the elastic modulus of cellulose crystal by molecular mechanics simulation. *Cellulose*. 13:509-517
- Terashima, N., Fukushima, K. (1988) Heterogeneity in formation of lignin, 11: An autoradiographic study of the heterogeneous formation and structure of pine lignin. *Wood Science and Technology*. 22:259-270
- Terashima, N., Seguchi, Y. (1988) Heterogeneity in formation of lignin, 9: Factors affecting the formation of condensed structures in lignin. *Cellulose Chemistry and Technology*. 22:147-154
- Tobolsky, A., Eyring, H. (1943) Mechanical properties of polymeric materials. *Journal of Chemical Physics*. 11:125-134
- Urquhart, A. R. (1929) The mechanism of the adsorption of water by cotton. *Journal of the Textile Institute*. 20:T125-T132
- Urquhart, A. R., Eckersall, N. (1930) The moisture relations of cotton, VII: A study of hysteresis. *Journal of the Textile Institute*. 21:T499-T510

- van der Put, T. A. C. M. (1989) Deformation and damage processes in wood. DSc thesis. Delft University of Technology, Delft, The Netherlands
- Vanderhart, D. L., Atalla, R. H. (1984) Studies of microstructure in native celluloses using solid-state C-13 NMR. *Macromolecules*. 17:1465-1472
- Vintila, E. (1939) Untersuchungen über Raumgewicht und Schwindmass von Früh- und Spätholz bei Nadelhölzern. *European Journal of Wood and Wood Products*. 2:345-357
- Voigt, W. (1889) Ueber die Beziehung zwischen den beiden Elasticitätsconstanten isotroper Körper. *Annalen der Physik*. 274:573-587
- Vrentas, J. S., Duda, J. L., Ling, H. C. (1988) Antiplasticization and volumetric behavior in glassy-polymers. *Macromolecules*. 21:1470-1475
- Vrentas, J. S., Vrentas, C. M. (1991) Sorption in glassy-polymers. *Macromolecules*. 24:2404-2412
- Vrentas, J. S., Vrentas, C. M. (1996) Hysteresis effects for sorption in glassy polymers. *Macromolecules*. 29:4391-4396
- Wada, M., Okano, T. (2001) Localization of I-alpha and I-beta phases in algal cellulose revealed by acid treatments. *Cellulose*. 8:183-188
- Weatherwax, R. C., Stamm, A. J. (1956) The coefficients of thermal expansion of wood and wood products. Tech. Rep. 1487, US Department of Agriculture, Forest Service, Forest Products Laboratory, Madison, WI, USA
- Weichert, L. (1963) Investigations on sorption and swelling of spruce, beech and compressed beech wood at temperatures between 20 C and 100 C. *Holz als Roh- und Werkstoff*. 21:290-300
- Wickholm, K., Larsson, P. T., Iversen, T. (1998) Assignment of non-crystalline forms in cellulose I by CP/MAS C-13 NMR spectroscopy. *Carbohydrate Research*. 312:123-129
- Wissinger, R. G., Paulaitis, M. E. (1987) Swelling and sorption in polymer-CO₂ mixtures at elevated pressures. *Journal of Polymer Science Part B-Polymer Physics*. 25:2497-2510
- Wynne-Jones, W. F. K., Eyring, H. (1935) The absolute rate of reactions in condensed phases. *Journal of Chemical Physics*. 3:492-502
- Xu, P., Donaldson, L. A., Gergely, Z. R., Staehelin, L. A. (2007) Dual-axis electron tomography: a new approach for investigating the spatial organization of wood cellulose microfibrils. *Wood Science and Technology*. 41:101-116
- Yamamoto, H., Horii, F., Hirai, A. (1996) In situ crystallization of bacterial cellulose, 2: Influences of different polymeric additives on the formation of cellulose I-alpha and I-beta at the early stage of incubation. *Cellulose*. 3:229-242
- Yui, T., Nishimura, S., Akiba, S., Hayashi, S. (2006) Swelling behavior of the cellulose I beta crystal models by molecular dynamics. *Carbohydrate Research*. 341:2521-2530
- Åkerholm, M. (2003) Ultrastructural aspects of pulp fibers as studied by dynamic FT-IR spectroscopy. PhD thesis. Royal Institute of Technology, KTH, Stockholm, Sweden
- Åkerholm, M., Salmén, L. (2001) Interactions between wood polymers studied by dynamic FT-IR spectroscopy. *Polymer*. 42:963-969
- Åkerholm, M., Salmén, L. (2003) The oriented structure of lignin and its viscoelastic properties studied by static and dynamic FT-IR spectroscopy. *Holzforschung*. 57:459-465
- Åkerholm, M., Salmén, L. (2004) Softening of wood polymers induced by moisture studied by dynamic FTIR spectroscopy. *Journal of Applied Polymer Science*. 94:2032-2040

Appended papers

PAPER I

Water sorption in wood and modified wood at high values of relative humidity.

Part I: Results for untreated, acetylated and furfurylated Norway spruce

Thygesen L. G., Englund E. T. and Hoffmeyer P.

Holzforschung (2010) 64:315-323

Water sorption in wood and modified wood at high values of relative humidity. Part I: Results for untreated, acetylated, and furfurylated Norway spruce

Lisbeth G. Thygesen^{1,*}, Emil Tang Englund^{2,3}
and Preben Hoffmeyer³

¹ Forest and Landscape, University of Copenhagen,
Frederiksberg C, Denmark

² Wood and Textile, Danish Technological Institute,
Taastrup, Denmark

³ Department of Civil Engineering, Technical University of
Denmark, Lyngby, Denmark

*Corresponding author.

Forest and Landscape, University of Copenhagen, Rolighedsvej
23, DK-1958 Frederiksberg C, Denmark
E-mail: lgt@life.ku.dk

Abstract

Desorption isotherms at 20°C for untreated, acetylated, and furfurylated Norway spruce [*Picea abies* (L.) Karst.] sapwood were established in the 91.9–99.9% relative humidity (RH) range. Three methods were employed to secure various constant RH levels: saturated salt solutions, climate chambers, and the pressure plate technique. The curve form for the untreated samples did not show an upward bend, except perhaps above 99.5% RH, indicating that – contrary to what has hitherto been assumed – capillary condensation does not play a significant role for water sorption in wood below fiber saturation. Three additional results corroborate this conclusion: (1) calculation of the theoretical contribution of capillary condensation to the moisture content (MC) in wood based on idealized microstructural geometries by means of the Kelvin and Laplace equations resulted in very small contributions to the equilibrium moisture content (EMC), i.e., below 0.35% moisture at 99.9% RH. (2) The ratio between the EMC of acetylated and untreated samples did not show an increasing trend for increasing RH, as would have been the case if capillary condensation had taken place in both untreated and acetylated wood. (3) Low field time domain nuclear magnetic resonance results showed that only the relaxation curves from the furfurylated samples were affected systematically by freezing, indicating that neither untreated nor acetylated wood contained significant amounts of capillary condensed water.

Keywords: acetylation; capillary condensation; furfurylation; isotherm; sorption; wood-water relations.

Introduction

Moisture in wood has been studied for decades. Several explanations have been suggested regarding the way water

molecules are bound in the wood structure as a function of the relative humidity (RH). One such explanation often cited relates the uppermost part of the sorption isotherm to capillary condensation in voids in the material (Sheppard 1933; Barkas 1937; Babbitt 1943; Stamm 1950; Spalt 1958; Kollmann 1962; Simpson 1973). However, the question of capillary condensation at high levels of RH has not yet been resolved. The present study employs three techniques (saturated salt solutions, climate chambers, and the pressure plate technique) to examine the nature of moisture in wood in the RH range from 91.9% to 99.9%. Furthermore, two different types of chemically modified woods are included in the experiments as a tool to highlight the sorption behavior of untreated wood.

Void radii and capillary condensation

In the following, cavities, pores, voids, etc., in wood are categorized and termed according to their dimensions (Griffin 1977). This system complies better with wood anatomy than the IUPAC definition of pore size classes (Sing et al. 1985; Rouquerol et al. 1994). *Macrovoids* comprise the lumina of cells with radii from approximately 5 μm to 200 μm or greater. *Microvoids* include the pointed ends of lumens, pit apertures, pit-membrane voids, and other small voids with radii in the range from 5 nm to 5 μm . *Nanovoids* are found in the cell wall and range in size from 5 nm down to the level of single water molecules bound to hydrophilic sites of the wood polymer, at which level the concept of pore radii becomes meaningless. It is a generally accepted assumption that the dry cell wall is essentially non-porous (Griffin 1977; Fahlén and Salmén 2005; Salmén and Fahlén 2006) and that nanovoids emerge as a result of the presence of water. Measurements on different wood species in either green or saturated condition show a maximum nanovoid size of 1.8 nm for green spruce (Stone and Scallan 1968), 0.9–1.0 nm for green Sitka spruce (Tarkow et al. 1966), 0.8 nm for saturated sweetgum (Flournoy et al. 1991), and 2 nm for saturated Corsican pine (Hill et al. 2005).

The Kelvin equation relates the relative humidity to the void radius that leads to capillary condensation within voids of these dimensions. Corresponding values of RH and void radius are given in Table 1. It has long been debated in what range the Kelvin equation is valid. Skaar (1988) argued that below 80% RH the concept of capillary condensation is questionable, as at this RH the corresponding pore radius of 4.9 nm was only approximately 15 times the diameter of a water molecule (0.3 nm). Measurements of menisci in mica capillaries of 5 nm diameters confirm that the Kelvin equation is valid down to approximately 80% RH (Kohonen and

Table 1 Values of relative humidity (RH), capillary radius, and corresponding matrix component, ψ_m , of water potential at 20°C.

RH (%)	Water potential (MPa)	Capillary radius (μm)	Void type
99.999	-0.00136	108	Macro
99.99	-0.0136	10.8	
99.98	-0.0271	5.42	
99.9	-0.136	1.08	Micro
99.8	-0.271	0.542	
99.5	-0.679	0.216	
99	-1.36	0.108	
98	-2.74	0.0537	
97	-4.13	0.0357	
95	-6.95	0.0211	Nano
90	-14.3	0.0103	
85	-21.9	0.0067	
80	-30.2	0.00487	
75	-69.2	0.00378	

Christenson 2000). Other studies (Lastoskie et al. 1993; Rouquerol et al. 1999) have shown that the Kelvin equation cannot be extended below a void radius of 3.75 nm and a relative water vapor pressure of 75%. Below this pressure, the capillary condensation is controlled by the specific interaction between sorption sites and the condensed vapor and not by the Kelvin equation (Evans 1990). However, capillary condensation can still take place below 75% RH. For instance, Branton et al. (1995) have studied the capillary condensation in the porous silicate material MCM-41, which has a specific pore size of narrow distribution. They found that capillary condensation occurs in a narrow range of RH of approximately 55%. At such low RH, however, the mechanisms controlling the condensation cannot be described by the Kelvin equation. Consequently, the values of pore radii are presented in Table 1 as calculated from the Kelvin equation down to 75% RH.

Table 1 also lists water potentials as given by the Young-Laplace equation. This equation is very useful in pore size studies if the pressure plate technique (PPT) is used, also known as the suction technique, which is a method for studying desorption isotherms and pore size distributions at very high levels of RH. The pressure-EMC (equilibrium moisture content) relation can be transformed into a desorption isotherm for high values of RH and subsequently used for pore size assessment (Tremblay et al. 1996; Defo et al. 1999) by combining the Kelvin and the Laplace equations. However, caution should be exercised when interpreting such assessments because the method is strictly valid only for pores in a rigid material. However, the number and sizes of pores in wood are functions of RH. A drop in RH, therefore, results in pores losing some of their water while at the same time collapsing to the size in equilibrium with the new RH (Robertson 1965; Alinec 2002).

Water in wood

The general concept of water in wood used here is largely based on Berthold et al. (1996) and Salmén (1997). According to these authors, water is held as non-freezing bound water, freezing bound water, and free water. This classification is a refinement of that used by Stamm (1950), who did not distinguish between the two bound water types. *Non-freezing bound water* is water specifically bound to hydrophilic sites (hydroxyl groups) of the three main wood polymers, mainly hemicelluloses. In uncharged carbohydrates, each polar hydroxyl group has on average approximately one water molecule adsorbed at 92% RH, increasing to approximately 1.3 at 98% RH (Berthold et al. 1994). Non-freezing bound water is found in nanovoids and as wall lining of macrovoids and microvoids. *Freezing bound water* is the more loosely bound water in the larger water clusters. Thus, freezing bound water is only indirectly bound to the hydrophilic sites of the wood polymers. Freezing bound water is found at high RH in nanovoids and as wall lining of macrovoids and microvoids. This type of water exhibits freezing point lowering. Berthold et al. (1994) did not find by differential scanning calorimetry any freezing bound water down to -90°C in uncharged carbohydrates for EMCs up to 98% RH. Freezing bound water was only found in carbohydrates containing charged groups. *Free water* in wood is held in microvoids and macrovoids. The term *free* only signifies that water molecules are not bound to specific sorption sites; it is still bound by capillary forces and has a negative water potential. Stamm (1950) refers to this type of water in wood as capillary water. This type of water exhibits little freezing point lowering.

Water in modified wood

One of the purposes of the present work was to study moisture in acetylated wood and in furfurylated wood at high RH. Both treatments are chemical modifications aimed at reducing the moisture uptake thus enhancing dimensional stability and decay resistance.

Regarding acetylation, each acetyl group is known to be linked covalently to a hydroxyl sorption site in the cell wall (Papadopoulos and Hill 2003). Acetylation therefore should not be capable of filling cavities significantly larger than the acetyl group themselves, but only form a layer on part of the walls of the cavity. The size of an acetyl group is influenced by its nearby environment (Kwon et al. 2007). However, computer simulations of acetylated galactopyranose by Thibodeaux et al. (2002) can give an idea of the size. In these simulations the bond lengths of the O-C and C-CH₃ bonds was found to be 0.135 nm and 0.149 nm, respectively (Thibodeaux et al. 2002). If the C-H bond length is estimated to 0.109 nm (Demaison and Wlodarczak 1994) and the van der Waals radius of the hydrogen to 0.120 nm (Bondi 1964), the maximum distance from the oxygen of the wooden substrate to the end of the acetyl group is approximately 0.52 nm (assuming a linear O-C-C-H structure). This should be seen in relation to the size of the initial hydroxyl group where an

O-H bond length of 0.0946 nm (Szalay et al. 2002) results in a distance from the oxygen to the end of approximately 0.22 nm. Thus, based on estimates of bond lengths, the acetyl groups add approximately 0.3 nm at each sorption site where it bonds. Capillary sorption in pores with a radius significantly larger than the dimension of the acetyl group should therefore remain unaffected by acetylation, provided that there is no change of contact angle. There are, however, indications that the contact angle in macrovoids is affected by acetylation (Thygesen and Elder 2008). A theoretical quantification of the influence of contact angle on capillary moisture uptake is found in Part 2 of this article. For RH values where EMC is governed by sorption directly at hydroxyl sorption sites, an almost constant ratio between the EMCs of acetylated and untreated wood would be expected, largely reflecting the degree to which the acetyl group is blocking access of water molecules to hydroxyl sorption sites. An EMC ratio increment in the range of high RH could indicate contribution from capillary sorption (Strømdahl 2000), which is supposed to be unaffected by acetylation. This reasoning is valid only if it can be assumed that acetylation does not create new voids of a size relevant for capillary sorption at high RH. Microvoids and macrovoids caused by acetylation have not been reported in the literature. Based on these findings, acetylated wood samples were included here as a type of modified wood where direct blocking of hydroxyl groups through the formation of covalent bonds presumably played a more important role for the sorption properties than bulking of voids in the 91.9–99.9% RH range.

It is presently not exactly known how furfurylation reduces moisture uptake. It was recently shown (Nordstierna et al. 2008) that furfuryl alcohol can form covalent bonds to lignin model compounds. However, such a reaction has not been shown for wood lignin *in situ*. Furthermore, bonds to lignin will not directly block sorption sites in the carbohydrate part of the wood cell wall material, i.e., the part of the wood where most of the primary sorption takes place. Other recent studies indicate that a furfuryl alcohol based polymer (FAP) is formed within the wood, a polymer which is bulking the cell wall (Venås 2008; Thygesen et al. 2010; Thygesen and Elder 2009). Furfurylated wood was included here as a type of modification where bulking presumably played a more important role for the sorption properties than direct blocking of hydroxyl groups through the formation of covalent bonds.

Materials and methods

Wood samples

Two differently shaped sapwood samples were included: cylinders and cuboids. Cylinder shaped samples with a diameter of 14 mm were drilled from the sapwood of 10 mm thick discs taken from a stem of Norway spruce [*Picea abies* (L.) Karst.], whereas cuboids measuring 1×40×40 mm were cut from the sapwood of other discs from the same stem. Processing of the stem took place within a few days after harvest, and care was taken throughout to prevent samples from drying out. After processing, the samples were stored in sealed plastic bags with an excess of demineralized water. All samples

were then subjected to neutron radiation (1×15 kGy) to prevent biological degradation during storage (mould fungi). As a further precaution, samples were stored at +5°C.

Three types of wood samples were produced:

- *Untreated samples (denoted U)* were dried at 103°C and then vacuum saturated with demineralized water containing sodium azide (NaN_3 , 200 mg l^{-1}). The samples were saturated in the water for 2–3 h at 2.6–3.0 kPa followed by 24 h at atmospheric pressure.
- *Acetylated samples (denoted A)* were treated in a lab-scale set-up adapted from Rowell (1986). The samples were dried at 103°C and then subjected to vacuum drying for 18 h, after which enough acetic anhydride was added to cover all samples. After 1 h, the pressure was equilibrated, and the samples were boiled ($\sim 140^\circ\text{C}$) in acetic anhydride for 4 h. Finally, the samples were dried at 103°C for approximately 24 h. The average weight percent gain (WPG) was 20%. After acetylation the samples were vacuum saturated in the same way as the untreated samples (type U).
- *Furfurylated samples (denoted F)* were treated in a lab-scale set-up. Samples were pre-dried at 103°C for 16 h and impregnated in an autoclave (full vacuum for 30 min followed by a pressure of 1.2 MPa for 120 min). Excess liquid was wiped off, and the solvent was partly evaporated in an oven using a temperature ramp from 20°C to 40°C during 4 h. Subsequently, the samples were wrapped in aluminum foil and cured for 16 h at 103°C. The foil was removed, and the samples were dried for 7 h at 103°C to evaporate condensed water and unreacted monomer. The impregnation fluid consisted of furfuryl alcohol (55 wt-%), ethanol (39 wt-%), citric acid (catalyst, 2 wt-%), and deionized water (4 wt-%). The average WPG was 63%, indicating that the impregnation was successful even though the samples were made from spruce. This is most likely as a result of the small sample dimensions used. After furfurylation, the samples were vacuum saturated in the same way as the untreated samples (type U).

Relative humidity levels and equilibrium moisture contents

Relative humidity levels (21 totally) were established at 20°C by three methods: saturated salt solutions, climate chambers, or the PPT. All EMCs were reached from higher MCs, i.e., through desorption. The criterion employed for determining whether EMC had been reached was that the sample weight did not vary more than 0.5% over 2 weeks, or, for the PPT method, that there had been no outflow of water for 2 weeks.

Saturated salt solutions in desiccators were employed to reach the following RH levels: (1) 91.9% RH (BaCl_2), according to a linear regression between temperature and RH based on values from Apelblat (1992), (2) 94.1%, and (3) 97.7% RHs obtained with saturated KNO_3 and K_2SO_4 solutions, respectively, according to Hansen and Jensen (2002). The desiccators were placed in a 20°C water bath in an isolated chamber. Magnetic stirring of the solution was used throughout the experiment to ensure a homogeneous RH distribution within the desiccators. The samples were taken out and weighed once every 1–2 weeks. The time to equilibrium was approximately 5 months. Both cuboids and cylindrical samples were conditioned.

Other samples were conditioned in climate chambers at the Department of Civil Engineering, Technical University of Denmark (Strømdahl 2000). This system allows weighing of the samples within the chambers. Two chambers were available in parallel, and

the RH levels were 98.0%, 96.0%, and 94.7%, respectively, 97.6%, 96.2%, and 94.9%. Samples were weighed once or twice a week, and the time to equilibrium was 2–5 months for each RH level. The total duration of the experiment was approximately 1 year. Both cuboids and cylindrical samples were treated as described.

The principle of the PPT method is to expose water saturated samples to a pressure of up to 10 MPa while they are in hydraulic contact with atmospheric pressure through a ceramic disc or a cellulose membrane with fine pores. Water will then flow out of the samples until they are in equilibrium with the applied pressure. By combining the Kelvin and the Laplace equations the RH that corresponds to the applied pressure can be calculated, assuming that the sample is stiff and porous and partially water filled. For a given pressure it is then hypothesized that pores with a diameter larger than a limit value corresponding to the applied pressure are emptied of liquid water. A description of the method can be found in Penner (1963) and Cloutier and Fortin (1991).

Two different systems placed in two different laboratories were employed, one at the Technical University of Denmark (DTU), and one at Lund University (LU), Sweden. Both systems were based on equipment from Soilmoisture (Santa Barbara, CA, USA) and three different extractors intended for different pressure ranges were employed at both laboratories (0–0.5, 0–1.5, and 0–10 MPa). However, the 0–10 MPa unit of the Danish system had been slightly modified as described in Thygesen and Hansen (2007). Table 2 gives an overview of the PPT experiments carried out. All three types (U, A, and F) were always included in each run, i.e., situated in the same extractor and subjected to the exact same pressure. The outflow of water from the extractors was checked 2–5 times a week, and the time to equilibrium was in each case 2–3 months. Only cylindrical samples were used for the PPT experiments, and they were always placed with one of the two flat faces facing the disk, i.e., water was made to move along the grain, which should ensure the shortest possible time to equilibrium (Cloutier et al. 1995).

Following all types of conditioning experiments, samples were dried at 103°C and weighed. Mean MCs were calculated for each sample type based on the total dry weight of all samples of the same type subjected to the same RH level within the same experiment. It has recently been suggested to calculate MCs of modified wood samples based on their dry weight before modification, thus excluding the weight of the added substances (Hill 2008; Venås 2008). However, in this study, only average WPG values for each

modification type (acetylation and furfurylation) were known. We consequently report for each sample the MC results based on an estimated dry weight of an unmodified sample. If the results were reported on the basis of the dry weight of the modified sample, the WPG variation between samples would still be included in the results. Thus, no additional uncertainty is introduced by estimating the dry weight of the unmodified samples.

Low field time domain nuclear magnetic resonance (LF TD NMR)

A subset of the samples was subjected to LF TD NMR at two temperatures. For each measurement four cylindrical samples of the same type (U, A, or F) conditioned to the same RH level were measured together to achieve the recommended tube filling for each NMR measurement. For each sample type, 36 such samples were prepared. Instrument: 23 MHz ¹H NMR Maran (from Resonance Instruments, now part of Oxford Instruments, UK) set to a temperature of +20°C. The free induction decay was recorded by a recycle delay of 2 s and 32 acquisitions. In total, 8000 data points with a spacing of 0.5 ms were recorded. Just before measurement, the samples were weighed to allow MC determination.

After measurements the samples were put in a freezer at -18°C for at least 24 h. Then they were placed in a cooling bath at -20°C for at least 1 h. The temperature just below the position of the tube inside the NMR instrument was set to -20°C by a custom-built cooling system based on evaporation of liquid nitrogen. The samples were then remeasured at this temperature before they were dried at 103°C to constant weight to determine their MC during the +20°C measurement.

Results and discussion

Sorption isotherms

The desorption data are presented in Figure 1. As can be seen, the experiment was designed with overlaps between the three methods. These overlaps show that the EMCs found for the same sample type and at the same RH level, but by different methods, are not systematically different. In other words, there are no discontinuities between methods; a feature that lends the isotherms high credibility.

As seen from Figure 1, the EMCs of the untreated samples at the high end of the RH scale (above 98%) are around 40%, i.e., well above the rule-of-thumb value of approximately 30% often assumed to be the fiber saturation point (FSP) of European softwood. However, as pointed out already by Stamm (1971), the FSP depends on the method applied, and our results for RH >98% obtained by the PPT method are in fact well in line with earlier PPT results regarding the FSP of untreated softwood (Stone and Scallan 1967; Stamm 1971; Griffin 1977; Hill et al. 2005).

Sorption isotherms in the 96–99% RH range are often drawn with an upward bend (Spalt 1958; Kollmann 1962; Simpson 1973). Typically, it is assumed that at very high humidity levels, capillary sorption in microvoids in the cell wall structure is of crucial importance to the MC. However, such an upward bend is not seen in our data for untreated samples, except perhaps a weak tendency above approxi-

Table 2 Overview of the pressure plate technique (PPT) experiments.

Laboratory ^a	Extractor, max pressure (MPa)	Pressure (MPa)	RH (%)
LU	10	5.60	95.9
LU	10	4.05	97.0
DTU	10	2.73	98.0
DTU	10	1.36	99.0
LU	1.5	1.36	99.0
DTU	1.5	0.66	99.5
DTU	0.5	0.38	99.7
DTU	0.5	0.27	99.8
LU	0.5	0.28	99.8
DTU	0.5	0.14	99.9

^aLund University (LU), Technical University of Denmark (DTU).

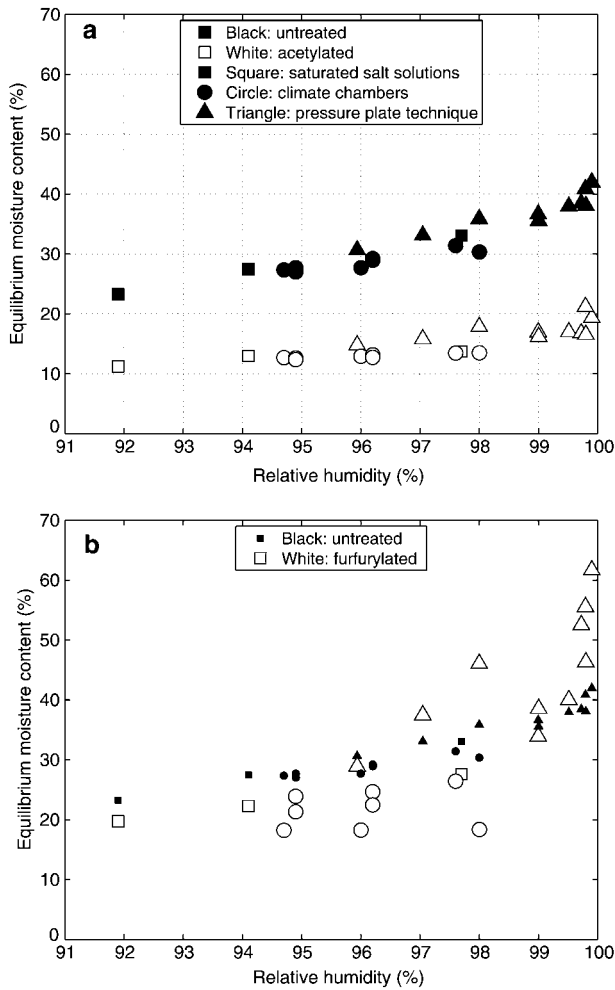


Figure 1 Desorption data for untreated, acetylated, and furfurylated samples. For each data point it is also indicated which of the three different methods mentioned in the legend that was employed for establishing a constant relative humidity level.

mately 99.5% RH. The highest RH value (99.9%) obtained in the present study corresponds to capillary sorption in microvoids of a radius equal to $1 \mu\text{m}$, i.e., the very high end of the range of microvoid radii as defined in Table 1. The results therefore can be interpreted as though capillary condensed water in microvoids plays at most a modest role with regard to EMC reached through desorption.

Theoretical calculation of capillary condensation in microvoids

In an attempt to better understand the sorption isotherm for untreated wood presented in Figure 1a, a theoretical calculation of the contribution from capillary condensation in the 99.0–99.9% RH range was undertaken based on the Kelvin equation and idealized microstructural geometries. These derivations and calculations are shown *in extenso* in Part 2 of this article. The result of the theoretical exercise was that the effect of capillary sorption in microvoids is expected to be insignificant with regard to the overall MC of wood even

at very high RH, below 0.35% moisture at 99.9% RH. This result supports the validity of the isotherm for untreated wood recorded and shown in Figure 1.

Modified wood

Figure 1a also illustrates that, as expected, the EMCs of the acetylated samples are systematically lower than those of the untreated samples. But more interestingly, the moisture ratio $MR_A = EMC_A/EMC_U$ between the EMCs of the acetylated and the untreated samples is more or less independent of RH. As can be seen in Figure 2a, MR_A is approximately 0.48 throughout the entire range of RH from 92% to approximately 99.6%. This result is in the same range as results for similar WPG by Papadopoulos and Hill (2003) shown in Figure 2b. Based on the hypothesis on MR_A presented in the introduction, MR_A should increase significantly with increasing RH if capillary condensation took place in both sample types. The inference of the constant moisture ratio MR_A , as seen in Figure 2a, is therefore that for desorption isotherms for untreated wood as well as for acetylated wood, capillary condensed water does not contribute to sorption below 99.9% RH.

The moisture ratios ($MR_F = EMC_F/EMC_U$) for the furfurylated samples are presented in Figure 3. For RH below 96%, the moisture ratio is of the order $MR_F = 0.8$, indicating that the furfurylated samples at equilibrium contain 80% of the water present in untreated samples at the same RH levels, i.e., in spite of a much higher WPG, furfurylation was not as effective as acetylation. Above 96% RH the MR_F gradually increases. For $RH > 99\%$, $MR_F > 1$ indicating that at such high RH, furfurylated wood could hold significantly more water than untreated wood. At $RH = 99.9\%$ untreated wood holds approximately 40% moisture, whereas furfurylated wood holds 50–60% moisture. The results of the present study confirm the findings of Venås (2008) who established adsorption isotherms for furfurylated Scots pine

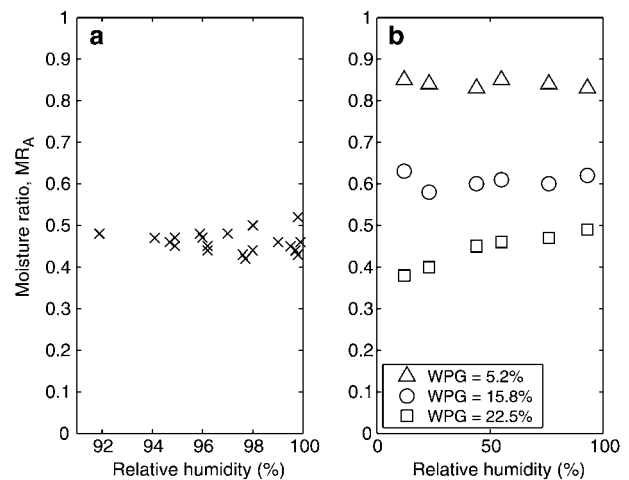


Figure 2 Moisture ratios (MR_A) for acetylated samples. (a) Results from the present study. (b) Samples acetylated to obtain a WPG of 5.4% (triangles), 15.8% (circles), and 22.5% (squares) (Panel b is based on data from Papadopoulos and Hill 2003).

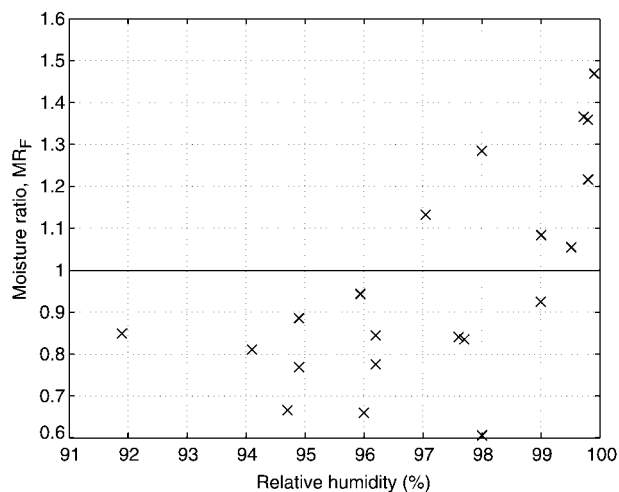


Figure 3 Moisture ratios (MR_F) as a function of relative humidity (RH) for furfurylated samples.

samples with a WPG of approximately 28%. Below $RH=85\%$ the MR_F stayed at an almost constant value of approximately 0.56. However, somewhere in the interval $85\% < RH < 100\%$ the moisture ratio started to increase to eventually reach a value of approximately $MR_F=1.0$ at a RH value characterized as 'close to 100%'. At the very high WPG levels in the present study, it is probable that the cell walls were bulked to such an extent that they were damaged and/or that the cell lumina of some cells were (partially) filled. The cause of the change in sorption behavior of furfurylated wood compared with untreated wood can thus be related to (1) sorption of the FAP itself, (2) an increase in accessibility of the sorption sites caused by less effective blocking by the FAP, or (3) capillary condensation in cracks created by the bulking of the cell wall.

Venås (2008) exposed ground FAP, i.e., the glassy, hydrophobic polymer formed by *in vitro* homopolymerization of furfuryl alcohol to saturated water vapor. The EMC was 2.6%. For the furfurylated samples in the present study with a WPG of 63%, this amount of water corresponds approximately to 1.6% moisture bound in the FAP phase. Firstly, this is a very modest contribution, and secondly there is nothing to indicate that this polymer differs from most polymers with regard to showing smooth running isotherms with no particular increase of water uptake at very high RH. The results presented in Thygesen et al. (2009) indicate that the same homopolymer is formed inside the wood. Thus, water uptake in the FAP itself does not offer a likely explanation.

Increasing the MC causes the molecular mobility of the hemicelluloses to increase (Salmén 1982; Olsson and Salmén 1997). It might therefore be hypothesized that such softening makes access to blocked sorption sites easier. However, such a mechanism would be expected to show over a considerable range of RH and not to be confined to a narrow range of the very highest RH values. In addition, such a mechanism would be incapable of explaining moisture uptake in excess of that of untreated wood. Consequently, softening can at best offer part of the explanation.

Capillary condensation can offer a better explanation. In fact, a crossing at high RH of sorption isotherms, as seen for untreated wood and furfurylated wood, is also known from other types of wood modification. Heat treatment reduces the number of available sorption sites particularly by decomposing hemicelluloses. This results in a reduced moisture sorption at intermediate levels of RH. However, the decomposition of hemicelluloses also creates voids, which result in increased moisture uptake as a result of capillary condensation at high levels of RH (Hoffmeyer et al. 2003). A related mechanism is suggested for furfurylated wood with high WPG. Water sorption is reduced by furfurylation blocking the access to sorption sites at normal levels of RH. At high levels of RH, capillary sorption in microvoids becomes active. We suggest that the microvoids are generated by the pressure impregnation with furfuryl alcohol. They might show as microcracks emerging from the bulking of the cell wall or as microvoids between cell wall matter and bulk FAP deposited, e.g., in cell lumens. The RH range from $RH=99.0\%$, where $MR \approx 1$ up to $RH=99.9\%$, which is the highest RH value of the study, corresponds to capillary radii in the range $0.1\text{--}1.0\ \mu\text{m}$. An exploratory attempt to identify such microvoids by environmental scanning electron microscopy (ESEM) was unsuccessful, perhaps because the microvoids are shut at the insufficient moisture conditions available in the ESEM (results not shown). The ESEM did, however, reveal that the lumina of ray cells were filled to some extent by the FAP.

If the marked increase of the sorption isotherm of furfurylated wood at high RH is related to capillary sorption, it would be expected that such behavior is reflected by the swelling of the wood. Either the wood will exhibit a slightly negative swelling as a result of capillary forces or a low or zero swelling caused by the filling of existing voids in the structure. Thus, the ratio of swelling over MC would decrease in the region where the sorption isotherm changes. It remains unresolved whether this is the case.

Freezing and non-freezing water as detected using LF TD NMR

The LF TD NMR method is an alternative to swelling experiments for the study of the state(s) of water in wood, i.e., for answering the question to what extent the water is 'bound' or 'free'. The method is suited for measurements both above and below the freezing point of the 'free' water. Figure 4 shows the mean free induction decay (FID) relaxation curve for the three sample types measured at $+20^\circ\text{C}$ and at -20°C . The figure demonstrates that only the mean relaxation curve of the furfurylated wood is affected by freezing the samples. This indicates that on average only the furfurylated samples contained freezing water. To make sure that the difference seen was not simply an effect of a difference in average MC between sample types, a principal component analysis (PCA) was carried out of all FIDs recorded. The PCA included data for all three sample types (untreated, acetylated, and furfurylated) and for two measurements per sample ($+20^\circ\text{C}$ and -20°C). To avoid clutter, the scores plot for factors 1 vs. 2

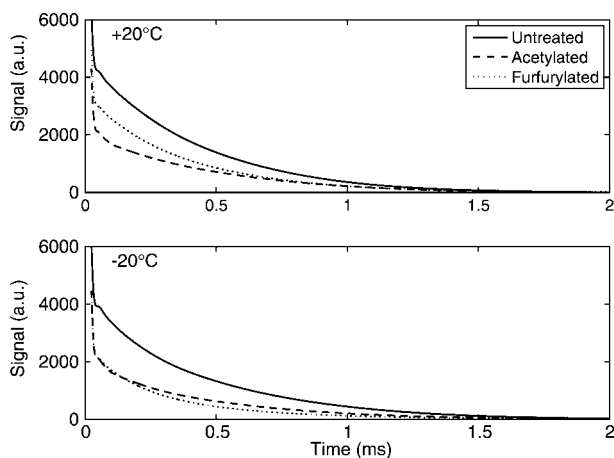


Figure 4 Mean free induction decay (FID) relaxation curves from LF TD NMR of 36 samples of each of the three sample types (untreated, acetylated, and furfurylated) at +20°C and at -20°C. Data for different moisture contents have been pooled.

for this PCA are presented as three subplots (Figure 5a,b,c), each showing data for one of the three sample types. Furthermore, the two points corresponding to the same sample are connected by a line and a circle shows which end of the line corresponds to -20°C. It is obvious that the untreated and the acetylated samples form groups that are separate from each other, regardless of the temperature. Within each of these two groups, no systematic effect of the temperature can be discerned. Contrary to this, the furfurylated samples at the -20°C group (situated within a narrow area) are well separated from the position of the samples at +20°C. At +20°C they are positioned more or less with the untreated samples, at -20°C they are positioned close to the acetylated samples.

Figure 6 shows the length of the ‘vectors’ in Figure 5 vs. the MCs of the samples. This plot demonstrates for the furfurylated samples that the higher the MC the longer the ‘vector’, i.e., the more was the FID at -20°C different from the FID at +20°C. Accordingly, the difference in signal is related to the amount of freezing water. This trend is not seen for the two other sample types indicating that they did not contain any significant amounts of freezing water. According to Petrov and Furó (2009), water in cylindrical pores with a radius down to 3 nm will freeze at -20°C. This indicates that also water in very large clusters – as those that might exist around charged groups at RH levels close to 100% – could freeze at this temperature, but so large clusters are not found around uncharged groups such as hydroxyl groups (Berthold et al. 1996). Charged (carboxylic) groups exist only in acetylated wood, not in untreated or furfurylated wood. However, no freezing occurred in the acetylated wood. Consequently, we find it probable that the water that froze in the furfurylated samples was capillary condensed water (perhaps in damaged cell walls), i.e., free water and not freezing bound water.

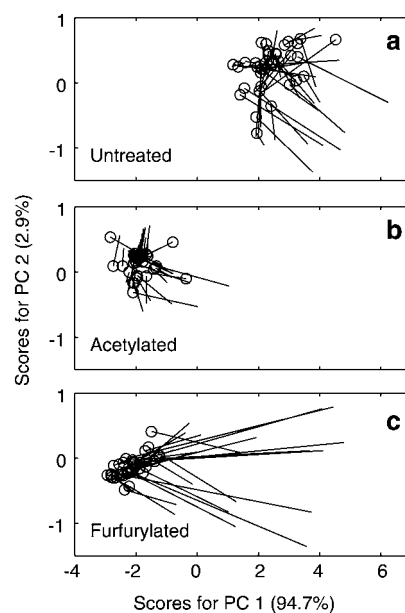


Figure 5 Principal component analysis of the 3 (sample types) × 36 (samples) × 2 (temperatures) = 216 FID relaxation curves summarized in Figure 4. Scores for factor 1 vs. scores for factor 2 are shown in three separate subplots to avoid clutter, i.e., one subplot per sample type. Within each subplot each line connects the position of a sample at +20°C with its position at -20°C (marked by a circle).

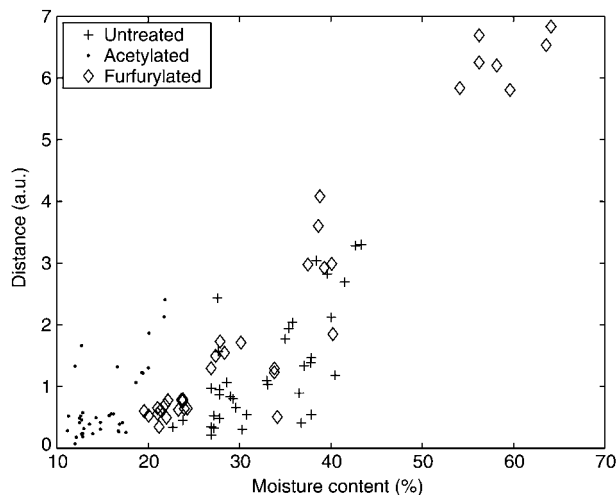


Figure 6 The distances in the PCA scores plot between the positions at +20°C and at -20°C (as seen in Figure 5) vs. the moisture content of the samples at +20°C.

Conclusions

Desorption isotherms at 20°C for untreated, acetylated, and furfurylated Norway spruce sapwood were established in the 91.9–99.9% RH range. The curve for the untreated samples did not show an upward bend, except perhaps above 99.5% RH, indicating that – contrary to what has hitherto been assumed – capillary condensation does not play a significant

role for water sorption in wood below fiber saturation. Three additional results from the present study point in the same direction:

- The theoretical contribution of capillary condensation to the MC in wood – based on idealized microstructural geometries – was calculated by the Kelvin and Laplace equations. Only very small contributions to the EMC were found, namely below 0.35% moisture at 99.9% RH.
- The moisture ratio between acetylated and untreated samples did not show an increasing trend for increasing RH, as would have been the case if capillary condensation had taken place in both untreated and acetylated wood.
- Low field time domain NMR results showed that only the relaxation curves from the furfurylated samples were affected systematically by freezing, indicating that neither untreated nor acetylated wood contained significant amounts of capillary condensed water.

Acknowledgements

The authors wish to thank Ulla Gjør Jacobsen for her invaluable and never tiring technical support during the cumbersome experiments that formed the basis of this work. Thomas Mark Venås is acknowledged for performing the furfurylation. L.G.T. acknowledges funding from The Danish Research Council for Technology and Production Science (project no. 26-02-0100).

References

- Alinec, B. (2002) Porosity of swollen pulp fibres revisited. *Nordic Pulp Paper Res.* 17:71–73.
- Apelblat, A. (1992) The vapour pressures of water over saturated aqueous solutions of barium chloride, magnesium nitrate, calcium nitrate, potassium carbonate, and zinc sulfate, at temperatures from 283 K to 313 K. *J. Chem. Thermodyn.* 24:619–626.
- Babbitt, J.D. (1943) On the adsorption of water vapour by cellulose. *Can. J. Res.* 20:143–172.
- Barkas, W.W. (1937) Wood-water relationships, part III – molecular sorption of water by Sitka spruce wood. *Proc. Phys. Soc.* 49:237–247.
- Berthold, J., Desbrières, J., Rinaudo, M., Salmén, L. (1994) Types of adsorbed water in relation to the ionic groups and their counter-ions for some cellulose derivatives. *Polymer* 35:5729–5736.
- Berthold, J., Rinaudo, M., Salmén, L. (1996) Association of water to polar groups; estimations by an adsorption model for lignocellulosic materials. *Colloids Surf. A Physicochem. Eng. Asp.* 112:117–129.
- Bondi, A. (1964) Van der Waals volumes + radii. *J. Phys. Chem.* 68:441–451.
- Branton, P.J., Hall, P.G., Sing, K.S.W. (1995) Physisorption of alcohols and water vapour by MCM-41, a model mesoporous adsorbent. *Adsorption* 1:77–82.
- Cloutier, A., Fortin, Y. (1991) Moisture content-water potential relationship of wood from saturated to dry conditions. *Wood Sci. Technol.* 25:263–280.
- Cloutier, A., Tremblay, C., Fortin, Y. (1995) Effect of specimen structural orientation on the moisture content-water potential relationship of wood. *Wood Sci. Technol.* 29:235–242.
- Defo, M., Fortin, Y., Cloutier, A. (1999) Moisture content-water potential relationship of sugar maple and white spruce wood from green to dry conditions. *Wood Fiber Sci.* 31:62–70.
- Demaison, J., Włodarczyk, G. (1994) The equilibrium C-H bond length. *Struct. Chem.* 5:57–66.
- Evans, R. (1990) Fluids adsorbed in narrow pores: phase equilibria and structure. *J. Phys. Condens. Matter* 2:8989–9007.
- Fahlén, J., Salmén, L. (2005) Pore and matrix distribution in the fiber wall revealed by atomic force microscopy and image analysis. *Biomacromolecules* 6:433–438.
- Flournoy, D.S., Paul, J.A., Kirk, T.K. (1991) Wood decay by brown rot fungi. Changes in pore structure and cell wall pore volume. *Holzforschung* 45:383–388.
- Griffin, D.M. (1977) Water potential and wood-decay fungi. *Annu. Rev. Phytopathol.* 15:319–329.
- Hansen, P.F., Jensen, O.M. (2002) Dew point meter – for high accuracy measurements of water activity by Dynamic Dew point Analysis. Department of Building Technology and Structural Engineering, Aalborg University, Denmark.
- Hill, C.A.S. (2008) The reduction in the fibre saturation point of wood due to chemical modification using anhydride reagents: a reappraisal. *Holzforschung* 62:423–428.
- Hill, C.A.S., Forster, S.C., Farahani, M.R.M., Hale, M.D.C., Ormondroyd, G.A., Williams, G.R. (2005) An investigation of cell wall micropore blocking as a possible mechanism for the decay resistance of anhydride modified wood. *Int. Biodeterior. Biodegradation* 55:69–76.
- Hoffmeyer, P., Jensen, S.K., Jones, D., Klinke, H.B., Felby, C. (2003) Sorption properties of steam treated wood and plant fibres. In: Proceedings of the First European Conference on Wood Modification, Eds. Van Acker, J., Hill, C., Ghent University, Ghent, April 3–4, pp. 177–189.
- Kohonen, M.M., Christenson, H.K. (2000) Capillary condensation of water between rinsed mica surfaces. *Langmuir* 16:7285–7288.
- Kollmann, F.F.P. (1962) Eine Gleichung der Sorptionsisotherme. *Naturwissenschaften* 49:206–207.
- Kwon, J.H., Hill, C.A.S., Ormondroyd, G.A., Karim, S. (2007) Changes in the cell wall volume of a number of wood species due to reaction with acetic anhydride. *Holzforschung* 61:138–142.
- Lastoskie, C., Gubbins, K.E., Quirke, N. (1993) Pore size distribution analysis of microporous carbons: a density functional theory approach. *J. Phys. Chem.* 97:4786–4796.
- Nordstierna, L., Lande, S., Westin, M., Karlsson, O., Furó, I. (2008) Towards novel wood-based materials: chemical bonds between lignin-like model molecules and poly(furfuryl alcohol) studied by NMR. *Holzforschung* 62:709–713.
- Olsson, A.-M., Salmén, L. (1997) Humidity and temperature affecting hemicellulose softening in wood. In: Proceedings of the COST Action E8 international conference on wood-water relations, Ed.: Hoffmeyer, P., Technical University of Denmark, Lyngby, June 16–17, pp. 269–279.
- Papadopoulos, A.N., Hill, C.A.S. (2003) The sorption of water vapour by anhydride modified softwood. *Wood Sci. Technol.* 37:221–231.
- Penner, E. (1963) Suction and its use as measure of moisture contents and potentials in porous materials. In: Humidity and Moisture. Vol. 4. Ed. Wexler, A. Reinhold Publ. Co., New York, NY. pp. 245–252.
- Petrov, O.V., Furó, I. (2009) NMR cryoporometry: principles, applications and potential. *Prog. Nucl. Magn. Reson. Spectros.* 54:97–122.

- Robertson, A.A. (1965) Investigation of the cellulose water relationship by the pressure plate method. *Tappi* 48:568–573.
- Rouquerol, J., Avnir, D., Fairbridge, C.W., Everett, D.H., Haynes, J.H., Pernicone, N., Ramsay, J.D.F., Sing, K.S.W., Unger, K.K. (1994) Recommendations for the characterization of porous solids. *Pure Appl. Chem.* 66:1739–1758.
- Rouquerol, F., Rouquerol, J., Sing, K.S.W. (1999) Assessment of mesoporosity. In: *Adsorption by powders and porous solids: principles, methodology and applications* (Rouquerol, F., Rouquerol, J., Sing, K.S.W.), Academic Press, London. pp. 191–218.
- Rowell, R.M. (1986) A simplified procedure for the acetylation of hardwood and softwood flakes for flakeboard production. *J. Wood Chem. Technol.* 6:427–448.
- Salmén, L. (1982) Temperature and water induced softening behavior of wood fiber based materials. Royal Institute of Technology, Stockholm, Sweden.
- Salmén, L. (1997) The sorption behaviour of wood. In: *Proceedings of the COST Action E8 international conference on wood-water relations*, Ed.: Hoffmeyer, P., Technical University of Denmark, Lyngby, June 16–17, pp. 33–44.
- Salmén, L., Fahlén, J. (2006) Reflections on the ultrastructure of softwood fibers. *Cellulose Chem. Technol.* 40:181–185.
- Sheppard, S.E. (1933) The structure of xerogels of cellulose and derivatives. *Trans. Faraday Soc.* 29:77–85.
- Simpson, W.T. (1973) Predicting equilibrium moisture content of wood by mathematical models. *Wood Fiber* 5:41–49.
- Sing, K.S.W., Everett, D.H., Haul, R.A.W., Moscou, L., Pierotti, R.A., Rouquerol, J., Siemieniowska, T. (1985) Reporting physisorption data for gas/solid systems with special reference to the determination of surface area and porosity. *Pure Appl. Chem.* 57:603–619.
- Skaar, C. *Wood-Water Relations*. Springer-Verlag, Berlin/Heidelberg, 1988.
- Spalt, H.A. (1958) The fundamentals of water sorption by wood. *Forest Prod. J.* 10:288–295.
- Stamm, A.J. (1950) Bound water and hydration. *Tappi* 33:435–439.
- Stamm, A.J. (1971) Review of nine methods for determining the fiber saturation points of wood and wood products. *Wood Sci.* 4:114–128.
- Stone, J.E., Scallan, A.M. (1967) The effect of component removal upon the porous structure of the cell wall of wood. II. Swelling in water and the fiber saturation point. *Tappi* 50:496–501.
- Stone, J.E., Scallan, A.M. (1968) The effect of component removal upon the porous structure of the cell wall of wood. III. A comparison between the sulfite and the kraft processes. *Pulp Paper Mag. Canada* 69:69–74.
- Strømdahl, K. (2000) Water sorption in wood plants. PhD thesis. Department of Structural Engineering and Materials, Technical University of Denmark. Report Series R78. ISBN 87-7740-293-6.
- Szalay, V., Kovacs, L., Wohlecke, M., Libowitzky, E. (2002) Stretching potential and equilibrium length of the OH bond in solids. *Chem. Phys. Lett.* 354:56–61.
- Tarkow, H., Feist, W.C., Southerland, C.F. (1966) Interaction of wood with polymeric materials. Penetration versus molecular size. *Forest Prod. J.* 16:61–65.
- Thibodeaux, D.P., Johnson, G.P., Stevens, E.D., French, A.D. (2002) Crystal structure of penta-O-acetyl-beta-D-galactopyranose with modeling of the conformation of the acetate groups. *Carbohydr. Res.* 337:2301–2310.
- Tremblay, C.A., Cloutier, A., Fortin, Y. (1996) Moisture content-water relationship of red pine sapwood above the fiber saturation point and the determination of the effective pore size contribution. *Wood Sci. Technol.* 30:361–371.
- Thygesen, L.G., Hansen, K.K. (2007) Improved suction technique for the characterization of construction materials. *J. ASTM Int.* 4:1–9.
- Thygesen, L.G., Elder, T. (2008) Moisture in untreated, acetylated and furfurylated Norway spruce studied during drying using time domain NMR. *Wood Fiber Sci.* 40:309–320.
- Thygesen, L.G., Elder, T. (2009) Moisture in untreated, acetylated and furfurylated Norway spruce monitored below fibre saturation using time domain NMR. *Wood Fiber Sci.* 41:194–200.
- Thygesen, L.G., Bartsberg, S., Venås, T.M. (2010) The fluorescence characteristics of furfurylated wood studied by fluorescence spectroscopy and confocal laser scanning microscopy. *Wood Sci. Technol.* 44:51–65.
- Venås, T.M. (2008) A study of mechanisms related to the fungal decay protection rendered by wood furfurylation. PhD thesis. Forest and Landscape, University of Copenhagen, Copenhagen, Denmark.

Received June 30, 2009. Accepted November 30, 2009.
Previously published online February 17, 2010.

PAPER II

Water sorption in wood and modified wood at high values of relative humidity.

Part II: Appendix. Theoretical assessment of the amount of capillary water in wood microvoids

Engelund E. T., Thygesen L. G. and Hoffmeyer P.

Holzforschung (2010) 64:325-330

Water sorption in wood and modified wood at high values of relative humidity. Part 2: Appendix. Theoretical assessment of the amount of capillary water in wood microvoids

Emil Tang Engelund^{1,3}, Lisbeth G. Thygesen^{2,*} and Preben Hoffmeyer³

¹ Wood and Textile, Danish Technological Institute, Taastrup, Denmark

² Forest and Landscape, University of Copenhagen, Frederiksberg C, Denmark

³ Department of Civil Engineering, Technical University of Denmark, Lyngby, Denmark

*Corresponding author.

Forest and Landscape, University of Copenhagen, Rolighedsvej 23, DK-1958 Frederiksberg C, Denmark
E-mail: lgt@life.ku.dk

Abstract

A theoretical study of the amount of moisture held in wood as capillary condensed water in the relative humidity (RH) range of 90–99.9% is carried out. The study is based on idealized geometries of the softwood structure related to micrographs. It is confined to structural elements such as bordered pits and the pointed ends of tracheids. The theoretical amount of water in these elements is found by employing the Kelvin equation. An equal amount of earlywood and latewood cells with different geometries and with different amounts of pits is assumed. The effect of pit aspiration is considered, and different degrees of pit aspiration are assigned to earlywood and latewood. We suggest based on the results that capillary condensation makes only a very small contribution to the equilibrium moisture content. At 99.9% RH the contribution amounts to less than 0.0035 kg water per kg dry wood. This is in line with the experimental results presented in Part 1 of this study.

Keywords: capillary condensation; isotherm; Kelvin equation; sorption; wood-water relations.

Introduction

In Part 1 of this article a variety of techniques were employed to shed light on wood-water relations with regard to capillary condensation. In the present Part 2 of this article, a detailed account is given of the theoretical assessment of capillary condensation already utilized in Part 1. The study is confined to structural elements such as bordered pits and the pointed ends of tracheids for the 90–99.9% range of relative water vapor pressures. Idealized geometries based on

micrographs of softwood structure are used and the Kelvin equation is employed. Geometrical dimensions, capillary radius, and contact angle are the only variables.

Theory

The condensation of vapor in narrow pores can occur below the saturation pressure. This phenomenon is termed capillary condensation. The critical pressure at which capillary condensation occurs is determined, among other factors, by the shape and size of the pores; the narrower the pore, the lower the critical pressure. The relation between critical pressure and pore size is described by the Kelvin equation shown as Eq. (1). The critical pressure is often expressed as relative pressure. For water vapor, the relative pressure is termed relative humidity (RH).

$$r = \frac{-2\sigma \cdot M_w}{\rho \cdot R \cdot T \cdot \ln(RH)} \quad (1)$$

where σ is the surface tension of water (72.74 mN m⁻¹ at 20°C), M_w is the molecular weight of water (18.01 g mol⁻¹), ρ is the density of water (998 kg m⁻³ at 20°C), R is the universal gas constant, and T is absolute temperature. The parameter r is the mean curvature of the formed meniscus of condensed vapor in the pore. For cylindrical pores r is equivalent to the radius of the pore, whereas for slit-shaped pores it designates half the distance between the two parallel pore walls (Evans et al. 1986).

The Kelvin equation is only valid above a certain relative pressure (Sing 2004). Below this pressure, capillary condensation can occur but it is not described by the Kelvin equation (Evans 1990). For instance, Branton et al. (1995) have studied the capillary condensation in the porous silicate material MCM-41, which has a specific pore size of narrow distribution. They found that capillary condensation occurs in a narrow range of RH of approximately 55%. However, at such low levels of RH, the capillary condensation is controlled by the specific interaction between sorption sites and the condensed vapor and not by the Kelvin equation (Evans 1990). Computer simulations indicate that the Kelvin equation is accurate down to pore widths of approximately 7.5 nm (Lastoskie et al. 1993; Rouquerol et al. 1999) which corresponds to a cylindrical pore radius of 3.75 nm and a relative water vapor pressure of 75% RH. Thus, for studying moisture adsorption by capillary condensation in wood in the

range of 90–99.5% RH, the Kelvin equation is fully applicable.

Occasionally, the Kelvin equation is modified to take into account adsorbed layers of vapor molecules on the wall surfaces (Evans 1990; Lastoskie et al. 1993). However, for 90% RH the corresponding capillary radius is 10.3 nm (see Part 1). If it is assumed that each sorption site only adsorb 1.35 water molecules on average even at high RH (Berthold et al. 1996), the capillary radius of 10.3 nm is more than 30 times larger than the layer (0.3 nm for one water molecule) of adsorbed water molecules on the cell wall surfaces. Thus, it is reasonable to model the contribution of capillary condensation in the idealized wood structure without taking into account the water adsorbed to specific sorption sites.

Pointed ends of tracheids

Idealized, the capillary water volume in tracheid ends has the shape of a cone with a concave bottom (see Figure 1a). The volume of water can thus be found as the volume of a cone minus the volume of a spherical cap. The curvature of the latter is determined by the capillary radius corresponding to the given ambient relative humidity. The height of the cone is determined both by tracheid geometry and the capillary radius. The variable which connects the cone height with the capillary radius is the width D (see Figure 1a). D is the diameter of the flat circular face of the spherical cap.

The volume of water, V_{water} can be calculated from Eq. (2):

$$V_{water} = V_{cone} - V_{cap} = \frac{\pi}{12} \cdot h_{cone} \cdot D^2 - \frac{\pi}{3} \cdot h_{cap}^2 \cdot (3r - h_{cap}) \quad (2)$$

where V_{cone} and V_{cap} are the volumes of the cone and spherical cap, respectively. The height of the cone, h_{cone} is related to D by Eq. (3):

$$h_{cone} = \frac{h_{max}}{D_{max}} \cdot D \quad (3)$$

The angle β gives the relation between D and h_{cap} .

$$\tan \beta = \frac{\frac{1}{2}D}{h_{cap}} \quad (4)$$

By using Pythagoras equation on the triangle ABC , the parameter D can be determined.

$$r^2 = (r - h_{cap})^2 + \left(\frac{1}{2}D\right)^2 \quad (5)$$

$$0 = h_{cap}^2 - 2r \cdot h_{cap} + \frac{1}{4}D^2 \quad (6)$$

$$0 = \left(\frac{D}{2 \tan \beta}\right)^2 - r \cdot \frac{D}{\tan \beta} + \frac{1}{4}D^2 \quad (7)$$

$$D = \frac{r}{\tan \beta} \left(\frac{1}{4 \tan^2 \beta} + \frac{1}{4} \right)^{-1} \quad (8)$$

By trigonometric considerations, the angles α and β can be found.

$$\alpha = \text{Arc tan} \left(\frac{\frac{1}{2}D_{max}}{h_{max}} \right) \quad (9)$$

As the triangle ABC is an isosceles triangle, β can be found from Eq. (10).

$$\beta = \frac{1}{2} \left(\pi - \left(\frac{1}{2} \pi - \alpha - \theta \right) \right) = \frac{1}{2} \left(\frac{1}{2} \pi + \alpha + \theta \right) \quad (10)$$

The height of the spherical cap, h_{cap} can then be found from D from Eq. (11).

$$h_{cap} = \frac{D}{2 \tan \beta} \quad (11)$$

Aspirated pits

The capillary water volume in aspirated pits is assumed to be shaped like a ring with a sharp rim. The volume can be calculated by solids of revolution, i.e., rotating a plane object around an axis. In Figure 1b the gray area marks the water. To obtain the volume of water, the space between the volume of the rotated gray area and the rotational axis has to be extracted.

The volume of water can be found from Eq. (12). In general, the volume of a rotational body can be found by the integral of the squared function multiplied with π .

$$\begin{aligned} V_{water} &= \pi \int_0^D f(x)^2 dx - \pi \int_0^D g(x)^2 dx \\ &= 2\pi \int_0^{D/2} \left(\frac{1}{2} h_{open} + h_{max} - \frac{h_{max}}{\frac{1}{2}D_{max}} x \right)^2 dx \\ &\quad - 2\pi \int_0^{D/2} \left(h_{rot} + \sqrt{r^2 - x^2} \right)^2 dx \end{aligned} \quad (12)$$

The first integral is related to the area lines indicating the pit geometry. The second integral is related to the area between the water meniscus and the rotational axis (see Figure 1b).

The height and width of the water volume are related by Eq. (13).

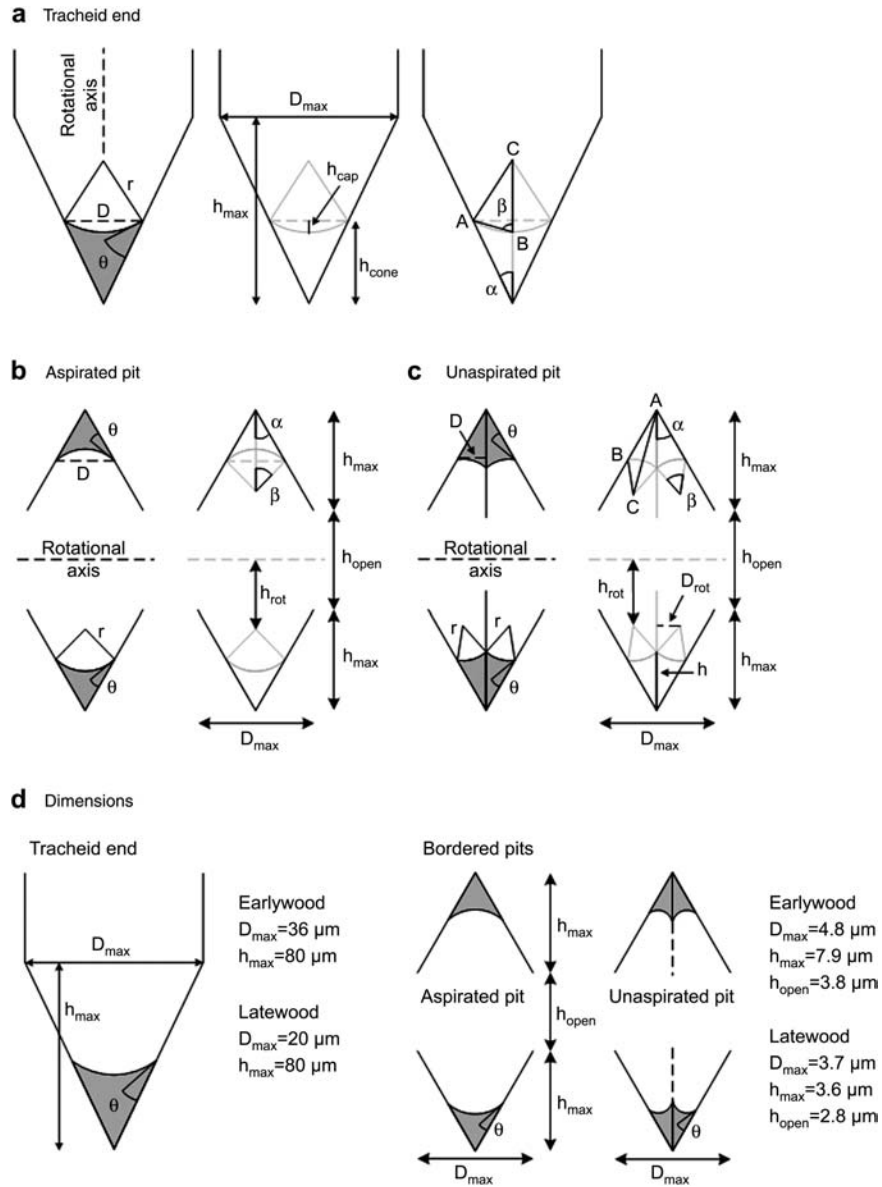


Figure 1 (a) Water volume (gray area) in an idealized tracheid end. (b) Water volume (gray area) in an idealized aspirated pit. (c) Water volume (gray area) in an idealized unaspirated pit. (d) Dimensions of earlywood and latewood tracheid ends and pits based on Côté and Day (1969).

$$h = \frac{h_{\max}}{\frac{1}{2}D_{\max}} \cdot \frac{1}{2}D = \frac{h_{\max}}{D_{\max}} \cdot D \quad (13)$$

$$\alpha = \text{Arc tan} \left(\frac{\frac{1}{2}D_{\max}}{h_{\max}} \right) \quad (15)$$

The offset of the circular center from the rotational axis can be found from Eq. (14).

$$\begin{aligned} h_{\text{rot}} &= \frac{1}{2}h_{\text{open}} + h_{\max} - h \cdot r \cdot \cos \beta \\ &= \frac{1}{2}h_{\text{open}} + h_{\max} - \frac{h_{\max}}{D_{\max}} \cdot D \cdot r \cdot \cos \beta \end{aligned} \quad (14)$$

$$\beta = \pi - \left(\frac{1}{2}\pi + \alpha + \theta \right) = \frac{1}{2}\pi - \alpha - \theta \quad (16)$$

The capillary radius and the parameter D are related by Eq. (17).

$$\text{By trigonometric considerations, the angles } \alpha \text{ and } \beta \text{ can be found.} \quad \frac{1}{2}D = r \cdot \sin \beta \quad (17)$$

The following integral is part of the second integral of the water volume equation. The solution to the integral is given by Eq. (18).

$$\int \sqrt{r^2 - x^2} dx = \int r \cdot \cos^2 u du = r \cdot \left(\frac{1}{2} u + \frac{1}{4} \sin(2u) \right) \quad (18)$$

$$\text{where } u = \text{Arc sin} \left(\frac{x}{r} \right) \quad (19)$$

Unaspirated pits

The idealized capillary water volume in unaspirated pits differs in shape from the water in aspirated pits only by two concave curvatures within the ring instead of one. Therefore, the second part of the volume Eq. (12) differs from the one for aspirated pits. It is also important to note that the boundaries have changed from $[0 \frac{1}{2} D]$ to $[0 D]$, see Figure 1c for further information on the parameters. It is assumed that the margo is located in the center of the pit.

The volume of water can be found from Eq. (20).

$$V_{\text{water}} = 2\pi \int_0^D \left(\frac{1}{2} h_{\text{open}} + h_{\text{max}} - \frac{h_{\text{max}}}{\frac{1}{2} D_{\text{max}}} \cdot x \right)^2 dx - 2\pi \int_0^D (h_{\text{rot}} + \sqrt{r^2 - (x - D_{\text{rot}})^2})^2 dx \quad (20)$$

The offset of the center for the capillary curve can be found from Eqs. (21) to (24).

$$D_{\text{rot}} = r \cdot \cos \theta \quad (21)$$

$$h_{\text{rot}} = \frac{1}{2} h_{\text{open}} + h_{\text{max}} - h \cdot r \cdot \sin \theta \quad (22)$$

$$h = \frac{D}{\sin \alpha} \quad (23)$$

$$\text{where } \alpha = \text{Arc tan} \left(\frac{\frac{1}{2} D_{\text{max}}}{h_{\text{max}}} \right) \quad (24)$$

The relation between D and r is given by Eqs. (25) to (27).

$$h \cdot \sin \left(\frac{1}{2} \alpha \right) = r \cdot \sin \left(\frac{1}{2} \beta \right) \quad (25)$$

$$\frac{D}{\sin \alpha} \cdot \sin \left(\frac{1}{2} \alpha \right) = r \cdot \sin \left(\frac{1}{2} \beta \right) \quad (26)$$

$$D = \frac{\sin \alpha \cdot \sin \left(\frac{1}{2} \beta \right)}{\sin \left(\frac{1}{2} \alpha \right)} \cdot r \quad (27)$$

The angle β can be found in triangle ABC and is given by Eq. (28).

$$\frac{1}{2} \beta + \frac{1}{2} \alpha + \frac{1}{2} \pi + \theta = \pi \quad (28)$$

$$\beta = \pi - 2\theta - \alpha \quad (29)$$

The following integral is part of the second integral of the water volume equation. The solution to the integral is given by Eq. (30).

$$\begin{aligned} \int \sqrt{r^2 - (x - r \cdot \cos \theta)^2} dx &= \int r \cdot \sqrt{1 - \left(\frac{x}{r} - \cos \theta \right)^2} dx \\ &= \int r^2 \cdot \cos^2 u du \\ &= r^2 \cdot \left(\frac{1}{2} u + \frac{1}{4} \sin(2u) \right) \end{aligned} \quad (30)$$

$$\text{where } u = \text{Arc sin} \left(\frac{x}{r} - \cos \theta \right) \quad (31)$$

Idealized softwood structure

The total water volume can be calculated on the basis of the previous equations and assumptions regarding the dimensions and number of pits and tracheids. Wood is a very variable material and shows a large variation between the cells in earlywood (EW) and latewood (LW). For instance, the dimensions of cell lumen and pits of the EW are greater than those in LW. Furthermore, a larger amount of pits are aspirated in the EW than in the LW. These factors are included in the calculations by defining two types of cells (EW and LW tracheids) and four types of pits (aspirated and unaspirated pits in EW and LW, respectively). The dimensions of the six different geometries are seen in Figure 1d. The dimensions are based on micrographs from Côté and Day (1969).

To calculate the amount of moisture held as capillary condensed water, the amount of tracheids and pits needs to be established. The number of tracheids is set to 80 per mm^3 based on their dimensions which typically are 50 μm in width and 5 mm in length (Dinwoodie 2000). This corresponds to 160 tracheid ends per mm^3 available for capillary condensation. An equal amount of thin-walled EW and thick-walled LW cells is assumed. The number of pits is set to 300 per EW tracheid and 100 per LW tracheid based on Dinwoodie (2000). This results in an amount of 8000 pits per mm^3 wood. The percentage of aspirated pits is at first assumed to be 75% in EW and 10% in LW. The dry density

of wood is assumed to be 480 kg m^{-3} , which enables a calculation of the MC content as weight percentage of water in wood.

Results and discussion

Figure 2 shows the contribution of capillary water to the MC as a function of the relative humidity in the ambient climate. For this Figure, the contact angle between cell wall and water is set to zero. A zoom of the range of 99–100% RH is included in Figure 2. It is clear that even at very high relative pressures, the amount of moisture held as capillary water does not exceed $0.0035 \text{ kg water per kg dry wood}$. An interesting feature is seen for the LW where the slope of the curve decreases above 99.8% RH, whereas the EW slope continues to increase. This is as a result of a complete filling of the smaller LW pits. This is also clear from Figure 3 that depicts

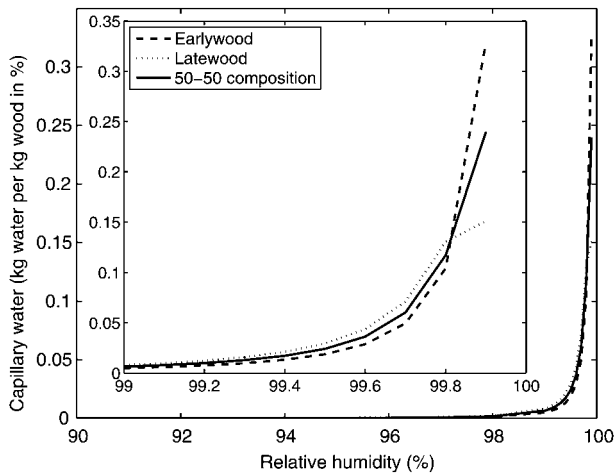


Figure 2 The contribution of capillary water to the moisture content as a function of the ambient relative humidity. Inserted is a zoom of the 99–100% RH range.

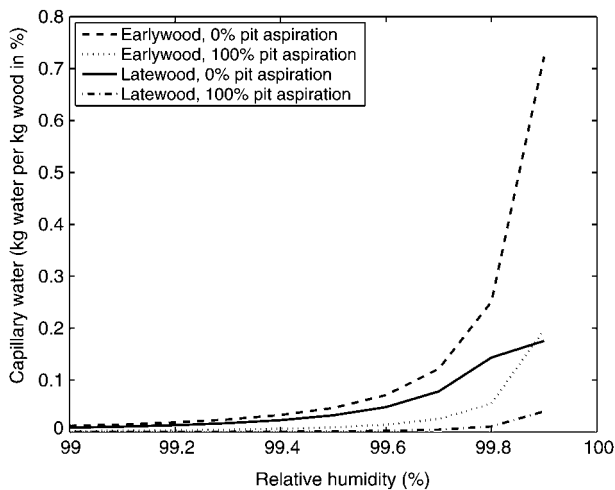


Figure 3 Influence of pit aspiration in earlywood and latewood on the contribution of capillary water to the moisture content.

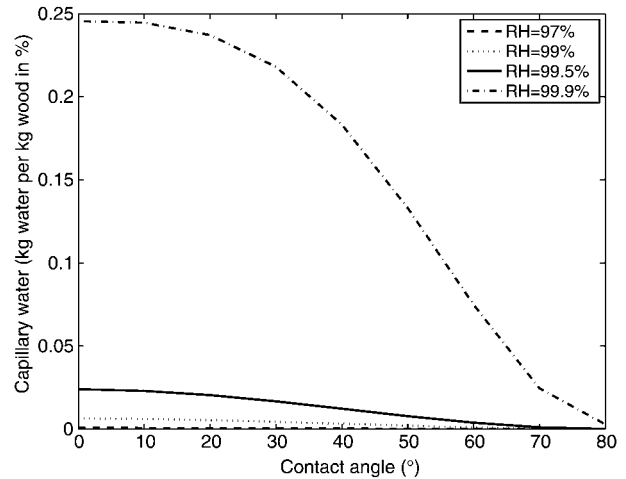


Figure 4 The influence of contact angle between water and wood on the contribution of capillary water to the moisture content for selected values of relative humidity.

the sorption curves for EW and LW with either completely aspirated or unaspirated pits, respectively.

The contact angle between water and wood was initially set to zero. However, the influence of contact angle on the contribution of capillary water is shown in Figure 4 for selected values of relative humidity. The diagram shows that the largest contribution of capillary water is achieved if the contact angle equals zero.

Conclusions

The theoretical calculations indicate that capillary condensation in structural elements such as bordered pits and the pointed ends of tracheids plays an insignificant role in the adsorption of moisture in wood even at a relative humidity as high as 99.9% RH. This is in line with the experimental results shown in Part 1 of this study.

Acknowledgements

L.G.T. acknowledges funding from The Danish Research Council for Technology and Production Science (project no. 26-02-0100).

References

- Berthold, J., Rinaudo, M., Salmen, L. (1996) Association of water to polar groups; estimations by an adsorption model for lignocellulosic materials. *Colloids Surf. A Physicochem. Eng. Asp.* 112:117–129.
- Branton, P.J., Hall, P.G., Sing, K.S.W. (1995) Physisorption of alcohols and water vapour by MCM-41, a model mesoporous adsorbent. *Adsorption* 1:77–82.
- Côté, W.A., Day, A.C. (1969) Wood ultrastructure of the Southern yellow pines. Technical Report No. 95. State University College

- of Forestry at Syracuse University, Syracuse, New York, NY. pp. 52–53.
- Dinwoodie, J.M. *Timber – Its Nature and Behaviour*. E&FN Spon, London, 2000.
- Evans, R. (1990) Fluids adsorbed in narrow pores: phase equilibria and structure. *J. Phys. Condens. Matter* 2:8989–9007.
- Evans, R., Marconi, M.B., Tarazona, P. (1986) Fluids in narrow pores: adsorption, capillary condensation, and critical points. *J. Chem. Phys.* 84:2376–2399.
- Lastoskie, C., Gubbins, K.E., Quirke, N. (1993) Pore size distribution analysis of microporous carbons: a density functional theory approach. *J. Phys. Chem.* 97:4786–4796.
- Roquerol, F., Roquerol, J., Sing, K.S.W. (1999) Assessment of mesoporosity. In: *Adsorption by powders and porous solids: principles, methodology and applications*. Eds. Roquerol, F., Roquerol, J., Sing, K.S.W. Academic Press, London, 1999. pp. 191–218.
- Sing, K.S.W. (2004) Characterization of porous materials: past, present and future. *Colloids Surf. A Physicochem. Eng. Asp.* 241: 3–7.

Received June 30, 2009. Accepted November 30, 2009.
Previously published online February 17, 2010.

PAPER III

Equilibrium moisture content in Norway spruce during the first and second desorptions

Hoffmeyer P., Thygesen L. G. and Engelund E. T.

Holzforschung (2011) 65:875-882

Equilibrium moisture content (EMC) in Norway spruce during the first and second desorptions

Preben Hoffmeyer¹, Emil Tang Englund^{1,2} and Lisbeth G. Thygesen^{3,*}

¹ Department of Civil Engineering, Technical University of Denmark, Brovej, Building 118, DK-2800 Kgs. Lyngby, Denmark

² Wood Technology, Danish Technological Institute, Gregersensvej, DK-2630 Taastrup, Denmark

³ Forest and Landscape, University of Copenhagen, Rolighedsvvej 23, DK-1958 Frederiksberg C, Denmark

*Corresponding author.

Forest and Landscape, University of Copenhagen, Rolighedsvvej 23, DK-1958 Frederiksberg C, Denmark
E-mail: lgt@life.ku.dk

Abstract

It is a commonly accepted notion that the equilibrium moisture content (EMC) of wood at a given relative humidity (RH) is highest during initial desorption of green wood due to an irreversible loss of hygroscopicity during the 1st desorption. The basis for this notion is investigated by assessing how drying and saturation procedures influence the differences between the 1st and the 2nd desorption curves for Norway spruce (*Picea abies* (L.) Karst.) sapwood. The study establishes 1st and 2nd desorption isotherms for a variety of initial conditions and it covers the RH range from 60.1% to 99.9%. The state of the water is not affected by oven-drying and rewetting as demonstrated by time domain low field NMR relaxometry. The results challenge the conclusions of earlier studies and indicate that in these studies the 2nd desorption was initiated at much too low EMC and therefore fails to describe a boundary desorption isotherm. Instead, it becomes an intermediate desorption isotherm starting at the adsorption boundary curve and crossing over to eventually meet the desorption boundary curve. The results also show that vacuum drying at room temperature only gives a modest loss of hygroscopicity compared to the green state. Conversely, oven-drying at 103°C results in a more significant loss of hygroscopicity, except for RH above 96% where an increase in EMC surprisingly is seen.

Keywords: fiber saturation; first and second desorption isotherms; green wood; time domain low field NMR spectroscopy; wood-water relations.

Introduction

It is a commonly accepted notion that the equilibrium moisture content (EMC) of wood at a given relative humidity

(RH) is highest during initial desorption of green wood. More specifically, it is commonly accepted that after drying, any subsequent desorption from saturated condition produces lower values of EMC at RH above 60%–70% “indicating that there is an initial irreversible loss in hygroscopicity” (Skaar 1988). The scientific basis for the notion that the 2nd desorption universally gives lower EMCs than the 1st is often ascribed to Spalt (1958), though similar observations had earlier been reported for cotton (Urquhart 1929; Urquhart and Eckersall 1930), beech wood (Barkas 1936), wood pulp (Seborg et al. 1938) and cellulose objects (Hermans 1949). Spalt (1958) subjected specimens of four different coniferous species to both a 1st and a 2nd desorption. By use of saturated salt solutions, six different RHs were obtained, the highest of which was 94%. At this RH, a species dependent value of the moisture ratio (MR), defined as the ratio between the EMCs at the 1st and 2nd desorption, was recorded in the range of 1.1–1.2. At decreasing values of RH the MR also decreased, resulting in a merging of the two desorption isotherms somewhere between RH 62% and 78%. Spalt initiated his specimens to the 2nd desorption from a condition reached by heating a water reservoir to a temperature that caused condensation in the weighing tubes held at room temperature. In other words, the specimens were presumably exposed to air saturated with water vapor. The specimens in the weighing tubes were thought to be in a saturated condition after prolonged exposure to this climate. However, it may be questioned whether this procedure is a suitable reference condition for saturation of the wood fibers. If this is not the case, Spalt’s 2nd desorption curves are intermediate desorption curves initiated from a moisture state less than fiber saturation. Spalt’s results show increasing MRs for increasing RH. Even higher MRs for RH values exceeding Spalt’s maximum RH value of 94% would therefore be expected. However, results for the 92.6%–99.9% RH range produced as an unpublished spin-off from an earlier study (Thygesen et al. 2010) surprisingly suggested decreasing MR ratios, which prompted the present study.

The study of potential differences between the 1st and 2nd desorption is intimately linked to the concept of the fiber saturation point (FSP). A brief review of the FSP concept is therefore included here. The original definition (Tiemann 1906) relates FSP to the EMC where, the free water in the cell lumina has disappeared, the cell wall begins to dry and the strength begins to increase. However, as discussed by Hill (2008), these effects do not normally occur at the same EMC, so in practice the FSP is less well defined. Furthermore, both free water and unsaturated cell wall may exist simultaneously in different cells within the same specimen (Almeida and Hernández 2006a,b; Hernández and Pontin 2006; Hernández and Bizoñ 1994; Araujo et al. 1992; Menon

Table 1 Overview of sequence of events for the five different procedures employed to subject specimens to desorption measurements. The digit in the procedure label is a hint to 1st or 2nd desorption, respectively.

	Procedure labels				
	GREEN1 ^a	VACUUM1	SATVAP2 ^b	VACUUM2	OVENDRY2
Drying	N/A	N/A	Vacuum (20°C)	Vacuum (20°C)	Oven-drying (103°C)
Saturation	N/A	Vacuum	Water vapor	Vacuum	Vacuum

^aSimulating 1st and ^b2nd desorption according to Spalt (1958).

et al. 1987). Stamm (1964) lists FSP determined from a variety of strength tests of Sitka spruce and arrives at an FSP in the 27%–30% range, or much the same as the FSP value obtained by extrapolation of the sorption isotherm from 98% RH. Hence, for purposes of calculating the moisture dependency of physical and mechanical properties of wood, such an approach to find FSP is perfectly suitable. However, such an FSP is a nominal value. It represents neither a particular point on the sorption isotherm nor an upper value of EMC above which no more bound water is taken up. Stone and Scallan (1967) related FSP to “the amount of water contained within the water saturated cell wall”. They then argued that the FSP must be where there is a discontinuity in the range of void dimensions, and they defined this FSP in terms of water potential. The quoted authors exposed black spruce to humidity in a pressure plate apparatus and found such a discontinuity at about 99.75% RH, equivalent to a matrix water potential of about $\psi_m = -0.3$ MPa and a void radius of about 0.4 μm , i.e., large microvoids (Thygesen et al. 2010). The corresponding FSP was 40%. The same authors found, by means of a solvent exchange technique (dextran 110), a FSP value of 42% for the same specimens. Griffin (1977) reanalyzed the results of Stone and Scallan (1967) and added his own results from pressure plate tests including two other coniferous species. The author then defined FSP as the water content of wood that is in equilibrium with $\psi_m = -0.1$ MPa (99.93% RH and 1.5 μm void radius) during desorption from the saturated state and arrived at FSP = 43%. Hill et al. (2005) calculated FSP = 38% for Corsican pine sapwood by the solute exclusion method. Hernández and Bizoñ (1994) investigated sugar maple by the pressure membrane technique combined with measurements of strength and shrinkage and found that loss of bound water begins in desorption around 42% EMC. The present paper is based on the FSP definition as “the amount of water contained within the water saturated cell wall” (Stone and Scallan 1967). More specifically, FSP is chosen as the EMC of wood in equilibrium with $\psi_m = -0.1$ MPa (RH = 99.93%, void radius = 1.5 μm) (Griffin 1977).

The hypothesis of the present study is that a more detailed understanding is needed in terms of the question how drying and saturation procedures affect the relation between the 1st and 2nd desorption isotherms and that the concept of Spalt (1958) and Skaar (1988) “indicating that there is an initial irreversible loss in hygroscopicity” needs to be revisited and reassessed. The study establishes 1st and 2nd desorption iso-

therms for a variety of initial conditions and it covers the 60.1%–99.9% RH range. The study comprises two test series. One series covers the RH range from 60.1% to 98.4% and thus includes the full RH range for which Spalt (1958) reported differences between the 1st and the 2nd desorption curves. The state of water in the various specimens is also studied by NMR relaxometry. Advanced versions of both high and low field NMR relaxometry have been introduced to the wood and paper sciences during the last decade (see for example Topgaard and Södermann 2001; Garvey et al. 2006; Johannessen et al. 2006; Kekkonen et al. 2009; Cox et al. 2010). In the present study, standard time domain low field NMR relaxometry (TD LF NMR) above and below the freezing point of free water was performed.

Materials and methods

Rectangular cuboids measuring $3 \times 23 \times 47$ mm³ were cut from the sapwood of discs taken from a stem of Norway spruce (*Picea abies* (L.) Karst.). Processing of the stem took place within a few days after harvest, and care was taken throughout to prevent specimens from drying out. After processing, the specimens were stored in sealed plastic bags with an excess of demineralized water. The bags and their content were then subjected to neutron radiation (1×15 kGy) to prevent biological degradation by mold fungi during storage. As a further precaution, the sealed plastic bags were stored at 5°C. Prior to further use, the specimens were removed from the bags and placed in demineralized water containing sodium azide (NaN_3 , 200 mg l⁻¹) for more than 24 h. Specimens prepared like this are here referred to as green specimens.

Saturation and drying procedures

Table 1 presents the procedure labels together with the five different procedures employed to subject specimens to desorption measurements. The digit 1 or 2 in the procedure label is a hint to 1st or a 2nd desorption, respectively. The GREEN1 procedure corresponds to that of Spalt (1958) to establish the 1st desorption curve. The VACUUM1 procedure then reveals whether the green condition represents full saturation of the cell wall. The saturation over water vapor (SATVAP2) procedure attempts to mimic the water vapor saturation and vacuum drying procedure – as described by Spalt (1958) – applied for the 2nd desorption. The efficiency of this procedure is assessed by the procedure VACUUM2, which employs liquid water instead of water vapor for the saturation prior to the 2nd desorption. Finally, the OVENDRY2 procedure allows an assessment of any additional change of hygroscopicity arising from drying at elevated temperature.

Demineralized water containing sodium azide (NaN_3 , 200 mg l^{-1}) was used for the vacuum saturation. The specimens were first exposed to water for 1 h at 2.6–3.0 kPa followed by 0.5 h at atmospheric pressure. They were then exposed to the water for more than 24 h at 2.6–3.0 kPa followed by more than 6 h at atmospheric pressure. Vacuum drying was carried out in desiccators containing magnesium perchlorate as desiccant (20°C and 0.1–1.0 kPa). After two weeks, the desiccant was removed and constant pumping (20°C and 0.1 kPa) was carried out for an additional three days. At that point, the weight change of the specimens was about 0.03% per day. Exposure to saturated water vapor was started in desiccators at 20°C at a pressure of about 2.6–3.0 kPa. After 7 days, vacuum was replaced by atmospheric pressure to allow EMC to be reached under conditions comparable to those used by Spalt (1958). The total time for water vapor saturation was ten days. At that point, the weight change of the specimens was about 0.02% per day. Oven-drying was carried out at 103°C for a duration of about 24 h. Specimens were taken directly from green condition to oven-drying.

Conditioning ($60.1\% \leq \text{RH} \leq 98.4\%$)

Six different levels of RH were achieved by saturated salt solutions in desiccators (NaBr, NaCl, KCl, BaCl_2 , KNO_3 and K_2SO_4). The desiccators were placed in a 20°C water bath in an isolated chamber. The solutions were magnetically stirred to promote a uniform RH distribution within the desiccators. Five sets of cuboid specimens, corresponding to the five procedures, were placed in weighing glasses in each of the six desiccators. The 30 specimens were generally taken out and weighed once every 1–2 weeks. The lids of the weighing glasses were mounted when opening a desiccator and taking out the glasses for weighing. Atmospheric pressure was re-established immediately before opening any desiccator. This was done by filling the desiccator with air having a RH matching that of the desiccator. Air used for the filling of the dry desiccators had a dew point temperature of about -100°C corresponding to a $\text{RH} < 0.01\%$. The maximum time to equilibrium was about five months. The criterion for having reached EMC was a change of mass corresponding to $< 0.01\%$ MC per day. Following the completion of the desorption measurements, all specimens were oven-dried at 103°C for a minimum of 24 h and then weighed.

In a preceding paper (Thygesen et al. 2010), RH values corresponding to the saturated salt solutions were taken from literature. The present investigation demonstrated that stirring of the saturated salt solutions results in RH values in the desiccators slightly higher than would be expected from literature. The RH was therefore measured in situ by placing moisture data loggers in the desiccators. Instrument: Tinytag Explorer Version 4.6 (from Gemini Data Loggers Ltd., Chichester, UK). A Hygromer[®] HR 100A (from Rotronic AG, Bassersdorf, Switzerland) was used to calibrate the Tinytag data loggers. Traceability of measurements was assured by using the Rotronic calibration chamber in a combination with Rotronic's certified salt solution ampoules. The following calibrated RH values were found based on the in situ moisture measurements: 60.1% (NaBr), 76.9% (NaCl), 87.1% (KCl), 92.6% (BaCl_2), 95.1% (KNO_3) and 98.4% (K_2SO_4). These RH values, which are used in the following, exceed those reported in literature by about 1%.

Additional test series ($92.6\% \leq \text{RH} \leq 99.9\%$)

A subset of the specimens were treated according to the processes GREEN1 and OVENDRY2. RH levels (21 totally) in the 92.6%–99.9% range were established at 20°C by three different methods: saturated salt solutions, climate chambers, and the pressure

plate technique (PPT). For details about the methods see Thygesen et al. (2010).

Time domain low field NMR relaxometry (TD LF NMR)

A subset of the specimens from the additional test series were subjected to TD LF NMR (23 MHz ^1H NMR Maran instrument, from Resonance Instruments, now part of Oxford Instruments, Abingdon, UK) at +20°C and -20°C. The free induction decay (FID) was recorded with a recycle delay of 2 s and 32 acquisitions. Eight thousand data points with a spacing of 0.5 ms were recorded. For further details see Thygesen et al. (2010).

Results and discussion

Particular features of desorption isotherms at very high RH values

Results from the additional test series ($92.6\% \leq \text{RH} \leq 99.9\%$) allow a discussion of characteristic features at the very high end of RH. Figure 1a shows the isotherms corresponding to the procedures GREEN1 and OVENDRY2. The markers refer to the three different methods employed for establishing the RH levels. As can be seen, the experiment was designed with overlaps between the three methods and the overlaps show that the EMCs recorded (obtained at the same RH by two or three methods for samples prepared using the same procedure) are not systematically different. In other words, the results show no discontinuities between methods and this feature lends the isotherms high credibility. Neither the green nor the dried and remoistened specimens show any signs of an upward bend as a result of capillary condensation, except perhaps above 99.5% RH. For the OVENDRY2 specimens, this has been discussed elsewhere (Thygesen et al. 2010; Engelund et al. 2010). The results do not indicate that the green specimens behave any differently, which supports the conclusion of (Thygesen et al. 2010; Engelund et al. 2010) that “capillary condensation does not play a significant role for water sorption below the FSP”.

Figure 1 shows FSP values of the order $\text{FSP} \approx 38\%$ for the GREEN1 procedure and $\text{FSP} \approx 42\%$ for the OVENDRY2 procedure. This order of magnitude is consistent with the results from the literature discussed in the preceding section on fiber saturation. It should be noted that the two isotherms cross around 96% RH leaving the oven-dried specimens with a higher FSP than the green specimens.

The significance of saturation procedures

Green specimens are used throughout the tests as a reference representing never dried and fully saturated wood. A comparison of the desorption isotherm for the two types of green specimens GREEN1 and VACUUM1 (obtained by additional vacuum saturation with water) show very little difference (Figure 2a). It can be concluded that the GREEN1 specimens were indeed water saturated.

Figure 2b shows MRs as a function of RH for each of the three 2nd desorption procedures. The three procedures lead

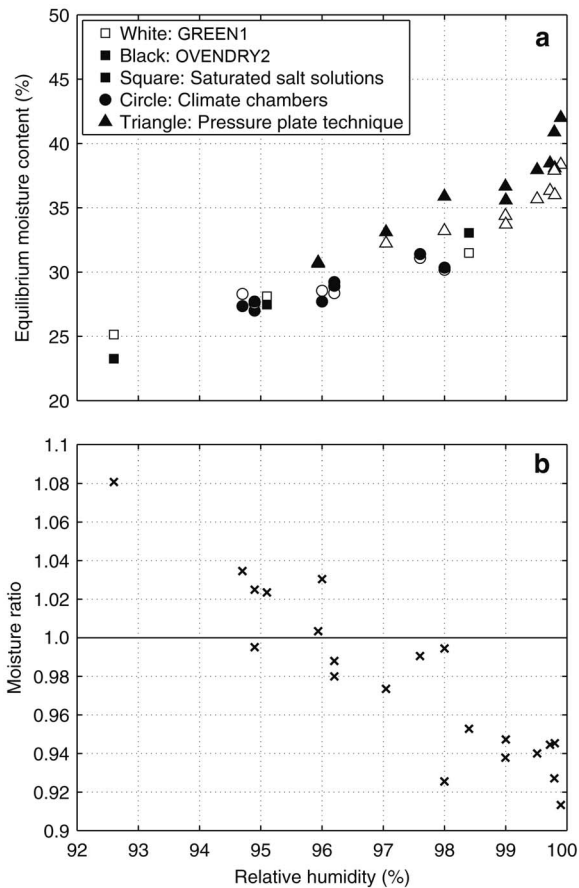


Figure 1 a) Comparison of desorption isotherms for Norway spruce sapwood for relative humidity (RH) in the range $92.6\% \leq RH \leq 99.9\%$. First desorption isotherm (GREEN1) and second desorption isotherm (OVENDRY2). b) Corresponding moisture ratio (MR) as a function of RH. MR is expressed as the ratio between the equilibrium moisture content (EMC) from procedure GREEN1 (1st desorption) and the EMC for OVENDRY2 (2nd desorption).

to very different results. This underlines the importance of the choice of procedure prior to the 2nd desorption when attempting to assess a measure of irreversible change of hygroscopicity. The MR for the SATVAP2 desorption is representative of the procedure of Spalt (1958) and Urquhart and Eckersall (1930). A general trend is recognized towards increasing MR the higher the RH. At RH = 98.4%, the MR is elevated to about 1.07 (Figure 2b). This behavior is in accordance with the findings of the quoted papers and we suggest that they are a result of an insufficient saturation prior to the 2nd desorption. In order to test this hypothesis, SATVAP2 is compared with vacuum saturation with water (VACUUM2) (Figure 2c): at 98.4% RH, the EMC of the SATVAP2-desorption was 30.1% while the EMC of the VACUUM2-desorption was 32.2%. At higher RH values, this difference increases: the EMC of the SATVAP2 specimens after prolonged exposure to saturated water vapor was on average 31.2% or only marginally higher than the EMC obtained at 98.4% RH. Thus, exposure to an atmosphere of saturated water vapor does not result in saturation of the

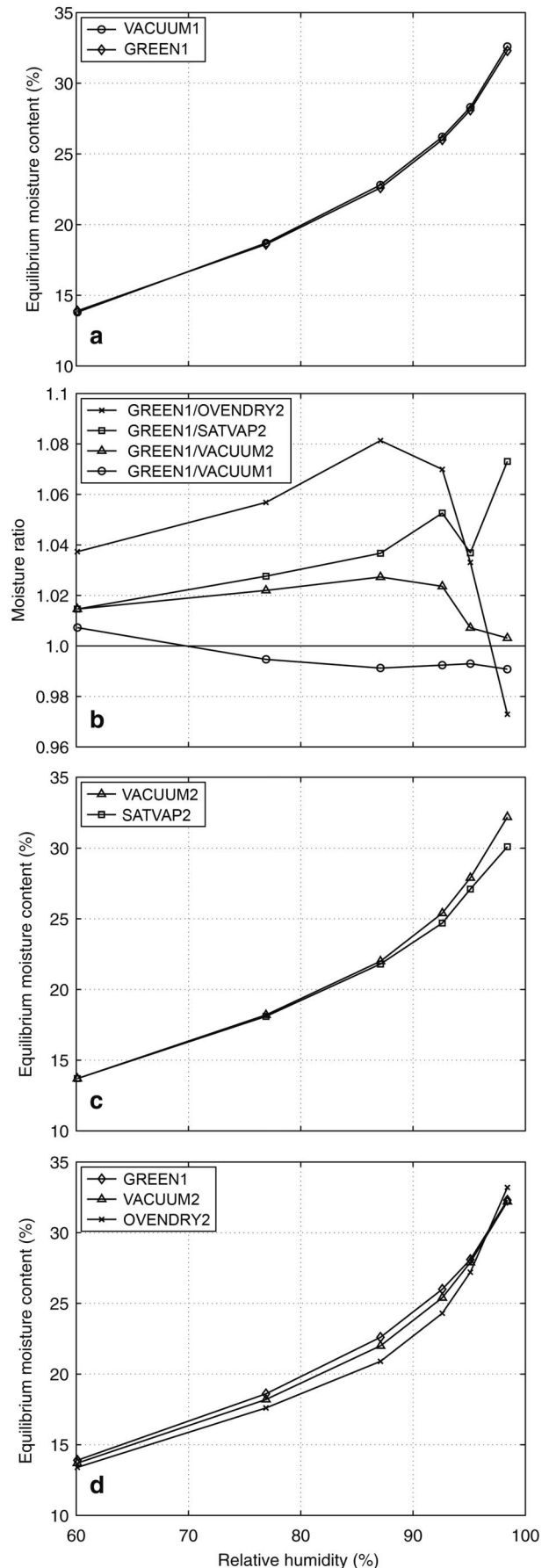


Figure 2 a) Desorption isotherms for Norway spruce sapwood. Green specimens (GREEN1) and green specimens subjected to additional vacuum saturation with water (VACUUM1). b) Moisture ratio (MR) as a function of relative humidity (RH) for Norway spruce sapwood in the range $60.1\% \leq RH \leq 97.7\%$. MR is expressed as the ratio between the equilibrium moisture content (EMC) from procedure GREEN1 (1st desorption) and the EMC for VACUUM1 and for each of the three 2nd desorption procedures. c) Desorption isotherms for Norway spruce sapwood. Second desorptions initiated from exposure to saturated water vapor (SATVAP2) or from vacuum saturation with water (VACUUM2). d) Desorption isotherms for Norway spruce sapwood. Illustration of irreversible change of hygroscopicity as a result of vacuum drying (GREEN1 vs. VACUUM2) or oven-drying at 103°C (GREEN1 vs. OVENDRY2).

wood cell wall, but rather produces an EMC representative of a RH around 98.5%. In contrast, vacuum saturation of the specimens ensures initiation of the 2nd desorption from a MC surpassing the FSP. The FSP for the green specimens was found to be 38%. Thus, the SATVAP2-desorption is initiated at too low EMC. It therefore represents an intermediate isotherm starting at the adsorption boundary curve well below the FSP and then crossing over to eventually meet the desorption boundary curve at a RH value around 75%–80% (Figure 2c). The very fact that the SATVAP2 curve merges with the boundary curve (VACUUM2) shows the SATVAP2-desorption curve to be an intermediate curve crossing the hysteresis area. Consequently, the results of Spalt (1958) do not give a quantitative assessment of irreversible loss of hygroscopicity. However, this does not exclude that such loss takes place as discussed below.

The significance of drying procedures

The impact of drying is illustrated in Figure 2b and 2d where the GREEN1-desorption is compared with the VACUUM2 and OVENDRY2 desorption isotherms. As would be expected, the Figures show that drying from the green state generally reduces the hygroscopicity, and also that oven-drying reduces hygroscopicity more than vacuum drying. Only at high values of RH, the reverse turns out to be true.

Softening may explain the general decrease in hygroscopicity, and may also explain the difference seen between vacuum drying and oven-drying. Above the glass transition point (T_g), amorphous polymers are in a rubbery state of mobility, whereas the mobility is highly restricted in the glassy state below this point. T_g depends on both MC and temperature; the higher the MC, the lower the T_g . In situ, lignin has a T_g around 50–60°C at full saturation while it approaches 100°C as the MC drops below 10% (Kelley et al. 1987). Hemicelluloses have a lower T_g , i.e., below 0°C for full saturation and about room temperature for an MC of 10% (Kelley et al. 1987). During vacuum drying at room temperature in the VACUUM2 procedure, the hemicelluloses pass from the rubbery state present in the green wood to the glassy state, while the lignin remains in its glassy state. In the OVENDRY2 procedure, the specimens experience an initial short period of simultaneously high MC and high temperature. This means that both the lignin and the hemicelluloses

have been in their rubbery states allowing greater mobility and thus facilitating a stress relaxation and a rearrangement of the wood polymers into an energetically more favorable state than what was possible at any time during the VACUUM2 procedure. The more mobile the lignin and the hemicelluloses, the more stable polymer-polymer hydrogen bonds will presumably form. Consequently, upon a subsequent re-saturation and desorption, the hygroscopicity will be slightly lower due to a decrease in available sorption sites, thus yielding a MR above unity. This effect has been found for other materials, such as polymers (Watt 1980), collagen (Green 1948), and textile fibers (Jeffries 1960).

For both types of drying, the MR in Figure 2b shows that a change occurs around 85% RH. Below this humidity, the MR decreases with decreasing RH, whereas it decreases with increasing humidity above 85% RH. For the VACUUM2 specimens, the decrease in MR at high RH is less pronounced than that for the OVENDRY2 specimens. For VACUUM2, MR approaches unity for RH close to saturation. This implies that vacuum saturation restores the MC of vacuum dried wood to that of green wood, but that the sorption isotherm nevertheless lies below that of green wood throughout the RH range included in the study. The MR of OVENDRY2 specimens is below unity for very high RH. At 98.4% RH, $MR \approx 0.97$ corresponding to slightly higher MCs in the oven-dried specimens at high RH than in green wood following vacuum saturation, i.e., the desorption isotherm of the oven-dried specimens crosses that of green wood at approximately 96% RH. The same tendency was found in the additional tests at very high RH (Figure 1b), confirming that at these RH values the OVENDRY2-desorption isotherm lies above the GREEN1-desorption isotherm. To the best of the authors' knowledge this has not been documented earlier.

Capillary sorption could theoretically explain the higher MC in oven-dried wood at high RH compared to green wood. It is well known that heat treatment of wood can cause chemical degradation and removal of cell wall material (Stamm 1956). The microvoids left behind due to loss of material can cause an increased hygroscopicity at high RH due to capillary condensation, whereas the hygroscopicity at lower RH is decreased due to loss of sorption sites in the cell wall (Hoffmeyer et al. 2003). A similar change in hygroscopicity is evident for the OVENDRY2 specimens in Figure 2b. In this study, however, the temperature and duration of drying are considered insufficient to cause significant chemical degradation of the wood cell wall (Kollmann et al. 1969).

Water in green and rewetted wood studied by TD LF NMR

Drying stresses may cause microcracks which could lead to capillary condensation at high RH. A possible presence of such capillaries to allow condensation of water in the cell wall of the OVENDRY2 specimens may be assessed by testing a possible presence of freezable water (Petrov and Furó 2009). Therefore, TD LF NMR was carried out at +20 and at -20°C for a subset of the OVENDRY2 and the GREEN1 specimens. Figure 3 shows the mean FIDs of the two sample

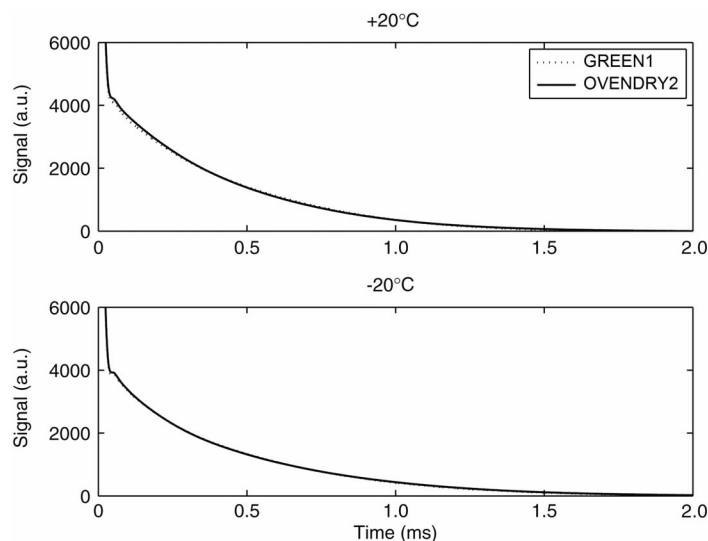


Figure 3 Mean free induction decay (FID) relaxation curves from LF TD NMR of 36 specimens of each of the two sample types GREEN1 and OVENDRY2 at +20°C and at -20°C. Data for different moisture contents have been pooled.

types. All four mean curves appear to be almost identical. This indicates that neither sample type contained freezable water at temperatures as low as -20°C. This comparison based solely on mean FIDs may, however, be misleading as the specimens within the two samples contained different amounts of water, as seen in Figure 1a. In order to check for possible individual effects of freezing, a principal component analysis was carried out of the FIDs from both samples at both temperatures (Figure 4). This analysis shows that freezing did not affect the FIDs of the individual specimens systematically (Figure 4a and Figure 4b), albeit the amplitude of the effect does seem to be somewhat related to the MC (Figure 4c), regardless of treatment. In any case, the lack of systematic differences in the FIDs between the two samples and temperatures means that the state of the water in all specimens is similar, and that neither of the two samples contained any water that froze at -20°C. This temperature corresponds to freezing of water in microvoids with a radius down to 3 nm (Petrov and Furó 2009). Thus, the extra water present in OVENDRY2 specimens compared to GREEN1 specimens at high RH was not due to capillary condensation in microvoids, but must have been caused by increased amounts of bound water. That the EMC of oven-dried wood is higher than that of green wood close to saturation thus remains unexplained.

Conclusions

The study compares the desorption isotherms in the range from 60.1% to 99.9% RH for green Norway spruce sapwood (1st desorption) with the sorption isotherms of similar specimens that had been dried and remoistened using a variety of procedures (2nd desorptions). All desorption tests were carried out at 20°C. The main conclusions are as follows:

- Exposure to an atmosphere of saturated water vapor does not result in saturation of the wood cell wall, but rather produces an EMC representative of a RH of around 98.5%.
- A 2nd desorption curve initiated from a state of water vapor saturation represents an intermediate isotherm starting at the adsorption boundary curve well below the FSP and then crossing over to eventually meet the desorption boundary curve at a RH value around 75%–80%. Vacuum saturation restores full saturation of the cell wall.
- The 2nd desorption curve reveals only little change of hygroscopicity caused by drying at room temperature. At high RH no change is seen.
- Oven-drying at 103°C produces a loss of hygroscopicity for RH below 96%. The loss is ascribed to the process history allowing a short period of both high temperature and MC. Both lignin and hemicelluloses then pass their glass transition and enter into a rubbery state. The resultant softening allows a rearrangement of the cell wall polymers into an energetically more favorable state resulting in fewer available sorption sites.
- Oven-drying at 103°C produces an increase of hygroscopicity for RH above 96%. It is shown that the increase is not caused by capillary sorption in voids. The cause of this increase in hygroscopicity remains unexplained.
- The FSP defined as the EMC at a matrix potential $\psi_m = -0.1$ MPa (RH = 99.93%, void radius = 1.5 μm), is of the order FSP $\approx 38\%$ for the 1st desorption of green specimens and FSP $\approx 42\%$ for the desorption of oven-dried specimens that are subsequently vacuum saturated.
- The shape of the desorption isotherm at high values of RH for green specimens confirms the findings reported in an earlier study (Thygesen et al. 2010; Englund et al. 2010) regarding the modest role of capillary condensation in wood-water relations below the FSP.

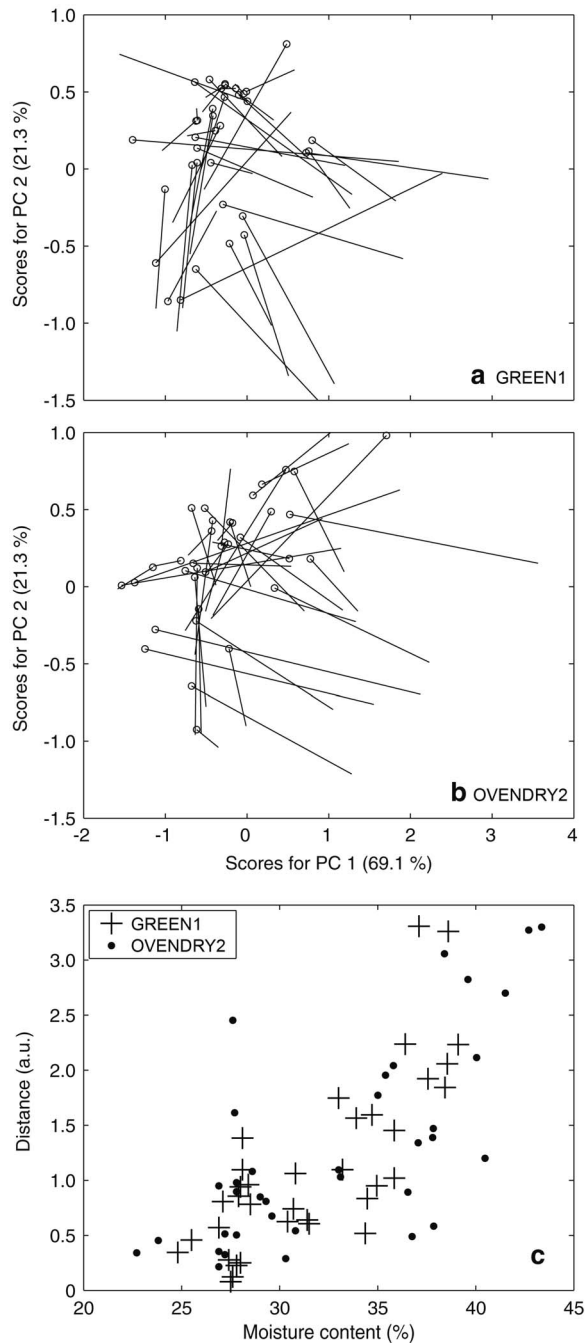


Figure 4 Principal component analysis of the 2 (sample types) \times 36 (specimens) \times 2 (temperatures) = 144 FID relaxation curves summarized in Figure 3. Scores for factor 1 vs. scores for factor 2 are shown separately for the two sample types, green specimens in a) and dried and remoistened specimens in b). Each line connects the position of a sample at +20°C with its position at -20°C (marked by a circle). c) The distances between the positions at +20 and at -20°C (as seen in Figures 4a and 4b) vs. the moisture content of the specimens at +20°C.

Acknowledgements

The authors wish to thank Ulla Gjøel Jacobsen for her invaluable and never tiring technical support during the cumbersome experi-

ments that formed the basis of this work. LGT acknowledges funding from The Danish Research Council for Technology and Production Science (project no. 26-02-0100).

References

- Almeida, G., Hernández, R.E. (2006a) Changes in physical properties of yellow birch below and above the fiber saturation point. *Wood Fiber Sci.* 38:74–83.
- Almeida, G., Hernández, R.E. (2006b) Changes in physical properties of tropical and temperate hardwoods below and above the fiber saturation point. *Wood Sci. Technol.* 40:599–613.
- Araujo, C.D., MacKay, A.L., Hailey, J.R.T., Whittall, K.P., Le, H. (1992) Proton magnetic resonance techniques for characterization of water in wood: application to white spruce. *Wood Sci. Technol.* 26:101–113.
- Barkas, W.W. (1936) Wood-water relationships, 2: the fibre saturation point of beech wood. *Proc. Phys. Soc.* 48:576–588.
- Cox, J., McDonald, P.J., Gardiner, B.A. (2010) A study of water exchange in wood by means of 2D NMR relaxation correlation and exchange. *Holzforchung* 64:259–266.
- Engelund, E.T., Thygesen, L.G., Hoffmeyer, P. (2010) Water sorption in wood and modified wood at high values of relative humidity. Part 2: Appendix. Theoretical assessment of the amount of capillary water in wood microvoids. *Holzforchung* 64:325–330.
- Garvey, C.J., Parker, I.H., Simon, G.P., Whittaker, A.K. (2006) The hydration of paper studied with solid-state magnetisation-exchange ^1H NMR spectroscopy. *Holzforchung* 60:409–416.
- Green, R.W. (1948) Adsorption of water vapour on collagen and elastin. *Trans. Roy. Soc. New. Zeal.* 77:24–46.
- Griffin, D.M. (1977) Water potential and wood-decay fungi. *Ann. Rev. Phytopathol.* 15:319–329.
- Hermans, P.H. (1949) *Physics and Chemistry of Cellulose Fibers*. New York-Amsterdam-London-Brussels Elsevier Publishing Co. Inc. pp. 180–196.
- Hernández, R.E., Bizoñ, M. (1994) Changes in shrinkage and tangential compression strength of sugar maple below and above the fiber saturation point. *Wood Fiber Sci.* 26:360–369.
- Hernández, R.E., Pontin, M. (2006) Shrinkage of three tropical hardwoods below and above the fiber saturation point. *Wood Fiber Sci.* 38:474–483.
- Hill, C.A.S. (2008) The reduction in the fibre saturation point of wood due to chemical modification using anhydride reagents: a reappraisal. *Holzforchung* 62:423–428.
- Hill, C.A.S., Forster, S.C., Farahani, M.R.M., Hale, M.D.C., Ormondroyd, G.A., Williams, G.R. (2005) An investigation of cell wall micropore blocking as a possible mechanism for the decay resistance of anhydride modified wood. *Int. Biodet. Biodeg.* 55:69–76.
- Hoffmeyer, P., Jensen, S.K., Jones, D., Klinke, H.B., Felby, C. (2003) Sorption properties of steam treated wood and plant fibres. In: *Proceedings of the First European Conference on Wood Modification*, Eds. Van Acker, J., Hill, C., Ghent University, Ghent, April 3–4, pp. 177–189.
- Jeffries, R. (1960) Sorption of water by cellulose and eight other textile polymers – part 2: the sorption of water vapour below 100°C by textile polymers other than cellulose. *J. Textil. Inst. Trans.* 51:T399–T418.
- Johannessen, E.H., Hansen, E.W., Rosenholm, J.B. (2006) Fluid self-diffusion in Scots pine sapwood tracheid cells. *J. Phys. Chem.* 110:2427–2434.

- Kekkonen, P.A., Telkki, V.V., Jokisaari, J. (2009) Determining the Highly Anisotropic Cell Structures of *Pinus sylvestris* in Three Orthogonal Directions by PGSTE NMR of Absorbed Water and Methane. *J. Phys. Chem. B* 113:1080–1084.
- Kelley, S.S., Rials, T.G., Glasser, W.G. (1987) Relaxation behaviour of the amorphous components of wood. *J. Mater. Sci. Lett.* 22:617–624.
- Kollmann, F., Schmidt, E., Kufner, M., Fengel, D., Schneider, A. (1969) Gefüge- und Eigenschaftsänderungen im Holz durch mechanische und termische Beanspruchung. *Holz Roh-Werks.* 27:407–425.
- Menon, R.S., MacKay, A.L., Hailey, J.R.T., Bloom, M., Burgess, A.E., Swanson, J.S. (1987) An NMR determination of the physical water distribution in wood during drying. *J. Appl. Polymer Sci.* 33:1141–1155.
- Petrov, O.V., Furó, I. (2009) NMR cryoporometry: principles, applications and potential. *Progr. Nucl. Magn. Reson. Spectros.* 54:97–122.
- Seborg, C.O., Simmonds, F.A., Baird, P.K. (1938) Sorption of water vapour by papermaking materials: irreversible loss of hygroscopicity due to drying. *Paper Trade J.* 107:223–228.
- Skaar, C. (1988) *Wood-Water Relations*. Springer-Verlag, Berlin Heidelberg.
- Spalt, H.A. (1958) The fundamentals of water sorption by wood. *Forest Prod. J.* 10:288–295.
- Stamm, A.J. (1956) Thermal degradation of wood and cellulose. *Ind. Eng. Chem.* 48:413–417.
- Stamm, A.J. (1964) *Wood and Cellulose Science*. The Ronald Press Company, New York.
- Stone, J.E., Scallan, A.M. (1967) The effect of component removal upon the porous structure of the cell wall of wood. II. Swelling in water and the fiber saturation point. *Tappi* 50:496–501.
- Topgaard, D., Södermann, O. (2001) Diffusion of water absorbed in cellulose fibers studied with $^1\text{H-NMR}$. *Langmuir* 17:2694–2702.
- Thygesen, L.G., Engelund, E.T., Hoffmeyer, P. (2010) Water sorption of wood and modified wood at high values of relative humidity. Part 1: results for untreated, acetylated and furfurylated Norway spruce. *Holzforschung* 64:315–323.
- Tiemann, H.D. (1906) Effect of moisture upon the strength and stiffness of wood. *USDA For. Serv. Bull.* 70.
- Urquhart, A.R. (1929) The mechanism of the adsorption of water by cotton. *J. Text. Inst.* 20:T125–T132.
- Urquhart, A.R., Eckersall, N. (1930) The moisture relations of cotton, VII – A study of hysteresis. *J. Textil. Inst. Trans.* 21:T499–T510.
- Watt, L.C. (1980) Adsorption-Desorption Hysteresis in Polymers. *J. Macromol. Sci-Chem.*, A14:245–255.

Received December 1, 2010. Accepted May 6, 2011.

Previously published online July 8, 2011.

PAPER IV

Modelling time-dependant behaviour of softwood using deformation kinetics

Engelund E. T. and Svensson S.

Holzforschung (2011) 65:231-237

Modelling time-dependent mechanical behaviour of softwood using deformation kinetics

Emil Tang Engelund^{1,2,*} and Staffan Svensson²

¹ Wood Technology, Danish Technological Institute, Taastrup, Denmark

² Department of Civil Engineering, Technical University of Denmark, Lyngby, Denmark

*Corresponding author.

Wood Technology, Danish Technological Institute, Gregersensvej 4, DK-2630 Taastrup, Denmark
E-mail: ete@teknologisk.dk

Abstract

The time-dependent mechanical behaviour (TDMB) of softwood is relevant, e.g., when wood is used as building material where the mechanical properties must be predicted for decades ahead. The established mathematical models should be able to predict the time-dependent behaviour. However, these models are not always based on the actual physical processes causing time-dependent behaviour and the physical interpretation of their input parameters is difficult. The present study describes the TDMB of a softwood tissue and its individual tracheids. A model is constructed with a local coordinate system that follows the microfibril orientation in the S2 layer of the cell wall. The inclination of the local system to the global coordinate system reflects the microfibril angle of the tracheid. Normal excitations in the local system perform linear elastically, whereas shearing excitation in the local system produces both elastic and inelastic responses. The results of the model are compared with experimental results of different types. It was observed that the model is able to describe the results. Moreover, to some surprise, the introduction of only elastic and viscous properties on the microscopic scale leads to an apparent macroscopic viscoelasticity, i.e., the time-dependent processes are to a significant degree reversible.

Keywords: constitutive modelling; creep; kinetics; relaxation; time-dependent behaviour.

Introduction

The time-dependent mechanical behaviour (TDMB) of wood is far greater than that of most other building materials. Owing to the desired longevity of buildings, predicting the mechanical behaviour of timber many decades ahead is important. This has typically been done by using rheological mathematical models (Morlier and Palka 1994). Often these models assume contributions from elastic, viscoelastic, and viscous components. However, the physical interpretation of

the parameters applied in such models is often difficult (Hunt 1997; Gril et al. 2004). This is because these mathematical models typically are not related to the physical mechanisms behind the observed mechanical behaviour (Hunt 1997).

The aim of this study was to describe the mechanical behaviour of softwood xylem and individual tracheids. This is done by considering the basic composition and material structure of the tracheid. Assumptions are included into simple mathematical equations with regard to the mechanism causing TDMB.

Tracheid structure and mechanical behaviour

The significant component of the tracheid in terms of load bearing is the cellulose microfibril (MF). These highly ordered aggregates of aligned cellulose chains (Atalla et al. 2008) have a helical structure with inclinations varying in the layers of the tracheid walls. However, the thick S2 layer of the cell wall constitutes approximately 80% of the whole cell wall (Brändström 2001). Therefore, the mechanical behaviour of tracheids is dominated by the contribution from the MFs in the S2 layer and is closely connected to the microfibril angle (MFA), i.e., the inclination of the MFs in the S2 layer. For instance, the modulus of elasticity (MOE) decreases with increasing MFA (Persson 2000). Also, the TDMB of wood is influenced by the MFA (Gril et al. 2004; Kojima and Yamamoto 2004).

When a constant load is applied to wood, the deformation will increase over time, whereas if a constant deformation is applied, the required load will decrease over time. These two processes are termed creep and relaxation, respectively. The effect of MFA on these processes has been illustrated, for instance, by Kojima and Yamamoto (2004) who found that the tensile creep in the longitudinal direction increases dramatically with increasing MFA.

The mechanism behind the TDMB has been ascribed to sliding between the MFs (Balashov et al. 1957; Lotfy et al. 1972; Olsson and Salmén 2001). This sliding over time is controlled by flow processes within the material, where the internal hydrogen bonds between the constituents are broken, moved and reformed in new configurations (van der Put 1989; Hanhijärvi 1995; Bonfield et al. 1996).

Modelling mechanical behaviour of tracheids

In this study, numerical modelling is used to describe the mechanical behaviour of tracheids. This behaviour is assumed to be controlled by the behaviour of its dominant S2 layer. Thus, the composition and structure of only this layer is considered in this study.

Figure 1 is a schematic illustration of the S2 layer of a tracheid along with two different coordinate systems. The

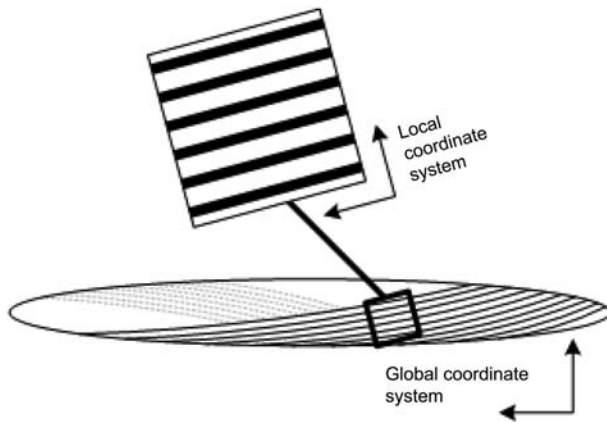


Figure 1 Global and local coordinate systems for a single cell.

local coordinate system is oriented along the MFs, whereas the global coordinate system is oriented in the longitudinal direction of the cell. These two coordinate systems are used to incorporate contributions of both composition and structure in the model. For instance, the mechanical properties are defined in the local system by the composition of the constituents and their mechanical properties. By contrast, the effect of the tracheid structure is reflected in the angle between local and global coordinate systems which is similar to the MFA of the tracheid. With this approach, Berg and Gradin (1999) modelled the elastic behaviour of single wood cells with accurate results.

In the local coordinate system, the mechanical properties of the cell wall can be derived from those of the cellulose MFs and the embedding matrix (composed of hemicelluloses and lignin) using composite theory. Sliding between the MFs on the microscopic scale is equivalent to shearing deformations. The basic assumption in this study is that time-dependent properties of the cell wall composite are only relevant for shearing modes. Thus, normal excitations in the local coordinate system cause only linear elastic responses. These properties are a result of the lengthening and/or rotation of covalent and hydrogen bonds (Hinterstoisser et al. 2003). By contrast, shearing excitations in the local system will cause both elastic and inelastic responses. The elastic shear response is thought to be caused by lengthening and/or rotation of hydrogen bonds, whereas the inelastic response is a result of the sliding between MFs controlled by the rate of breaking and reformation of hydrogen bonds.

Shearing modelled with deformation kinetics

The rate of processes such as the one occurring in shearing can be described by the theory of deformation kinetics. This theory has already been applied to the TDMB of wood (for example, van der Put 1989; Hanhijärvi 1995; Bonfield et al. 1996). However, the novelty in this study is that time-dependent processes are only active in shearing modes.

The breaking and reforming of hydrogen bonds can be described by a deformation kinetics approach in terms of a potential energy surface. A visualisation of this surface is the symmetrical energy barrier seen in Figure 2. In a stress-free

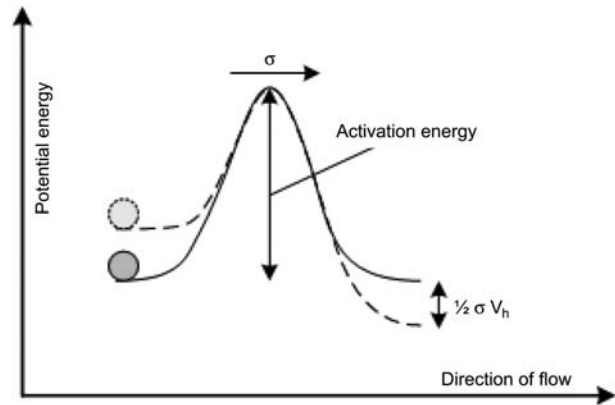


Figure 2 Symmetrical energy barrier for a flow process. The height of the energy barrier is the activation energy. When a force is applied the energy barrier is tilted, favouring movement in the force direction.

state, the probability of moving both forwards and backwards is equal. However, if a force is applied, the energy needed to cross the energy barrier is shifted, favouring movement along the direction of the force.

The strain rate for a fully viscous flow process governed by a single energy barrier can be described (Krausz and Eyring 1975) by Eq. (1):

$$\frac{d\varepsilon}{dt} = \frac{1}{G} \frac{d\sigma}{dt} + \frac{V_h}{V_m} \frac{kT}{h} \exp\left(-\frac{\Delta G^\ddagger}{kT}\right) 2\sinh\left(\frac{V_h\sigma}{2kT}\right) \quad (1)$$

where ε is the shear strain, t is time, G is the shear modulus, and σ is the shear stress. The parameters V_h and V_m are the volume swept by the motion and the volume of the moving segment itself, respectively, whereas k is Boltzmann's constant, h is Planck's constant, and T is the temperature. The difference in potential energy between the non-activated and the activated states is termed the activation energy (Eyring 1935) and is related to the Gibbs' free energy of activation, ΔG^\ddagger .

Under isothermal conditions, Eq. (1) can be simplified to the following form:

$$\frac{d\varepsilon}{dt} = \frac{1}{G} \frac{d\sigma}{dt} + A \cdot 2\sinh(B\sigma) \quad (2)$$

Materials and method

The numerical modelling is performed on commercially available numerical software. The theory presented here should, however, be applicable to any mechanics software which can handle user-defined partial differential equations.

Geometry

To simulate the TDMB of tracheids without having too many degrees of freedom, only a length section of 250 μm of a single

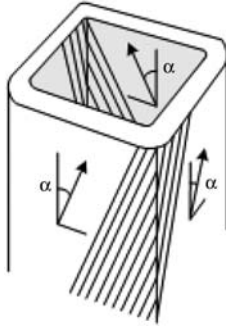


Figure 3 Schematic illustration of geometry of the numerical model.

tracheid is modelled. The cross-section of the tracheid is quadratic with rounded corners, see Figure 3. The wall thickness is set to 2 μm for earlywood (EW) and to 4 μm for latewood (LW) fibres. The width of the EW and LW fibres are set to 40 μm (EW) and 20 μm (LW), based on cell dimensions for Norway spruce according to Fengel and Stoll (1973).

Mechanical cell wall properties

The local cell wall properties are assigned based on literature data of elastic mechanical properties of the chemical constituents, see Table 1. These can be calculated from composite theory for laminar structures assuming a structure with relatively stiff cellulose MFs embedded in a matrix with average properties of hemicelluloses and lignin. The MOE along the MFs and perpendicular to them can thus be approximated by Reuss and Voigt bounds (McCullough et al. 1976), respectively, due to the assumed laminar structure. The Poisson's ratio between the longitudinal and transverse direction can be derived from the same basic assumptions as the Reuss model (McCullough et al. 1976). The Poisson's ratio between the transverse directions is assumed to be equal to that of the matrix. The shear modulus of the transverse and longitudinal material directions is determined by applying composite theory, whereas the shear modulus of the two transverse directions can be derived under the assumption of in-plane isotropy.

The local coordinate system of the cell wall is tilted with regards to the global coordinate system with an angle corresponding to the assumed MFA of the tracheid. This is done in such a way that two opposing sides have the same inclination but with opposing sign, hereby representing the helical arrangement of the MFs (Figure 3). The local shear behaviour is modelled by deformation kinetics with literature data for wood (Bonfield et al. 1996) and for rayon cellu-

lose (Krausz and Eyring 1975) as input parameters. The kinetic parameters are summarized in Table 2. To account for the influence of water on the kinetics, the effect of varying the kinetic parameter A in Eq. (2) was investigated. This was done based on the hypothesis that the influence of moisture is more related to the height of the energy barrier, i.e., the activation energy than any other kinetic input parameter.

Loading conditions and constraints

The loading conditions in terms of a constant deformation (relaxation) or constant load (creep) are based on experimental results (Lotfy et al. 1972; Eder et al. 2006). The results cover several different sets of literature data for tensile testing of both softwood single fibres and softwood tissues. The literature data for single fibres include relaxation experiments with EW fibres in a moisture saturated condition (Eder et al. 2006). The literature data for tensile testing of tissues include relaxation experiments with EW tissue in a saturated condition (Eder et al. 2006) and creep experiments with normal wood tissue at 23°C, 50% RH (Lotfy et al. 1972). It is vital that the MFA is stated or can be approximated for each set of data for the numerical model to be properly evaluated. Often, however, not all necessarily input data in terms of MFA, cell wall area or either wood or cell wall stiffness are given in the evaluated literature. Therefore, assumed values for the straining of the model fibres are used which yield reasonable stresses on the cell wall level.

The constraint applied on the modelled fibres differ between simulations of single fibres and tissues. For the previous, the rotation of one end of the fibre is restricted simulating a single fibre which is free to rotate. The influence of freedom of rotation is examined by including simulations where rotation is restricted in both ends. This simulates single fibres with both ends clamped. For the tissue, the rotation along the entire length of the fibre is restricted simulating the constraint from neighbouring fibres in a tissue.

Results and discussion

Elastic behaviour

The results for both the local elastic cell wall properties as well as the elastic properties of the cell as a whole are in accordance with the calculated values from the literature (Berg and Gradin 1999). In Table 3, the properties along the MFs and for the cell wall with an MFA of 15° are given. The only values that deviate markedly are the transverse Young's modulus and the shear moduli, all in the saturated condition. The probable explanation for the very low values

Table 1 Mechanical properties of the different cell wall components at 20°C.

Component	Property	Dry condition	12% MC	Saturated
Cellulose	Fraction of cellulose in the cell wall	$c=0.5$	$c=0.5$	$c=0.5$
	Longitudinal modulus of elasticity	$E_L=134$ GPa	$E_L=134$ GPa	$E_L=134$ GPa
	Transverse modulus of elasticity	$E_T=27.2$ GPa	$E_T=27.2$ GPa	$E_T=27.2$ GPa
	Shear modulus	$G=4.4$ GPa	$G=4.4$ GPa	$G=4.4$ GPa
	Poisson's ratio	$\nu=0.2$	$\nu=0.2$	$\nu=0.2$
Hemicellulose/lignin matrix	Longitudinal modulus of elasticity	$E_L=6$ GPa	$E_L=4$ GPa	$E_L=2$ GPa
	Transverse modulus of elasticity	$E_T=4$ GPa	$E_T=3$ GPa	$E_T=2$ GPa
	Shear modulus	$G=2$ GPa	$G=1.5$ GPa	$G=1$ GPa
	Poisson's ratio	$\nu=0.3$	$\nu=0.3$	$\nu=0.3$

Values are based on Berg and Gradin (1999) and Peura et al. (2007).

Table 2 Kinetic parameters used in the present study.

Parameter	Explanation	Value
V_h	Volume of hole swept by the flow motion	$5.22 \times 10^{-27} \text{ m}^3$
V_m	Volume of flowing segment	$1.09 \times 10^{-27} \text{ m}^3$
k	Boltzmann's constant	$1.38 \times 10^{-23} \text{ J K}^{-1}$
T	Absolute temperature	293 K
h	Planck's constant	$6.63 \times 10^{-34} \text{ J s}$
ΔG^\ddagger	Change in Gibbs' free energy	$1.12 \times 10^5 \text{ J mol}^{-1}$
N_A	Avogadro's constant	$6.02 \times 10^{23} \text{ mol}^{-1}$

Parameters are taken from Bonfield et al. (1996) and Krausz and Eyring (1975).

Table 3 Elastic results from this study compared with numerical modelling (Berg and Gradin 1999).

Condition	Berg and Gradin (1999)		This study	
	12% MC (GPa)	Saturated (GPa)	12% MC (GPa)	Saturated (GPa)
S2 layer				
Young's modulus, L	69.2	67.1	69.5	68
Young's modulus, T	7.33	0.32	5.40	3.73
Shear modulus, LT	2.73	0.02	2.22	1.92
Shear modulus, TT	2.83	0.02	2.08	1.43
Cell wall, MFA=15				
Young's modulus, L	46	42	41.9	38.0

The properties in the S2 layer are determined in the material direction, i.e., along the microfibrils, whereas the cell wall properties are in the longitudinal direction of the cell.

in the paper of Berg and Gradin (1999) is that the elastic properties of the hemicelluloses are set very low in the saturated condition due to the softening effect of water (Olsson and Salmén 2004). In this study, such low values are not used because it is the opinion of the authors that these low values rather reflect TDMB of the hemicelluloses than actual elastic behaviour. The softening of the hemicelluloses should therefore be incorporated in the time-dependent shearing. Young's moduli for the entire cell based on its gross cross-section are in the ranges 5.2–12.4 GPa.

Experimental results for spruce fibres, tissues and solid wood with MFAs in the range 0–5° at around 12% moisture content (MC) was 9.9–12.1 GPa and 26.2–29.4 GPa for the gross and the actual cross-sectional area, respectively (Keunecke et al. 2008). The reason why the current model predicts a modulus of 12.4 GPa for MFA of 15° could be partly due to a swelled cross-sectional area at 12% MC, which is not accounted for in the current model. Also, the entire cell wall is assigned S2 layer properties, whereas only approximately 80% of the cross-section of a real EW cell consists of the S2 layer (Brändström 2001).

Time-dependent behaviour

Figure 4 compares results from experimental findings with the numerical model. The legends of the figure show a variation in the input parameter A in Eq. (2).

The relaxation of single Norway spruce fibres is illustrated in Figure 4a and b. It is clear from the previous that the rotational freedom of the fibre is seen to have a major influence on the relaxation behaviour. This has also been found

to be the case in the elastic domain, where freedom of rotation decreases the MOE of the fibre (Marklund and Varna 2009). In the time-dependent case, larger freedom of rotation results in faster stress relaxation. Moreover, the stress relaxation appears to stop after a certain time duration. However, the stress level, after relaxation has died out, depends on the freedom of rotation. It is clear from Figure 4a that the partial restriction of rotation better explains the experimental results. In Figure 4b, this restraining condition is the basis for the presented modelling results. It is clear that for MFAs of between 7 and 10 and with a kinetic input parameter in the range of 10–20 A_0 , the model is fully capable of describing the TDMB. The value A_0 is calculated on the basis of the parameters presented in Table 3. In Figure 4c, the same kinetic input parameters and MFAs are used to model a Norway spruce tissue in relaxation. Again, the model is able to describe the observed experimental behaviour. However, there is a difference in behaviour between the relaxation of tissues and single fibres in that the single fibres seem to converge to a more or less stable stress level, whereas the stress relaxation process continues in the tissues case. This can be seen in Figure 4d, where the declination of the stress-time curve is larger for tissues than for single fibres, even though the results for the latter do not extend beyond 400 s. This can perhaps be explained by an additional component of the TDMB of tissues, i.e., the shear time-dependent behaviour of the middle lamella. As it is now, the model is fully capable of explaining single fibre behaviour while only considering the behaviour of the S2 layer. This is possibly due to the lower longitudinal stiffness of the other cell wall

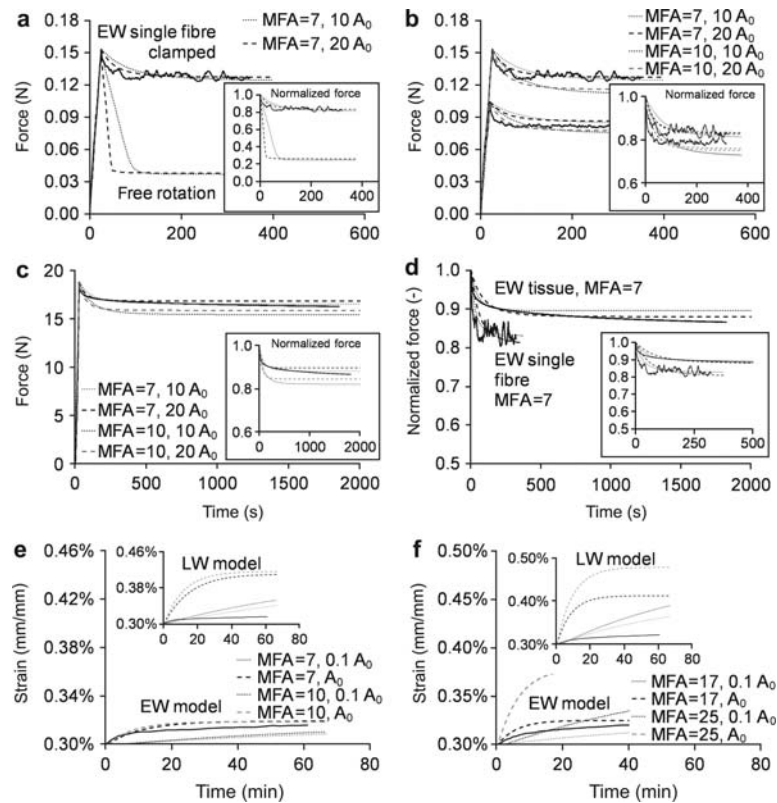


Figure 4 (a) Experimental results for relaxation of single Norway spruce fibres (MFA = 7–10°) from Eder et al. (2006) compared with numerical EW model with the model fibre either clamped in both ends or with free rotation ability. (b) Experimental results for relaxation of single Norway spruce fibres (MFA = 7–10°) from Eder et al. (2006) at two different load levels compared with numerical EW model. In this case the model fibres are clamped in both ends. (c) Experimental results for relaxation of Norway spruce tissues (MFA = 7–10°) from Eder et al. (2006) compared with numerical EW model. (d) Experimental results for relaxation of both single fibres and tissues of Norway spruce compared (MFA = 7–10°), from Eder et al. (2006). Also inserted are the results from the numerical EW model. (e) Experimental results for creep of Sitka spruce tissue (MFA = 9.2°) from Lotfy et al. (1972) compared with numerical EW and LW models. (f) Experimental results for creep of Douglas fir tissue (MFA = 21.6°) from Lotfy et al. (1972) compared with numerical EW and LW models.

layers and the dominant contribution of the S2 layer. Thus, the mechanical behaviour of single fibres can be illustrated by a system of individual layers connected in parallel with the contribution of the dominating S2 layer. If other cell wall layers were also incorporated, only minor improvements in the predictions of single fibre behaviour should be expected. In tissues, however, the middle lamella is responsible for transferring load between the individual cells. It is possible that the mechanical response of this intercellular layer cannot be regarded as being connected in parallel with the mechanical response of the individual cells. Thus, if the TDMB of wood tissues should be predicted, the effect of the middle lamella should be incorporated.

Creep of different softwood tissues is presented in Figure 4e and f. Here, it is also evident that the geometry of the model fibre influences the TDMB. Thus, the EW fibre with its higher polar moment of inertia seems better capable of describing the experimental results than the thick-walled, smaller LW model fibre. As remarked before, the TDMB related to shearing of the middle lamella might be needed to fully predict the mechanical behaviour.

In the simulation of all the experimental results, the kinetic input parameter A has been varied in the range of 0.1–20

A_0 . This variation is based on an expectation of the influence of moisture on the barrier height, i.e., the activation energy of the shearing process. The fitting of the numerical model to the experimental results by varying the kinetic parameter A seems to follow the expected tendency of smaller activation energy with greater MC. However, more accurate experimental accounts of creep and relaxation of fibres and tissues with known MFA are needed to fully fit the numerical model to the experimental data.

A somewhat surprising result of the present model is that it is capable of simulating apparent viscoelastic behaviour, even though only elastic and viscous behaviour are permitted on a microscopic scale. This can be seen in Figure 5 which illustrates the TDMB of the numerical models of EW and LW for a load history with constant load for a little over 0.5 h followed by an equal amount of time without load. It is clear that the macroscopic behaviour is apparent viscoelastic, and that no viscoelastic component in the local coordinate system is needed to predict macroscopic apparent viscoelasticity. The shearing of the MFs past each other is dependent on the breaking and reforming of intermolecular hydrogen bonds. This process is viscous in that the only potential for reversing this process is the elastic energy stored

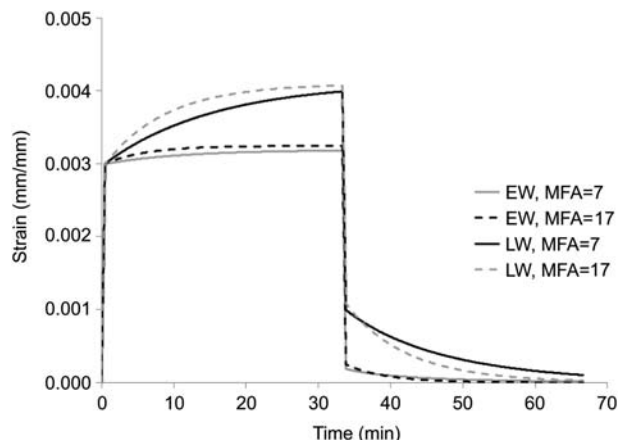


Figure 5 Creep and creep recovery for models of both EW and LW models with two different MFA levels. The load has been tuned so similar elastic strains are produced by both models.

in the covalent bonds of the MFs. Therefore, the fact that only elastic and viscous components are needed to explain macroscopic wood behaviour is in line with theories regarding the very nature of the causal mechanisms.

Conclusions

The present study uses very simple basic assumptions regarding the mechanism of TDMB of wood. One assumption is that the elastic properties derive from lengthening of covalent bonds, whereas the TDMB of wood is caused by breaking and reforming of hydrogen bonds. This is modelled by only allowing time-dependency, described by kinetic theory, in the shearing modes on the microscopic scale, whereas all other modes are purely elastic. Thus, no viscoelastic property is assigned to the model. The mechanical behaviour on macro-scale is nonetheless apparent viscoelastic, i.e., the TDMB is to a significant degree reversible. The results indicate that TDMB such as creep and relaxation originate from complex interactions of very simple molecular mechanisms and the structural arrangement of the components in wood cell walls.

Furthermore, the numerical model was fitted to different sets of experimental data of creep and relaxation behaviour. This was done by varying the MF angle and the kinetic input parameter related to the activation energy of the shearing process. The model was capable of describing the various experimental findings well, and the changes in the kinetic parameter was in line with the expectation of lower activation energy of the shearing process with greater MC.

The model was only partly able to describe relaxation behaviour of wood tissues, perhaps due to a missing component in the macroscopic TDMB: viscous shearing in the middle lamella. This is, however, very speculative and further experimental investigations on this topic are needed.

Acknowledgements

The authors would like to gratefully thank Dr. Michaela Eder and her colleagues at Max Planck Institute, Potsdam, Germany for providing experimental data.

References

- Atalla, R.H., Brady, J.W., Matthews, J.F., Ding, S.-Y., Himmel, M.E. (2008) Structures of plant cell wall celluloses. In: *Biomass Recalcitrance – Deconstructing the Plant Cell Wall for Bioenergy*. Ed. Himmel, M.E. Blackwell Publishing Ltd., Oxford, UK. pp. 188–212.
- Balashov, V., Preston, R.D., Ripley, G.W., Spark, L.C. (1957) Structure and mechanical properties of vegetable fibres 1: the influence of strain on the orientation of cellulose microfibrils in sisal leaf fibre. *Proc. R. Soc. Lond. B Biol. Sci.* 146:460–468.
- Berg, J.E., Gradin, P.A. (1999) A micromechanical model of the deterioration of a wood fibre. *J. Pulp Pap. Sci.* 25:66–71.
- Bonfield, P.W., Mundy, J., Robson, D.J., Dinwoodie, J.M. (1996) The modelling of time-dependant deformation in wood using chemical kinetics. *Wood Sci. Technol.* 30:105–115.
- Brändström, J. (2001) Micro- and ultrastructural aspects of Norway spruce tracheids: a review. *IAWA J.* 22:333–353.
- Eder, M., Burgert, I., Stanzl-Tschegg, S. (2006) Relaxation experiments on wood fibres and tissues. In: *Proceedings of the Third International Conference of the European Society of Wood Mechanics*. Vol. 1. Eds. Morlier, P., Morais, J., Dourado, N. FCT, Vila Real, Portugal. pp. 141–147.
- Eyring, H. (1935) The activated complex and the absolute rate of chemical reactions. *Chem. Rev.* 17:65–77.
- Fengel, D., Stoll, M. (1973) Variation of cell cross area, thickness of cell-wall and of wall layers of sprucewood tracheids within an annual ring. *Holzforschung* 27:1–7.
- Gril, J., Hunt, D., Thibaut, B. (2004) Using wood creep data to discuss the contribution of cell-wall reinforcing material. *C. R. Biol.* 327:881–888.
- Hanhijärvi, A. (1995) Modelling of Creep Deformation Mechanisms in Wood. VTT Publications 231. Technical Research Centre of Finland, Espoo. pp. 79–91.
- Hinterstoisser, B., Åkerholm, M., Salmén, L. (2003) Load distribution in native cellulose. *Biomacromolecules* 4:1232–1237.
- Hunt, D.G. (1997) Dimensional changes and creep of spruce, and consequent model requirements. *Wood Sci. Technol.* 31:3–16.
- Keunecke, D., Eder, M., Burgert, I., Niemz, P. (2008) Micromechanical properties of common yew (*Taxus baccata*) and Norway spruce (*Picea abies*) transition wood fibers subjected to longitudinal tension. *J. Wood Sci.* 54:420–422.
- Kojima, Y., Yamamoto, H. (2004) Effect of microfibril angle on the longitudinal tensile creep behavior of wood. *J. Wood Sci.* 50:301–306.
- Krausz, A.S., Eyring, H. *Deformation Kinetics*. Wiley, New York, 1975.
- Lotfy, M., El-osta, M., Wellwood, R.W. (1972) Short-term creep as related to microfibril angle. *Wood Fiber Sci.* 4:26–32.
- Marklund, E., Varna, J. (2009) Modeling the effect of helical fiber structure on wood fiber composite elastic properties. *Appl. Compos. Mater.* 16:245–262.
- McCullough, R.L., Wu, C.T., Seferis, J.C., Lindenmeyer, P.H. (1976) Predictions of limiting mechanical performance for anisotropic crystalline polymers. *Polym. Eng. Sci.* 16:371–387.

- Morlier, P., Palka, L.C. (1994) Basic knowledge. In: Creep in Timber Structures. Rilem Report 8. Ed. Morlier, P. E&FN Spon, New York. pp. 9–42.
- Olsson, A.M., Salmén, L. (2001) Molecular mechanisms involved in creep phenomena of paper. *J. Appl. Polym. Sci.* 79:1590–1595.
- Olsson, A.M., Salmén, L. (2004) The softening behavior of hemi-celluloses related to moisture. *ACS Symp. Ser.* 864:184–197.
- Persson, K. (2000) Micromechanical modelling of wood and fibre properties. PhD thesis, Lund University, Lund, Sweden.
- Peura, M., Kölln, K., Grotkopp, I., Saranpää, P., Müller, M., Serimaa, R. (2007) The effect of axial strain on crystalline cellulose in Norway spruce. *Wood Sci. Technol.* 41:565–583.
- van der Put, T.A.C.M. (1989) Deformation and damage processes in wood. DSc thesis, Delft University of Technology, Delft, The Netherlands.

Received June 18, 2010. Accepted September 3, 2010.
Previously published online November 1, 2010.

PAPER V

Tensile creep and recovery of Norway spruce influenced by temperature and moisture

Engelund E. T. and Salmén L.

Tensile creep and recovery of Norway spruce influenced by temperature and moisture

Emil Tang Engelund^{1,2} and Lennart Salmén³

¹ Industrial PhD-student, Wood Technology, Danish Technological Institute,
Gregersensvej 4, DK-2630 Taastrup, Denmark
ete@teknologisk.dk

² Department of Civil Engineering, Technical University of Denmark
Brovej, Building 118, DK-2800 Kgs. Lyngby, Denmark

³ Assoc. Prof. and Research Manager, Fiber and Materials Science, Innventia AB
Drottning Kristinas Väg 61, SE-11486 Stockholm, Sweden
lennart.salmen@innventia.com

Key words

Creep, dynamical mechanical analysis, numerical modelling.

Abstract

The time-dependent mechanical behaviour (TDMB) of wood is of important when using the material for structural purposes. Recently, a new method for predicting TDMB by numerical modelling was established (Engelund and Svensson 2011) based on the assumption that TDMB is caused by sliding of microfibrils past each other. In this study, TDMB is examined via creep experiments on small specimens of Norway spruce latewood. The results of these are compared with results from the numerical modelling. The experiments include results at two levels of moisture content and three levels of temperature, enabling an investigation of these two climatic factors on TDMB of wood. It was found that the mechanical response of wood tissue is the sum of responses from both tracheids and middle lamella, with only the previous being reversible. The effect of moisture and temperature differed in that the latter affected the elastic and time-dependent responses equally. Moisture, on the other hand, reduced both elastic properties and activation energy barrier for sliding of microfibrils, but furthermore changed the MFA of the sample as a result of swelling. Hereby, moisture had a larger effect on the time-dependent response than the elastic. All of these effects were predicted by the numerical model.

Introduction

Moisture and temperature have a significant impact on the time-dependent mechanical behaviour (TDMB) of wood, and thus also influence the applicability of the material for structural purposes. When water molecules enter wood cell walls, some of the internal hydrogen bonds between wood polymers are replaced with bonds to water molecules. Hereby, the material is weakened yielding a lower wood stiffness. Water does not enter the aggregated cellulose microfibrils (Matthews et al. 2006) but may absorb on microfibril surfaces or to the surrounding matrix of hemicelluloses and lignin (Hill et al. 2009). Therefore, it is the decrease in stiffness of these two latter components that cause the decrease in wood stiffness. Increasing temperature is also accompanied by a decrease in stiffness for constant moisture contents (Gerhards 1982). The TDMB is also influenced by both moisture and temperature in that an increasing creep rate is observed when either moisture content (Kojima and Yamamoto 2005) or temperature (Navi and Stanzl-Tschegg 2009) is increased.

Predicting TDMB of wood is of importance when using the material for structural purposes. Therefore, several mathematical models have been established over the years in an attempt to predict this behaviour (Morlier and Palka 1994). The input parameters to these models, however, are often difficult to assign any physical meaning. Thus, most of these mathematical models cannot be said to be describing actual physical processes causing TDMB (Hunt 1997). Recently, a new method for numerical modelling of TDMB of wood was established (Engelund and Svensson 2011). The basic assumption of the numerical model is that time-dependency is caused by sliding of microfibrils past each other. This was modelled by allowing viscous behaviour in shear deformation modes in material directions of the cell wall but only allowing elastic behaviour in all other deformation modes. Engelund and Svensson (2011) showed that such a model was capable of describing different types of TDMB. However, more complete experimental data sets are needed in order to evaluate some of the input parameters in the model.

This study examines creep behaviour of specimens from spruce latewood of the same annual ring, cut adjacent to each other. This enables a detailed investigation of the effect of both temperature and moisture content on creep behaviour. Besides the experimental results, this study includes numerical modelling of TDMB influenced by moisture and temperature. The actual cell geometry of the samples, found by ESEM microscopy, is used in the model.

Materials and method

The study includes an investigation of TDMB of Norway spruce at two different moisture contents (8 % and 20 %) at three different temperature levels (10 °C, 25 °C, and 40 °C), i.e. six different climatic conditions. In order to generate the desired moisture content in the samples, sorption isotherms were first established. The results of these experiments were then used to set the air humidity at each temperature in the main experiment.

Sample preparation

The sample material was Norway spruce of Danish origin with a dry density of about 470 kg m⁻³ and an annual ring width of approximately 2.3 mm. The wood was sawn into blocks of 2.5 x 3 x 5 cm, and thin slices were cut from these blocks in a fully water saturated condition using a microtome. The slices were cut in the LT plane and care was taken to secure a fibre orientation along the cut. Among the many slices, those with a large proportion of latewood were selected. From one such slice six samples were cut with a razor blade. Thus, all samples originate from the same annual ring close to each other. It is therefore safe to assume a high degree of similarity between samples. The effect of difference in microfibril angle (MFA) which has a high impact on the creep behaviour (Kojima and Yamamoto 2004) was hereby minimized. The cross sections of the final samples were on average 0.12 x 0.50 mm.

Sorption isotherms

The adsorption isotherms at three different temperature levels were determined using the dynamic vapour sorption equipment (DVS Advantage 2, Sorption Measurement Systems, Alpertown, UK) located at the Danish Technological Institute (DTI), Taastrup, Denmark. Sample amounts of 60-75 mg were used to determine adsorption isotherms at 10 °C, 25 °C, and 40 °C. The resolution in the regions 35-55 % RH and 70-90 % RH was high since in these two humidity regimes, the moisture content for all samples was expected to be around 8 % and 20 %, respectively.

Time dependent mechanical behaviour

The creep and recovery behaviour of the samples were determined using dynamic mechanical analysis equipment (DMA7, Perkin Elmer, Waltham, USA) located at Innventia, Stockholm, Sweden. Each sample was mounted between the grips of the equipment with a distance between grips of 6.8 mm on average. To be certain that each sample was straight a small load of 50 mN was

shortly applied after which the sample was left stress-free. Thereafter, each sample was conditioned for 240 minutes at the selected climate for the given experimental run. Six different combinations of relative humidity and temperature were selected corresponding to moisture contents of either 8 % or 20 %. The air humidity surrounding the sample inside the test chamber was controlled using a Wetsys Controlled Humidity Generator, Setaram, France. Nitrogen was used as carrier gas. Hereafter, load was applied for 90 minutes and the creep of the sample recorded followed by a stress-free period of 90 minutes in which the creep recovery was recorded. A load level of 10 MPa was selected. The load level was adjusted for differences in sample cross-section at room climate. However, they were not adjusted for swelling during conditioning in the test chamber. The applied force where therefore approximately equal in proportion to amount of cell wall material for all samples.

Cell geometry

In order to get a more accurate description of the TDMB, the cell wall geometry and area of the samples were evaluated. This was done using an Environmental Scanning Electron Microscope (ESEM) located at DTI. The samples were investigated in low vacuum mode, and therefore the recorded geometry and area of the samples corresponds to dry conditions. The characteristic cell wall thickness was 4.5 μm , whereas the width and height of the typical sample cell were 35 μm and 19 μm , respectively. For cells with a moisture content of 8 % and 20 %, the dimensions are expected to be about 2 % and 5 % larger, respectively, based on results from swelling experiments (Keylwerth 1968).

Numerical modelling

The geometry from microscopy investigations was used as basis for generating a representative model fibre for each sample. Input parameters regarding elastic properties of wood constituents are different from those used in the study by Engelund and Svensson (2011) which only considered the cell wall as a composite of two components: the cellulose microfibrils embedded in a hemicellulose/lignin matrix. In this study, the matrix material is lignin which embeds both cellulose microfibrils and hemicelluloses. From this the elastic moduli and Poisson's ratio of the composite cell wall in the material directions can be calculated from Reuss and Voigt bounds (Engelund and Svensson 2011). The composite shear modulus is found from a mathematical model by Kerner (1956). The variation of elastic properties of the three constituents with temperature and moisture

content are derived from the theory of hydrogen-bonded dominated solid materials (Caulfield 1990; Nissan 1976a; Nissan 1976b; Nissan and Batten 1990). Nissan's model states that the elastic moduli are related to the number of internal hydrogen bond and force constant of these. Introduction of moisture into the substance will reduce the number of hydrogen bonds between wood polymers, whereas an increase in temperature will weaken these remaining wood-wood hydrogen bonds. Thus, the variation of the elastic and shear moduli can be described by the relation:

$$M(MC, T) = M_0 \cdot \exp[-K_{MC}(MC - MC_0) - K_T(T - T_0)] \quad (1)$$

where M is modulus [GPa], MC is moisture content in the constituent [%], T is temperature [K], and index zero refers to the reference condition. The parameters K_{MC} and K_T are linked to the decline in modulus with moisture and temperature, respectively. The value of K_T is 0.0024 K^{-1} for solids dominated by hydrogen bonding (Caulfield 1990; Nissan and Batten 1990) derived from the Lippincott-Schroeder potential function for hydrogen bonds (Lippincott and Schroeder 1955). In the longitudinal direction of the cell wall, however, the dominant effect of the covalent bonds in the microfibrils reduce K_T to 0.00075 K^{-1} (Engelund 2011). The value of K_{MC} for hemicellulose and lignin is $6.7 \cdot 10^{-2} \text{ /\%}$ and $7.2 \cdot 10^{-2} \text{ /\%}$, respectively (Caulfield 1990; Nissan 1977). Since water does not affect the mechanical properties of cellulose, the value of K_{MC} for cellulose is zero. The elastic and shear moduli of the three constituents are illustrated in figure 1, along with experimental data for some of the moduli of hemicelluloses and lignin. According to the Nissan model, the properties does not change much below about 5 % moisture content (Nissan 1976b), whereas above the change is more pronounced. The abscissa of figure 1 has been converted from moisture content in the constituent to wood moisture content based on figure 2. The data shown in figure 2 are based on sorption isotherms of the wood constituents at various climatic conditions. These conditions are used to convert the results in wood moisture content based on the standard softwood sorption isotherm (Forest Products Laboratory 2010).

The TDMB of samples was modelled using the method described in (Engelund and Svensson 2011) in which the rate of viscous shearing is described by

$$\frac{d\varepsilon_v}{dt} = A(MC, T) \cdot 2\sinh[B(T) \cdot \sigma] \quad (2)$$

where σ is shear stress [MPa], and A [s^{-1}] and B [MPa^{-1}] are kinetic parameters. In the following, only the kinetic parameter A is varied in order to generate differences in shearing rates.

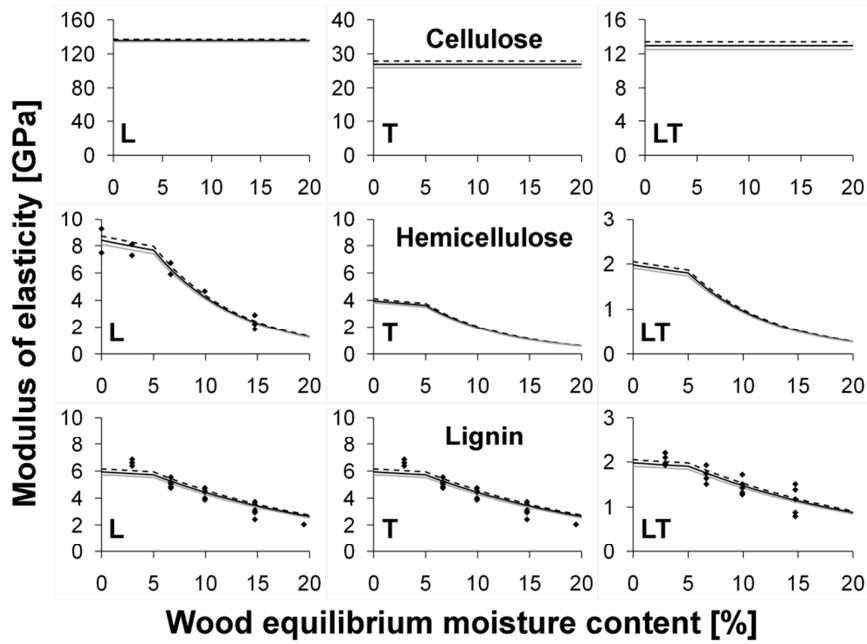


Figure 1. Moduli of elasticity in the normal (*L*, *T*) directions and shear plane (*LT*) for cellulose, hemicellulose and lignin as function of moisture content at the three experimental temperatures employed in this study. The dotted black line is the curve for $T = 10\text{ }^{\circ}\text{C}$, the solid black is for $T = 25\text{ }^{\circ}\text{C}$, and the grey line is for $T = 40\text{ }^{\circ}\text{C}$. Experimental data from (Cousins et al. 1975; Cousins 1976; Cousins 1978; Srinivasan 1941) are included for hemicellulose and lignin.

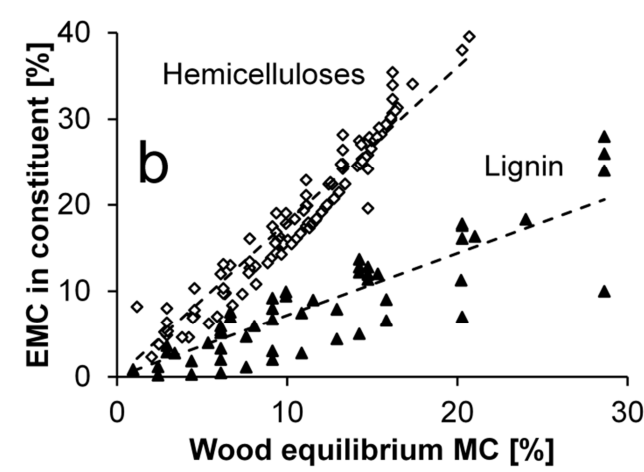


Figure 2. Relation between wood moisture content and moisture content of hemicellulose and lignin based on experimental data by (Christensen and Kelsey 1958; Christensen and Kelsey 1959; Cousins 1976; Cousins 1978; Goring 1963; Olsson and Salmen 2004; Reina et al. 2001; Sadoh 1960; Sadoh and Christensen 1964; Seborg et al. 1938). The wood moisture content is based on the standard softwood isotherm given by (Forest Products Laboratory 2010).

The parameter A is varied as multiples of A_0 which has a value corresponding to an activation free energy of about 100 kJ mol^{-1} at room temperature, which is within the range of $85\text{-}140 \text{ kJ mol}^{-1}$ reported for time-dependent deformation of viscose rayon (Eyring and Halsey 1946; Halsey et al. 1945; Holland et al. 1946), cotton (Holland et al. 1946; Lasater et al. 1953), cellulose acetate (Halsey et al. 1945; Reichardt et al. 1946; Reichardt and Eyring 1946), and wood (Bonfield et al. 1996; Kingston and Clarke 1961). The value of B used in the following is based on the volume of a hemicellulose unit.

The applied stress on the model fibre was adjusted based on the actual cell wall area obtained from ESEM investigations considering the effect of moisture content on dimensions. The effect of temperature on dimensions was assumed to be negligible.

Results and discussion

Experimental results

Unfortunately, the insulation surrounding the test chamber proved insufficient to prevent condensation in the chamber at the 20 % MC, 40 °C condition. Therefore, results for this climate were discarded. Figure 3 shows the effect of moisture content and temperature on the creep behaviour. For the selected range of these two parameters, it is clear that moisture has a significant effect whereas temperature has a minor effect on behaviour. However, considering the normalized strain development it is clear that temperature affects the elastic and creep compliances equally since the normalized curves coincide. Thus, the scaling with temperature of elastic strain and creep strain rate is similar. The same phenomenon is seen for creep recovery in Figure 4, except for the sample at 40 °C and 8 % MC.

The effect of moisture content on creep and recovery behaviour is not similar for the elastic and time-dependent compliances. From Figures 3 and 4 it is clear that moisture influences the time-dependent compliances more than the elastic compliances. Thus, there is a difference in the effect of temperature and moisture on the compliances of wood. This may be linked to molecular mechanisms responsible for these compliances. Whereas the elastic compliance is controlled by lengthening and/or rotation of covalent and hydrogen bonds, the time-dependent compliance is thought to be a result of breaking, moving and re-forming of hydrogen bonds (Engelund and Svensson 2011).

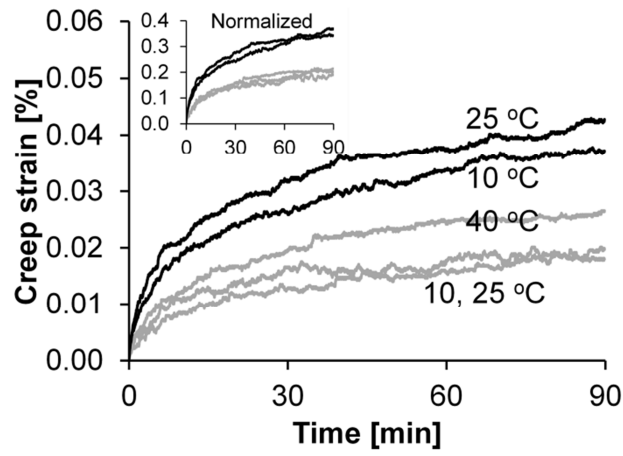


Figure 3. Creep strain as function of time, temperature and moisture content (black = 20 % MC, grey = 8 % MC). Inserted is the creep response normalized with elastic strain.

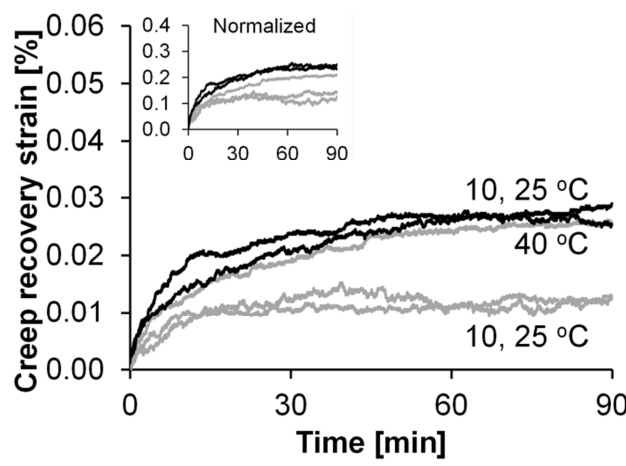


Figure 4. Creep recovery strain as function of time, temperature and moisture content (black = 20 %MC, grey = 8 %MC). Inserted is the creep recovery response normalized with elastic strain.

Increasing temperature will affect all chemical bonds, whether covalent or secondary, hereby increasing bond length and weakening the bonds. Moisture within cell walls, however, only interferes with hydrogen bonds and therefore affects the time-dependent compliance more than the elastic compliance.

There is a marked difference in behaviour during creep and recovery. Whereas the creep strain continues developing, the creep recovery seems to converge to a stable level, at least for samples at 10 °C and 25 °C. This may be a result of the difference in driving potential for creep and recovery processes. Whereas the previous is driven by the applied external load, recovery is driven by the elastic energy stored while external load was applied. As this energy is used during creep

recovery, the driving potential is decreasing thus slowing the processes. Eventually, recovery is halted due to insufficient elastic energy to drive the recovery process.

Another possible explanation is related to TDMB of the middle lamella (Engelund and Svensson 2011). During loading both wood cells and middle lamellas gluing these together are subjected to load which will cause viscous responses in both. When the load is removed, elastic energy in microfibrils causes a full or almost full reversal of the response of wood cells. This is predicted by the numerical model of a single fibre reported in (Engelund and Svensson 2011). However, nowhere in the structure is elastic energy stored which could reverse the viscous response of the middle lamella. Thus, creep recovery curves will tend towards a stable value only due to the creep recovery in wood cells. As an approximation it is assumed that the plane of shearing in the middle lamella does not change orientation over time with respect to the axis of loading. Therefore, the viscous response of middle lamellas must be linear with time under constant load. This response can be found by taking the difference between the normalized curves of Figures 3 and 4, and fitting a linear function to each of these differences. The average inclination of the lines for 8 % MC and 20 % MC are then used to subtract the middle lamella contribution from the creep curves. The result is seen in Figure 5 where assumed cell creep curves are compared with their respective unmodified recovery curves.

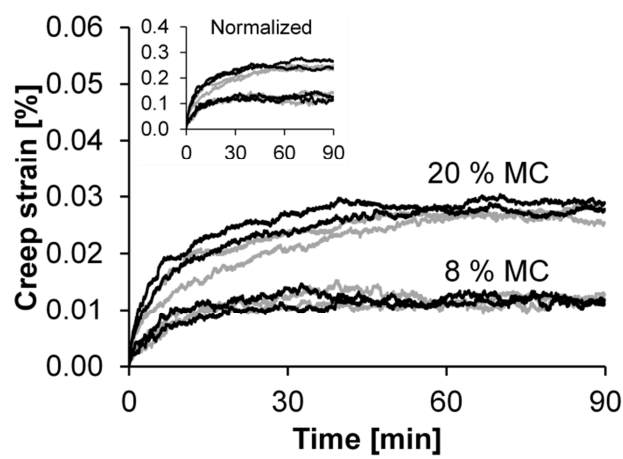


Figure 5. Assumed creep strain in cell wall (black) and actual recovery strain of tissue (grey) for samples at 10 °C and 25 °C.

Apparently, the difference between creep and creep recovery curves in Figures 3 and 4 could be due to a viscous linear response of the middle lamella. The behaviour of single fibres can by this way of reasoning be regarded as a response of several constituent layers connected in parallel. Upon

unloading, stored elastic energy in S2 microfibrils causes a reversal of developed strains. On the tissue scale, however, TDMB of tissues can be regarded as the response of cell and middle lamella connected in series. Upon unloading only the cells will exhibit creep recovery. This explanation, however, fails in describing the creep and creep recovery response of the sample at 40 °C and 8 % MC as seen in Figure 3 and 4. Also, full recovery of creep strain is in contrast with experimental results of Hill (1967) on single latewood pine holocellulose fibres from a pulp. These results show unrecoverable strain after creep. On the other hand, the numerical model was capable of describing experimental results by Eder and co-workers (2006) for stress relaxation of single fibres as illustrated by Englund and Svensson (2011). However, the model was unable to predict the observed continuing stress relaxation of tissues in the data from (Eder et al. 2006). Although it seems as the results by Eder and co-workers (2006) and Hill (1967) contrast, it should be noted that the separation of fibres in the previous study was done mechanically using tweezers and in the latter by pulping. The latter process highly modifies the fibres which may influence results significantly.

Numerical modelling

The tracheid model is fully capable of describing the TDMB observed in figure 5. As illustrated by the results from a simulated creep test in figure 6, the numerical model predicts levelling off of strain. This supports the hypothesis that the TDMB response of wood tissue is the sum of elastic and viscous responses of tracheids and middle lamella.

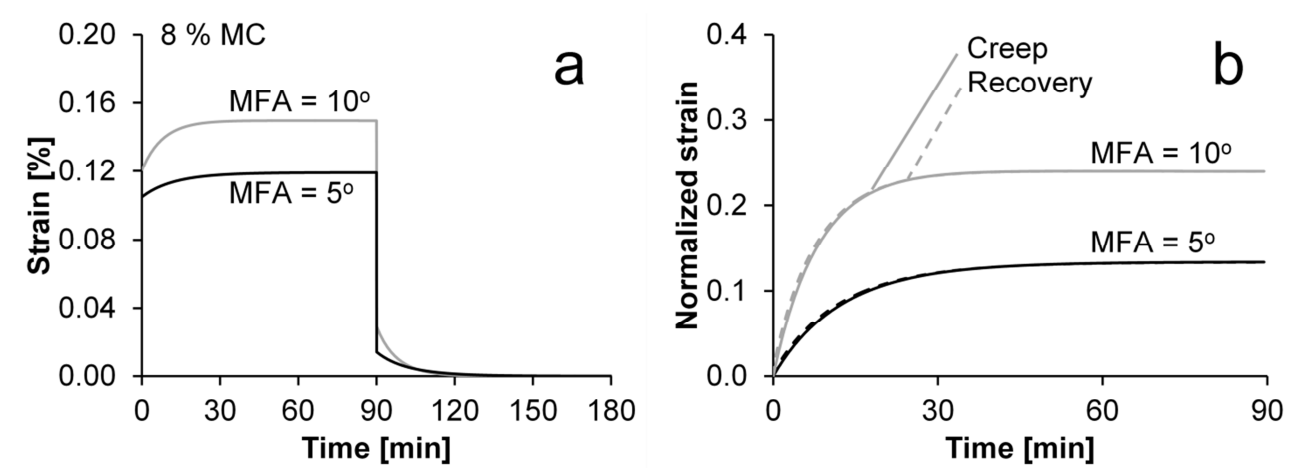


Figure 6. Predicted mechanical response of the numerical model to constant tensile stress of 10 MPa in 90 min. followed by 90 min. without applied stress.

From Figure 7 it is clear that the magnitude of the final level of strain is determined by MFA and elastic properties, but not the rate of time-dependent processes. Whether the time-dependent process is fast, i.e. high value of parameter A in (2) or slow, the final level of strain is the same. This observation implies that TDMB of tracheids is controlled by moisture and MFA. Part of the observed difference between creep at 8 % MC and 20 % MC must therefore be explained by a difference in MFA in these two moisture states. This hypothesis is in fact supported by the numerical model by incorporating a swelling coefficient of 0.4 typical of tracheid cell walls (Hartley and Avramidis 1996; Murata and Masuda 2006; Seifert 1972) in directions perpendicular to the microfibrils. The results is that the MFA of tracheids at 20 % MC is about 3° higher if an initial MFA of about 5° in the tracheids at 8 % MC is assumed. These findings are furthermore supported by some, although scarce, experimental results (Jentzen 1964).

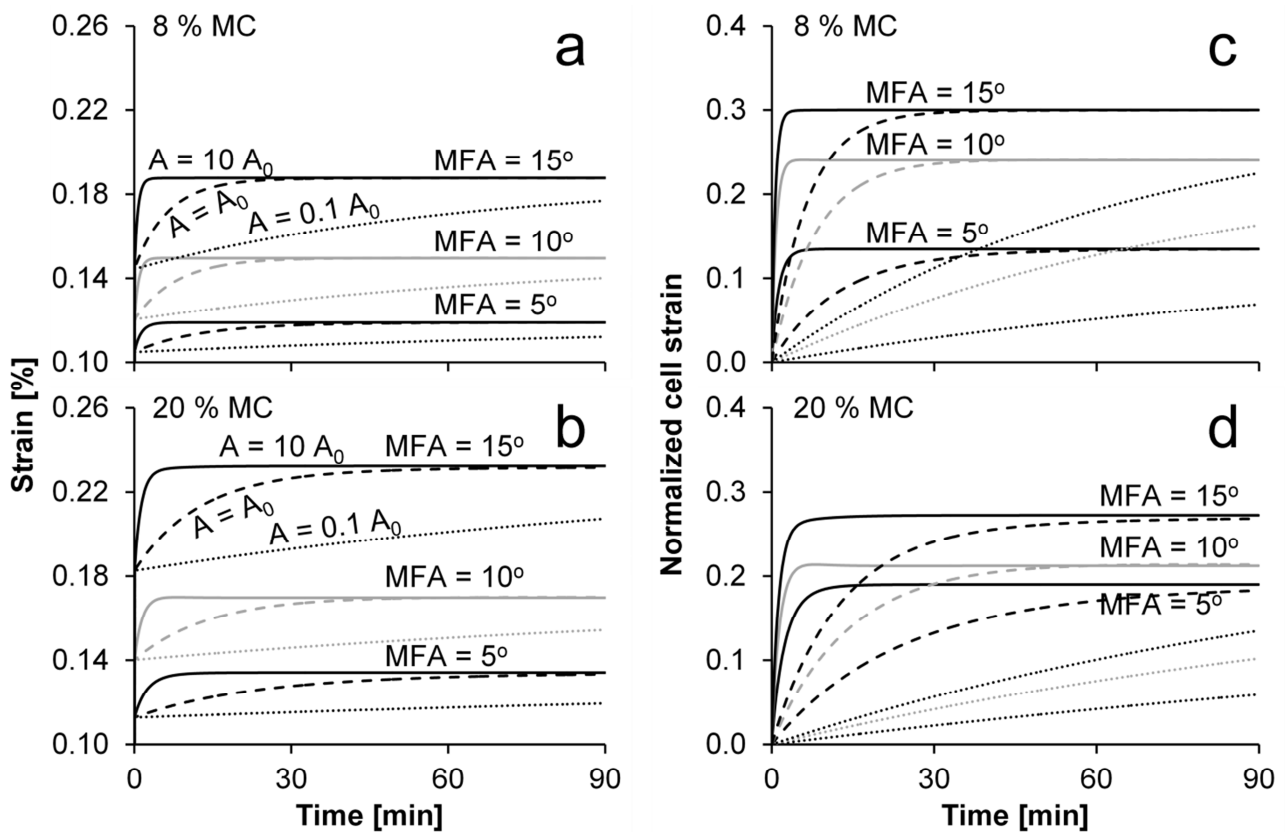


Figure 7. Predicted mechanical response of the numerical model at room temperature as function of MFA and moisture content.

In figure 8, experimental results are fitted with good agreement by the numerical model with such two levels of MFA. Moreover, the kinetic parameter A is doubled for the 20 % MC model in order

to achieve a better fit to data. This corresponds with an expected decreased activation free energy with increased moisture content.

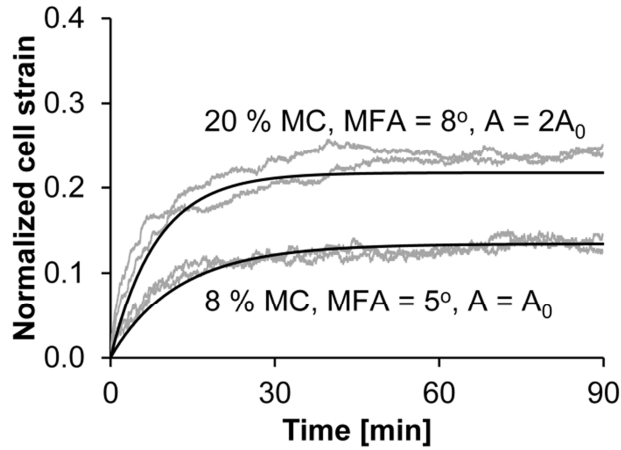


Figure 8. Comparison of predicted mechanical response of the numerical model with experimental results.

The effect of temperature on the normalized strain response is fully predicted by the numerical model as illustrated in figure 9. Although temperature changes elastic properties, the time-dependent response is proportional to these changes in accordance with the experimental results.

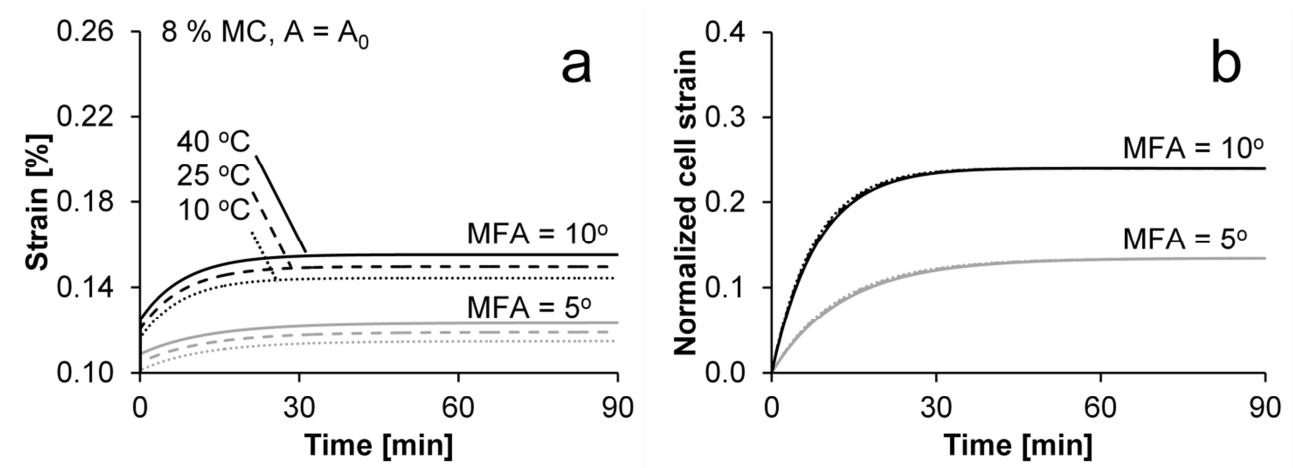


Figure 9. Predicted mechanical response of the numerical model at the three temperature levels employed in the experiments.

These findings contradict, however, experimental results for bending tests which show that creep recovery (Davidson 1962) are in fact affected by temperature in the range 20-60 °C. Although a different mode of loading is employed in the quoted study, further tensile experiments on softwood

tissue are needed to draw final conclusions. In general, more experimental data are needed to fully evaluate the parameters of the numerical model and the findings of this study.

Conclusions

In this study, it was found that the TDMB response of wood tissue is the sum of responses from both tracheids and middle lamella, with only the previous being reversible. Water molecules entering cell walls result in fewer hydrogen bonds between wood polymers. Hereby, elastic properties and activation energy barrier for sliding of microfibrils are reduced. Furthermore, swelling that accompany an increase in moisture results in a change in MFA which also has an effect on the TDMB response of tracheids. All of these effects are predicted by the numerical model of this study. The simple theoretical basis of the model and agreement of predictions with experimental results lend the model credibility. The model is also able to predict the effect of temperature on the TDMB responses seen in experiments. These are, however, in contradiction with previous findings.

Acknowledgements

ETE would like to thank Anne-Mari Olsson, Innventia for her invaluable technical support. Also, the financial support of COST Action FP0802 “Experimental and computational micro-characterization techniques in wood mechanics” is gratefully acknowledged.

References

- Bonfield, P. W., Mundy, J., Robson, D. J., Dinwoodie, J. M. (1996) The modelling of time-dependant deformation in wood using chemical kinetics. *Wood Sci Technol* 30:105-115.
- Caulfield, D. F. (1990) Effect of moisture and temperature on the mechanical properties of paper. *Solid mechanics advances in paper related industries: Proceedings of National Science Foundation workshop*, 50-62.
- Christensen, G. N., Kelsey, K. E. (1958) The sorption of water vapour by the constituents of wood: determination of sorption isotherms, *Austr J Appl Sci* 9:265-282.
- Christensen, G. N., Kelsey, K. E. (1959) The sorption of water vapor by the constituents of wood. *Holz Roh Werkst* 17:189-203.
- Cousins, W. J. (1976) Elastic modulus of lignin as related to moisture content. *Wood Sci Technol* 10:9-17.

Cousins, W. J. (1978) Youngs modulus of hemicellulose as related to moisture-content. *Wood Sci Technol* 12:161-167.

Cousins, W. J., Armstrong, R. W., Robinson, W. H. (1975) Youngs modulus of lignin from a continuous indentation test. *J Mater Sci* 10:1655-1658.

Eder, M., Burgert, I., Stanzl-Tschegg, S. (2006) Relaxation experiments on wood fibres and tissues. *Proceedings of the Third International Conference of the European Society of Wood Mechanics*, 141-147.

Engelund, E. T. (2011) Wood – water interactions: Linking molecular level mechanisms with macroscopic performance. PhD thesis. Technical University of Denmark, Lyngby.

Engelund, E. T., Svensson, S. (2011) Modelling time-dependent mechanical behaviour of softwood using deformation kinetics. *Holzforschung* 65:231-237.

Eyring, H., Halsey, G. (1946) The mechanical properties of textiles 3. *Text Res J* 16:13-25.

Forest Products Laboratory (2010) Wood handbook - wood as an engineering material. Tech. Rep. FPL-GTR-190. Madison, WI, USA.

Gerhards, C. C. (1982) Effect of moisture content and temperature on the mechanical properties of wood - an analysis of immediate effects. *Wood Fiber* 14:4-36.

Goring, D. A. I. (1963) Thermal softening of lignin, hemicellulose and cellulose. *Pulp Pap Mag Can* 13:T517-T527.

Halsey, G., White, H. J., Eyring, H. (1945) Mechanical properties of textiles 1. *Text Res J* 15:295-311.

Hill, C. A. S., Norton, A., Newman, G. (2009) The water vapor sorption behavior of natural fibers. *J Appl Polym Sci* 112:1524-1537.

Hill, R. L. (1967) Creep behavior of individual pulp fibers under tensile stress. *Tappi* 50:432-440.

Holland, H. D., Halsey, G., Eyring, H. (1946) Mechanical properties of textiles 6 - a study of creep of fibers. *Text Res J* 16:201-210.

Hunt, D. G. (1997) Dimensional changes and creep of spruce and consequent model requirements. *Wood Sci Technol* 31:3-16.

Kerner, E. H. (1956) The elastic and thermo-elastic properties of composite media. *Proc Phys Soc B* 69:808-813.

Keylwerth, R. (1968) Wood species with dimensional stability. *Holz Roh Werkst* 26:413-416.

Kingston, R. S. T., Clarke, L. N. (1961) Some aspects of the rheological behavior of wood II - analysis of creep data by reaction-rate. *Austr J Appl Sci* 12:227-240.

Kojima, Y., Yamamoto, H. (2004) Effect of microfibril angle on the longitudinal tensile creep behavior of wood. *J Wood Sci* 50:301-306.

Kojima, Y., Yamamoto, H. (2005) Effect of moisture content on the longitudinal tensile creep behavior of wood. *J Wood Sci* 51:462-467.

Lasater, J. A., Nimer, E. L., Eyring, H. (1953) Mechanical properties of cotton fibers 1 - relaxation in air and water. *Text Res J* 23:237-242.

Lippincott, E. R., Schroeder, R. (1955) One-dimensional model of the hydrogen bond. *J Chem Phys* 23:1099-1106.

Matthews, J. F., Skopec, C. E., Mason, P. E., Zuccato, P., Torget, R. W., Sugiyama, J., Himmel, M. E., Brady, J. W. (2006) Computer simulation studies of microcrystalline cellulose I beta. *Carbohydr Res* 341:138-152.

Morlier, P., Palka, L. C. (1994) Basic knowledge. In: *Creep in timber structures* (Morlier, P., ed.), Rilem Report 8, E & FN Spon, 9-42.

Navi, P., Stanzl-Tschegg, S. (2009) Micromechanics of creep and relaxation of wood. A review COST Action E35 2004-2008: Wood machining - micromechanics and fracture. *Holzforschung* 63:186-195.

Nissan, A. H. (1976a) Three modes of dissociation of H-bonds in hydrogen-bond dominated solids. *Nature* 263:759.

Nissan, A. H. (1976b) H-bond dissociation in hydrogen-bond dominated solids. *Macromolecules* 9:840-850.

Nissan, A. H. (1977) Elastic modulus of lignin as related to moisture content. *Wood Sci Technol* 11:147-151.

Nissan, A. H., Batten, G. L. (1990) On the primacy of the hydrogen bond in paper mechanics. *Tappi* 73:159-164.

Olsson, A. M., Salmen, L. (2004) The softening behavior of hemicelluloses related to moisture. *Hemicelluloses: Science and Technology*. 864:184-197

Reichardt, C. H., Eyring, H. (1946) Mechanical properties of textiles 11 - application of the theory of the 3-element model to stress-strain experiments on cellulose acetate filaments. *Text Res J* 16:635-642.

Reichardt, C. H., Halsey, G., Eyring, H. (1946) Mechanical properties of textiles 10 - analysis of Steinberger data on creep of cellulose acetate filaments. *Text Res J* 16:382-389.

- Reina, J. J., Dominguez, E., Heredia, A. (2001) Water sorption-desorption in conifer cuticles: the role of lignin. *Physiol Plant* 112:372-378.
- Sadoh, T. (1960) Studies on the sorption of water vapour by wood hemicellulose 2 - amount of vapour adsorbed. *The scientific reports of Kyoto Prefectural University. Agriculture* 12, 113-118.
- Sadoh, T., Christensen, G. N. (1964) Rate of sorption of water vapour by hemicellulose. *Austr J Appl Sci* 15:297-308.
- Seborg, C. O., Simmonds, F. A., Baird, P. K. (1938) Sorption of water vapor by papermaking materials: irreversible loss of hygroscopicity due to drying. *Pap Trade J* 107:223-228.
- Srinivasan, P. S. (1941) The elastic and thermal properties of timber. *Q J Indian Inst Sci* 4:222-314. Quoted from (Cousins et al. 1975).

PAPER VI

Predicting the reorientation of microfibrils in plant fibres under tensile strain

Engelund E. T. and Svensson S.

Predicting the reorientation of microfibrils in plant fibres under tensile strain

Emil Tang Engelund^{a,b,*} and Staffan Svensson^b

^aWood Technology, Danish Technological Institute,

Gregersensvej 4, DK-2630 Taastrup, Denmark

ete@teknologisk.dk

Phone (+45) 72 20 23 55

Fax (+45) 72 20 20 19

^bDepartment of Civil Engineering, Technical University of Denmark

Brovej, Building 118, DK-2800 Kgs. Lyngby, Denmark

nss@byg.dtu.dk

* Corresponding author

Key words

Microfibril angle; natural fibres; continuum mechanics; linear elastic; orthotropic

Abstract

Prediction of the mechanical behaviour of natural fibres is important for their use. Despite difference in size, shape and chemical composition natural fibres often share many common features. The most important of these in terms of mechanical behaviour is the cellulose microfibrils. Microfibrils are oriented at an angle to the fibre axis. Although the orientation may vary between different layers of the cell wall, one layer is dominating and the average orientation in this layer is termed the microfibril angle (MFA) of the fibre. This common structural organization of the cell walls of different natural fibres enables a general approach for describing their mechanical behaviour. When stretching a natural fibre, the microfibrils are reoriented resulting in a decreasing MFA. Models describing the mechanical performance of natural fibres should be able to predict this fundamental and important feature. It is shown here, however, that existing analytical models for predicting this reorientation upon straining only provide reasonable results for plant fibres with a high initial MFA. An analytical model is therefore presented based on composite theory and

continuum mechanics with high accuracy and precision predicts material re-orientation caused by stretching. The model is verified against experimental results presented by different research groups on a wide range of different natural fibres.

1. Introduction

Understanding the mechanical behaviour of plant fibres is paramount when using these natural and renewable resources. Natural fibres govern the performance of paper, textiles and reinforced polymer, clay or mortar. Although plant fibres may come in different shapes, sizes and chemical composition, they often share many common features. This enables an analysis of the mechanical behaviour of various plant fibres in general which will be attempted in this study. The most important common feature of plant fibres in terms of load bearing and stiffness is the cellulose microfibrils in the cell walls of the fibres. Microfibrils are highly ordered aggregates of long aligned cellulose chains [1]. The microfibrils have a helical structure with an inclination which may vary between different layers of the cell wall. The cells of most plant fibres can be divided into primary and secondary walls, among which the latter typically is significantly thicker and consists of several layers. The microfibrils in these secondary wall layers have a high degree of orientation [2]. Although this orientation may differ between the different layers, often the central layer is significantly thicker than the others. For example, wood cells typically have three secondary cell wall layers of which one of them, the S2 layer constitutes about 80 % of the cell wall [3]. The mechanical behaviour in the longitudinal direction of plant fibres is to a great extent linked to the properties of the central layer which again depends of the helical inclination of its microfibrils [4]. Therefore, the inclination of such layer is often referred to as the microfibril angle (MFA) of the specific plant fibre.

When load is applied in the longitudinal direction of the plant fibres, several mechanisms are responsible for the load bearing. Their relative contribution depends on the shape and structure of the specific cell. Hearle [5] suggests that upon straining fibres, deformation may occur as a result of three modes: lengthening and shearing of the microfibrils and the interfibrillar matrix and bending and twisting of the microfibrils as spiral springs. If the MFA is high, i.e. in the range 14° - 65° , a significant decrease in MFA upon straining is observed [6-10]. For low MFA, the load strains the cellulose microfibrils [11]; an effect which is insignificant when the initial MFA is high [8]. In the case of low MFA, the change in MFA is therefore small and often complicated to measure [11-12].

In order to describe the mechanical behaviour of plant fibres, mathematical models are useful tools. If these are not based on coherent physical theory, however, a deeper scientific understanding of the mechanical behaviour is impossible. In this study, experimental results presented in the literature of the change in MFA for four different kinds of plant fibres under tensile loading will be discussed. Two analytical mathematical models presented in literature will be evaluated. Furthermore, a continuum mechanical model based on coherent physical theory will be presented. It is derived directly from continuum mechanics for orthotropic and linear-elastic materials. Two versions of the model are presented based on infinitesimal strain theory and finite strain theory.

The experimental results used for evaluation of the different models covers five different natural fibres: coir, flax, sisal leaf fibres, pipevine schlerenchyma fibres and Norway spruce wood. The literature sources for these experimental results are summarized in Table 1 including the initial MFA of the fibres and the moisture condition during experiments.

Table 1: Overview of experimental results from literature. Fibre types are listed after initial MFA, except for spruce.

Fibre type	Latin name	Initial MFA	Moisture	Reference
Coir	<i>Cocos nucifera</i>	46	Unknown	[13]
Coir	-	45.9	12-15 %	[9]
Sisal leaf	<i>Agave sisalana</i>	38.6	Wet	[6]
Pipevine	<i>Aristolochia macrophylla</i>	15.9	Wet	[25]
Flax	<i>Linum usitatissimum</i>	6.2	10 %	[23]
Spruce	<i>Picea abies</i>	46.0	Wet	[8]
Spruce	-	24.0	10 %	[23]
Spruce	-	15.3	Wet	[12]
Spruce	-	4.6	Wet	[12]

2. Materials and methods

2.1 Study of existing models

In the literature, two mathematical models have been found; a model by Balashov et al. [6] which is similar to an expression given by Stern [13] and a recent model by Keckes et al. [8]. Both sources use the same assumption of inextensible microfibrils in the cell wall, however, arriving at two different relations between strain and MFA. The assumed deformation of the cell wall in both models is illustrated in Figure 1.

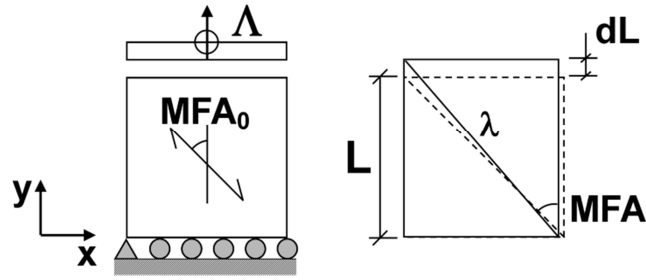


Figure 1: Assumed deformation of the cell wall in the Balashov (3) and Keckes (5) models.

Tensile strain in the fibre direction causes an elongation in this direction and contraction in the perpendicular-to-load direction. Inextensibility of the microfibrils results in the following relation; geometric entities L , λ , and MFA are defined in Figure 1.

$$L = \lambda \cdot \cos(MFA) \quad (1)$$

Stretching the cell wall in the longitudinal direction, i.e. the y -direction of Figure 1, the length L is increased by dL . From here the two literature models use different approaches in the derivation of the strain versus MFA relation and hence come up with two quite different results. Balashov et al. [6] deduces the following relation of MFA and strain, where MFA_0 is the initial MFA illustrated in Figure 1

$$\frac{dL}{L} = \frac{\lambda \cdot \cos(MFA) - \lambda \cdot \cos(MFA_0)}{\lambda \cdot \cos(MFA_0)} = \frac{\cos(MFA)}{\cos(MFA_0)} - 1 \quad (2)$$

which gives

$$MFA = \text{Arccos}[\cos(MFA_0)(1 + \varepsilon_y)] \quad (3)$$

Keckes et al. [8] on the other hand use the derivative of (1) to calculate the strain as

$$\frac{dL}{L} = \frac{d(\lambda \cdot \cos(MFA))}{\lambda \cdot \cos(MFA)} = \frac{d(\cos(MFA))}{\cos(MFA)} = -\tan(MFA)d(MFA) \quad (4)$$

From (4), Keckes et al. [8] conclude that strain versus MFA has a negative slope of $\cot(MFA_0)$ and defines the following relation between strain and MFA

$$MFA = MFA_0 - \cot(MFA_0)\varepsilon_y \quad (5)$$

2.2 Continuum mechanical model

The deformation of a cell wall as a result of stretching in an arbitrary direction in regards to material directions 1 and 2, where initial MFA coincides with 2, can be found by using simple continuum mechanics under assumptions of plane stress and orthotropic, linear-elastic materials. The applied

operation for this is shown in the appendix. Deformation of the cell wall involves both normal and shear deformations, see Figures 2 and 3. The re-orientation of the cell wall described as MFA in the deformed state as a consequence of straining and initial MFA, denoted MFA_0 , is given by (6).

$$MFA = \text{Arctan} \left(\frac{\sin(MFA_0)(1+\varepsilon_x)}{\cos(MFA_0)(1+\varepsilon_y)} \right) + \gamma \quad (6)$$

where the normal strains ε_x and ε_y and the shear strain γ are related to the xy-coordinate system of the cell wall in Figure 2. In the appendix, the strains are derived from both infinitesimal strain theory and finite strain theory.

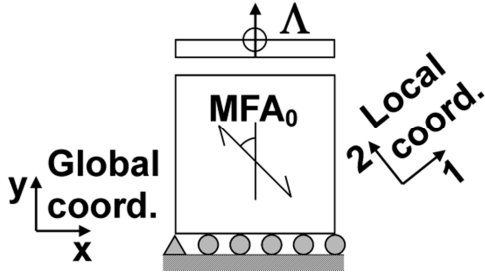


Figure 2: Plane model of a cell wall partition. The local coordinate system coincides with material directions.

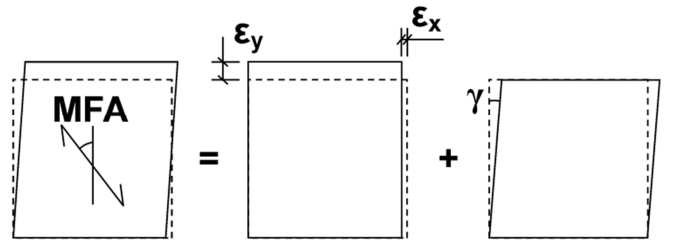


Figure 3: Fundamental normal and shear deformations from the complex deformation state of the cell wall.

The deformation of the cell wall depends on its mechanical material properties. These originate from the properties of the cell wall constituents, their orientation and concentrations. The mechanical properties of the constituents are given in Table 2 for a reference condition (12 % moisture content). However, the properties vary with moisture and since the moisture conditions differ between experiments, the properties are corrected using the method employed in [14] to fit the experimental conditions. The chemical composition of the different natural fibres studied here varies and is listed in Table 3.

Table 2: Elastic properties of cellulose, hemicellulose and lignin in the reference condition (12 % MC). Based on the mechanical properties given in [14].

	Cellulose	Hemicellulose	Lignin
Modulus of elasticity, E_2 [GPa]	137	2.9	3.7
Modulus of elasticity, E_1 [GPa]	27	1.4	3.7
Shear modulus, G [GPa]	13	0.7	1.3
Poisson's ratio, ν_{21}	0.20	0.20	0.33

Table 3: Chemical composition of the dominant cell wall layer [26-27] in various natural fibres and calculated mechanical properties in reference condition in the directions along and perpendicular to the microfibrils. The chemical composition of pipevine has been estimated.

	Coir	Flax	Pipevine	Sisal	Spruce
Cellulose content [%]	48.5	77.6	70.0	70.8	45.0
Hemicellulose content [%]	0.3	22.4	15.0	15.1	35.0
Lignin content [%]	51.2	0.0	15.0	14.2	20.0
Modulus of elasticity, E_2 [GPa]	68.3	107.0	96.9	98.0	63.4
Modulus of elasticity, E_1 [GPa]	6.3	5.3	5.8	5.8	3.1
Shear modulus, G [GPa]	3.1	3.9	4.4	4.4	2.3
Poisson's ratio, ν_{21}	0.27	0.20	0.22	0.22	0.23

For the different fibres the vast majority of cellulose is oriented in the same direction. Furthermore, experimental studies indicate that other cell wall components are also oriented coinciding with the cellulose [15-20]. It is therefore reasonable for the plane problem studied here to determine mechanical properties of the cell wall from composite theory of lamellar material structures. The modulus of elasticity in the 1 and 2 directions of Figure 2 is found from [21] by Voigt and Reuss bounds, respectively. For the previous, the composite modulus perpendicular to the lamellas is

$$E_1 = \left(\sum \frac{c_i}{E_{1,i}} \right)^{-1} \quad (7)$$

where E_1 is the composite modulus of elasticity, $E_{1,i}$ is the modulus of elasticity of the i -th component and c_i its concentration. The sum of concentrations is unity. The Reuss bound gives the composite modulus along the lamellas by

$$E_2 = \sum c_i E_{2,i} \quad (8)$$

where E_2 is the composite modulus of elasticity and $E_{2,i}$ is the modulus of elasticity of the i -th component. The Poisson's ratio for the 2 and 1 directions is found from the Reuss bound assuming unity strain in one direction.

$$\varepsilon_2 = 1 \quad (9)$$

$$\varepsilon_1 = \sum \varepsilon_{1,i} = - \sum c_i \nu_i \quad (10)$$

$$\nu_{21} = \frac{-\varepsilon_1}{\varepsilon_2} = \sum c_i \nu_i \quad (11)$$

The shear modulus is found from composite theory by the model of Kerner [22]

$$G = G_0 \cdot \left(C_2 + \sum G_i \cdot C_{1,i} \right) / \left(C_2 + \sum G_0 \cdot C_{1,i} \right) \quad (12)$$

where the index zero refers to the matrix material and

$$C_{1,i} = c_i / \left((7 - 5 \cdot \nu_0) \cdot G_0 + (8 - 10 \cdot \nu_0) \cdot G_i \right) \quad (13)$$

and

$$C_2 = c_0 / (15(1 - \nu_0)) \quad (14)$$

The matrix material is selected as lignin for all species of fibres, except for flax in which no lignin is present, see Table 3. Thus, for flax the hemicelluloses act as matrix material in the calculations.

3. Results and discussion

The elastic mechanical properties of the cell wall have been calculated employing (7)-(14) for the five different plant fibre species based on their chemical composition. Results of the calculations are listed in Table 3 and illustrated in Figure 4.

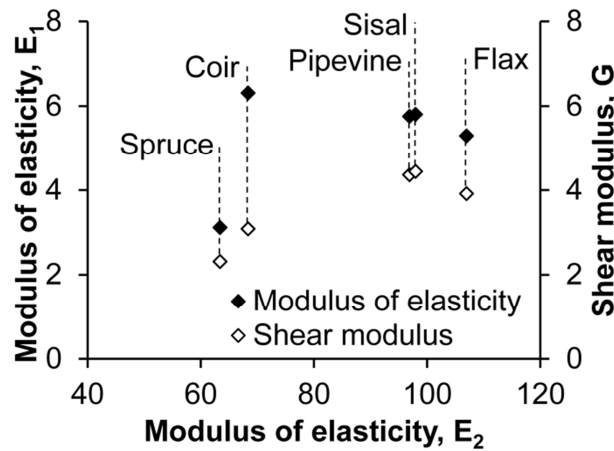


Figure 4: Modulus of elasticity perpendicular to the microfibrils, E_1 and shear modulus, G plotted against modulus of elasticity along the microfibrils, E_2 for the five different fibres. All moduli are given in GPa.

It is clear that there is a huge variation in material properties between fibres. In terms of absolute values, flax, sisal and pipevine constitute one extreme and spruce another. In terms of the relation between the three moduli, however, the moduli of spruce and flax are both around 27 : 1.3 : 1.0 for $E_2 : E_1 : G$, whereas the relations for sisal and pipevine are about 22 : 1.3 : 1.0, and 22 : 2.0 : 1.0 for coir. Thus, calculated composite material properties are very different between fibres and depend on

their chemical composition. However, if the moisture content is changed, the properties also change in proportion to concentration of moisture sensitive constituents in the cell wall, i.e. hemicelluloses and lignin. The predictions of the mathematical models from literature and based on continuum mechanics are illustrated in Figures 5-7.

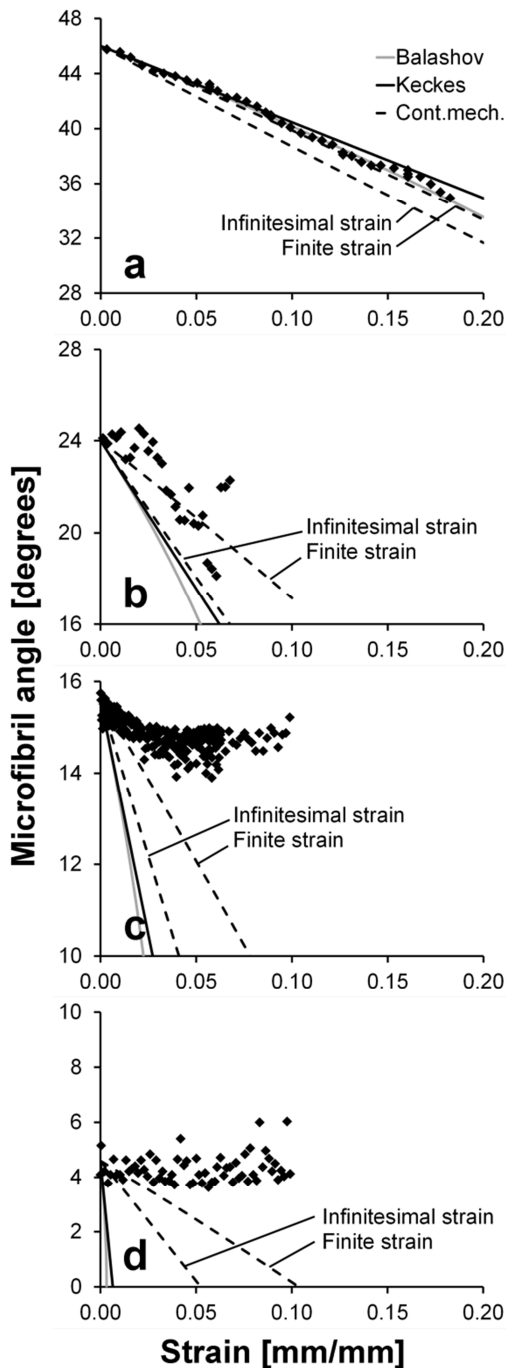


Figure 5: Experimental results and predictions of MFA as function of strain for Norway spruce wood: a) [8], b) [23], c)-d) [12].

Among the literature sources, Kölln [23] does not report the results for flax as MFA versus strain but rather an orientation function versus strain. Therefore, these specific results have been translated to MFA based on the assumption of high degree of microfibrillar orientation of the microfibrils in the secondary wall [23]. From Figures 5-7 it is clear that the Keckes model (5) fit well with the data when the initial MFA is extremely high, i.e. in the range 35-50°. In this range the Balashov model (3) only fits the experimental data adequately. In the lower range of MFA both of these models fail in describing the experimental data. It can, therefore, only be deduced that none of the models found in literature are able to predict the change in MFA upon straining for all initial values of MFA. The continuum mechanical model on the other hand fit the experimental results surprisingly well. The exceptions are found for the data for wood at low initial MFA and normal strain above 5 % as shown in Figure 5c-d. There is, however, a reasonable explanation for these deviations. The failure strain of normal wood fibres with low MFA is around 3-5 % [24], and the wood fibres in Figure 5c-d are subjected to strain far beyond the failure strain. It is therefore very likely, that the wood fibres beyond strains of 3-5 % are showing fracture behaviour in which case the basic assumptions of continuum

mechanics are violated. Furthermore, the predictions of the continuum mechanical model do not follow the experimental results of Figure 7a. This might be caused by a flawed initial value of the MFA in the experiments, since the first data point appears to be an outlier.

If an initial MFA of around 14-15° is used in the continuum mechanical model, correspondence between predictions and experimental results is achieved. In general, the continuum mechanical model presented in this study can predict the observed reorientation of the microfibrils in a range of different natural fibres with various chemical compositions, material properties and MFAs. Furthermore, the model is based on sound physical principles from continuum mechanics and composite theory which lends the model high credibility.

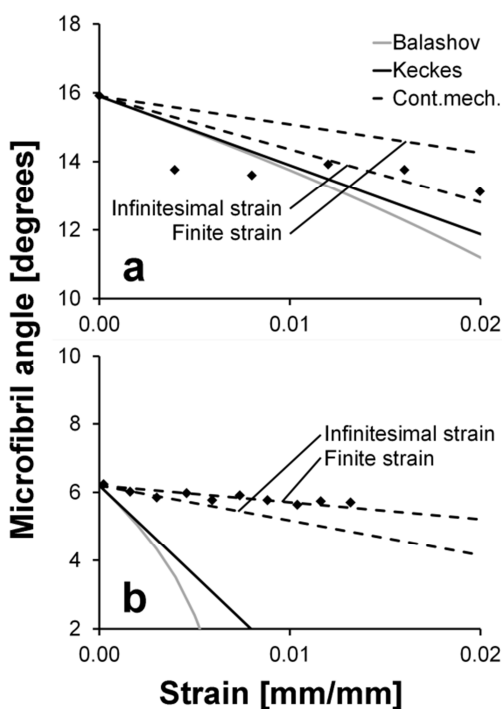


Figure 7: Experimental results and predictions of MFA as function of strain for a) flax [25] and b) pipevine [23].

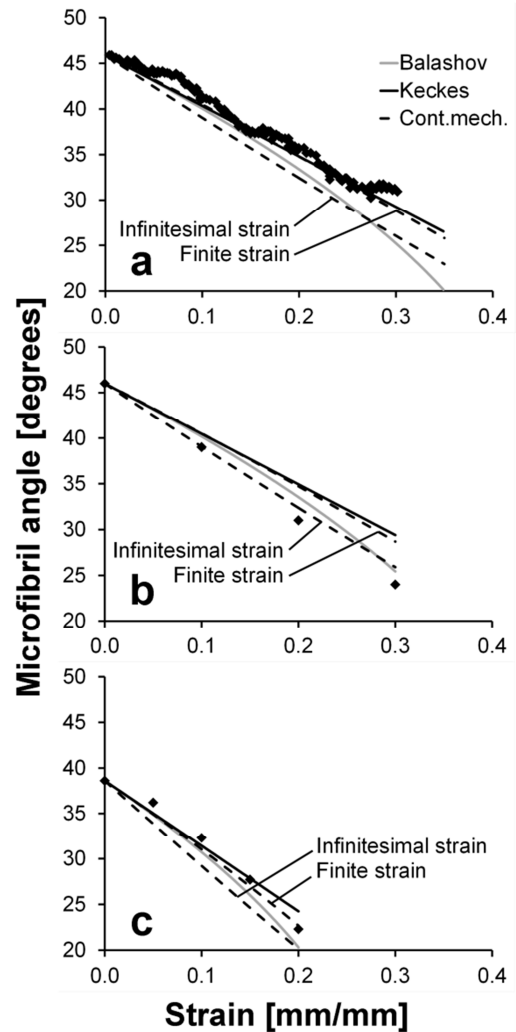


Figure 6: Experimental results and predictions of MFA as function of strain for coir, a) [9] b) [13], and sisal leaf fibres, c) [6].

4. Conclusions

The mathematical models from literature for predicting the reorientation of microfibrils upon straining are showed to only provide reasonable fit to the experimental results for natural fibres with a high initial MFA. On the other hand, the results of the continuum mechanical model presented in this study show

surprisingly good correspondence for a wide range of natural fibres with differences in chemical composition, microfibrillar orientation and mechanical material properties. Despite the large variation between the fibre species in all these aspects, the continuum mechanical model is able to predict the microfibrillar re-orientation when the fibres are stretched. This is verified by comparing the results of the continuum mechanical model with experimental results from a range of literature sources from various research groups. Hereby, the predictive power of models based on sound physical principles is illustrated.

5. References

- [1] Atalla RH, Brady JW, Matthews JF, Ding SY, Himmel ME. Structures of plant cell wall celluloses. In Himmel ME editor. *Biomass Recalcitrance – Deconstructing the Plant Cell Wall for Bioenergy*, Oxford: Blackwell Publishing; 2008. p 188-212.
- [2] Satyanarayana KG, Sukumaran K, Mukherjee PS, Pillai SGK. Materials science of some lignocellulosic fibers. *Metallography*. 1986; 19:389-400.
- [3] Brändström J. Micro- and ultrastructural aspects of Norway spruce tracheids: a review. *IAWA J*. 2001; 22:333-353.
- [4] Barnett JR, Bonham VA. Cellulose microfibril angle in the cell wall of wood fibres. *Biol Rev*. 2004; 79:461-472.
- [5] Hearle JWS. The fine structure of fibers and crystalline polymers 3: interpretation of the mechanical properties of fibers. *J Appl Polym Sci*. 1963; 7:1207-1223.
- [6] Balashov V, Preston RD, Ripley GW, Spark LC. Structure and mechanical properties of vegetable fibres 1: the influence of strain on the orientation of cellulose microfibrils in sisal leaf fibre. *P Roy Soc Lond B Bio*. 1957; 146:460-468.
- [7] Kamiyama T, Suzuki H, Sugiyama J. Studies of the structural change during deformation in *Cryptomeria japonica* by time-resolved synchrotron small-angle X-ray scattering. *J Struct Biol*. 2005; 151:1-11.
- [8] Keckes J, Burgert I, Frühmann K, Müller M, Kölln K, Hamilton M, Burghammer M, Roth SV, Stanzl-Tschegg S, Fratzl P. Cell-wall recovery after irreversible deformation of wood. *Nat Mater*. 2003; 2:810-814.
- [9] Martinschitz KJ, Boesecke P, Garvey CJ, Gindl W, Keckes J. Changes in microfibril angle in cyclically deformed dry coir fibers studied by in-situ synchrotron X-ray diffraction. *J Mater Sci*. 2008; 43:350-356.
- [10] Roy SC, Das S. Small-angle x-ray scattering of cellulose 1: shape and extent of scattering in some vegetable fibers. *J Appl Polym Sci*. 1965; 9:3427-3437.
- [11] Peura M, Kölln K, Grotkopp I, Saranpää P, Müller M, Serimaa R. The effect of axial strain on crystalline cellulose in Norway spruce. *Wood Sci Technol*. 2007; 41:565-583.

- [12] Peura M, Grotkopp I, Lemke H, Vikkula A, Laine J, Müller M, Serimaa R. Negative Poisson ratio of crystalline cellulose in kraft cooked Norway spruce. *Biomacromolecules*. 2006; 7:1521-1528.
- [13] Stern F. A note on the structure and mechanical properties of coir fibre. *J Text I*. 1957; 48:T21-T25.
- [14] Engelund ET, Salmen L. Tensile creep and recovery of Norway spruce influenced by temperature and moisture. Unpublished; 2011.
- [15] Liang CY, Bassett KH, McGinnes EA, Marchessault RH. Infrared spectra of crystalline polysaccharides VII – thin wood sections. *Tappi*. 1960; 43:1017-1024.
- [16] Marchessault RH, Liang CY. Infrared Spectra of Crystalline Polysaccharides .8. Xylans. *J Polym Sci*. 1962; 59:357-378.
- [17] Fromm J, Rockel B, Lautner S, Windeisen E, Wanner G. Lignin distribution in wood cell walls determined by TEM and backscattered SEM techniques. *J Struct Biol*. 2003; 143:77-84.
- [18] Åkerholm M. Ultrastructural aspects of pulp fibers as studied by dynamic FT-IR spectroscopy. PhD thesis. Stockholm: Royal Institute of Technology, KTH; 2003.
- [19] Åkerholm M, Salmen L. The oriented structure of lignin and its viscoelastic properties studied by static and dynamic FT-IR spectroscopy. *Holzforschung*. 2003; 57:459-465.
- [20] Stevanic JS, Salmen L. Orientation of the wood polymers in the cell wall of spruce wood fibres. *Holzforschung*. 2009; 63:497-503.
- [21] McCullough RL, Wu CT, Seferis JC, Lindenmeyer PH. Predictions of limiting mechanical performance for anisotropic crystalline polymers. *Polym Eng Sci*. 1976; 16:371-387.
- [22] Kerner EH. The elastic and thermo-elastic properties of composite media. *P Phys Soc Lond B*. 1956; 69:808-813.
- [23] Kölln K. Morphology and mechanical characteristics of cellulose fibres: investigations with x-ray and neutron scattering (in German). PhD thesis. Kiel: Christian-Albrechts-Universität; 2004.
- [24] Eder M, Terziev N, Daniel G, Burgert I. The effect of (induced) dislocations on the tensile properties of individual Norway spruce fibres. *Holzforschung*. 2008; 62:77-81.
- [25] Köhler L, Spatz HC. Micromechanics of plant tissues beyond the linear-elastic range. *Planta*. 2002; 215:33-40.
- [26] McDougall GJ, Morrison IM, Stewart D, Weyers JDB, Hillman JR. Plant fibers – botany, chemistry and processing for industrial use. *J Sci Food Agr*. 1993; 62:1-20.
- [27] Satyanarayana KG, Kulkarni AG, Rohatgi PK. Structure and properties of coir fibers. *P Indian AS-Eng Sci*. 1981; 4:419-436.

6. Appendix: Analytic evaluation of material re-orientation caused by uniform normal excitation on one boundary

Plane stress state in the cell wall, consisting of orthotropic, linear-elastic material, is assumed. The kinetics of an orthotropic domain for an excitation on one boundary oriented at angle β_0 in regards to one of the orthotropic material directions is shown in Figure 2. For brevity reasons, β is used instead of MFA to denote material orientation. Figure 3 illustrates the simple and fundamental parts of the deformed state. The fundamental deformations superimposed give the deformed state. The orientation angle as function of deformations is given by

$$\beta = \text{Arctan} \left(\frac{\sin(\beta_0)(1+\varepsilon_x)}{\cos(\beta_0)(1+\varepsilon_y)} \right) + \gamma \quad (6) \text{ and (A1)}$$

The variables ε_x , ε_y , and γ are determined as follows. From equilibrium conditions of force and moment the stress is

$$\sigma^* = \begin{bmatrix} 0 \\ \sigma_y \\ 0 \end{bmatrix} \quad (A2)$$

Where normal stress in the y-direction is a function of excitation $\sigma_y = \sigma_y(\Lambda)$. The stress is transformed into the (non-deformed) material directions with the transformation matrix T.

$$T = \begin{bmatrix} \cos^2 \beta_0 & \sin^2 \beta_0 & \cos \beta_0 \sin \beta_0 \\ \sin^2 \beta_0 & \cos^2 \beta_0 & -\cos \beta_0 \sin \beta_0 \\ -2\cos \beta_0 \sin \beta_0 & 2\cos \beta_0 \sin \beta_0 & \cos^2 \beta_0 - \sin^2 \beta_0 \end{bmatrix} \quad (A3)$$

The transformation is written

$$\sigma = T^T \sigma^* \quad (A4)$$

The exponent T stands for matrix operation transpose. Linear elasticity for orthotropic materials is

$$\varepsilon = C\sigma \quad (A5)$$

Where the compliance matrix for plane stress is

$$C = \begin{bmatrix} \frac{1}{E_1} & \frac{-\nu_{21}}{E_2} & 0 \\ \frac{-\nu_{12}}{E_1} & \frac{1}{E_2} & 0 \\ 0 & 0 & \frac{1}{G} \end{bmatrix} \quad (A6)$$

The strain is transformed back to global xy-coordinate system in order to find the deformed state as

$$\varepsilon^* = T\varepsilon \quad (A7)$$

If assuming infinitesimal strain, the strain vector in the local coordinate system becomes

$$\varepsilon = \mathbf{C}^T \mathbf{T} \sigma^* = \sigma_y \begin{bmatrix} \frac{\sin^2 \beta_0}{E_1} - \frac{\nu_{21} \cos^2 \beta_0}{E_2} & \\ \frac{\cos^2 \beta_0}{E_2} - \frac{\nu_{21} \sin^2 \beta_0}{E_1} & \\ -\frac{\cos \beta_0 \sin \beta_0}{G} & \end{bmatrix} \quad (\text{A8})$$

Which in component form transform into the strain in the global xy-coordinate system as

$$\varepsilon^* = \begin{bmatrix} \varepsilon_x \\ \varepsilon_y \\ \gamma \end{bmatrix} = \sigma_y \begin{bmatrix} \cos^2 \beta_0 \left(\frac{\sin^2 \beta_0}{E_1} - \frac{\nu_{21} \cos^2 \beta_0}{E_2} \right) + \sin^2 \beta_0 \left(\frac{\cos^2 \beta_0}{E_2} - \frac{\nu_{21} \sin^2 \beta_0}{E_1} \right) - \frac{\cos^2 \beta_0 \sin^2 \beta_0}{G} & \\ \sin^2 \beta_0 \left(\frac{\sin^2 \beta_0}{E_1} - \frac{\nu_{21} \cos^2 \beta_0}{E_2} \right) + \cos^2 \beta_0 \left(\frac{\cos^2 \beta_0}{E_2} - \frac{\nu_{21} \sin^2 \beta_0}{E_1} \right) - \frac{\cos^2 \beta_0 \sin^2 \beta_0}{G} & \\ -\sin 2\beta_0 \left(\frac{\sin^2 \beta_0}{E_1} - \frac{\nu_{21} \cos^2 \beta_0}{E_2} \right) + \sin 2\beta_0 \left(\frac{\cos^2 \beta_0}{E_2} - \frac{\nu_{21} \sin^2 \beta_0}{E_1} \right) - \frac{\cos 2\beta_0 \cos \beta_0 \sin \beta_0}{G} & \end{bmatrix} \quad (\text{A9})$$

The applied normal stress σ_y needed for a known corresponding engineering strain of the material is determined accordingly

$$\sigma_y = \varepsilon_y \frac{E_2}{\cos^4 \beta_0 + \left(\frac{E_2}{G} - 2\nu_{21} \right) \cos^2 \beta_0 \sin^2 \beta_0 + \frac{E_2}{E_1} \sin^4 \beta_0} \quad (\text{A10})$$

The assumption of infinitesimal strain is limited to strains below 1-2 %. For larger strain a better approximation of the re-orientation of the material as a result of deformation is found by using the Green-Lagrange definition of finite strain. The components of the finite strain tensor, in the material coordinate system for the studied case (A5) are

$$\bar{\mathbf{E}} = \begin{bmatrix} \frac{\sigma_y \sin^2 \beta_0}{E_1} - \frac{\sigma_y \nu_{21} \cos^2 \beta_0}{E_2} + \frac{1}{2} \left(\frac{\sigma_y \sin^2 \beta_0}{E_1} - \frac{\sigma_y \nu_{21} \cos^2 \beta_0}{E_2} \right)^2 & \\ \frac{\sigma_y \cos^2 \beta_0}{E_2} - \frac{\sigma_y \nu_{21} \sin^2 \beta_0}{E_1} + \frac{1}{2} \left(\frac{\sigma_y \cos^2 \beta_0}{E_2} - \frac{\sigma_y \nu_{21} \sin^2 \beta_0}{E_1} \right)^2 & \\ \frac{1}{2} \sin \left(\frac{\sigma_y \sin \beta_0 \cos \beta_0}{G} \right) \sqrt{\frac{2\sigma_y \sin^2 \beta_0}{E_1} - \frac{2\sigma_y \nu_{21} \cos^2 \beta_0}{E_2} + \left(\frac{\sigma_y \sin^2 \beta_0}{E_1} - \frac{\sigma_y \nu_{21} \cos^2 \beta_0}{E_2} \right)^2} + 1 \sqrt{\frac{2\sigma_y \cos^2 \beta_0}{E_2} - \frac{2\sigma_y \nu_{21} \sin^2 \beta_0}{E_1} + \left(\frac{\sigma_y \cos^2 \beta_0}{E_2} - \frac{\sigma_y \nu_{21} \sin^2 \beta_0}{E_1} \right)^2} + 1 & \end{bmatrix} \quad (\text{A11})$$

The strain in the global xy-coordinate system is then found by transformation (A7) as

$$\bar{\mathbf{E}}^* = \mathbf{T} \bar{\mathbf{E}} \quad (\text{A12})$$

The components of the finite strain in the global xy-coordinate system is left out here due to lengthily of the expressions.

In order to build safe and durable wood structures, reliable performance predictions are needed which require proper understanding of the physical characteristics of wood. The performance is closely related to the hierarchical wood structure as well as the interaction with water. Compared with other building materials, wood exhibits significant time-dependent deformations that are heavily affected by water. In this thesis, the interaction of wood with water is examined and the time-dependent response of wood is modelled based on physical mechanisms on the molecular level causing this response.

DTU Civil Engineering
Department of Civil Engineering
Technical University of Denmark

Brovej, Building 118
2800 Kgs. Lyngby
Telephone 45 25 17 00

www.byg.dtu.dk

ISBN: 9788778773401
ISSN: 1601-2917